NEGATIVE SKIN FRICTION INDUCED ON PILES IN COLLAPSIBLE SOILS DUE TO INUNDATION

SARAH TAHSIN NOOR KAKOLI

A PH.D. THESIS

IN

THE DEPARTMENT

OF

BUILDING, CIVIL AND ENVIRONMENTAL ENGINEERING

CONCORDIA UNIVERSITY

MONTREAL, QUEBEC, CANADA

JANUARY 2011

© SARAH TAHSIN NOOR KAKOLI, 2011

ABSTRACT

Negative skin friction induced on piles in collapsible soils due to inundation

Sarah Tahsin Noor Kakoli, Ph.D.

Concordia University, 2011

Collapsible soils experience significant volume decrease due to the increase of soil moisture content, with or without an increase in the in-situ stress level. These soils form large parts of North and South America, Eastern Europe, China, Central Asia, Northern and Southern Africa, Russia, Egyptian western dessert, and the continuous deposit from North China to South-East England. As human activities continue to increase in these regions, geotechnical engineers must learn how to deal with these problematic soils. Foundations on collapsible soils suffer from sudden settlement, which may contribute to serious damage or catastrophic failure due to inundation. For relatively light structures, the use of shallow foundations combined with soil replacement or treatment may constitute economical designs. For heavy structures, pile is perhaps the best of alternative available types of foundation.

This subject of significant practical interest has received little attention from the researchers mainly due to the complexity in conducting experimental study. Furthermore, numerical modeling is difficult at best due to the complexity associated in describing the behavior of collapsible soil during inundation. Analytical modeling is not suitable in this respect, as soil grains in collapsible soil undergo radical rearrangements during inundation. In the literature, no design theory can be found to predict the negative skin friction on pile foundation due to inundation of collapsible soil.

Present study presents a numerical model, which is capable to incorporate the effect of inundation of collapsible soil on an axially loaded vertical pile. It employs the theories of unsaturated soil mechanics; including the Soil-Water Characteristic Curve (SWCC) to include the effect of soil suction reduction resulted from the progressive inundation, from two different aspects: change in soil properties, and irrecoverable soil volume change. The proposed numerical model is used to predict negative skin friction

exerted on the pile during inundation of collapsible soil surrounding the pile. The numerical model is validated by comparing the numerical results and the experimental data from the literature. Moreover, another numerical modeling procedure is also proposed to design the pile (i.e., length and diameter) in collapsible soil, provided that the indirect load due to negative skin friction is known. An extensive numerical investigation is carried out to identify the parameters (e.g., collapse potential, radius of wetting, pile roughness, etc.) influencing the negative skin friction acting on a pile during inundation. Based on the numerical results, analytical models that can be directly used to predict the indirect load due to negative skin friction are established for both directions (i.e., from bottom and top) of inundation.

Design procedures that can provide adequate positive skin friction and pile capacity in accommodating indirect load due to negative skin friction, are proposed to design the length and diameter of a single pile in collapsible soil subjected to inundation. Present study is useful in reductions in the costs of construction, litigation and remediation in geotechnical engineering practice.

ACKNOWLEDGEMENTS

First and foremost, I am expressing my solemn gratitude to Almighty Allah, the most gracious and merciful. Without His help and kindness, I could not have finished my thesis.

I am forever grateful to my supervisor, Dr. Adel M. Hanna who has given me support from the beginning. His vast experience, immense knowledge and friendly attitude directed me to achieve my research goal. I want to express my heartfelt gratitude for the patience he showed when I was a novice researcher. Specially, I am thankful for the freedom he has provided me in deciding my goals and experimenting with the approaches towards achieving them. He has taught me and demonstrated what it means to be a professor.

I would like to thank the other members of my examination committee, Drs. Sai Vanapalli (University of Ottawa), Ahmed K. Elhakeem, Attila Zsaki and Lucia Tirca, for reviewing my thesis, and providing valuable comments and insight into my research. Thanks also to Dr. Tahar Ayadat in developing my background knowledge in collapsible soil and Ibrahim Mashhour for conducting experiments. I thank Dr. Kinh Ha for offering the Graduate course, 'Finite Element Method' in such a wonderful way.

Special thanks are due to the Natural Sciences and Engineering Research Council (NSERC) of Canada for granting me the Alexander Graham Bell Canada Graduate Scholarship (CGS), to Concordia University for awarding me several scholarships and to the American Association of Cost Engineering (AACE) International, Montreal section for providing me the Graduate Award. I would like to mention the initiative taken by Dr. Ted Stathopoulos (Associate Dean, Programs and Awards, Concordia University) in changing the policy for external award holders, which benefited me financially.

I am forever indebted to my mother, Prof. Hosne Ara and father, Dr. Nurul Amin (peace be upon them), as they taught, guided and loved me, and also showed me how meaningful a life could be. Unfortunately, I could not show them what I have achieved so far, before they left for their eternal lives. I specially show my respect to my mother for her devotion in raising and educating me. The shock from sudden death of my father, in May 2010, was very difficult for me to overcome and to finish my Ph.D. research

This thesis is dedicated to my
Beloved parents,
Prudent husband & inquisitive son

CONTENTS

LIST OF FIGURES

LIST OF TABLES

LIST OF SYMBOLS

C_p = Collapse potential

C = Calibration Factor

c = Cohesion

$c´$ = Effective cohesion (saturated condition)

D = Diameter of pile

H_s = Depth of collapsing soil

h = Radius of wetting

ΔH = Collapse settlement

$\Delta H/H_0$ = Collapse strain

Δe or $\Delta V/V_s$ = Change in void ratio

e_o = Natural (initial) void ratio

G_s = Soil specific gravity

H_o = Initial height of the specimen

V_0 = Total volume

E_p = Young's modulus

L = Pile Length

K_0 = Coefficient of earth pressure at rest

$K_{0(OC)}$ = Coefficient of earth pressure at-rest at over-consolidated state

$K_{0(NC)}$ = Coefficient of earth pressure at-rest at normally-consolidated state

P = Percentage of full collapse experienced during partial inundation

Q_u = Ultimate pile capacity

Q_s = Positive skin friction

Q_b = Tip resistance

Q_n = Indirect load due to negative skin friction

$Q_n/\pi D$ = Unit negative skin friction

q_n = Average negative shear stress

S_r = Degree of saturation = 1 (after full saturation)

S_b = Initial degree of saturation before major collapse

S_f = Final degree of saturation after major collapse

$(\sigma_f - u_a)$ = Net normal stress

$(u_a - u_w)$ = Matric suction

u_a = Pore air pressure

u_w = Pore water pressure

w_0 = Initial water content

w_n = Soil moisture content at natural condition

w_{sat} = Soil moisture content at saturated condition

φ = Angle of internal friction

φ_{inter} = Interface friction angle

γ_c = Unit weight of concrete

γ_{sat} = Soil unit weight at saturated condition

γ_{bulk} = Bulk unit weight

γ_{dry} = Dry unit weight

ρ_d = Initial Dry Density

I_p = Plasticity index

α_i = Correction factor

ε_v = Volumetric strain

ε_c = Collapse Strain

σ = Surcharge, stress or pressure due to Foundation Load

Θ = Normalized volumetric water content, θ_w/θ_s

κ = Fitting parameter

υ_p = Poisson's ratio

ψ = Angle of dialatancy

NSF = Negative skin friction

SWCC = Soil-water characteristic curve

MC = Mohr-Coulomb constitutive law

OCR = Over-consolidation ratio

ISRF = Interface strength reduction factor

CHAPTER 1

INTRODUCTION

1.1 General

Collapsible soils are known to experience significant volume decrease suddenly due to an increase in soil moisture content, with or without an increase in the in-situ stress level (Clemence and Finbarr 1981). These soils considered a problematic type of unsaturated soils, since the collapsible structure contains low soil moisture when they are formed naturally or artificially. Soils susceptible to inundation induced collapse include loessial soils, weak cemented sands and silts, certain residual soils, compacted soils and fills. Collapsible soils form large parts of North and South America, Eastern Europe, China, Central Asia, Northern and Southern Africa, the continuous deposit from North China to South-East England, Russia, and Egyptian western dessert (Derbyshire et al., 1995; Evans et al., 2004; Abdrabbo et al., 2006). As human activities continue to increase in these regions (Brandon et al. 1990; Lim and Miller 2004; Ayadat and Hanna 2007), geotechnical engineers must learn how to deal with these problematic soils. In arid and semi-arid climatic zones, natural soils of different geologic origins (e.g., alluvial, colluvial, aeolian, and residual soils) are of collapsible type. Collapsible soil can be found in the upper strata (e.g., aeolian soil) or at depth (e.g., buried residual soil). Moreover, granular material with angular particles compacted on the dry side of the optimum moisture content can also form a structure, which is susceptible to further densification or collapse due to inundation (Tadepalli and Fredlund 1991). Lawton et al. (1992) reported that nearly all types of compacted soils are subjected to collapse upon wetting.

Inundation of any soil is practically unavoidable, since it could take place naturally (e.g., due to rainfall) or accidentally (e.g., leakage from underground waterlines) either. Depending on the cause of inundation, collapsible soil can be subjected to inundation from both the top and the bottom. Surface runoff and percolation

of rain-water, irrigation, poor drainage, flood, etc. are some examples of inundation from the top. Rise in groundwater table and capillary rise from ground water table are the cause of inundation from the bottom. Collapsible soil layer may be subjected to local inundation because of leaking from swimming pool, underground storage tank (e.g., septic tank), water and sewer lines, etc. It is clear that there is high possibility of wetting collapsible soil (i.e., supporting the foundation) and of experiencing inundation induced collapse accordingly, during the lifetime of a structure in collapsible soils.

Unsaturated collapsible soils do not show significant deformations even under heavy loads and therefore, it can provide adequate support to heavily loaded structure. On the other hand, a significant volume reduction (up to 20% of its original volume) occurs only due to the inundation of collapsible layer without any change in the stress level. Dudley (1970) reported that soil collapsed by 10% of its volume when soaked though it settled insignificantly at its dry state under a stress of 670 kPa in excess of the natural overburden stress. Sudden soil volume reduction below or around the foundation causes several problems such as differential foundation settlement, tilting, cracks in the structure, etc. resulting catastrophic failure. According to past experience (reported by Lawton et al., 1991), corrective measures for fixing collapse induced foundation and structural problems are expensive, usually in the range of $20-36 billion in U.S.A for low-rise building. Thus, it is important to design foundation in collapsible soil considering the effect of inundation so that structures could survive during soil collapse without having any sign of distress.

For relatively light structures, the use of shallow foundations combined with soil replacement or treatment may constitute economical designs. However, in case of a deep bed of collapsible soil (existing near ground surface), the soil treatment or the soil replacement is not feasible either. Moreover, none of the techniques is suitable even for a thin bed of collapsible soil, if it exists at a depth (e.g., 5m or more) from the ground surface. In case of shallow foundation, the volume change behaviour of collapsible soil subjected to inundation, raised diversity in geotechnical concerns: costs of construction and extensive maintenance (due to structural distress), and excessive litigation.

Therefore, pile foundations driven to an existing bearing stratum underlying the collapsible soil layer is perhaps the only feasible alternative available, in case of heavy

loads and deep strata of collapsible soil or any load (light or heavy) and a thin bed of collapsible soil at a depth. To date, several cases of piles, supporting structures built in collapsible soil and experiencing sudden reduction in their bearing capacity and further excessive settlement (of pile) immediately after inundation of collapsible soils, are reported in the literature (Grigoryan, 1997). The presence of collapsible soil layer may also negatively impact the capacity and performance of these piles during the lifespan of the structure.

In the literature, little work can be found for foundations in collapsible soil. This is mainly due to the high cost and the long period of time, and the difficulties associated in achieving sensible experimental results (Gan and Fredlund, 1988; Escario and Juca, 1989; Vanapalli et al., 1996).

1.2 Problem Statement

If the soil around a pile settles faster than the pile, the skin friction developed on the pile surface is negative and acts downward. Due to immediate soil volume reduction (soil collapse) resulting from the inundation of a layer of collapsible soil (around the pile), the negative skin friction developed on the pile interface exerts indirect load on the pile in addition to the externally applied load on the pile head.

Therefore, a pile in collapsible soil can settle as a result of two different actions: application of external load and development of indirect load due to negative skin friction resulting from soil collapse around the pile. These two types of pile settlement are often noticed separately, since the collapsible soil layer (around the pile) is usually subjected to inundation after the pile attains the settlement due to external loads. When the pile settles due to an external load only and the collapsible soil is not subjected to any change in moisture, the settlement follows pile load displacement curve. In such condition, positive skin friction develops on the pile interface throughout the full length of the pile, as shown in Figure 1.1.

On the other hand, when the collapsible soil (near ground, as shown in Figure 1.2 or located at a depth, as shown in Figure 1.3) is subjected to inundation, skin friction, along the pile segment L_{NSF}, is negative, acting downward and called negative skin friction (NSF).

3
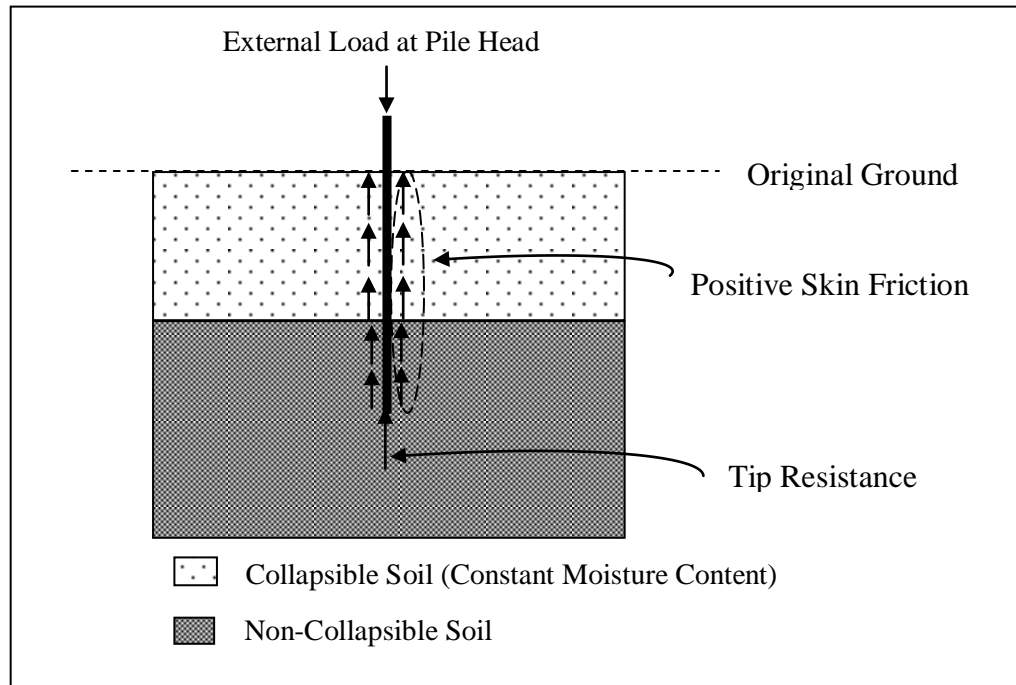
Figure 1.1: Load transfer mechanism of a single pile in unsaturated collapsible soil at constant moisture content

The soil collapse does not only increase the load on the pile but also reduces the capacity of the pile (due to reduction of positive skin frictional resistance). Both cases (shown in Figure 1.2 and Figure1.3) may equally approach critical conditions, regardless the magnitude of the drag load, if NSF appears on the equal length of pile segment (L_{NSF}, in Figure 1.2 and Figure 1.3) for a given pile. This is because the external load and the indirect load (i.e., drag load due to NSF) are resisted by the positive skin friction (developed on the pile surface having contact with non collapsible soil underlying collapsible soil) and the tip resistance during soil collapse. If positive skin friction could develop throughout the pile surface (from head to tip), the additional load could easily be accommodated by the factor of safety applied. However, the pile performance deteriorates mainly because of reduction in the positive skin frictional resistance and the pile capacity accordingly.

Prediction of NSF is also important to investigate the performance of shallow foundation under such soil subjected to inundation, when the depth of foundation is greater than the depth of collapsible soil (existing near the ground

4
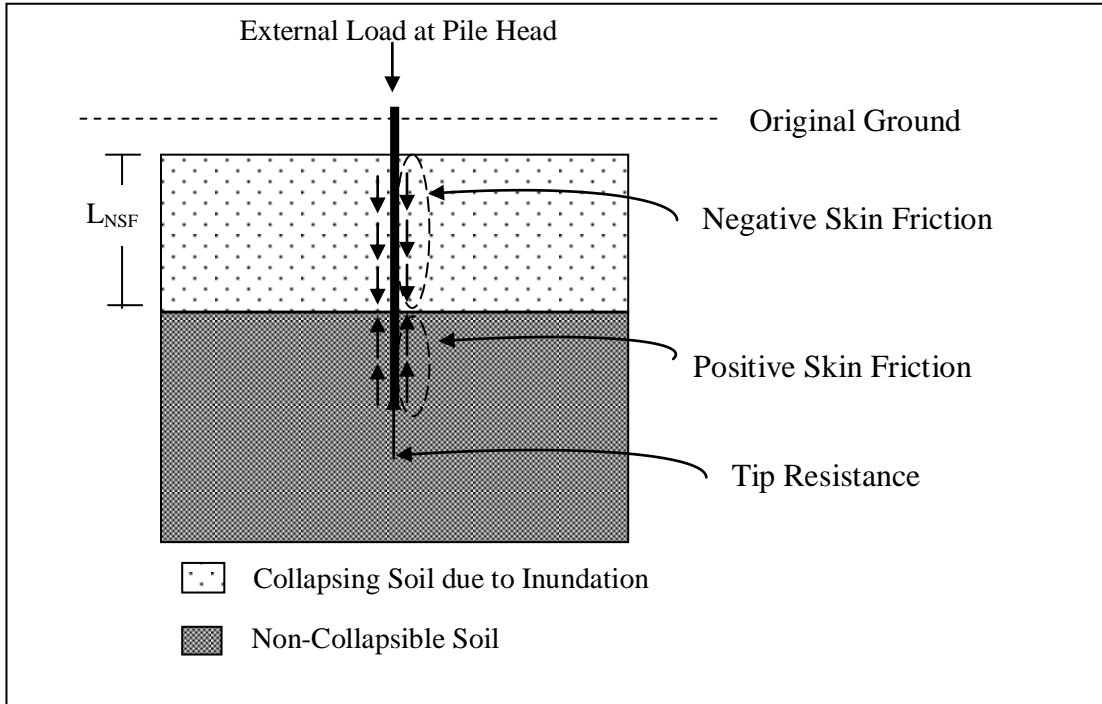
Figure 1.2: Load transfer mechanism of a single pile in collapsible soil (near the ground surface) during inundation
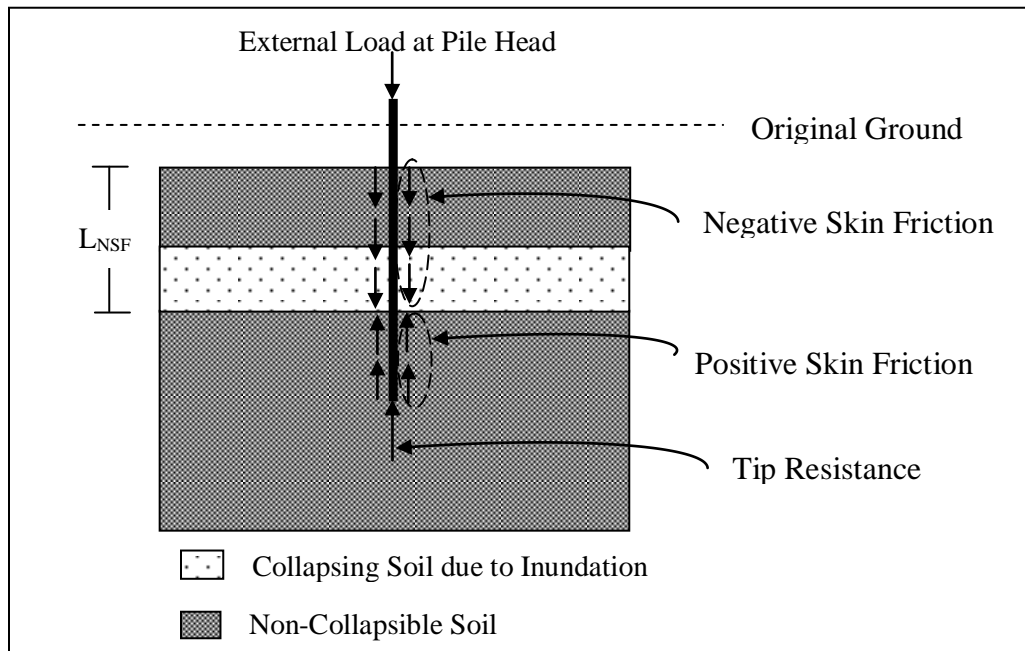
Figure 1.3: Load transfer mechanism of a single pile in collapsible soil (at depth) during inundation

surface). The stem of shallow foundation may also exert an additional, indirect load due to the development of NSF on its stem that has contact with collapsible soil subjected to inundation.

In order to obtain a safe design of pile in collapsible soil during inundation, two different aspects of developed NSF on the performance of pile must be addressed: magnitude of additional load (drag load) and reduction in positive skin frictional resistance. If the pile is not sufficiently embedded into the non collapsible layer, adequate safety of the structure under such situation can never be expected. To date, no theoretical framework is available to interpret, calculate or estimate the magnitude of the drag load (due to NSF) resulting from the inundation collapsible soil layer(s). The magnitude of the drag load for the case of Figure 1.2 could be greater or smaller than that of Figure 1.3, or both could be equal, depending on several factors, such as collapse potential, depth of collapsible soil subjected to inundation, radius of wetting, pile geometry and properties. Therefore, pile in collapsible soil must be designed considering the combined effects of different factors related to the inundation of collapsible soil.

1.3 Research Objectives

Extensive investigation is required to develop a theory to predict NSF. Experimental investigation is not suitable for the problem stated above as it involves several factors (such as collapse potential, depth of collapsible soil, radius of wetting, depth of collapsible layer, pile geometry and properties) those could have significant combined effect on the foundation performance and must be considered in developing theories. The experimental work is found very time consuming, e.g., 2-3 months to study the effect of inundation on pile excluding the preparation time for establishing the method of inundation and pile installation (Grigoryan, 1997). Furthermore, technical problems are often encountered in measuring devices installed along the pile, as they broke up during installation or due to water entering inside (during inundation). While numerical modeling may sound appealing to researchers, developing numerical models to simulate the case of unsaturated soil, especially during inundation is not easy. To date, only a few numerical studies involving the development of computer programs for coupling stress equilibrium and water flow for unsaturated soil can be found to study the effect of

6

inundation of collapsible soil on earth-dam (Miranda 1988; Pereira 1996). To our knowledge, foundation problems due to inundation induced collapse have not been investigated numerically due to the difficulties in describing the sudden volume reduction behavior of collapsible during inundation. Sudden decreases of soil stiffness and of lateral support along the pile's shaft (Lawton et al. 1991), and radical rearrangement of soil grains constitute the major stumbling blocks in modeling this condition. Furthermore, most of the available computer programs for saturated soil do not take into account the consequences of the transient unsaturated-saturated water flow. Also, consequences of inundation of collapsible soil are clearly more complicated than a transient unsaturated-saturated flow problem of any volume insensitive unsaturated soil.

The objectives of the research could be summarized as follows:

1. To conduct a literature review and to prepare a state-of-the-art report on collapsible soil and pile in collapsible soil. Special emphasis is given to develop knowledge regarding the behaviour of collapsible soil during inundation and also to study inundation induced NSF on pile.

2. To develop a numerical model capable of incorporating the effect of inundation of collapsible soil to study the performance of foundation in collapsible soil.

3. To validate the numerical model using experimental results, while predicting NSF on a vertical pile.

4. To perform a parametric study to establish the effect of the governing parameters that may affect the performance of a single pile in collapsible soil subjected to inundation.

5. To develop analytical models for practicing geotechnical engineers to predict NSF and drag load.

6. To propose a numerical approach to analyze the pile design during soil collapse, when the magnitude of drag load is known.

CHAPTER 2

LITERATURE REVIEW

2.1 General

This chapter presents the state-of-the art literature review and background information about the collapsible soils and the performance of foundation in collapsible soils. The effect of inundation on important soil parameters (e.g., strength parameters) are addressed in terms of matric suction, the governing parameter for describing collapsible soil behavior during inundation. The performance and research on pile foundation in collapsible soil subjected to inundation and negative skin friction are reported.

2.2 Inundation-induced Volume Reduction of Collapsible Soil

Unsaturated collapsible soil experiences sudden volume reduction (collapse settlement) during inundation, without any change in the stress level. The term 'unsaturated' refers to both dry and partially saturated conditions. Partially saturated collapsible soil, with low water content, is usually encountered in natural deposits. However, unsaturated soils, having stable soil structure, show insignificant volume reduction as compared to collapse settlement (i.e., experienced by collapsible soil having meta-stable structure) due to inundation. This sudden volume change behavior of collapsible soil makes it difficult to predict the performance of foundation in collapsible soil during inundation.

The volume sensitivity of collapsible soil, due to the change of soil moisture, is quite different from shrinkage and swelling, as experienced by other type of unsaturated soils. Expansive soil is a stable structured unsaturated soil that increases in volume (swell) during inundation. When the swelled soil (after wetting) is further subjected to drying (e.g., due to evaporation), it decreases in volume (subsidence) due to shrinkage and desiccation cracks are formed. The cracks (formed during the drying process the soil previously experienced) become closed during wetting. When the percentage of sand (in a clay-sand mixture) exceeds a certain value, the volume change of expansive soil (during drying and wetting) becomes negligible (Kodikara et al., 1999). It is to note that

8

collapsible soil experiences irrecoverable volume change (reduction) while the volume change behavior of swelling (expansive) soil is recoverable.

Practically, open and unstable (meta-stable) structure causes collapsible soil susceptible to immediate collapse during inundation. At initial state, collapsible soil has highly porous unsaturated structure, and has low unit weight accordingly. Its porosity and unit weight (unsaturated) usually range 0.8–1.0 and 12–15 kN/m^3 (Grigoryan, 1997) respectively. Figure 2.1 shows the microstructure of collapsible loess, which is formed by wind action. Collapsible sediments have honeycomb type particle arrangements, as shown in Figure 2.2.

| (a) | (b) |
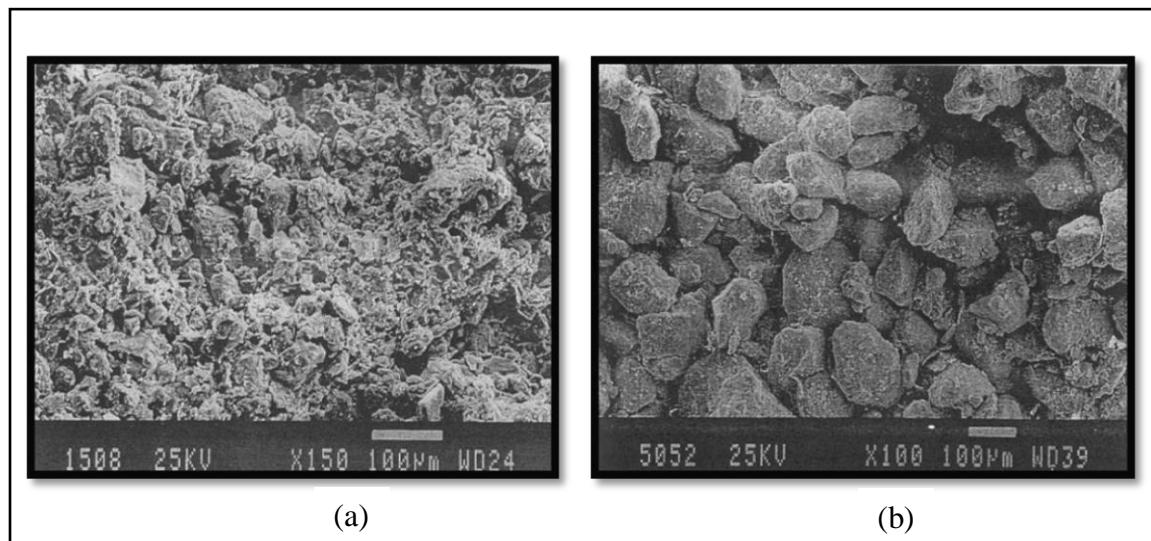
Figure 2.1: Skeletal microstructures; (a) typical loess, (b) sandy loess (Klukanova and Frankovska, 1995)

Different bonds due to cementation and capillary force constitutes the inter-particle bonds between the coarse grains and/or macro grains. Fine silt bond, clay bond, bond by autogenesis, ring buttress, clay-bridge, etc. are different types of bonds, acting as cementing agents between the coarse particles. In addition, capillary force, in micro-pores of unsaturated soil, provides significant bond strength, as shown in Figure 2.3. Micro-pores are located within the cementing material, connecting coarse grains and large flocs.
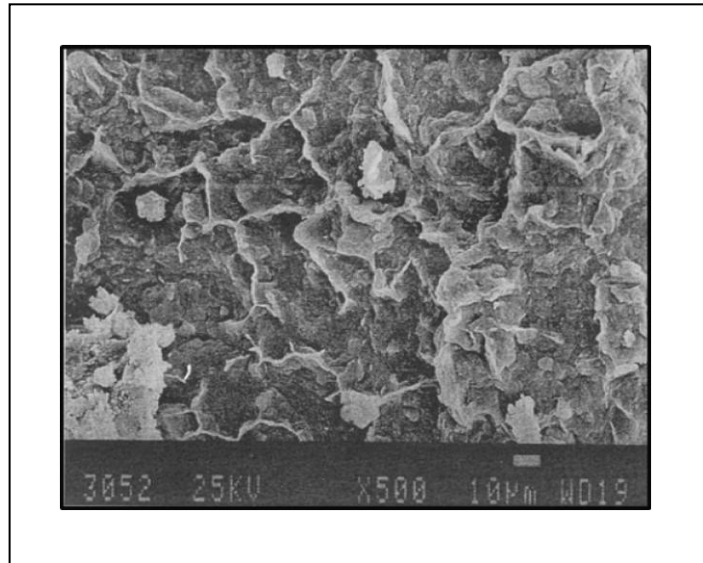
Figure 2.2: Honeycomb type of microstructure of loess like sediments (Klukanova and Frankovska, 1995)
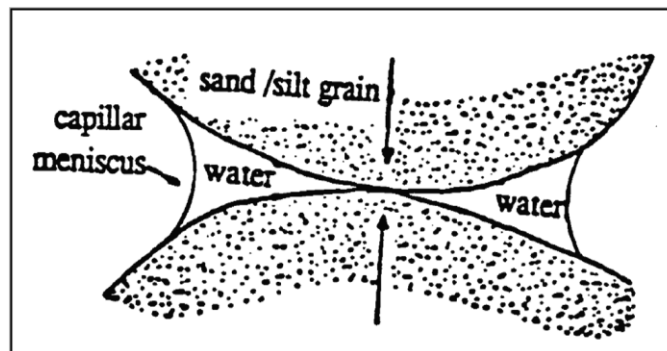
Figure 2.3: Bond in unsaturated soil by capillary action (Dudley, 1970)

Capillary action within unsaturated soil matrix causes the development of negative pore water pressure ($-u_w$), as the moisture content (i.e., very low in unsaturated collapsible soil) exists within the micro-pores only, rather than in the large macro-pores between the large flocs and/or coarse grains. Negative pore water pressure ($-u_w$), with respect to atmospheric pressure, is termed matric suction ($u_a - u_w$) in unsaturated soil mechanics. Pore air pressure is denoted by u_a. Typically, the pore air pressure in collapsible soils is in atmospheric pressure condition. The higher the matric suction is, the higher the additional bond strength (due to capillary force) is. Therefore, if the soil moisture content remains constant at its initial (unsaturated) value, the original porous structure of collapsible soil can be maintained under heavy external load. In such case, the combined action of inter-

10

particle bonds (cementation and capillary bonds) between coarse particles (e.g., sand and silt) resist any slip between soil grains and maintain the flocculated structure of collapsible soil.

The bond strength due to capillary action (or matric suction) is available only when negative pore water pressure exists with the soil matrix. Inundation causes reduction in matric suction (or negative pore water pressure, $-u_w$) due to the increase of water (or water pressure) in the pore. During inundation of any unsaturated soil, matric suction diminishes continually and becomes zero when the soil attained full saturation. Among all unsaturated soils, only collapsible soil structure is highly dependent on this bond strength (of matric suction), because of having meta-stable structure and initial high void ratio (or porosity). As a result, collapsible soil experiences immediate volume reduction during inundation, as this bond strength is lost due to matric suction reduction. A stable-structured unsaturated soil may also experience volume reduction during inundation, only if the soil is subjected to a very high stress, though it has relatively low porosity as compared to collapsible soil.

All unsaturated soils (including meta-stable and stable structured) experience changes in the unsaturated soil property functions (e.g., shear strength parameters, and permeability) (Maswoswe, 1985; Lawton et al., 1991; Pereira and Fredlund, 1999, among others). Figure 2.4 shows the effect of increase in moisture content in apparent cohesion (i.e., a shear strength parameter). Apparent cohesion in natural unsaturated condition decreases during inundation. In Figure 2.4, apparent cohesion is found 30 kPa and 10 kPa when the soil has 5% and 15% moisture content respectively (Udomchoke, 1991). Therefore, it is important to know such parameters during inundation to develop reliable numerical models for different engineering problems. In addition, more details with respect to the influence of matric suction on collapsible soil behavior during inundation is important and addressed in the next section.
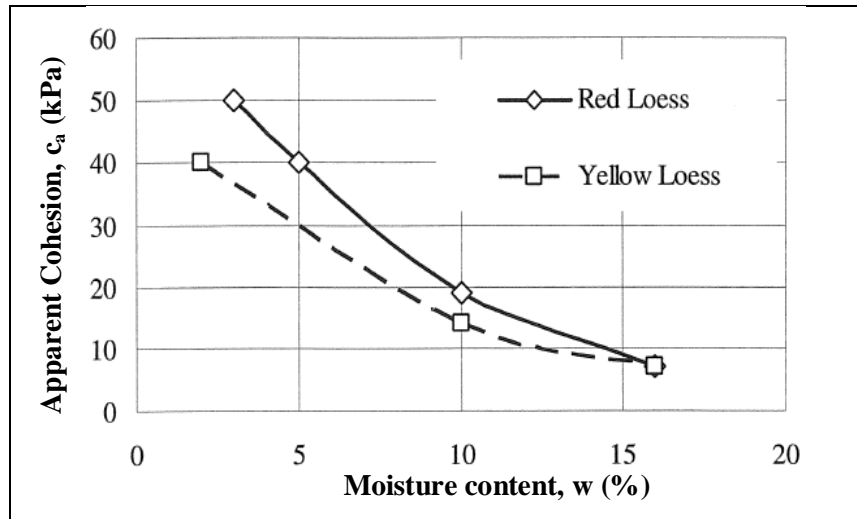
Figure 2.4: The effect of moisture content on apparent cohesion of Khon Kaen loess (Udomchoke, 1991)

The amount of expected collapse settlement due to full saturation depends on initial condition (in terms of initial moisture content, w_0 and initial dry density, γ_{dry}) of collapsible soil (Holtz, 1948; Hilf, 1956; Booth, 1977; Cox, 1978; Udommchoke, 1991; Fredlund and Gan, 1995; Sharma and Singhal, 2006 and Yasufuku et al., 2006 among others). The amount of collapse is expressed in terms of collapse strain ($\Delta H/H_0$), change in void ratio (Δe or $\Delta V/V_s$) or collapse settlement (ΔH). Collapse Strain ($\Delta H/H_0$) is the settlement (ΔH) of collapsible layer or sample due to inundation, as a percentage of the original height (H_0). Due to full saturation of a given collapsible soil under the same stress condition, less collapse strain results in the soil having relatively high initial moisture content, as shown in Figure 2.5, Figure 2.6 and Figure 2.7. Moreover, the higher the initial dry density is, the lower the collapse strain will be, as shown in Figure 2.5 and Figure 2.7. If the soil is inundated under constant pressure, collapse strain decreases when the relative density increases (Abbeche et al., 2007).
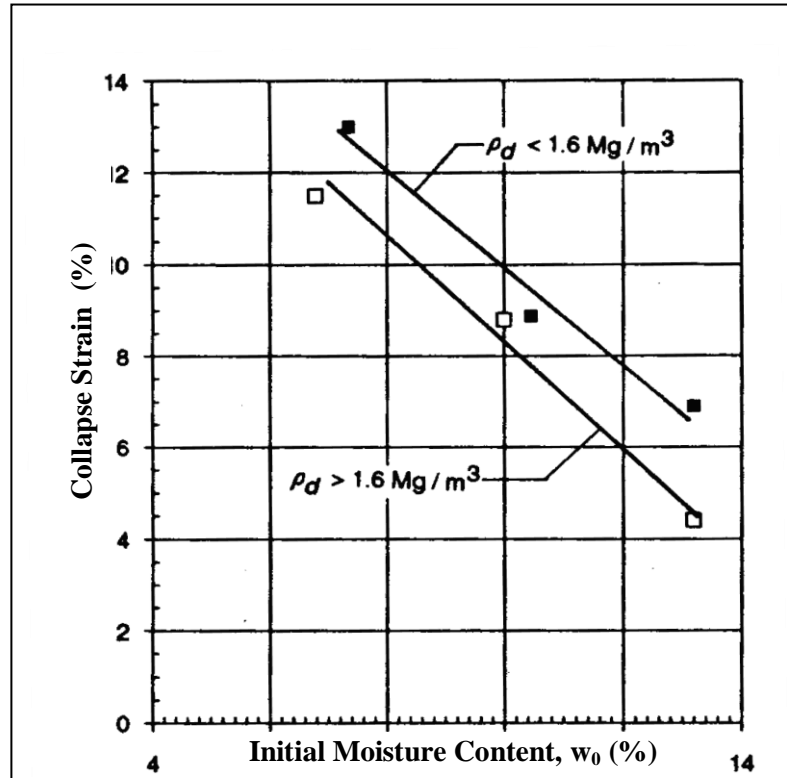
**Figure 2.5: Effect of initial water content on collapse strain
(Fredlund and Gan, 1995)**
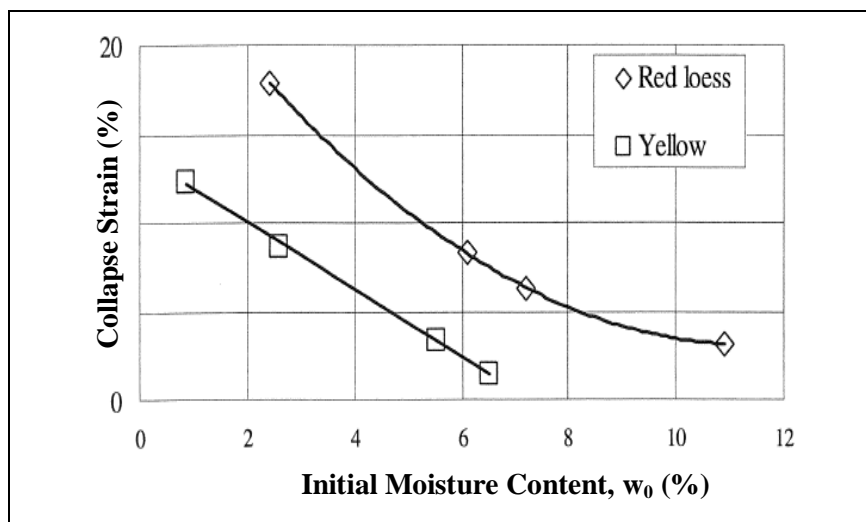
**Figure 2.6: Effect of initial water content on collapse strain
(Udommchoke, 1991)**

13
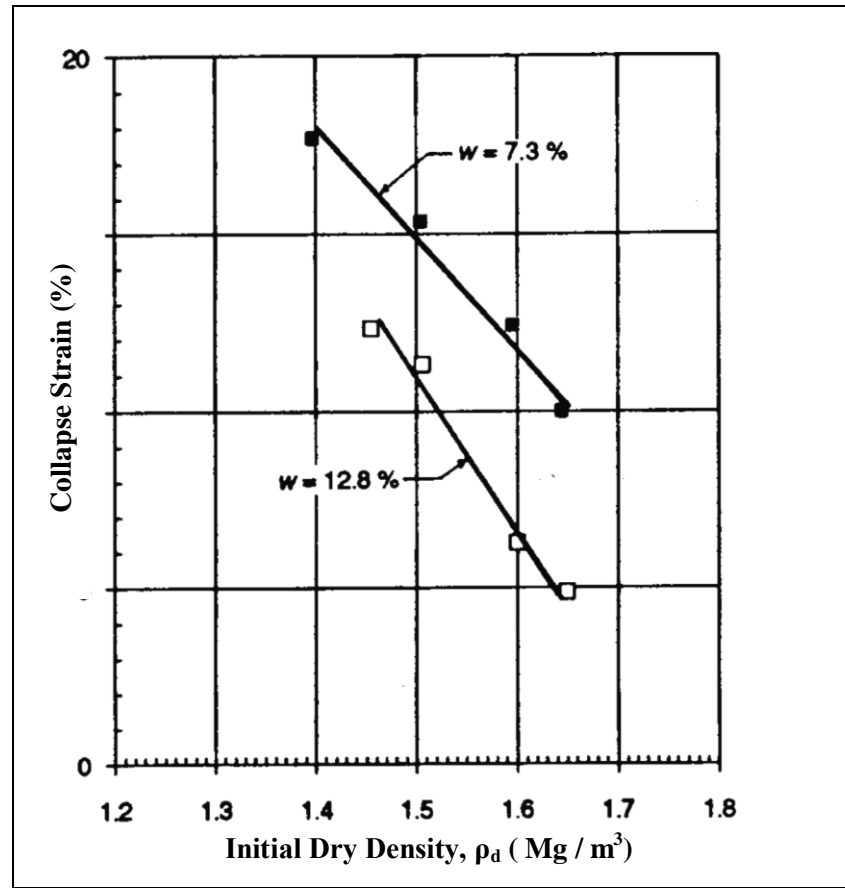
**Figure 2.7: Effect of initial dry density on collapse potential
(Fredlund and Gan, 1995)**

Therefore, for a given case, the amount of collapse decreases by increasing pre-collapse moisture content and increasing pre-collapse dry density. Pre-wetting (i.e., increase in moisture content) and compaction of unsaturated collapsible soil (i.e., increase in dry density) are often practiced before construction to avoid post-constructional catastrophic failure of foundation in collapsible soil subjected to inundation. Pre-wetting is not a feasible mitigation technique for a collapsible layer located at a depth (e.g., 5m or more). Moreover, it can cause collapse (of a collapsible soil near surface) under a given inundation pressure. Therefore, pre-wetted collapsible layer can show significant settlement, when the soil layer is subjected to increased stresses due to structural load after construction. Most of the conventional measures, such as avoiding of wetting, pre-wetting and controlled wetting, removal and replacement of the collapsible soil layer, are found ineffective in minimizing collapse problem. Chemical stabilization and grouting

14

are not economical for heavy structures. Therefore, in the literature, investigations, regarding mitigation and monitoring of foundations in collapsible soils, focus on advanced soil improvement techniques (e.g., dynamic compaction, rapid impact compaction and stone columns).

During compaction, collapsible soil requires significantly higher energy input than non collapsible soil (Rollins et al., 1998). Dynamic compaction can reduce void ratio from 1 ($e_{initial}$) to 0.7 (e_{final}), but that is not sufficient to eliminate the collapse problem, because such a reduction in void ratio is attained only at the drop-site hole. At the intermediate location of drop hole, collapsible soil has the potential to cause catastrophic failure of foundation during inundation. Figure 2.8 shows the effect of dynamic compaction in densification (at natural moisture content) of collapsible soil (in Western United States) in terms of void ratio.
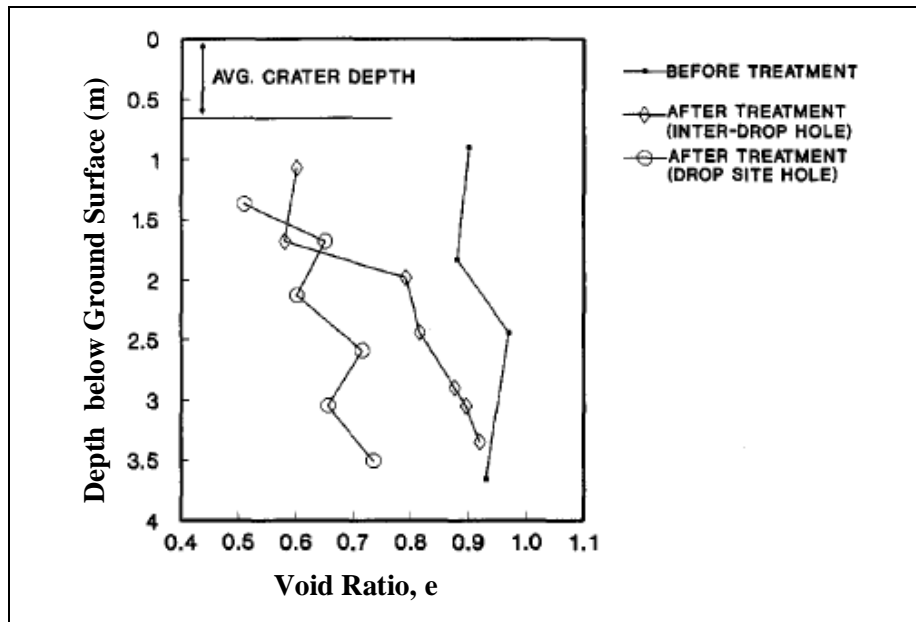
Figure 2.8: Void ratio before and after dynamic compaction (Rollins et al., 1994)

Pre-wetting and dynamic compaction cannot be combined to treat collapsible soil, as moisture content has significant influence on the degree of improvement due to on dynamic compaction (Rollins et al., 1998). Any significant improvement in soil densification cannot be achieved using moisture beyond the optimum moisture content. Rather, several difficulties, including formation of excessive crater depth and extraction

of the weight from deeper craters, were posed. Moreover, the use of down-hole nuclear moisture probe indicates that it is difficult to maintain uniform moisture content within the anticipated depth of improvement during dynamic compaction. Furthermore, reduction in collapse strain (i.e., improvement) due to dynamic compaction is not that much significant at depths greater than 3 m, as shown in Figure 2.9.
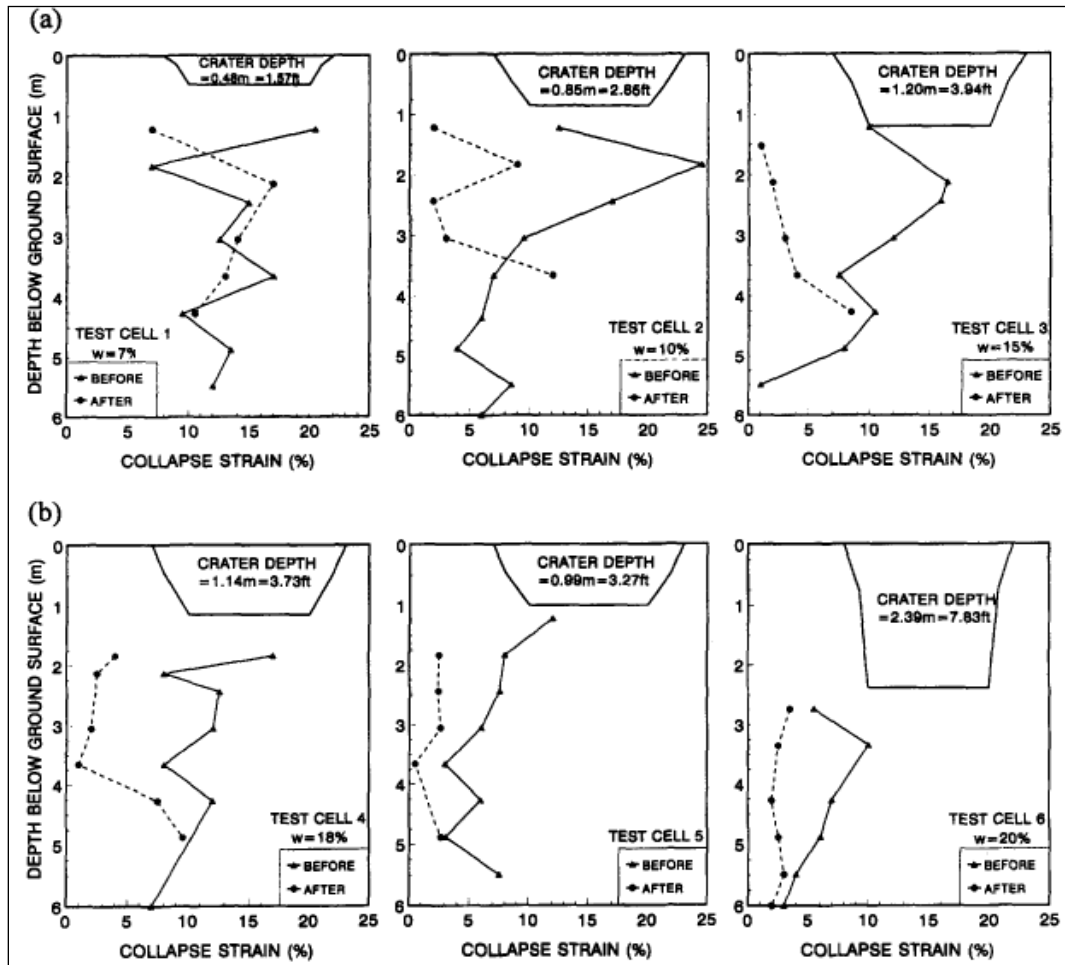
Figure 2.9: Collapse strain profiles before and after dynamic compaction (Rollins et al., 1998)

Rapid Impact Compaction (RIC) method for treating collapsible soil is also investigated on a large onshore oil and gas field development in Kazakhstan (Evans et al., 2004). Significant improvement up to 2.5–3 m was found in the area with deep ground water level, while no immediate improvement was attained in the area with shallow ground water level. In those sites, loess soil deposits were extending to a depth of 17 m.

As compared to dynamic compaction, RIC delivers less energy per blow but a large number of impacts per minute (about 40 blows per minute). Degree of compaction is achieved first on the top layers (i.e. top-down process) through RIC method, while dynamic compaction is generally viewed as a bottom up process. As a result, RIC could not increase dry density, reduce void ratio or decrease collapse strain at depths below 3 m.

Encapsulated stone column in geo-grid material is a recently introduced mitigation measure to avoid any further post-constructional disaster resulting from soil collapse. Ayadat and Hanna (2005) proposed a step-by-step procedure for the design of encapsulated stone columns and a calculation method for lateral deformation (the main contributor to the total settlement of stone column). However, this measure can sustain only light to moderately loaded structures built in collapsible soil.

Monitoring of collapsible soil has become an integral part of mitigation measure. Geophysical methods are recommended to assess the factors, including depth and lateral extent of collapsible deposits, depth of water table, moisture content, moisture movement and stiffness of soil, indicative to any potential future disaster during inundation (Evans et al., 2004). Such methods can trace the 'footprint' of loess deposits that would likely to undergo hydro collapse upon wetting. In recent years, British Geological Survey uses resistivity/moisture content imaging technique in monitoring moisture movements during a field collapse trial in loess deposits in UK. In a pilot study, the degree of ground improvement (due to dynamic compaction) was monitored through seismic survey (i.e., P wave propagation) by Evans et al. (2004). The optimum inundation depth due to a given rainfall event is expressed mathematically to avoid any disaster during inundation of collapsible soil (Abdrabbo et al., 2006).

Based on the literature review, building on pile or pier foundations is the only alternative available to avoid foundation failure. The following issues concerning soil collapse during inundation are addressed to assist in developing a numerical model of pile in collapsible soil incorporating the effect of inundation (i.e., the objective of the present study).

17
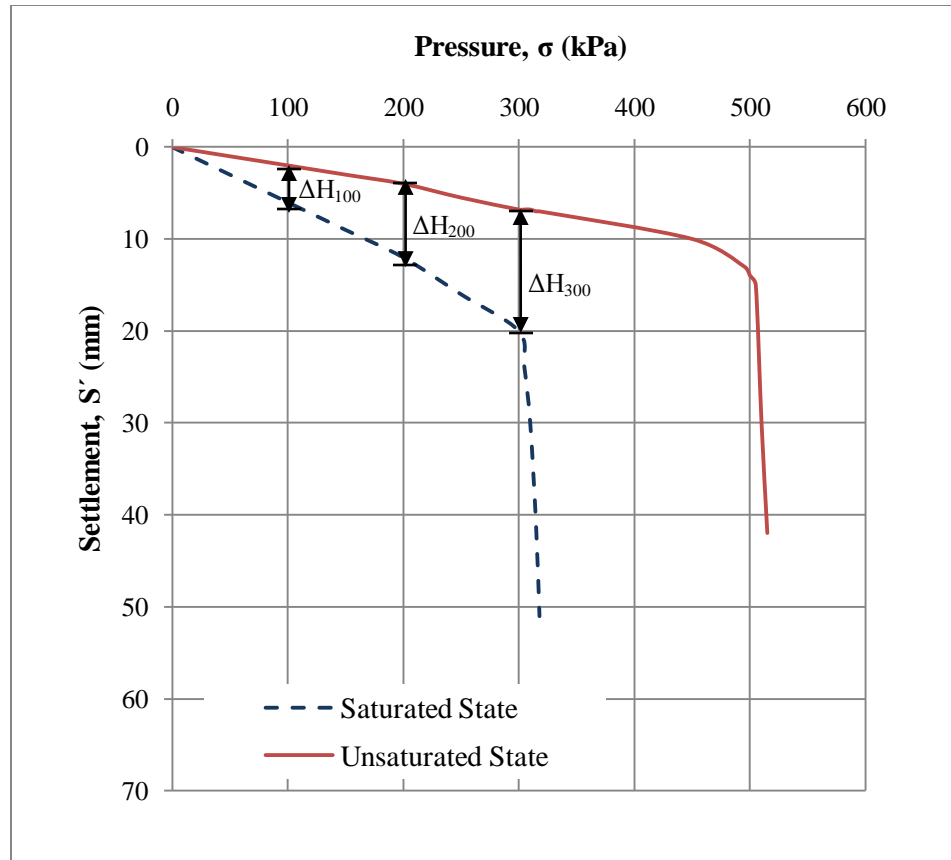
Figure 2.10: Typical load settlement curves of a bearing plate in collapsible soils (saturated and unsaturated) (Grigoryan, 1997)

Collapsible soil responds differently before and after inundation, as seen in Figure 2.10. The figure shows a typical pressure-settlement response of collapsible soil for a bearing plate in collapsible soil (unsaturated and saturated) (Grigoryan, 1997). This figure can explain the cause of excessive foundation settlement during inundation of collapsible soil. Foundations, supporting a structure on unsaturated collapsible soil, experience settlement, $\Delta H_{\sigma(un)}$, according to the pressure-settlement curve at unsaturated state. If the initially unsaturated collapsible soil is subjected to full inundation (reaching 100% degree of saturation) under a given foundation pressure (σ), the foundation will experience additional settlement ($\Delta H_{\sigma(inun)}$), which is the vertical distance between the unsaturated and saturated pressure response curves at foundation pressure (σ) in Figure 2.10. The pressure under which the soil is subjected to inundation is termed inundation pressure. In Figure 2.10, ΔH_{100}, ΔH_{200} and ΔH_{300} are the amount of collapse or

settlements ($\Delta H_{\sigma(inun)}$) due to inundation only under the inundation pressures (σ) of 100, 200 and 300 kPa, respectively. For a given soil, it can be noted that the higher the inundation pressure is, the greater the amount of collapse is. If the foundation rests on the top of collapsible soil (located at a depth), it will experience immediate settlement equals the significant amount of collapse. Therefore, the length of the pile must be greater than the full depth of collapsible soil and rest on non collapsible soil bed. On the other hand, since low foundation pressure on collapsible soil corresponds to low collapse settlement, only light structures can be built on shallow foundations after soil treatment (such as chemical stabilization, grouting, stone column and compaction).

Figure 2.10 demonstrates the effect of inundation on saturated collapsible soil behavior. Firstly, inundation causes a gradual increase in compressibility, which is also reported in Fredlund and Rahardjo, 1993. At initial unsaturated condition, collapsible soil can give only a small volume change due to the applied external load, as the fine cementing materials, within the soil structure, get compressed. On the other hand, saturated collapsible soil settles more than unsaturated one, under a constant pressure on the bearing plate in both cases. Secondly, inundation causes strength reduction. In the given example of Figure 2.10, unsaturated collapsible soil can support a pressure of 500 kPa, while the same soil can support only 300 kPa after inundation. It is to note that immediate foundation failure may result from inundation, if inundation pressure exceeds the ultimate limit of soil strength at saturated condition. According to Figure 2.10, if this soil is subjected to a pressure greater than 300 kPa (e.g., 400 kPa) before inundation, then bearing plate will fail and settle infinitely (as compared to ΔH_{300}) due to inundation under the same pressure.

For a given collapsible soil, the amount of collapse (in terms of collapse settlement, ΔH or change in void ratio, Δe) depends on inundation pressure (σ). Figure 2.11 shows the effect of inundation pressure (in terms of net confining pressure) on the change in void ratio (expressing the amount of collapse) during matric suction reduction (from 375 to 0 kPa) as a result of inundation. It is to note that different inundation pressures cause the same soil (having the same initial void ratio) to attain different final void ratios at the end of saturation (i.e., zero matric suction). Therefore, for a given soil,
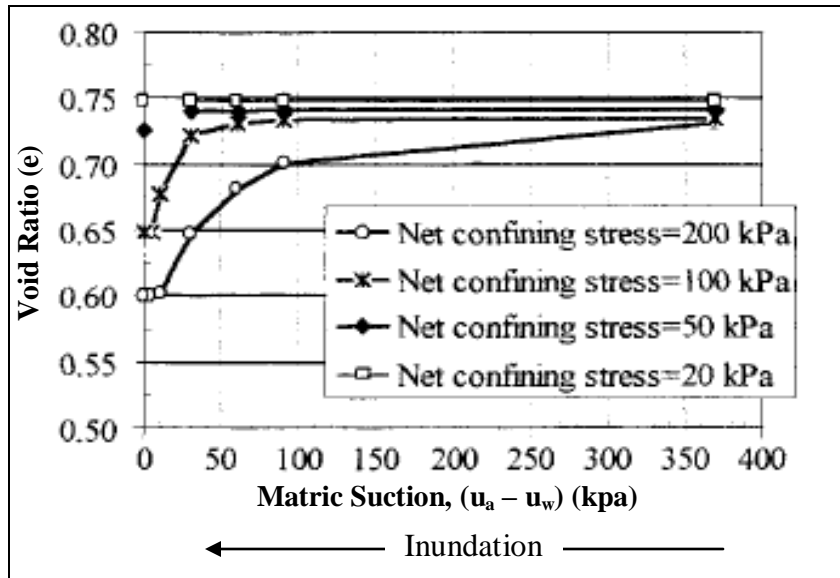
Figure 2.11: Void ratio changes during saturation (Pereira and Fredlund, 2000)

the depth of the layer from the ground is very important to assess the severity of collapse problem, as inundation pressure results from the overburden pressure of the soil above the collapsible layer subjected to inundation. The consequence of inundation of collapsible soil is more severe when the collapsible layer is at a depth (e.g., when underlying a non collapsible soil bed) than when that is located near ground surface. In case of 20 kPa net confining stress condition in Figure 2.11, highly porous soil and meta stable structured soil did not respond in showing volume reduction during inundation, as the inundation pressure is not sufficient to break the cementing bonds those show resistance against collapse upon inundation. As net confining stress increases, the soil gives increased amount of collapse. In an experimental program, Nouaouria et al. (2008) noted that greater collapse strain is expected under greater inundation pressure, for a given soil. From Figure 2.12, it can also be noted that collapse strain is directly proportional to inundation pressure up to a certain limit.
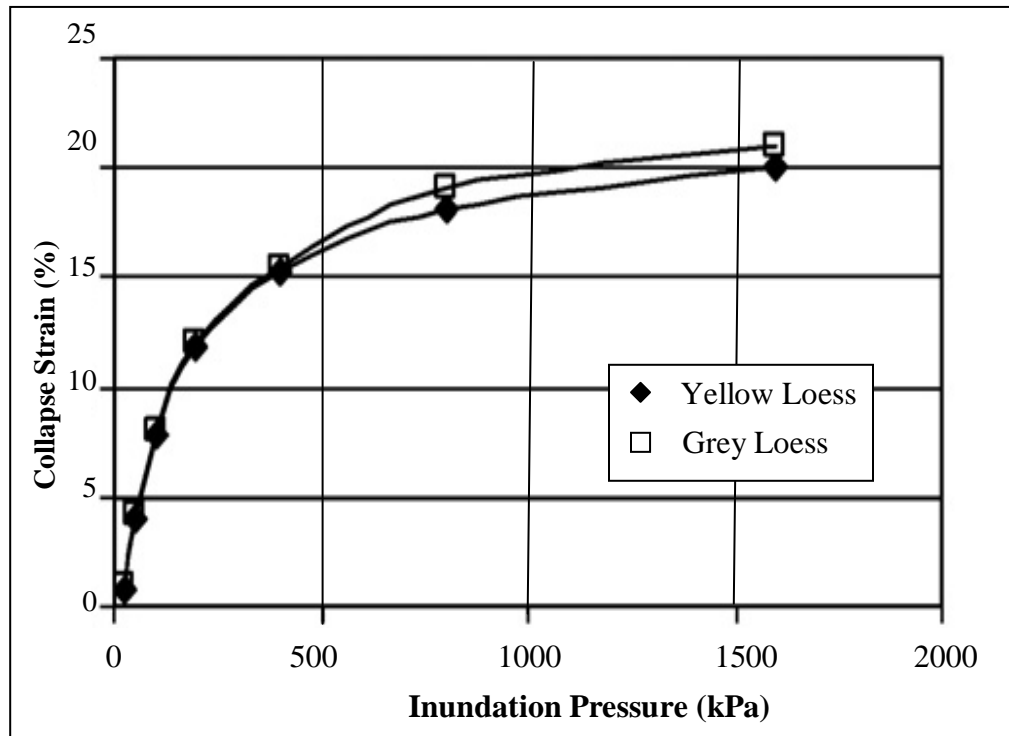
Figure 2.12: Effect of inundation pressure on collapse strain (Nouaouria et al., 2008)

Moreover, inundation pressure also influences the moment, when the significant changes in soil volume is commenced, in the process of saturating a collapsible soil from its initial condition to full saturation. The higher the inundation pressure is, the faster the soil volume reduction commences. When inundation pressure is low, the soil may not show volume reduction till the soil attains relatively high degree of saturation, as can be seen in Figure 2.11. This fact can be explained according to the concepts of bonds within the soil grains in collapsible unsaturated soil structure. Until a significant portion of bond strength due to matric suction is lost after attaining a certain degree of saturation, bonds (including fine silt bond, clay bond, etc. and the remaining bond strength due to matric suction) can maintain the original structure under the inundation pressure applied and therefore, the collapsible soil experiences a delayed collapse under low inundation pressure. If inundation pressure is high (e.g., the case of 200 kPa of net confining stress in Figure 2.11), volume reduces from the very beginning of saturation. Under high inundation pressure, diminishing bond strength due to matric suction (during inundation) causes high stress on the other bonds and further reduction in matric suction causes gradual break down of other bonds. Once the other bonds are destroyed under high

21

inundation pressure, volume reduction takes place along with the reduction of matric suction. For the case of 200 kPa confining stress in Figure 2.11, the moment of 100 kPa matric suction can be considered the moment when no other bonds, except the bond due to matric suction, exists. Beyond this stage of inundation, inundation induced collapse becomes fully dependent on the reduction of matric suction and major collapse begins. On the other hand, under the case of 100 kPa confining stress, major collapse begins until inundation causes matric suction to decrease below 50 kPa. It should be noted that high inundation pressure initiates the phase of major collapse faster than low inundation pressure.
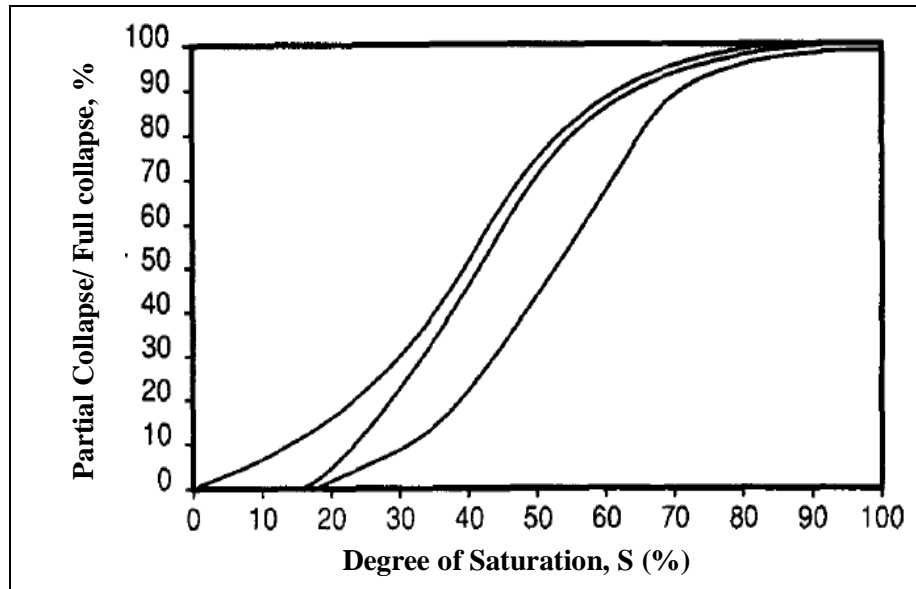
Figure 2.13: Partial collapse curves for three collapsible silts (Mahmoud, 1991)

Pre-collapse, major collapse and post collapse phases constitute collapse phenomena due to full saturation (Pereira and Fredlund, 2000). In a 'pre-collapse' phase, soil undergoes small volumetric deformations due to elastic compression without grain slippage, when the degree of saturation is usually below 30% (approximately), as in Figure 2.13. Phase 2 is the 'major collapse phase' where significant volumetric deformation results in response to reductions in matric suction, in the micro-structural level due to structural rearrangements and the occurrence of local shearing, of both connecting bonds and clay aggregations. Figure 2.13 shows that major collapse as a

22

percentage of full collapse under a given inundation pressure, which takes place at a constant rate for an increase of degree of saturation around 40%. This stage of deformation involves collapsing soil mass at both macro and micro-structural levels. Connecting bonds and clay aggregations break down at this phase and subsequently increase in number of contact points between large particles. At a given net normal stress, collapse continues until the new equilibrium configuration, which does not represent the total destruction of all connection bonds, is reached. In the final phase, termed as 'post collapse', smaller deformations are observed, which can be attributed to secondary compression of the soil skeleton (Pereira and Fredlund, 2000).

Collapse potential (C_p) is an index rating the potential of collapse for comparing different soils susceptible to collapse. According to the standard testing procedure (ASTM D 5333-96, 1998), collapse potential is the collapse strain due to inundation of the undisturbed sample under 200 kPa pressure in oedometer apparatus. Therefore, collapse potential (C_p) is defined as follows:

$$C_p = \frac{\Delta e_{200} * 100}{1 + e_o} = \frac{\Delta H_{200} * 100}{H_o}$$

where,

C_p = Collapse Potential (in %),

Δe_{200} = Change in void ratio upon wetting under 200 kPa pressure,

e_o = Natural (initial) void ratio,

ΔH_{200} = Change in sample height upon wetting under 200 kPa pressure, and

H_o = Initial height of the specimen.

While conducting oedometer test in evaluating collapse potential, both the single curve and the double curve methods are commonly used. However, both the methods give similar values. In the single curve method, three steps are followed on an undisturbed sample. In step 1, undisturbed soil sample (within the oedometer ring) is placed in the oedometer apparatus. In step 2, vertical pressure on the soil specimen is gradually increased up to 200 kPa (in determining C_p) or a pressure level equivalent to the new

pressure (on that soil) expected after construction. In step 3, the soil sample is inundated, after achieving nominal stabilization under the applied vertical pressure (in step 2). Therefore, loading and wetting of sample are carried out in the sequence as same as that observed in the nature, as shown in Figure 2.14. The relative soil compression (in terms of void ratio) is determined from the measurements of vertical settlements of the sample.
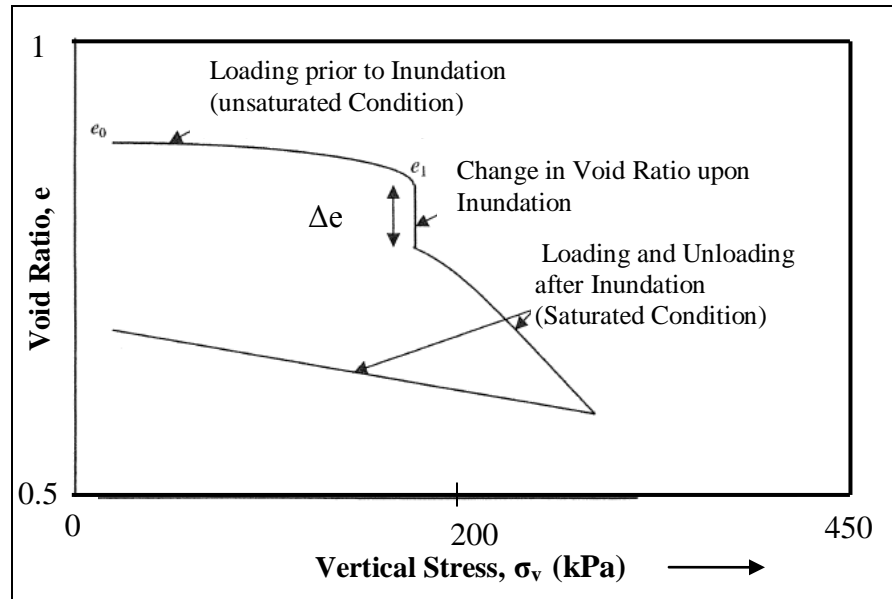
Figure 2.14: Single curve oedometer test to evaluate collapse potential (C_p)

In the two curve method, two oedometer tests are conducted on two identical samples. Two settlement-vertical stress curves, as shown in Figure 2.10, are obtained from two independent tests. After placing the sample in the oedometer apparatus, one test is performed by increasing the vertical stress on undisturbed sample at natural moisture content. The other test is performed after saturating the sample in the apparatus. The vertical distance between the curves, at any pressure, represents the settlement (ΔH) of specimen during inundation. Collapse strains can be obtained at different inundation pressures using two compression curves.

In the literature, several researchers gave further efforts to predict collapse potential in identifying collapsible soil. Ayadat and Hanna (2007) proposed a simple method to identify collapsible soils based on the results of the fall cone penetration test. Abbeche et al. (2007) presented the variations of the collapse potential with respect to the wide

ranges of relative density and clay content. Basma and Kallas (2004) proposed a model to predict collapse potential using Artificial Neural Network. To date, some empirical relations are available to predict collapse potential in identifying collapsible soil based on some soil parameters, including dry unit weight, initial (or compaction) water content, inundation pressure, percentages of sand and clay, percentage of clay-size fraction, coefficient of uniformity, and plasticity index (Lim and Miller, 2004; Lawton et al., 1992; Lutenegger and Saber 1988). Houston et al. (1995) developed an in-situ test system with the load-displacement measurement for identifying collapsible soils. Collapse potential (C_p) is used to assess the severity of the problem, as shown in Table 2.1 according to Jennings and Knight (1975).

Table 2.1: Collapse potential (C_p) and severity of foundation problem
(Jennings and Knight, 1975)

Collapse Potential, C_p (%)	Severity of problem
0-1	No problem
1-5	Moderate trouble
5-10	Trouble
10-20	Severe trouble
>20	Very severe trouble

In developing a numerical model incorporating the effect of inundation of collapsible soil, it is important to understand the continuous behavioral change of collapsible soil when collapse ($\Delta H_{\sigma(inun)}$) takes place due to the increase of degree of saturation from initial state to 100%, under a constant inundation pressure. In the literature, these behavioral changes (i.e., in terms of volume, permeability, and shear strength) due to inundation are related to matric suction, resulting from capillary forces within the unsaturated (or partially saturated) soil matrix. However, on microscopic level, van der Waals attraction, the double layer repulsion and the adsorbed water involve in causing such changes in soil behavior.

2.3 Effect of Matric Suction during Inundation

For collapsible soil, matric suction (u_a - u_w) is considered as one of the governing state variables (Fredlund and Morgenstern, 1977; Fredlund and Rahardjo, 1993; Lu and Likos, 2004, and others). Researchers also found that the matric suction (u_a - u_w) and the net normal stress (σ_f - u_a) are the most advantageous combination of state variables for partially saturated soils including collapsible soil, since only one of them becomes affected due to any changes in the pore water pressure (u_w). The theoretical and experimental justification of using two independent stress-state variables for unsaturated soil is given in Fredlund and Morgenstern (1977). Their proposed constitutive framework for unsaturated soil is equally applicable to volume increase (expansive soil) or decrease (collapsible soil) in response to any change in the state stress variables, e.g., matric suction.
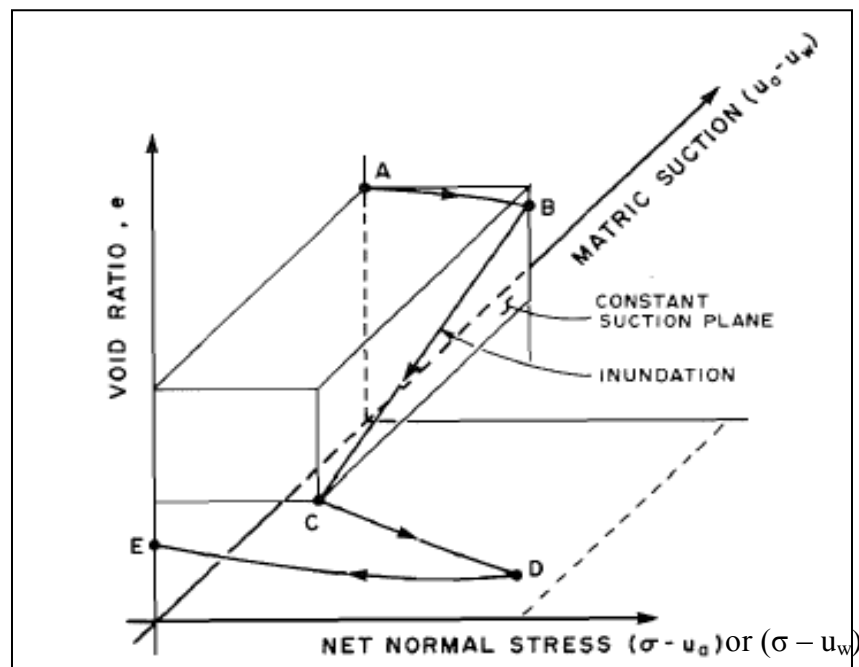
**Figure 2.15: Typical compression curve for collapsible soil
(Tadepalli and Fredlund, 1991)**

Figure 2.15 presents an idealized compression curve, typically plotted with respect to net normal stress (σ - u_a) and matric suction (u_a – u_w). As shown in Figure 2.15, stress path of a soil specimen is presented by the lines AB (before inundation) and BC (during

inundation), and the lines CD (loading under saturated condition) and DE (swelling line during unloading) after inundation.

Collapsible soil shows less compressibility before inundation than it exhibits at saturated condition, comparing the slopes of the lines AB and CD. During inundation it gives overall volume decrease that is irrecoverable and irreversible, while total stress (i.e., net normal stress) remains unchanged, as shown by the line BC. During inundation, the pore air pressure is commonly assumed constant, i.e., atmospheric condition. It appears that matric suction ($u_a - u_w$) is the only variable that changes during inundation and governs the soil behaviour. The effective stress concept of one stress state variable ($\sigma - u_w$) fails to explain the collapse behaviour of unsaturated (or partially saturated) soils during inundation (Tadepalli and Fredlund, 1991). However, this conventional concept of effective stress forms the fundamental basis of saturated soil mechanics and also very useful in predicting all mechanical aspects of saturated soils.
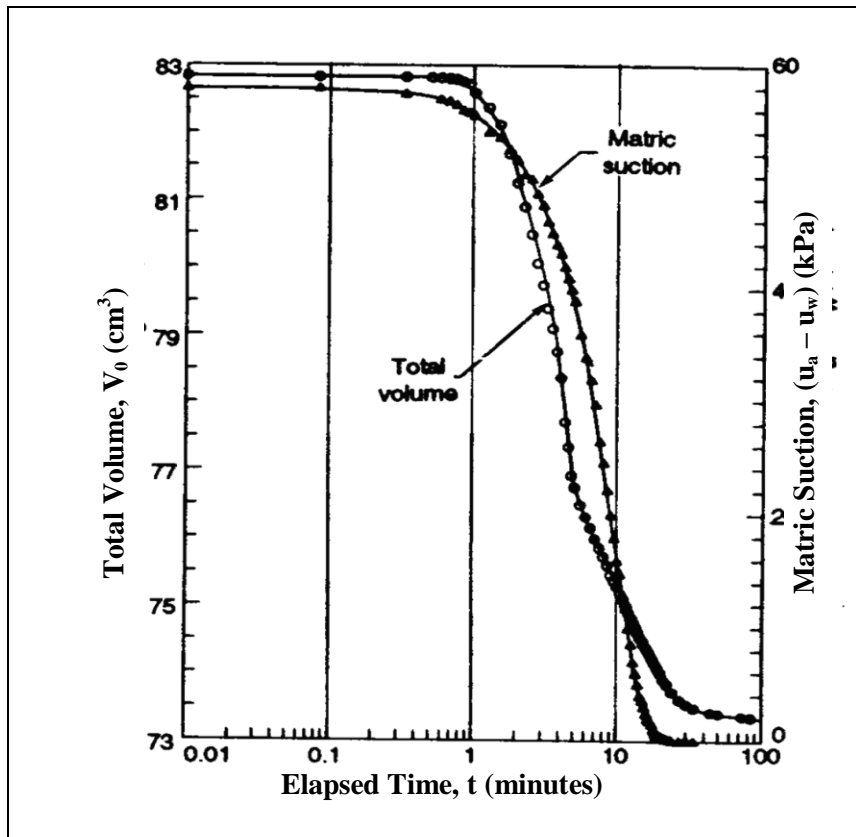
Figure 2.16: Reductions of soil volume and matric suction during inundation (Tadepalli and Fredlund, 1991)

Tadepalli and Fredlund (1991) showed that there exists a one-to-one relationship between the matric suction and the total volume change for a soil exhibiting collapse behaviour during inundation, as shown in Figure 2.16. Tadepalli and Fredlund (1991) and Tadepalli et al. (1992) verified the application of unsaturated soil mechanics to describe collapse mechanism. Pereira (1996) and Miranda (1988) applied the concepts of unsaturated soil mechanics in simulating the collapse behaviour of an earth dam during its first filling.

The process of direct measurements of different parameters defining hydro-mechanical behavior during inundation is time consuming and expensive. Therefore, research on 'estimation techniques' (to determine the properties of unsaturated soils, including collapsible soil during inundation) emerges over last few decades. In the recent conferences on unsaturated soils (e.g., Forth International Conference on Unsaturated Soils, Carefree, Ariz., 2006; Second International Symposium on Unsaturated Soils, Weimar, Germany, 2007; Third Asian Conference on Unsaturated Soils, Nanjing, China, 2007), studies on 'estimation techniques' have become one of the most common research topics, as reported by Fredlund and Houston (2009).

Soil water characteristic curve (SWCC) can be used as a tool in the estimation techniques to determine different unsaturated soil property functions (shear strength, permeability, volume change, etc.). SWCC relates the amount of water in a soil as a function of matric suction (ψ). The amount of water in soil is represented in terms of gravimetric water content, volumetric water content, degree of saturation, normalized water content and dimensionless water content. SWCC can provide the matric suction corresponding to the amount of water within the soil. An entire soil water characteristic curve (SWCC) can be divided into three distinct zones—residual zone, transition zone and boundary effect zone—as shown in Figure 2.17 (Fredlund and Houston, 2009). The residual value (unsaturated state) and the air entry value (nearly saturated state) subdivide the SWCC and the transition zone is defined between them. During drying and wetting SWCCs give hysteresis, as shown in Figure 2.18. Pham (2001) and Pham et al. (2002, 2003) suggested the approximate lateral shifts between the curves (as given in Table 2.2), if measured data showing the actual shift is not available.
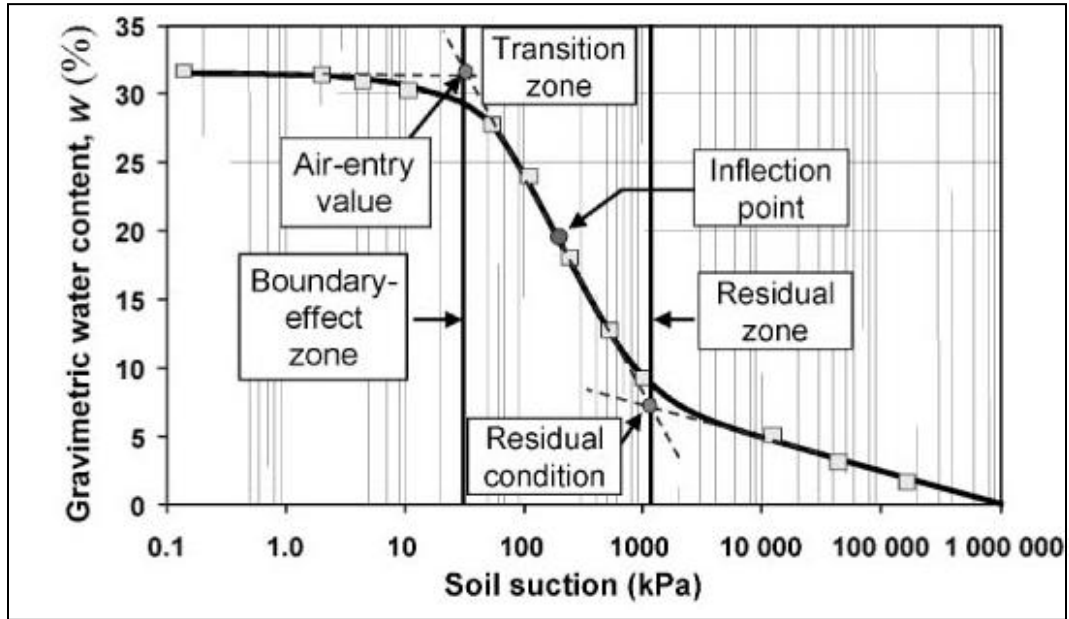
Figure 2.17: Typical soil water characteristic curve (Fredlund and Houston, 2009)
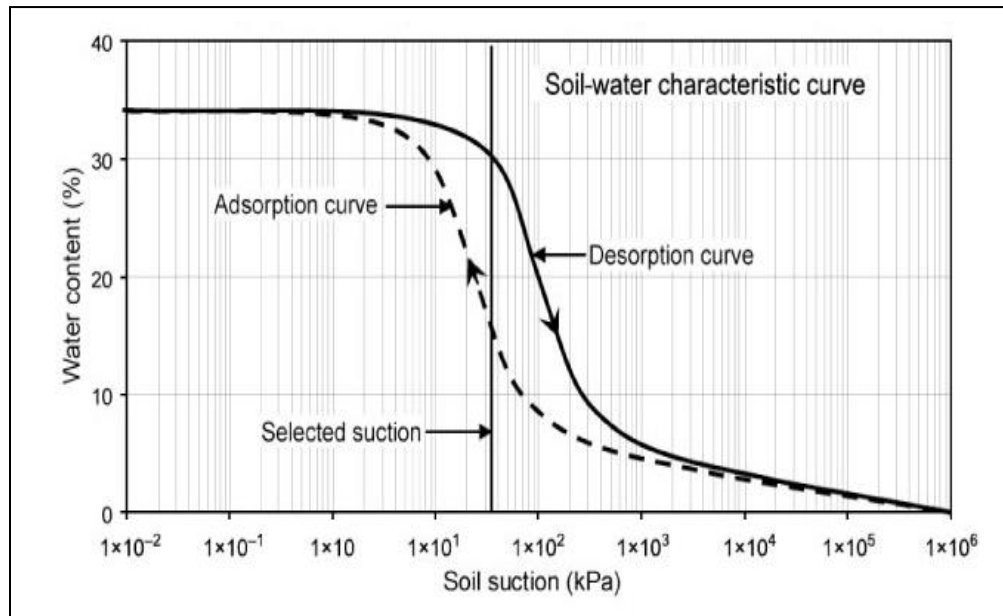
Figure 2.18: Hysteresis between drying (desorption) and wetting (adsorption) SWCC (Fredlund and Houston, 2009)

Table 2.2: Suggested shifts of the inflection point between the drying and the wetting curves for various soils (Pham, 2001)

Soil type	Range of typical shifts (% of a log cycle)	Average shift (% of a log cycle)
Sand	15-35	25
silt and loam	35-60	50
Clay	--	Up to 100
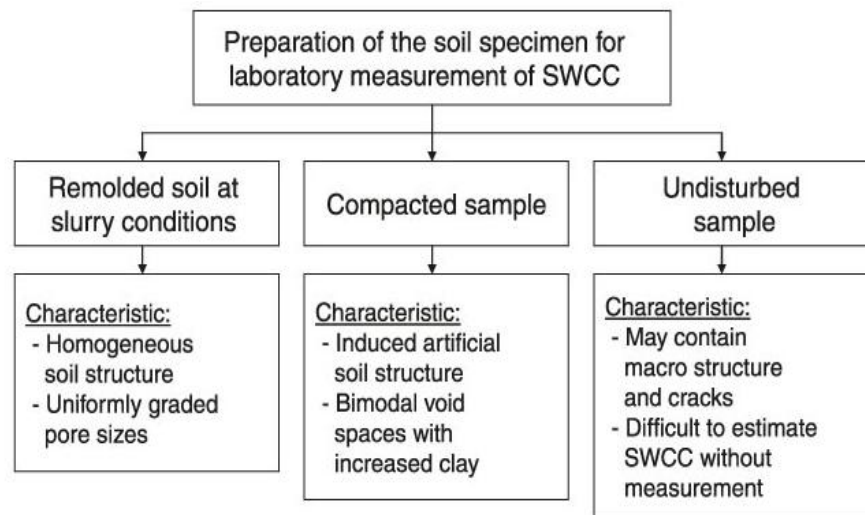
Figure 2.19: Effect of initial conditions of the soil specimens on the SWCC (Fredlund and Houston, 2009)

SWCC (drying curve) is estimated following one of the three ways: (i) database mining of previous test results, (ii) computations based on the grain size distribution curve, and (iii) 'correlation' of soil parameters (Fredlund and Houstan, 2009). Several researchers (Fredlund, 2006; Scheinost et al., 1997; Tyler and Wheatcraft, 1989; Vereecken et al., 1989; Rawls and Brakensiek, 1985; Arya and Paris, 1981) proposed the estimation of SWCC based on the grain size distribution curve, referred to as pedo-transfer functions (PTF). In the preliminary design stage, SWCC estimated from the grain size distribution curves is extremely useful and has been receiving rapidly increasing acceptance. Such estimation provides reasonable SWCC for sand and silt (or loam) soils. Soil Vision version 2.0 provides SWCC based on estimation techniques. Fredlund (1999)

technique performed better than other PTF for predicting SWCC, according to statistical evidences.

Laboratory determination of SWCC is recommended mainly for the final design of engineering projects involving unsaturated soils. If the results from the numerical simulations are sensitive to the input of unsaturated soil property functions, SWCC may need to be measured in the laboratory even at the 'preliminary design' stage. Besides, determination of the complete SWCC in the laboratory is time consuming and expensive. Therefore, a curve-fitting equation to best fit few data points along the SWCC is used to generate the entire SWCC from a few measured data points in the laboratory. In the literature, several empirical equations (Pereira and Fredlund, 2000; Feng and Fredlund, 1999; Fredlund and Xing, 1994; Mckee and Bumb, 1987; Mckee and Bumb, 1984; Tani, 1982; van Genuchten, 1980; Brutsaert, 1967; Brooks and Corey, 1964; Gardner, 1958) are available to best fit laboratory water content versus soil suction.
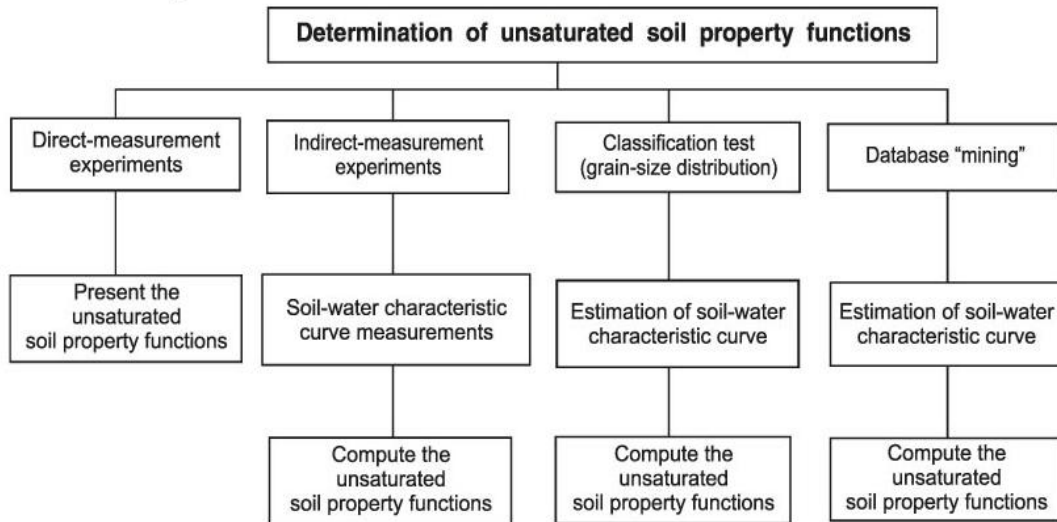
Figure 2.20: Different approaches in Determining Unsaturated Soil Property Functions (Fredlund and Houston, 2009)

Figure 2.20 presents different approaches in Determining Unsaturated Soil Property Functions.

SWCC can be determined from direct measurements using the pressure-plate type apparatuses. Research on modifying apparatus (e.g., advanced direct shear apparatus) to determine SWCC are also in progress (Hormdee et al., 2005). Initial conditions (i.e.,

initial density and amount of disturbance) of soil specimens have influences on the air entry value and the rate of desaturation measured in the laboratory, as shown in Figure 2.19. For soils with high clay content, sample disturbances are of great concern. Several unsaturated soil property functions, such as void ratio function, hydraulic conductivity function, water storage function, shear strength function and thermal conductivity function, are available in the literature for various types of unsaturated soil behavior; including soil collapse, steady state seepage, transient seepage, heave, slope stability, lateral earth pressure and steady state thermal analyses. It is important to note that void ratio (at constant vertical pressure), hydraulic conductivity, shear strength, etc. are constant parameters for saturated soil, while these are defined by the unsaturated soil property functions for unsaturated soils.

Some other researchers (Zapata et al., 2000; Kenneth et al., 1993) provide SWCC correlated to percent fines, plasticity index, etc. Figure 2.21 presents the effect of percent fines on SWCC. The accuracy of estimating unsaturated soil property function depends on the choice of the SWCC estimation techniques.
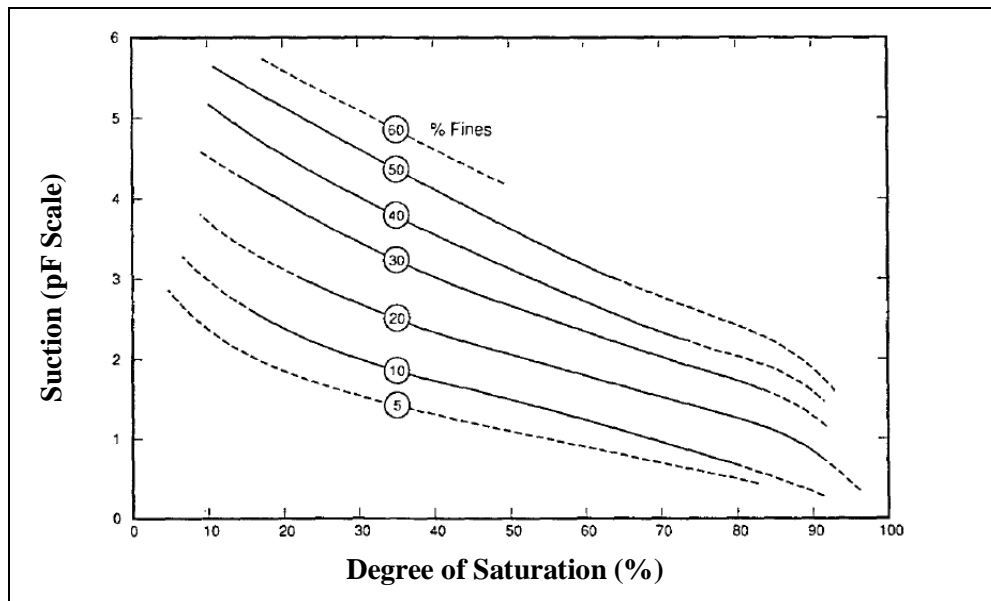
Figure 2.21: Soil Water Characteristic Curve for soils having different percent fines (Kenneth et al., 1993)

Like all unsaturated soils, collapsible soil exhibits significantly higher shear strength at initial natural state (of high matric suction) than its saturated state (i.e of zero matric suction). Shear strength of collapsible soil at partially saturated state is explained by an extended Mohr-Coulomb failure envelope, as shown in Figure 2.22. Extended Mohr-Coulomb failure criteria are formulated as follows (Fredlund and Rahardjo, 1993):

$$\tau = c' + (u_a - u_w)_f * \tan\varphi^b + (\sigma_f - u_a) * \tan\varphi'; \dots\dots\dots\dots\dots\dots\dots(2.1)$$
$$= c' + c'' + (\sigma_f - u_a) * \tan\varphi'; \quad c'' = 0 \text{ at fully saturated condition}$$

Apparent cohesion, $c = c' + (u_a - u_w) * \tan\varphi^b$;

c' = cohesion at saturated condition;

$\tan\varphi^b$ = slope of the shear strength vs. matric suction relation;

c = intercept of the extended Mohr-Coulomb failure envelope at a specific matric suction and zero net normal stress.

Shear strength is constituted as a combined contribution of apparent cohesion and frictional shearing resistance (i.e. developed by the effective normal force at the grain contacts). In Figure 2.22, the significant contribution of suction into the apparent cohesion component is explicit. The apparent cohesion includes the classical cohesion, c' (i.e. shearing resistance arising from inter-particle physicochemical forces, such as Van der Waals attraction) and suction induced cohesion, c'' (i.e. the shearing resistance arising from capillary effects). Figure 2.22 and Figure 2.23 give an explanation behind the spontaneous decrease in shear strength of collapsible soil during progressive saturation, because of corresponding suction reductions. Figure 2.23 shows a two dimensional projection of failure envelopes at various matric suctions.
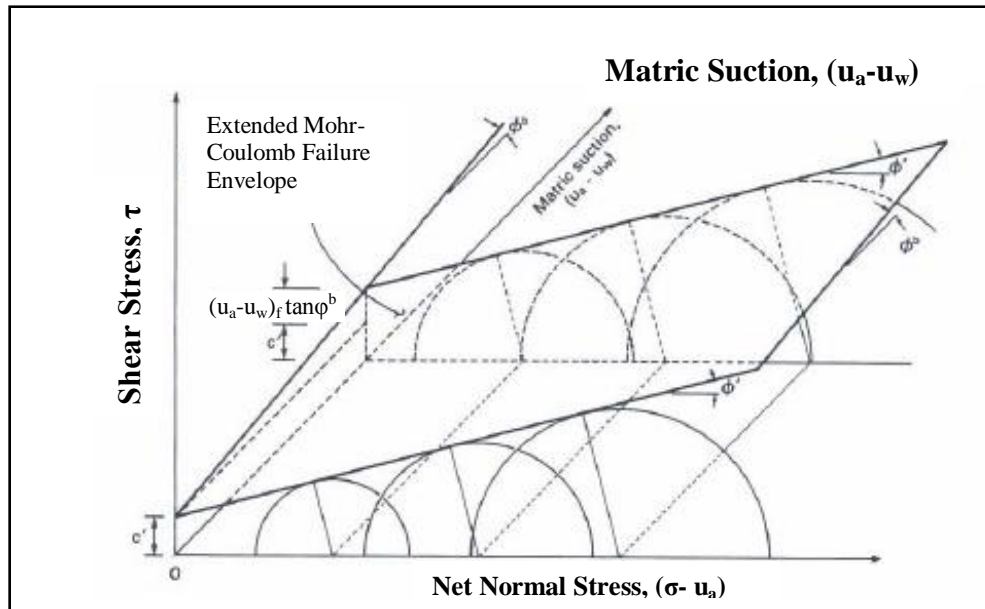
**Figure 2.22: Extended Mohr-Coulomb failure envelopes
(Fredlund and Rahardjo, 1993)**
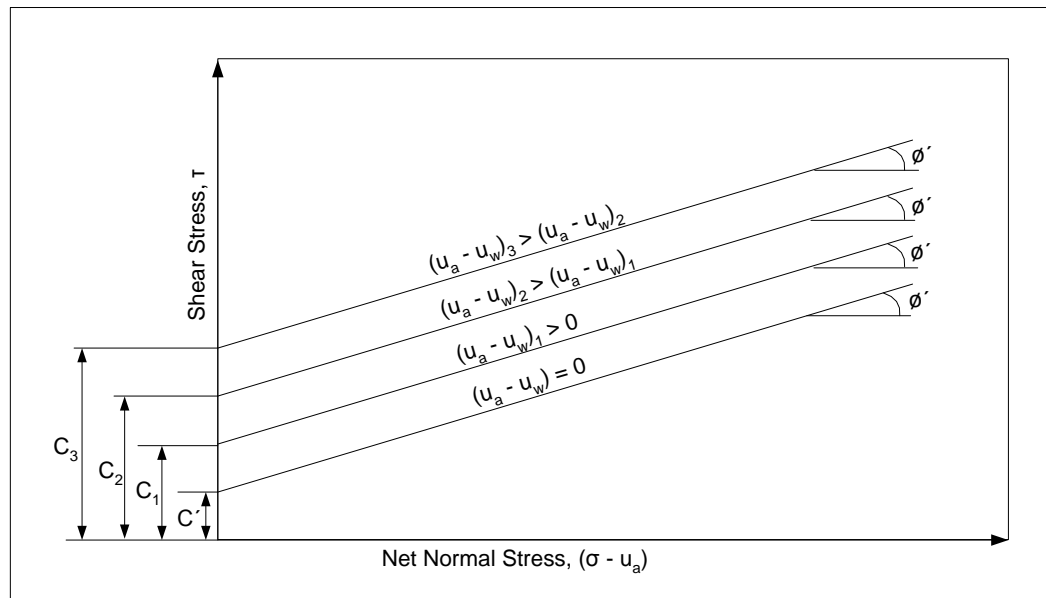
**Figure 2.23: Two dimensional projections of failure envelopes at various suctions
(Fredlund and Rahardjo, 1993)**

Several empirical shear strength functions were established in previous studies, based on the SWCC and the saturated shear strength parameters.

According to Oberg and Sallfors (1997),

$$\tau = [c' + (\sigma_n - u_a) \tan\varphi'] + S_w * (u_a - u_w) * \tan\varphi \ldots\ldots\ldots\ldots\ldots\ldots\ldots(2.2)$$

Where, S_w = water degree of saturation.

According to Vanapalli et al. (1996),

$$\tau = [c' + (\sigma_n - u_a) \tan\varphi'] + \theta_n . (u_a - u_w) \tan\varphi \ldots\ldots\ldots\ldots\ldots\ldots\ldots(2.3)$$

where, θ_n = normalized volumetric water content = $\dfrac{\theta - \theta_r}{\theta_s - \theta_r}$

θ = Volumetric water content

θ_s = Saturated volumetric water content

θ_r = Residual volumetric water content

According to Fredlund et al. (1996) and Vanapalli et al. (1996),

$$\tau = [c' + (\sigma_n - u_a) \tan\varphi'] + \Theta^\kappa (u_a - u_w) \tan\varphi' \ldots\ldots\ldots\ldots\ldots\ldots(2.4)$$

where,

τ = shear strength of unsaturated soil,

c' = effective cohesion,

φ' = angle of frictional resistance,

$(\sigma_n - u_a)$ = net normal stress,

$(u_a - u_w)$ = matric suction,

Θ = normalized volumetric water content, θ_w/θ_s,

κ = fitting parameter used for obtaining a best-fit between the measured and the predicted values

According to Khalili and Khabbaz (1998),

$$\tau = [c' + (\sigma_n - u_a) \tan\varphi'] + (u_a - u_w).((u_a - u_w)_f/(u_a - u_w)_b)^{-0.55}. \tan\varphi' \ldots\ldots(2.5)$$

where, $(u_a - u_w)_f$ = Matric Suction at failure

According to Futai et al. (2006), angle of internal friction,

$$\varphi\,(\psi) = \varphi\,' + (\varphi_{(ua\text{-}uw\,=\,\infty)} - \varphi\,')\,(1 - 10^{b(ua\text{-}uw)})\dots\dots\dots\dots\dots\dots\dots..(2.6)$$

where,

$\varphi\,(\psi)$ = variation of friction angle due to changes in matric suction;

$\varphi\,'$ = effective friction angle at saturated condition;

$\varphi_{(ua\text{-}uw\,=\,\infty)}$ = maximum friction angle;

b = friction angle adjustment factor.
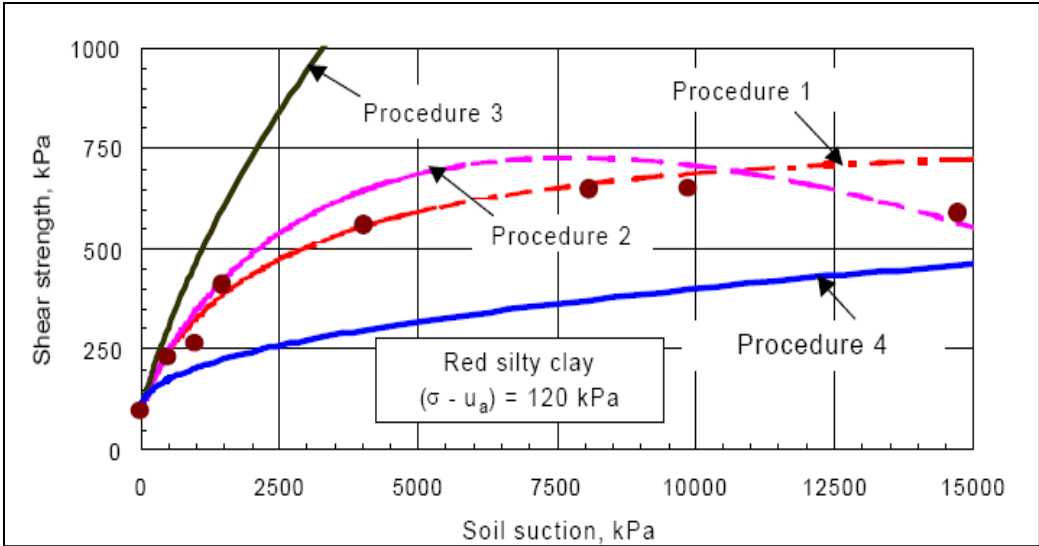
Figure 2.24: Comparison of the measured and the predicted shear strength values for red silty clay using four different procedures (Vanapalli and Fredlund 2000)

Vanapalli and Fredlund (2000) found the function of Eqn 2.3 that gives better results than other three procedures. Figure 2.24 and Figure 2.25 compare the performance of four different procedures for two different soils. In these figures, procedures are numbered 1 through 4: Fredlund et al. (1996) and Vanapalli et al. (1996) (Eqn 2.4), Vanapalli et al. (1996) (Eqn 2.3), Oberg and Sallfors (1997) (Eqn 2.2), and Khalili and Khabbaz (1998) (Eqn 2.5), respectively.
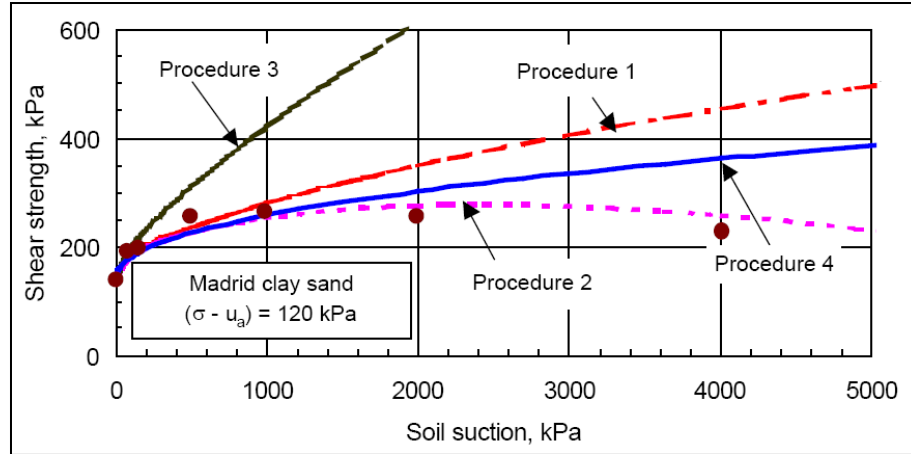
Figure 2.25: Comparison of the measured and the predicted shear strength values for Madrid clay sand using four different procedure (Vanapalli and Fredlund 2000)

In the literature, several hydraulic conductivity functions are available to establish the best fits data measured in the laboratory for unsaturated soils (Fredlund and Xing, 1994; Leong and Rahardjo, 1997). All the hydraulic conductivity functions have mathematical relationships with the hydraulic conductivity and the SWCC.

Pereira and Fredlund (2000) give Eqn 2.7 defining the void ratio function for collapsible soils in terms of any changes in matric suction (u_a-u_w),

$$e = e_u + \frac{e_f - e_u}{[1 + \left(\frac{(u_a - u_w)}{c}\right)^b]^a} \quad\text{...}(2.7)$$

i.e., e = e_u - (Δe)

where, e_u = initial void ratio of a soil specimen under a given net confining stress;

e_f = final void ratio of a soil specimen under a given net confining stress;

c = matric suction value at the inflection point (i.e., middle point of collapse phase);

b = slope parameter (i.e., slope of the collapse phase);

a = symmetry parameter that makes the logistic function asymmetric.

2.4 Performance of Pile Foundation in Collapsible Soil

In regions with collapsible soils, pile foundations are widely used to support the structures of single to 12 storied or even more (Grigoryan, 1997). Reduction in pile capacity in saturated collapsible soil, as compared to that in natural moisture, was

37

previously recognized the cause of such pile failures. Therefore, numerous static pile load tests were carried out to establish the range of reduction in the pile capacity resulting from saturation of collapsible soil (Grigoryan, 1997). It is found that pile settlement at P_{wetted} is always higher than the pile settlement in natural soil condition even under the same load. Table 2.3presents ultimate capacity of single pile in collapsible soil at natural moisture and saturated condition. All piles rest on collapsible soil bed. The data in Table 2.3 describes that pile capacity (P_{wetted}) in wetted collapsible soil is found significantly less than pile capacity ($P_{natural\ m/c}$) in the same soil at natural moisture content. The reduction in capacity is calculated as the difference in both pile capacities, as a percentage of $P_{natural\ m/c}$. In addition to that, the slopes of pile load-settlement curves are compared in two conditions. It is found that pile settlement at P_{wetted} is always higher than the pile settlement in natural soil condition even under the same load.

Table 2.3: Ultimate pile capacity in soil at natural moisture and at wetted condition (Grigoryan, 1997)

Pile Length, L (m)	Ultimate Capacity, Q_u (kN)		Settlement at Ultimate Capacity, S(ult) (mm)		S (ult at nat. m/c)*P (sat.)/P(nat. m/c)	Reduction of Ultimate Capacity, (%)
	Soil at Natural m/c	Wetted Soil	Soil at Natural m/c	Wetted Soil		
5.9	550	190	5.8	2.2	1.9	65.4
5.6	350	150	6	3	2.5	57.1
4.7	290	130	4.8	2.6	2.08	53
6.8	630	190	7	2.3	2.1	69.8
5.8	250	150	2.5	4.1	1.5	40
5.9	240	150	2.9	5.9	1.8	37.5

Since all the mitigation measures (such as control of wetting, soil improvement, pre-wetting, etc.) were found insufficient, the main concept of using pile foundation is to avoiding the collapsible soil by cutting its full depth to transfer the load into a deep non collapsible soil bed. However, pile in collapsible soil is designed according to the

conventional pile design theory and pile load test results. Though pile load tests are carried out under unsaturated (natural) soil condition and after saturation, many structures on pile foundations experienced foundation problems due to accidental wetting (Grigoryan, 1997; Evstaatiev, 1995). Therefore, several attempts of soil improvement (e.g., chemical stabilization) are found in the literature to be applied before pile construction (Isaev et al., 1989; Kalashnikova 1976). Mat'tsev et al. (1980) suggested pile construction on a compacted core in collapsible soil as they found pile in compacted core performed better than that in untreated collapsible soil during inundation. Grigoryan and Chinenkov (1990) examined the performance of long under-reamed pile in collapsible soil and found that it cannot provide additional tip resistance to total pile capacity to resist pile settlement during inundation, based on a field scale study. Similar efforts are also found in the literature investigating the pile capacity and settlement in unsaturated and saturated collapsible soil conditions (Gao et al., 2007). However, all of these investigations failed to study the effect of inundation on pile performance in collapsible soil. Later, negative skin friction, developed during collapse of soil, had been recognized.

Negative skin friction develops on pile-soil interface, where soil (around the pile) settles faster than the pile. Therefore, negative skin friction imposes additional (indirect) load, known as "negative skin friction force" or "drag load". It can cause serious damages to the structures (e.g., differential settlement, tilting, etc.). The development of negative skin friction is common in the case of a pile in soft soil, which settles due to consolidation over a period of time. Therefore, it increases incrementally, as consolidation (i.e., a time dependent phenomena) may occur in several years (as shown in Figure 2.26). Hanna and Sherif (2006) developed numerical model to investigate negative skin friction on a single pile in clay subjected to surcharge loading.

On the other hand, negative skin friction resulting from soil collapse during inundation develops fast, as collapsible soil experiences significant collapse suddenly. Note that soil settlement due to consolidation is much less than collapse settlement. Therefore, negative skin friction due to soil collapse is more critical than negative skin friction due to consolidation. The higher the soil settlement is, the greater the negative skin friction force is (Poulos 1997; Lee et al., 2001). Moreover, as the causes of both

types of negative skin frictions are quite different, the methods of numerical modeling must be different. Also empirical and analytical methods, to predict negative skin friction due to consolidation of cohesive or soft soils, are neither applicable nor reliable to predict negative skin friction due to soil collapse. Negative skin friction due to soil collapse exists for few hours and disappears after pile settlement. Therefore, many case studies reported only the settlement, as the moment of negative skin friction development could not be realized till the structure showed damage signs. In many cases, inundation is caused by underground problems (i.e., broken pipes, leakage of underground reservoir, etc).
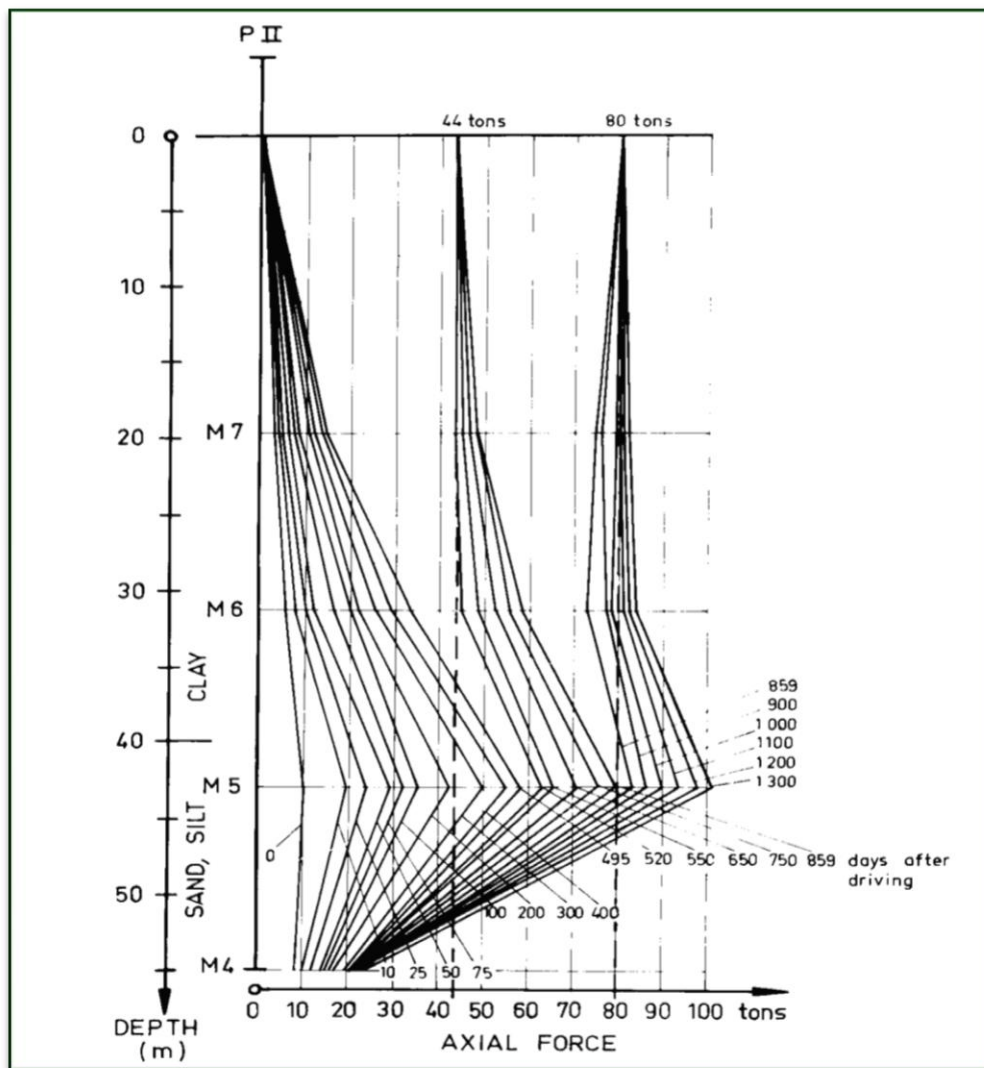
Figure 2.26 Vertical load distribution in piles PI at various times after the driving (Fellenius 1972)

Grigoryan and Grigoryan (1975) (i.e., also reported in Grigoryan, 1997) carried out for a full scale pile test to investigate negative skin friction forces on a floating and an end bearing piles in collapsible soils subjected to inundation from top.
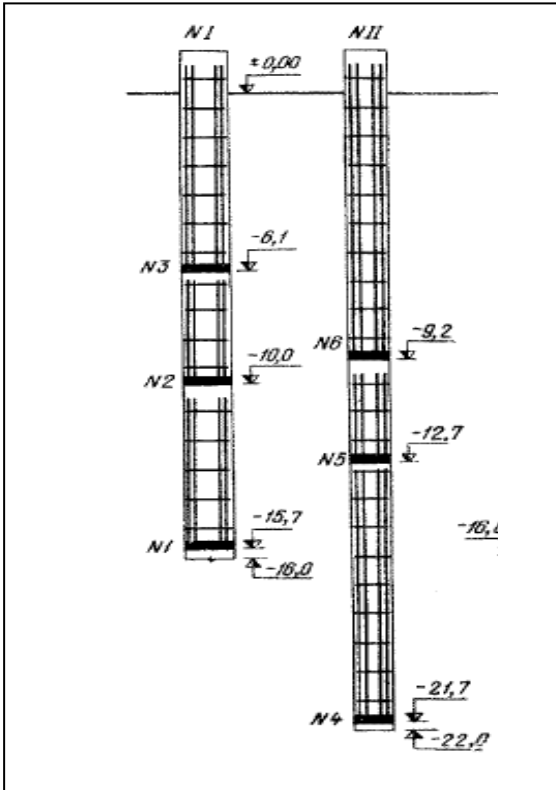
Figure 2.27: Test piles: NI and NII (Grigoryan and Grigoryan, 1975)

Two bored cast-in-situ testing piles, NI and NII (as shown in Figure 2.27) were equipped with strain gauges to measure the pile movement in the vertical direction. Dynamometers (N1 through N6) were installed at different depths to measure the forces along the pile shafts. NI and NII test piles were 16 m and 22 m in lengths, and 600 mm and 500 mm in diameter, respectively. The test pile NI did not cut the full depth of collapsible soil, while the test pile NII rested on non-collapsible soil. Collapsible soil exists up to 18 m from the ground. Depth markers (D1 through D6) were installed to monitor soil settlement.

Figure 2.28 shows the plan for the piles and depth markers. The depth markers were located at the depth of 6.2 m (D1), 9.1 m (D2), 11.3 m (D4), 15.5 m (D5) and 17.3 m (D6). Piles were loaded with a constant, static load all over the test in order to

introduce water and soak the soil; trenches have been constructed to be filled with water during the test. Figure 2.29 shows the records of the axial forces (i.e., T in kN) at a given pile section, the amount of water discharge (i.e., Q in thousand m^3) and the settlements (i.e., S in mm) of piles (NI and NII) and depth markers (D1 through D6).
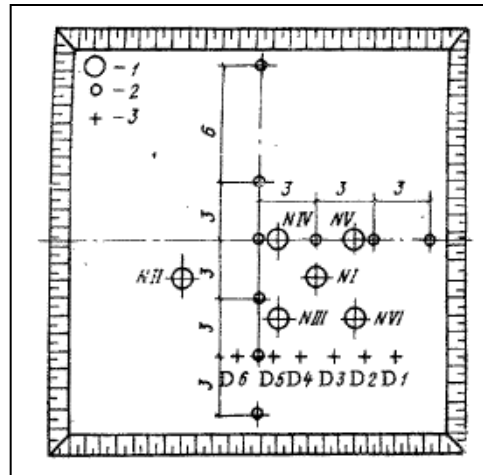
Figure 2.28: Plan of the test pit (Grigoryan and Grigoryan,1975)

The external loads on the test piles, NI and NII were 550 kN and 600 kN respectively. Axial loads were measured at four different levels (i.e., numbered as 1, 4, 5 and 6 in Figure 2.27) for more than a month, while settlements were recorded for 70 days after inundation commenced. The pile axial force at 9.2 m (marked 6 in T vs. Time plot in Figure 2.29) was low (about 40 kPa) before inundation, while no axial force was measured at other levels (lower than 9.2 m) of the test pile NII. This is because the external load (600 kN) was resisted by the positive skin friction developed on the pile interface from pile head to 9.2 m. When inundation (from top) begins, the upper layers were first subjected to inundation and experienced collapse. Then, the pile axial load at 9.2 m increased incrementally with time due two reasons: development of negative skin friction and diminishing positive skin friction on some parts between pile head and the pile section at 9.2 m. Until the depth marker (D1 at 6.2) showed settlement, which was just due to the soil collapse below 6.2 m, all the changes in the pile axial load at 9.2 m must be due to the collapse of the upper layer up to 6.2 m from the pile head. The depth marker D1 did not show any settlement during 25 days since inundation begun.
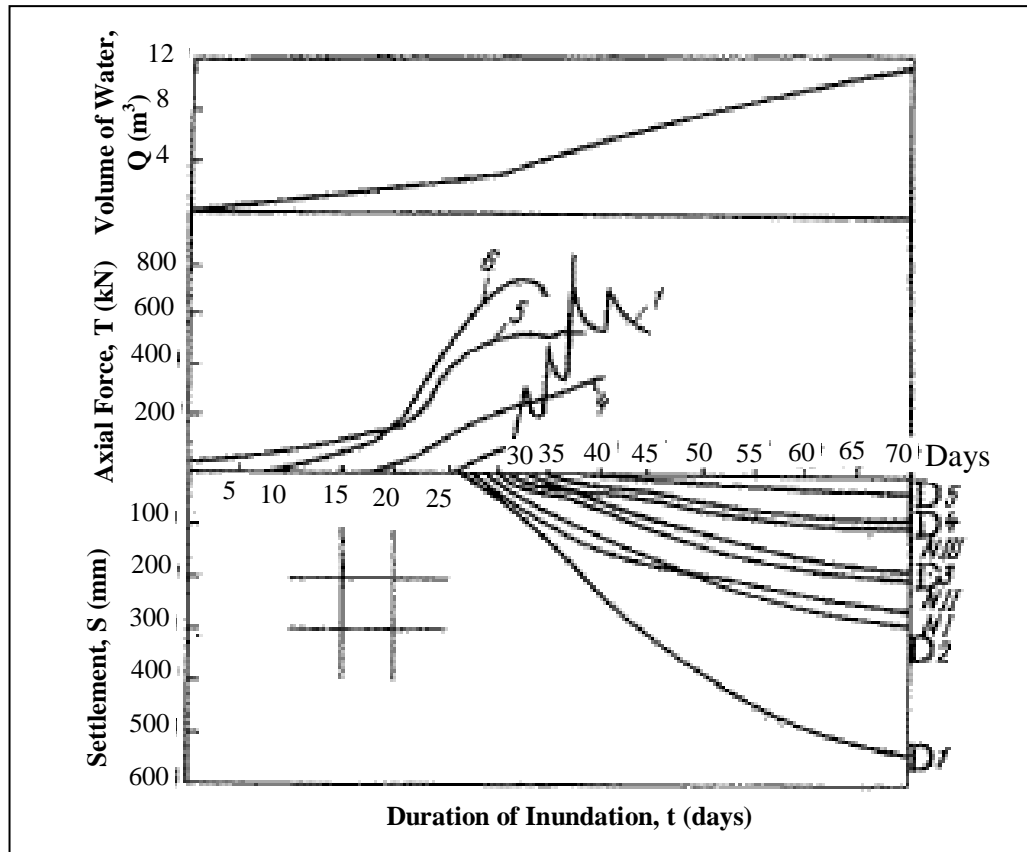
Figure 2.29: Experimental results: the amount of water discharge (Q), the axial forces (T) at different pile sections (1, 4, 5 & 6), and the settlements (S) of piles (NI and NII) & depth markers (D1 through D6) with time (Grigoryan and Grigoryan 1975)

By this time, axial load at 9.2 m increased up to 780 kN, a sum of external load (600 kN), pile weight (from pile head to 9.2 m) and additional indirect load (negative skin frictional force, about 280 kN). Axial loads at other level also increased with time consequently. As collapse due to collapsible soils between 6.2—18 m begun between 25—28th day, axial loads at the lower levels (at 12.7 m and 21.7 m) increased significantly due to the development of negative skin friction. At the pile tip (marked as 4 in T vs. Time in Figure 2.29), the axial load reached about 400 kN that was high but left to be supported by the end resistance of the pile NII. As a result, the pile settlements were observed. In case of the test pile NI, only the dynamometer (marked as 1 in Figure 2.27) installed near the pile tip indicated the change in the axial load at the pile tip. As the test pile NI was not supported at non collapsible soil, the test pile NI experienced settlement when axial load

43

at the pile tip increased significantly (like the test pile NII). Reduction in the axial load (at the pile tip) was observed since the pile settled and further increased axial load was due to progressive collapse. For this reason, oscillations are noted in T vs. time for NI pile.

Grigoryan (1997) also reported a full scale pile test in collapsible soil subjected to local wetting. In this region, the collapsible soil existed up to 15 m. The pile was 18 m long and 1 m in diameter. It was noted that negative skin friction developed up to 15 m (from the pile head) and only the last 3 m pile could mobilize positive skin frictional resistance. The pile was not subjected to any external load during inundation. When measurements indicated the development of negative skin friction, the external loading on pile began. Then pile settled faster than the soil, and the negative skin friction disappeared.

Chen et al. (2008) presented the pile load test (in collapsible soil subjected to inundation) results, as carried out in China. The test conditions and the experimental results of negative skin friction on pile in collapsible soil are given in Table 2.4 and Table 2.5 respectively. In China, the recommended value of negative skin friction is 10 kPa and 15 kPa for collapse settlement of 70─200 mm and over 200 mm, respectively. It can be noted that all the experimental data exceed this value, as given in Table 2.5.

Table 2.4: Test conditions of cast-in-situ piles in collapsible soil (Chen et al., 2008)

Location	Original Depth of Collapsible Soil (m)	Pit Dimension (m)	Pile Diameter (m)	Pile length (m)	Soil Settlement in Test Pit (cm)
Gansu Dongguang	12	12 (dia)	0.8	10	40
Gansu Hekou	15	15 (dia)	1	15	55
Puchen Power Plant	35	40 (dia)	1	40	6.3
Baoji 2nd Power Plant	20	50 x 30	0.8	22.85	8.5
Ningxia Yanghuang (ZH4)	35	30 (dia)	0.8	40	48.5

Table 2.5: Negative skin friction on pile in collapsible soil (Chen et al., 2008)

Index	Location	Negative Skin Friction (kPa)	
		Maximum	Average
1	**Gansu Dongguang**	-	18
2	**Gansu Hekou**	28	20
3	**Puchen Power Plant**	-	27, 44
4	**Baoji 2nd Power Plant**	52.3 & 57.6	35.7, 30.4
5	**Ningxia Yanghuang(ZH4)**	-	33.1
6	**Ningxia Yanghuang(ZH5)**	-	22

Mashhour (2009) conducted five small scale tests to investigate the development of negative skin friction during inundation of collapsible soil from bottom. The pile was of end bearing type.
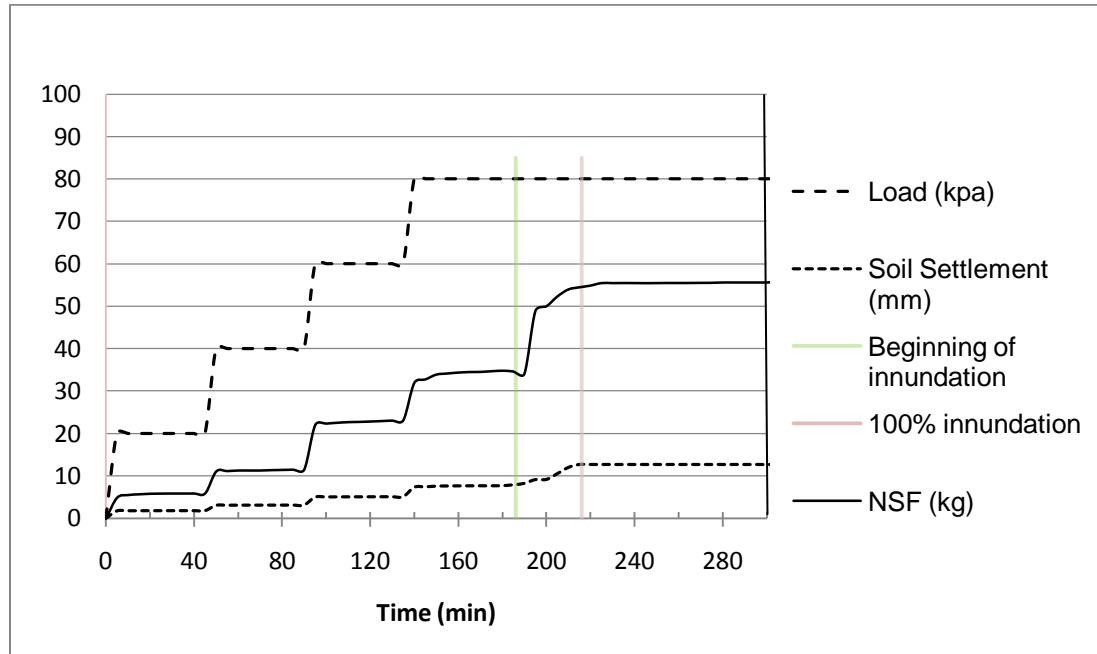
Figure 2.30: Surcharge, soil settlement and negative skin friction with time for C_p = 4.2% (Mashhour, 2009)

Figure 2.30 and Figure 2.31 show results of two experiments using two different collapsible soils. It appeared that negative skin friction developed during the periods

45

when collapse settlements took place. It can also be noted that the greater the collapse potential was, the higher the negative skin friction developed. The collapsible soil layer was about 50 cm thick and it took about 25 minutes to become fully saturated and accordingly collapsed.
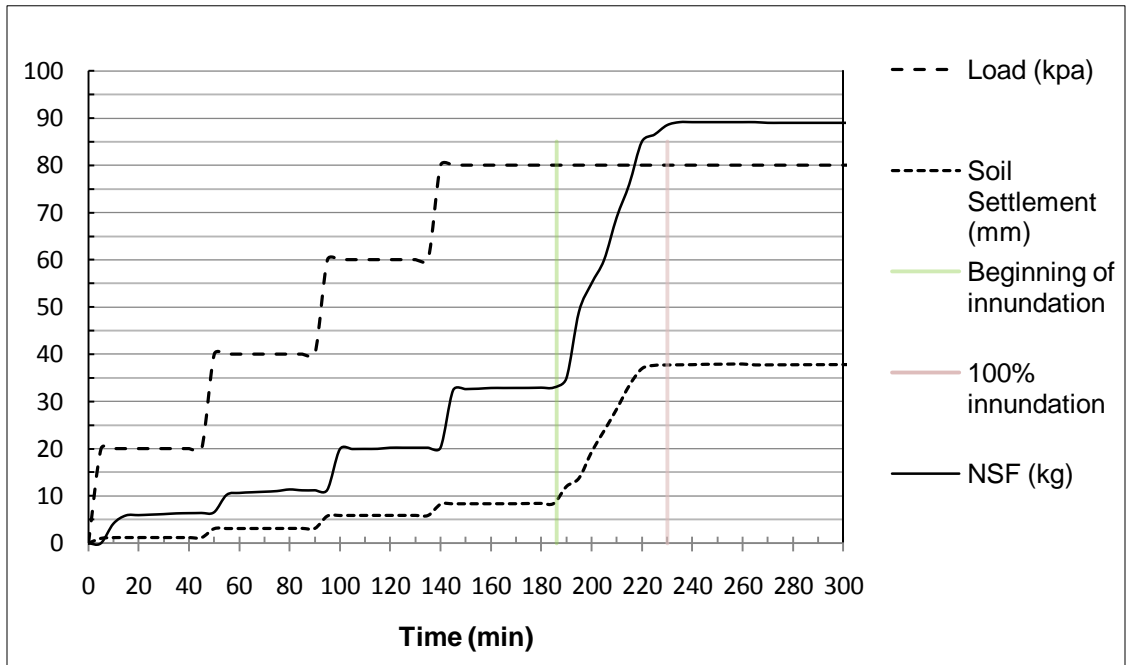
Figure 2.31: Surcharge, soil settlement and negative skin friction versus time for $C_P = 12.5\%$ (Mashhour, 2009)

2.5 Discussion

To date, a few investigations on negative skin friction (due to soil collapse) are carried out by testing full-scale pile in an immersion pit, as such tests (i.e., to measure negative skin friction and bearing capacity) are difficult, expensive and time consuming (Chen et al., 2008). To the best of our knowledge, no successful attempt of numerical modeling is found to investigate pile in collapsible soil during inundation. As collapsible soil undergoes radical rearrangements of particles during inundation while negative skin friction develops, the analytical modeling using the theory of mechanics has not been progressed. Only the few experimental results, of Grigoryan (1997) and Chen et al. (2008), provide some reference values for design of piles, having the same dimensions as the test pile, in the regions where the tests were carried out. No theory is developed to

predict negative skin friction due to soil collapse, because only one pile test is carried out in each location. Therefore, each set of test results gives the value of negative skin friction for a given pile geometry and for a given soil (i.e., profile and collapse potential) and inundation conditions.

The conventional method of estimating negative skin friction resulting from consolidation of soft soil is not applicable to calculate the value of negative skin friction due to soil collapse. Based on the literature review, it can be stated that there is a lack in experience to establish a theory and adequate limits of negative skin friction to guide the practitioners in designing pile in collapsible soil, because several factors (related to collapsible soil properties and pile geometry and its property) are involved in the development of such negative friction. In addition to negative skin friction estimation, the minimum depth of embedment in the non-collapsible soil (by the lower part of a pile) needs to be determined in designing a pile, because inadequate embedment causes sharp increase in the pile settlement during inundation of collapsible soil.

While numerical modeling may sound appealing to researchers, developing numerical models to simulate the case of unsaturated soil, especially during inundation is difficult, as it requires implementation of unsaturated soil property functions and it should model pile soil interface behavior as well. Currently, no such commercial Geotechnical software can handle such problem, as matric suction (the governing state variable) and its effects on soil parameters and soil volume during inundation are not included in the calculation. To date, a few numerical studies involving the development of computer programs for coupling stress equilibrium and water flow for unsaturated soil can be found in the literature (Miranda 1988; Pereira 1996). This is due to the difficulties associated in describing the behavior of collapsible soil. Furthermore, most of the available computer programs for saturated soil do not take into account the consequences of the transient unsaturated-saturated water flow. The present situation demands the use of numerical modeling to conduct an in depth study regarding negative skin friction due to soil collapse.

47

CHAPTER 3

NUMERICAL MODELING AND VALIDATION

3.1 General

Numerical models of foundations in regular soils (i.e., insensitive to moisture change, to cyclic loading, etc.) are available in the literature. On the other hand, limited numerical studies on foundations in problematic soils, such as collapsible and expansive soils (moisture sensitive) and sensitive clay (sensitive to remoulding/cyclic loading), have been carried out to date. The field of numerical investigation concerning foundation performance in such soils is lagging due to the complexities in describing the problematic behavior of such soils numerically. Numerical modeling of collapsible soil can be accomplished easily, if soil moisture remains unchanged. This model is inapplicable in examining the performance of foundations in collapsible soil during inundation, however. During inundation, collapsible soil affects the performance of pile (e.g., due to the development of negative skin friction and the separation of the pile from the pile cap) significantly due to its radical volume change behavior. Present study, to the best of our knowledge, is the first attempt in developing numerical model to incorporate the effect of inundation of collapsible soil in order to study the performance of an axially loaded vertical pile. The proposed numerical model is used to predict negative skin friction exerted on the pile during inundation of collapsible soil surrounding the pile. The numerical model is validated by comparing the numerical results and the experimental data from the literature. Moreover, another numerical modeling procedure is also proposed to design the pile (i.e., length and diameter) in collapsible soil, provided that the indirect load due to negative skin friction is known.

3.2 Development of Finite Element Model

The finite element model (i.e., a mathematical representation) of an embedded pile is developed using a Geotechnical software, PLAXIS. In choosing type (2 or 3 dimensional), order and number of the elements, size of the geometry model and pattern

of the mesh, computational time of the finite element analysis (FEA) is considered the most important deciding factor among other modeling-related issues, in order to attain the degree of accuracy desired without employing excessive number of degrees of freedoms (DOF).

In this study, an axisymmetric type of finite element model is developed to simulate a single-axially loaded-vertical pile. Development of two-dimensional (2D) finite element model becomes possible by taking the advantage of symmetry. In all the cases to be studied, the position of the pile and the direction of the external load (applied on the pile head) are vertical, while the soil layers and the groundwater table are horizontal. Otherwise, the number of elements would be very high using solid element (in three-dimensional analysis). The centerline of the axisymmetric geometry model coincides with the axis of the vertical pile. The outer vertical boundary is placed at 50 times the pile diameter (Hanna and Sharif, 2006). The horizontal boundary is placed at least at 0.7 L below the pile tip. The geometry model consists of soil and pile clusters.

Boundary condition of the geometry model is defined according to the rules of Standard fixities (PLAXIS BV). Figure 3.1 presents the applied boundary condition of the axisymmetric model of a pile embedded in a deep soil bed. Fixities are applied to geometry lines by defining their prescribed displacements equal zero.
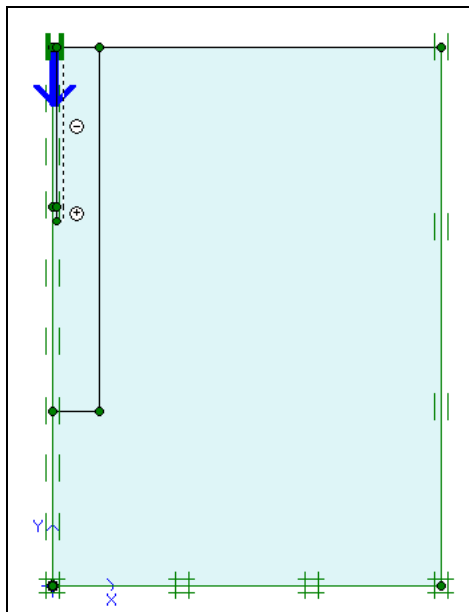
Figure 3.1: Boundary condition in an axisymmetric model

Horizontal fixity ($u_x = 0$) is imposed to the vertical geometry lines for which the x-coordinate equals the lowest or the highest x-coordinate in the geometry model. Therefore, the vertical boundaries are restrained in the horizontal direction, but free to move in the vertical direction. Total fixity ($u_x = u_y = 0$) is imposed to the horizontal geometry lines for which the y-coordinate equals the lowest y-coordinate in the model. It implies that the bottom of the geometry model is restrained in both the horizontal and the vertical directions. Therefore, the pile and the soil can show vertical settlements due to the application of external load and the inundation induced collapse.
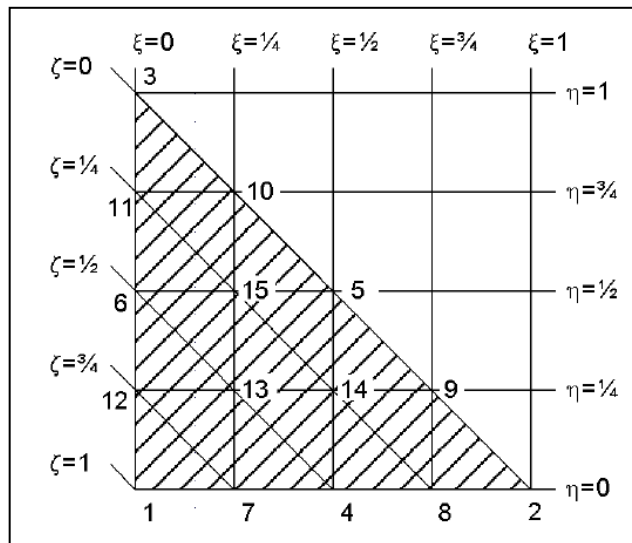
Figure 3.2: Numbering of nodes in a 15-node triangular element

Higher order triangular element, having 15 nodes (as shown in Figure 3.2), is chosen for both the soil and the pile clusters. 15-node triangular element performs better than quadrilateral (or rectangular) or any lower order triangular elements. In general, FEA is quick when model is meshed with triangular elements. This is because triangular elements involve less number of nodes (and DOFs accordingly) than quadrilateral element, if numerical models in both cases have the same number of elements and order of interpolation. Further, 15-node triangular element is chosen rather than any lower order (6- or 9-node) triangular element. Because of having more nodes (as compared to a lower order element), better accuracy is usually attained by using higher order element. The 15-node triangular element provides a fourth order interpolation for displacements.

Though a higher order element has more nodes than a lower order element, a mesh with higher order element has the total number of nodes less than that with lower order element. This is because more elements are required when meshed with lower order element than higher order element to reach a given accuracy in the results. Therefore, the choice of 15-node triangular element is found economical from the computational time requirement point of view. The numerical integration involves twelve stress points (Gauss Points).
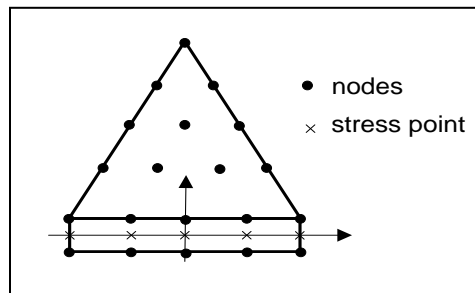
Figure 3.3: Connection between a 15 node triangular element and an interface element

Five-nodes line elements (termed as interface element in PLAXIS) are used along the pile-soil interface to capture a realistic interaction behavior between the pile surface and the soil during loading phase, to reduce the mesh dependency, and also to account for the relative pile-soil movement. Interface elements connect the elements of the soil clusters to those of the pile clusters. An interface element, compatible with 15-node triangular element, has five pairs of nodes. The coordinates of each node pair are identical in the finite element formulation. Each interface element is given an imaginary dimension (i.e., called 'virtual thickness'), which is necessary to define the material properties of the interface.

Some additional interface elements are provided extending the pile-soil interface for an additional length of 1 m below the pile tip. This provision of interface elements is to prevent non-physical stress oscillation and also to allow sufficient flexibility in the finite element mesh. Special attention is taken not to include any unrealistic weakness in the soil due to these elements by giving the full soil strength to these additional elements.

Figure 3.3 shows the connection between a 15-node triangular element and a compatible interface element, having five pairs of nodes.

Important mesh parameters, including size and types of elements and mesh coarseness, are provided to generate mesh automatically, skipping a laborious job of defining thousands of nodes and elements manually. Some important issues are given special attention in generating mesh. First of all, very coarse and very fine meshes are not created to avoid large errors in results and to reduce excessive computational time, respectively. Based on the experience, global fine mesh is considered inappropriate for the problem in hand, as it also involves excessive number of total DOFs. On the other hand, an acceptable mesh demands relatively large number of nodes in the vicinity of the pile's shaft, as deformations and stresses generally vary significantly around the pile and at the interface, respectively, as the objective of this modeling is to investigate shear stress distribution at the pile-soil interface. Mesh is considered acceptable, if it does not include any elongated element and aspect ratio ranges within the reasonable range. However, medium global coarseness applied allover cannot give the accuracy in results up to the mark. Therefore, considering the mesh dependency of the FEM results, mesh refinement technique is adopted in this study. A zone, 3 m horizontally from the pile axis and 1.5 L from the ground, is considered for this local mesh refinement. Secondly, any quick transition of element size (between the global elements and those in the refined mesh zone near the outer boundary of the refined mesh zone) is eliminated as the initial mesh is generated with medium global coarseness. Thirdly, the graphical display of the generated mesh is visually inspected for any possible errors, related to the shape of elements and the aspect ratio. If any element is distorted and/or elongated, the shape of the element is adjusted by refining adjacent geometry lines. Figure 3.4 shows the axi-symmetric model developed for a single pile in homogeneous soil. Finally, the 'Medium' global coarseness gives good results due to the advantage of using interface elements and mesh refinement, previously mentioned. As a result, FE computational time is reduced significantly. Mesh density is considered acceptable, if further mesh refinement does not give increased accuracy in computed results.

Pile is assumed to behave elastically. The pile cluster is modeled as non-porous material with linear-elastic (isotropic) constitutive relation, requiring only two input
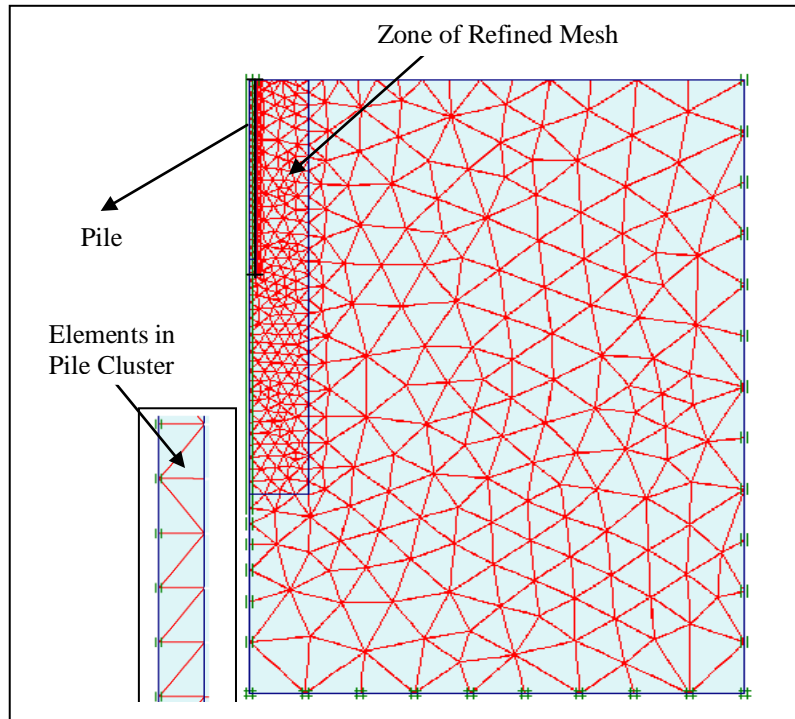
Figure 3.4: Generated Mesh in an axi-symmetric model

parameters: Young's modulus (E_p) and Poisson's ratio (υ_p). Pile is assumed to behave elastically. The pile cluster is modeled as non-porous material with linear-elastic (isotropic) constitutive relation, requiring only two input parameters: Young's modulus (E_p) and Poisson's ratio (υ_p).

Soil behavior is defined by Mohr-Coulomb (MC) constitutive law, which simulates the soil behavior based on soil parameters known in most of practical situations. The MC soil model operates with five material parameters; including angle of internal friction (φ), cohesion (c), angle of dilatancy (ψ), Young's modulus (E_p) and Poisson's ratio (υ_p). Any unsaturated soil clusters (of sandy or clayey type either), above the groundwater table are modeled as drained type of materials. On the other hand, saturated soil clusters are modeled as drained and undrained types of materials for sandy and clayey soils, respectively.

The behavior of the pile-soil interface is also defined by the Mohr-Coulomb (MC) Model. In this study, an additional material set with reduced strength parameters, is created to give input to the interface element properties. This approach was previously applied by Brore and Tol (2006) to include both the aspects of strength reduction and

dilatancy in interface modeling. The present study has found it more effective in achieving the full advantage of the pile-soil interface than using the strength reduction factor (R_{inter}) below 1, frequently used in the literature (Wehnert and Vermeer, 2004; and Dijkstra et al., 2006). In this study, the value of R_{inter} is kept equal to 1 for all material datasets: 'Soil', 'Pile' and 'Interface'. R_{inter} is to reduce the interface strength as compared to the surrounding soil. Elastic-plastic deformation analysis, termed 'Plastic' calculation, is performed according to small deformation theory, in simulating pile load test (static). Therefore, the stiffness matrix is based on the original undeformed geometry. As nodal displacements are caused due to the load, applied on the pile head (in case of the pile load test), this type of calculation is appropriate because of not being involved with the decay of excess pore pressures during the time period considered.

Each calculation is defined in separate phases of staged construction. Only one type of loading input can be activated in each calculation phase. In the Initial Phase, the initial soil effective stresses are automatically generated from the given general phreatic level and the input of coefficient of earth pressure at rest (K_0). The K_0-procedure is used to generate initial soil stresses. The initial horizontal effective stress ($\sigma'_{h, 0}$) and the initial vertical effective stress ($\sigma'_{v,0}$) are related by the coefficient of lateral earth pressure (K_0) as follows:

$$\sigma'_{h,0} = K_0 . \sigma'_{v,0}$$

In generating initial effective stresses, no external load or the weights of clusters of the pile and the interfaces are taken into account, and all clusters are given input the respective 'Soil' material sets.

The next phase (Phase I) is to install the bored pile by changing the material dataset, which had 'Soil' property (in Initial Phase), of the pile clusters with the 'Pile' property dataset. This simple procedure of bored pile installation is found useful in the literature (Wehnert and Vermeer, 2004). The unit weight of pile material is greater than that of the soil. Hence, the state of stress becomes slightly changed in this phase. According to Katzenbach et al. (1995), the change of the insitu stress state, next to the pile shaft, is only marginal due to the installation of a bored pile. At the end of calculation of this phase, displacements are reset to zero. The external load is simulated by both the approaches: 'prescribed displacements' and 'point load', applied at the pile

head. Both approaches give comparable numerical results. Prescribed displacements of 2, 4, 8, 16, 30, 70, 150 and 250 mm, are applied in consecutive phases from Phase 2 to Phase 9, respectively. In case of point load approach, a point load (per unit radian) is applied at the pile head in Phase II. The calculation phases, as defined above, can simulate pile load test in soil at constant moisture content. This model is further extended to incorporate the effect of inundation later on.

The finite element formulation in PLAXIS meets convergence requirements of finite element solution. The convergence requirements include compatibility and completeness of element formulation. In order to satisfy compatibility requirements, both inter-element and nodal (interconnection) compatibility are satisfied. Inter-element compatibility is met by choosing complete polynomial models, which are inherently continuous. Nodal compatibility at the interconnection is achieved by standard system assembly procedure. Displacement is compatible between adjacent elements only if there are no openings, overlap or discontinuities between elements. A completeness criterion is satisfied by including two terms for rigid body displacement and uniform strains in the displacement models. Therefore, shape functions for triangular and line elements are derived using polynomial displacement model. Both elements have the fourth order interpolation function (shape function). The polynomial terms for deriving the shape function of triangular element are the first 15 terms from Pascal triangle. The accuracy of the computed solutions is successfully checked by the mesh refinement. As a rule, the severity of violation of compatibility is less, if the mesh is refined.

Gaussian and Newton-cotes integrations are performed in PLAXIS for triangular and line elements, respectively. In case of 15-node triangular elements, 12 integration points are used. In Newton-Cotes integration, nodes are considered the integration points.

Different plots, including deformed mesh and contour plots of stresses, are used to interpret results produced by the post processing tool of PLAXIS. Plot of deformed mesh allows checking modeling errors, e.g. whether the displacement boundary conditions and external forces are properly applied. Contour plots of stresses allow checking the dimensions of the model, whether the size is adequate and the critical locations are not close to the boundary. Stresses are calculated at the integration point, and then are calculated using the shape function. Average nodal stress is calculated for each node

connecting two or more elements, because stress values at a node are different for different elements.

Shear stress distribution along the pile interface is obtained at the end of the finite element analysis. Figure 3.5 presents a typical shear stress distribution on pile interface. Using Trapezoidal Rule in EXCEL, the area of the shear stress distribution is determined. Therefore, the pile shaft resistance is calculated from this area times the pile perimeter (πD). The base resistance is obtained by subtracting the shaft resistance from the pile capacity. The pile capacity is known from the point of maximum curvature in the pile load displacement curve.
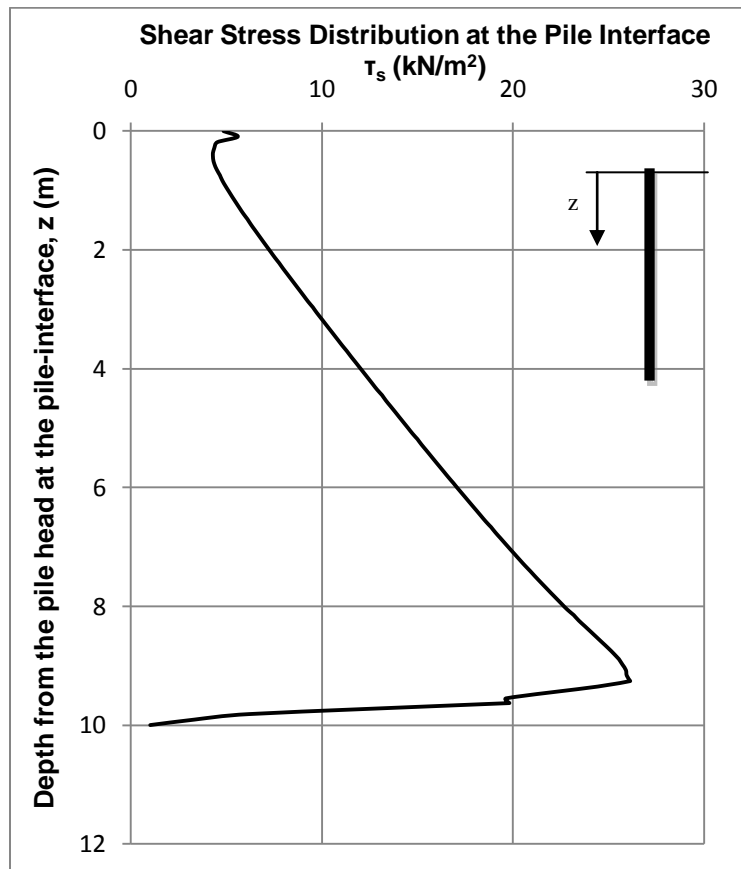
Figure 3.5: Present study - Typical shear stress distribution on pile-soil interface

3.3 Numerical Model Validation for Pile in Soil at Constant Moisture

The numerical model is validated for single pile in homogeneous and layered soils. All soils remain at constant moisture content, when the pile is subjected to external load. Table 3.1 presents the cases studied for the validation purposes.

Table 3.1: Cases to be studied

Case	Category	Soil Type	Soil Profile
1	Sand	Dense sand	Homogeneous
2		Medium Dense Sand	
3		Loose Sand	
4	Clay	Overconsolidated Clay	
5	Collapsible Soil	Silty Sand (unsaturated)	Layered
6		Silty Sand (Unsaturated)	
7		Silty Sand (Saturated)	

3.3.1 Validation of Numerical Model for Pile in Sandy Soils

The pile geometry, dimension and properties, of Cases 1─3, are given in Table 3.1. Table 3.2 presents the geometry, dimension and properties of piles. Properties of sandy soils, as given in Table 3.3, are used to model the homogeneous soil strata that exceed the depth of influence for the loaded pile under consideration. General phreatic line coincides the bottom of the geometry model. It implies that the groundwater table is located at the depth of 34 m from the ground level. Hence the pore water pressure remains zero for the full depth of the homogeneous strata. Homogeneous sand is considered as drained type of material. Interface elements are given the material properties similar to that of the surrounding soil. Only exception is that the interface friction angle (φ_{inter}) is taken as 66% of the angle of shearing resistance of the surrounding soil (φ). Initial stresses are generated using K_0 procedure. K_0 is calculated as $(1 - \sin\varphi)$ for normally consolidated soil.

Table 3.2: Pile geometry, dimension and properties

Pile Geometry and Dimension		Pile Properties		
Pile Length L (m)	Diameter of Pile D (m)	Poisson Ratio υ_p	Modulus of Elasticity E_p (kN/m^2)	Unit Weight γ_c (kN/m^3)
10	0.5	0.33	3E+07	24.5

Table 3.3: Sandy soil properties

Soil Properties	Dense Sand	Medium Dense Sand	Loose Sand
Cohesion, c (kPa)	1	1	1
Angle of internal Friction, φ (°)	45	35	26
Dialatancy, ψ (°)	15	5	0
Poisson Ratio, υ	0.35	0.28	0.2
Modulus of Elasticity, E (kPa)	6E+04	4E+04	2E+04
k_s/k_0	0.8	0.8	0.8
Interface friction angle, φ_{inter} (°)	0.66 φ	0.66 φ	0.66 φ

Pile load displacement curves, as shown in Figure 3.6, are obtained from the PLAXIS output program. The data point of maximum curvature of this curve (after multiplied by 2π) indicates the ultimate pile capacity.
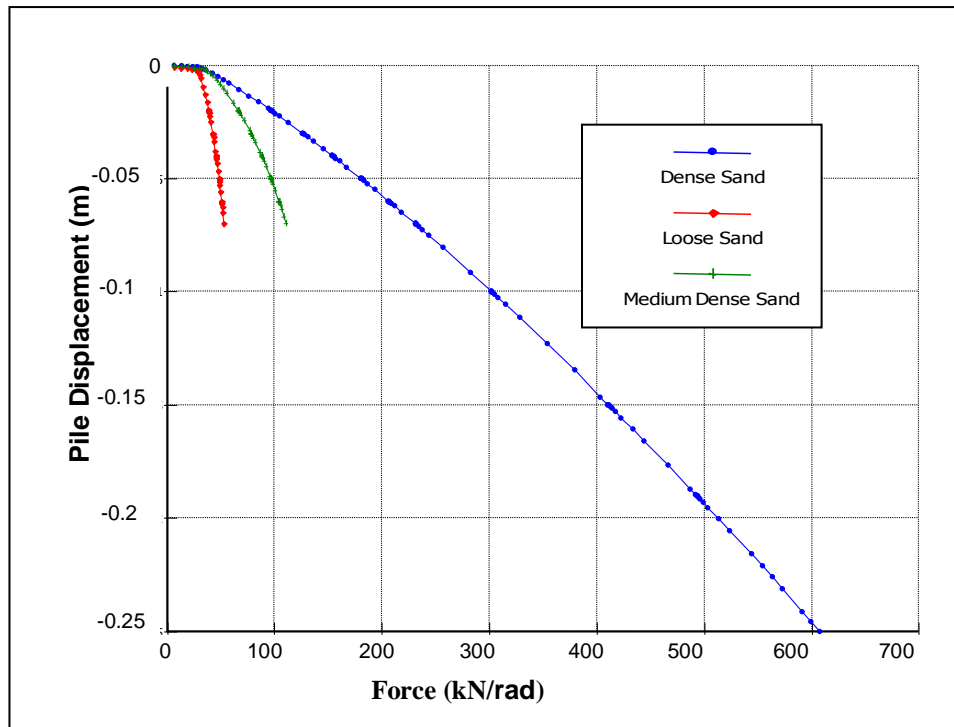
Figure 3.6: Present study - Load displacement curves for a 10 m long pile with 0.5 m diameter in dense, medium dense and loose sands

In numerical modeling, the initial stress is generated with K_0 (i.e., $1 - \sin\varphi$) that makes the finite element results higher than that obtained empirically (using $0.8*K_0$ for K_s). While using the empirical formula to predict pile shaft resistance in homogeneous sand, Canadian Foundation Engineering Manual recommends to use the value of K_s (in the formula) between 0.7 to 1.0 K_0 for bored piles, and thus a value equals $0.8*K_0$ is used. For this reason, initial stresses are regenerated with 80% of K_0 in the clusters immediate to the pile interface and below the pile tip and with full K_0 for the rest of the clusters.

Table 3.4: Comparison of numerical results with the values calculated from empirical formulae

Soil Type	Shaft Resistance (kN)		End Resistance (kN)		Ultimate Pile Capacity (kN)	
	Empirical Method	FEM	Empirical Method	FEM	Empirical Method	FEM
Dense Sand	240	224	1834	1817	2074	2041
Medium Dense Sand	212	219	299	295	511	514
Loose Sand	169	186	83	84	252	270

The ultimate pile capacity, the shaft resistance and the base resistance are calculated for a 10 m long pile with 0.5 m diameter in dense, medium dense and loose sands using finite element analysis and are compared well with those predicted from empirical formulae, as given in Table 3.4.

3.3.2 Validation of Numerical Model for Pile in Overconsolidated Clay

The numerical model is further validated with the experimental results of a pile subjected to vertical loading and embedded in stiff over-consolidated clay. The soil has a plastic limit of 20% and a liquid limit of 80%, and it has a natural water content of 22%. The groundwater table was located at a depth of 3.5 m below the ground surface. Its properties are taken from El-Mossallamy (1999), as given in Table 3.5. The load test results of a 9.5 m pile with a diameter of 1.3 m were obtained from Sommer and Hammbach (1974). Wehnert and Vermeer (2004) studied the same pile and the soil

condition stated using three different soil models in PLAXIS; the MC, the HS and the SS soil models. The finite element analysis with the MC soil model gave low values for the shaft friction, the base resistance and the pile capacity, as compared to the experimental results in that study. However, the effect of OCR was not included in any of the cases.

Table 3.5: Parameters of over-consolidated stiff clay and pile for the calculation (El-Mossallamy, 1999)

Properties	Stiff Clay	Pile
Unit Weight, γ (kN/m^3)	20	25
Cohesion, c (kpa)	20	-
Angle of internal Friction, φ ($°$)	20	-
Poisson Ratio, υ	0.3	0.2
Modulus of Elasticity, E (kPa)	6E+04	3E+07
$K_{0(NC)}$	0.8	-

Present study addresses the effect of overconsolidation ratio (OCR) that has an influence on the at rest coefficient of earth pressure (K_0) (i.e., $K_{0(OC)}$ at over-consolidated state). $K_{0(OC)}$, estimated according to Eqn 3.1, generates the initial stresses of heavily overconsolidated clay in the numerical model, as the stiff clay is at heavily over-consolidated state.

$$K_{0(OC)} = K_{0(NC)} . OCR^{0.5} \ldots\ldots..\ldots\ldots\ldots\ldots\ldots\ldots.(3.1)$$

where, $K_{0(NC)} = 0.8$.

The overconsolidation ratio (OCR) of the stiff clay under consideration is not mentioned in the literature. Therefore, for the heavily overconsolidated clay, three different OCRs, within the usual range from 5 to 8, are considered to estimate possible values of $K_{0(OC)}$. Table 3.6 summarizes the finite element results and compares the results with the experimentally measured values. For all three OCRs, numerical results are found reasonably closer to the experimental results. In case of OCR equals 7, numerical results are in a very good agreement with the experimental results, as shown in Table 3.6. The contrast of the pile load displacement curves, based on the numerical and the experimental results, is shown in Figure 3.7.

Table 3.6: The effects of OCR and K_0 on the shaft and the end resistances and the ultimate pile capacity

OCR	$K_{0(OC)}$	Shaft Resistance (kN)		End Resistance (kN)		Total Ultimate Pile Capacity (kN)	
		PLAXIS	Exp.	PLAXIS	Exp.	PLAXIS	Exp.
5.5	1.875	2086		766		2852	
6.25	2	2143	2100	837	1000	2980	3100
7	2.215	2200		909		3109	
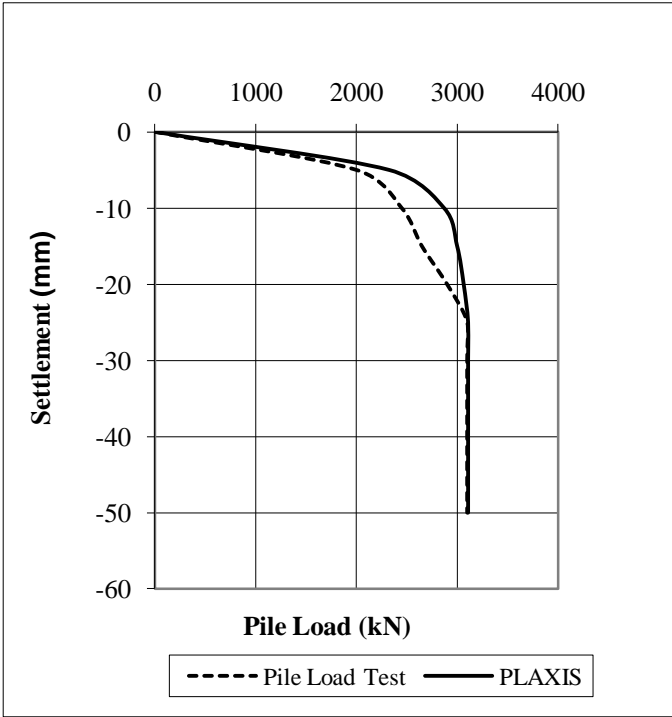
Figure 3.7: Load displacement curves of a pile in overconsolidated stiff clay (OCR = 6.25)

Hence, the application of $K_{0(NC)}$ by Wehnert and Vermeer (2004) could be the reason of getting low values of the shaft resistance and the pile capacity from the numerical modeling.

3.3.3 Validation of Numerical Model for Pile in Collapsible Soil at Constant Moisture Content

The developed numerical model is tested for the layered soil system, comprised of the natural deposits of collapsible and non-collapsible soils. The numerical and the experimental results (Grigorian, 1997) of pile load tests are compared at the initial unsaturated and the fully saturated soil conditions in Volgodon and Nikopol experimental regions, respectively. In Volgodon experimental regions, when the piles were installed and loaded externally, soil layers were at its initial unsaturated condition. In case of the pile tests at Nikopol region, load on the pile was applied after the soil was fully saturated. There was no possibility of inundation induced volume change (of collapsible soil) that may induce indirect load (Q_n) due to negative skin friction (NSF) during the loading of the pile externally.

Hydraulic jack of 5 MN capacity was used to apply static load on the test piles. At each stage of loading, a constant pressure was automatically maintained with an accuracy of 0.1 MPa of manometer deviations. Hydraulic jacks transferred load through the main longitudinal girder to the cross beams joined with anchor piles. Deflecto-meters were used to measure the pile settlements; moreover, settlements were controlled by means of precision leveling.

Collapsible soil behavior (at a constant moisture content, representing either partially or fully saturated state) is defined as drained material and modeled by the Mohr-Coulomb (MC) constitutive law. Material parameters (including cohesion (c), angle of shearing resistance (φ), Poisson's ratio (υ), Young's modulus (E) and angle of dilatancy (ψ)) in the MC model, are given input according to the soil constant soil moisture content state (corresponding to either the unsaturated or saturated condition). Unsaturated and saturated parameters are given to the collapsible soil clusters in the geometry models developed for the pile tests at Volgodon and Nikopol regions, respectively.

3.3.3.1 Pile Load Test at Initially Unsaturated Collapsible Soil

The developed numerical model is used to simulate the pile load tests at Volgodon Experimental Regions-1 and -2. Between the two experimental regions, there are also some differences in the soil profiles below the depth of 15 m, mainly because of the locations of groundwater level. Piles with different dimensions, as given in Table 3.7,

were tested at Volgodon Experimental Regions-1 and -2. Therefore, two different sets of experimental results are available.

Table 3.7: Pile geometry, dimension and properties

Experimental Region	Pile Geometry and Dimension		Pile Properties		
	Pile Length, L (m)	Diameter of Pile D (m)	Poisson Ratio υ_p	Modulus of Elasticity E_p (kN/m^2)	Unit Weight γ_c (kN/m^3)
Volgodon - 1	25	1	0.33	3E+07	24.5
Volgodon - 2	18	1	0.33	3E+07	24.5

In Volgodon Experimental Region-1, the ground water table is beyond the depth considered in numerical modeling. Collapsible soil is found up to a depth of 23 m. The last 2 m of the pile is embedded into a deep bed of non-collapsible soil. Therefore, the general phreatic level, representing the points with zero water pressure, coincides the bottom line of the geometry model. In other words, properties of each soil layer in the geometry model are of drained type. All clusters remain dry with zero steady state pore pressure and have the soil weight according to the unsaturated unit weight. The properties given to the pile and soil clusters are presented in Table 3.7 and Table 3.8.

Table 3.8: Soil properties at Voldogon Experimental Region-1 (Grigoryan, 1997)

Depth (m)	w_n (%)	γ_{bulk} (kN/m^3)	G_s	e	S_r %	c (kPa)	φ ($^\circ$)	Remarks
0 – 6	13.8	16.95	2.68	0.78	51	15	19	Collapsible
6 – 18	15	17.5	2.69	0.73	56	24	17	Collapsible
18 - 30	17.9	18.82	2.69	0.66	73	33	19	Collapsible up to 23 m.

On the other hand, in Volgodon Experimental Regions- 2, the ground water table is at a depth of 25 m. Figure 3.8 and Figure 3.9 show the soil profile of Volgodon Experimental Region-2 and the numerical model, respectively. Table 3.9 presents the soil properties of Volgodon Experimental Region-2. The general phreatic level, representing the points with zero water pressure, is at the depth of 25 m in the geometry model.

Collapsible soil is found up to a depth of 15 m. The last 3 m of the 18 m long pile is embedded into a deep bed of dense and non-collapsible soil. Up to the depth of 25 m from the ground surface, there are three distinct soil layers. Those are of drained type materials with zero steady state pore pressure. They have soil weights according to their respective unsaturated unit weights. Below the phreatic level (25 m), there exists a stable hydrostatic situation; the generated pore pressure is based on a hydrostatic pore pressure distribution, and the soil layer (Layer IV in Figure 3.8) is modeled as undrained type of material.

Table 3.9: Soil properties at Voldogon Experimental Region-2 (Grigoryan, 1997)

Depth (m)	w_n (%)	γ_{bulk} (kN/m^3)	G_s	e	S %	c (kPa)	φ ($^\circ$)	Remarks
0 – 6	13.8	16.95	2.68	0.78	51	15	19	Collapsible
6 – 15	15	17.5	2.69	0.73	56	24	17	Collapsible
15 - 25	17.9	18.82	2.69	0.62	73	33	19	Non-Collapsible, unsaturated
25-35	23.0	19.6	2.69	0.62	100	33	19	Non-Collapsible, saturated

The piles in layered soils, comprised of collapsible and non-collapsible type at Volgodon experimental regions, are studied using the numerical model. Initial condition and calculation phases are defined as described previously.
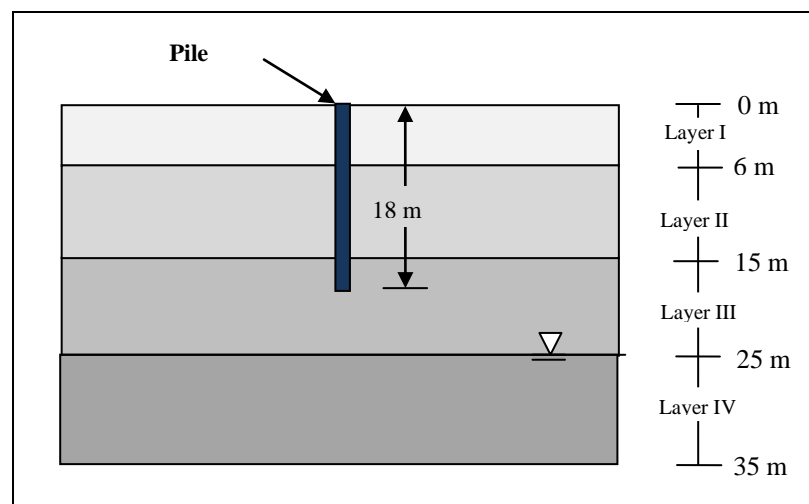
Figure 3.8: Soil profile at Volgodon Experimental Region-2
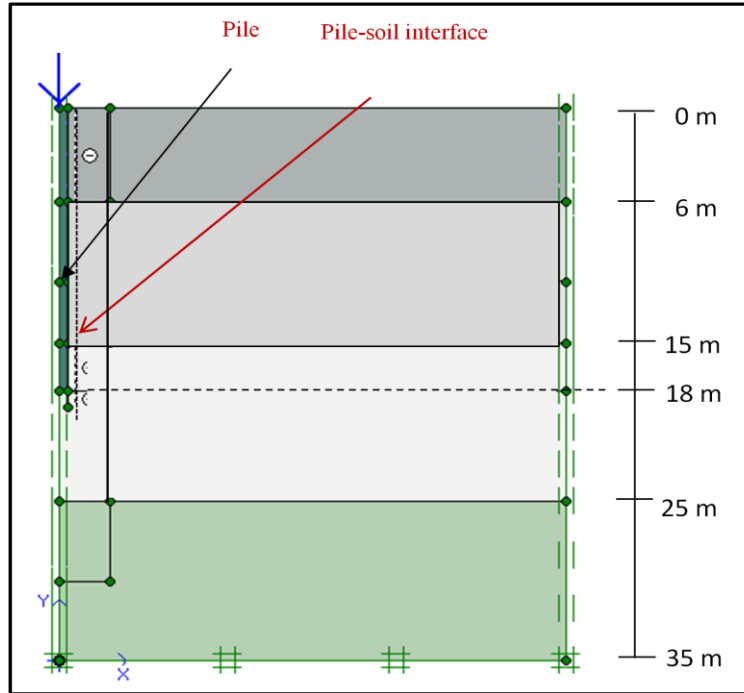
Figure 3.9: Numerical model of pile load test in Voldogon Experimental Region-2

In simulating pile load test under constant moisture condition, the contribution of suction stress is totally ignored in the finite element calculation. Unsaturated soil clusters are given unsaturated soil properties (known for the cases studied, e.g., Volgodon Experimental Region-2), and accordingly the contribution of suction to the soil properties at its unsaturated state are considered. Collapsible soil layer is given the value of E from Grigorian (1997). Though both the collapsible and non collapsible soil layers (as given in Table 3.7) have the same strength values, the reasonable value of E for non collapsible soil is chosen from the literature according to the values of c and φ. Differently, the input of low modulus of elasticity (into non collapsible soil layers) and the contribution of suction stress as neglected would make the finite element formulation to calculate unreliably high settlements of the piles. In that case, the finite element analysis may generate a load displacement curve below the corresponding experimental curve, and the pile settles less during field test than finite element simulation.

Good agreements are achieved between the numerical results and experimental data. Figure 3.10 and Figure 3.11 show the pile load displacement curves, from both the finite element analysis and the experiments, for the pile load tests at Volgodon Experimental Region-1 and -2, respectively.
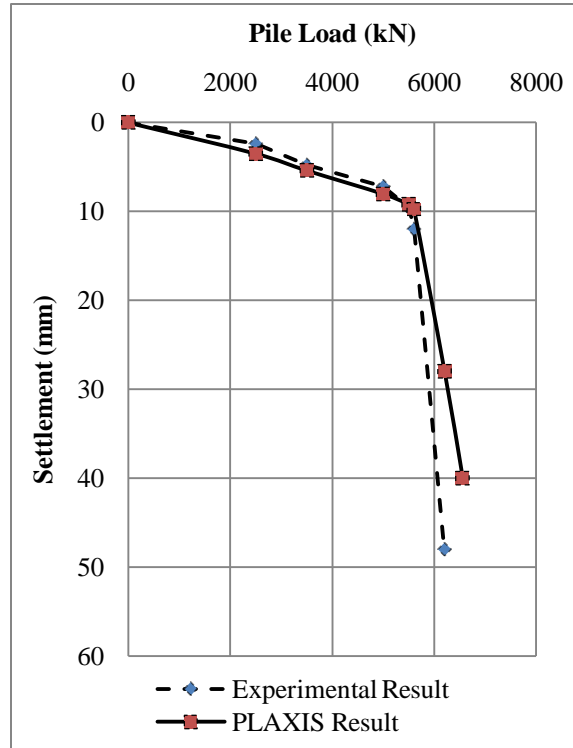
Figure 3.10: Pile load displacement curves at Volgodon Experimental Region-1
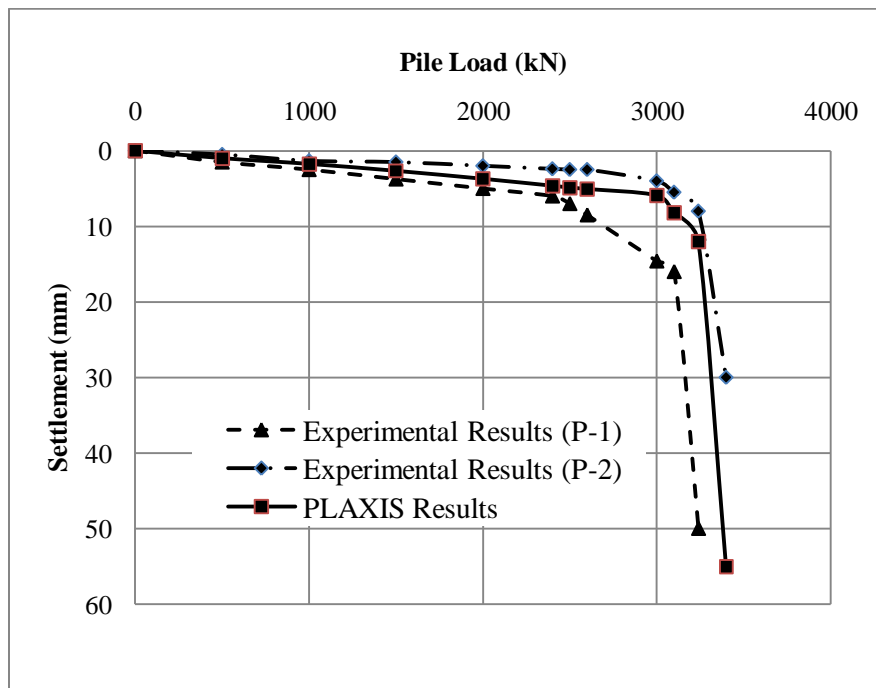
Figure 3.11: Pile load displacement curves at Volgodon Experimental Region-2

Table 3.10: Comparison between numerical results and experimental pile load test by (Grigoryan, 1997)

Pile Resistances	Present study	Experimental (Grigoryan, 1997)
Ultimate Pile Capacity, Q_u (kN)	3204	3240
Shaft Resistance, Q_s (kN)	2930	2948
End Resistance, Q_b (kN)	274	292

The numerical results, for Volgodon Experimental Region-2, are examined for the shaft resistance, the base resistance and the ultimate pile capacity; and are compared well with the experimental results, as given in Table 3.10. It is to note that only 10% of the ultimate pile capacity is supported by the pile tip resistance. It is clear that if positive skin friction would disappear (long a pile section) during inundation of collapsible soil, the pile will suffer from reduction in its capacity significantly.
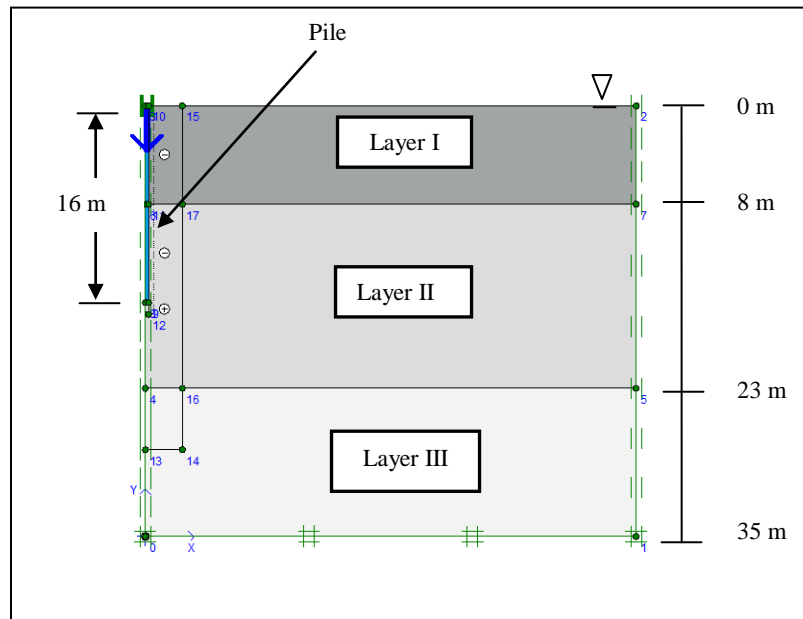
Figure 3.12: Numerical model of pile load test in wetted collapsible loess

3.3.3.2 Pile Load Test at Fully Saturated Collapsible Soil

The numerical model is further tested for a single pile in fully saturated layers of collapsible soil. Figure 3.12 shows the numerical model of a single pile in wetted

collapsible loess at Nikopol. The properties of pile and soil at Nikopol experimental region are given in Table 3.11 and Table 3.12, according to Grigoryan (1997).

Table 3.11: Pile geometry, dimension and properties (Grigoryan, 1997)

Experimental Region	Pile Geometry and Dimension		Pile Properties		
	Pile Length, L (m)	Diameter of Pile D (m)	Poisson Ratio υ_p	Modulus of Elasticity E_p (kN/m^2)	Unit Weight γ_c (kN/m^3)
Nikopol	16	0.5	0.33	3E+07	24.5

Table 3.12: Soil properties (saturated condition) at Nikopol (Grigoryan, 1997)

Depth (m)	w_n (%)	Void Ratio $e_{initial}$	w_{sat} (%)	γ_{sat} (kN/m^3)	c (kPa)	φ ($^\circ$)
0 – 8	7	0.91	28.7	17.57	5	20
8 – 23	4.3	0.86	30.82	18.34	6	16
23 - 30	11.3	0.71	21.2	18.4	5	18
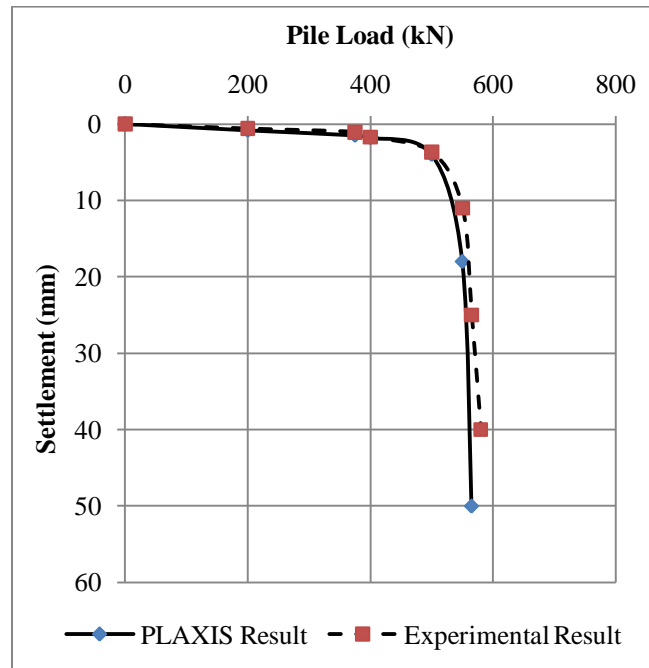
Figure 3.13: Pile load displacement curve at Nikopol Experimental Region

It can be noted that pile load displacement curves of Nikopol are in good agreement, as given in Figure 3.13.

3.4 Incorporating the Effect of Inundation of Collapsible Soil

In studying the performance of a single pile (in terms of skin friction and base resistance), collapsible soil is successfully modeled according to the Mohr-Coulomb theory regardless of the initial soil state (unsaturated or saturated), provided that the soil moisture does not change during the period of time under consideration. However, numerical modeling of collapsible soil subjected to inundation (alternatively soil collapse due to inundation), is a complex task, as compared to that of collapsible soil at constant moisture condition. During inundation, collapsible soil experiences irrecoverable volume reduction without any change in its stress level, while the Mohr-coulomb theory considers the soil as linear elastic-perfectly plastic with stress dependent properties, strain softening and can model irreversible load deformation response only. Moreover, the input soil parameters, in the Mohr-Coulomb model, are absolutely constant, but these may vary significantly for unsaturated soils (including collapsible soil) during inundation. Therefore, both volume change behavior and the change in the stress state are the effects of inundation (or matric suction reduction) on collapsible soil and demands consideration in developing a simulation procedure to incorporate the effect of soil collapse.

Before incorporating the effect of inundation of collapsible soil in the numerical model to investigate the foundation performance, this study identifies some important facts that make collapsible soil the most problematic one among all types of unsaturated soils. First of all, it becomes saturated very fast, as it is highly permeable due to its high porosity. Secondly, collapsible soil layer requires less amount of water to reach 100% saturation than expected for a volume insensitive (during inundation) soil (Statement 1). 'Statement 1' is examined by comparing collapsible soil (CS) with two different volume insensitive unsaturated soils (VIS): (i) CS and VIS have the same porous structure and (ii) VIS is denser than CS. It is to clarify here that an unsaturated porous soil may not collapse only due to inundation. In nature, there exists volume insensitive (to inundation) highly porous soil, in which other types of bond (including fine silt bond, clay bond, bond by autogenesis, ring buttress, clay bridge, etc) act as major bonds, giving high strength to

porous (flocculate) unsaturated soil, in combination with matric suction (i.e., relatively minor). The collapse problem, during inundation, is much less or insignificant to some extent of inundation pressure, because of other strong bonds in addition to matric suction (minor), as noted by Pereira and Fredlund (2000). During inundation, as the percentage of the water in the pore space increases, matric suction decreases and the bond of matrix suction diminishes. If the other bond is strong enough to resist the previously applied stress level alone, the porous unsaturated soil may not collapse. However, in previous studies, it is reported that such soil also experiences collapse, as that bond fails eventually after the applied stresses exceed the limiting stress. On the other hand, in case of collapsible soil, collapse takes place, when the other bonds, if any, cannot provide sufficient resistance against the previously acting stresses (due to overburden stress, load from foundation, etc.). Therefore, soil experiences sudden and significant deformations, as the major bond strength due to matric suction (holding soil grains in a porous structure) disappeared.

To examine 'Statement 1', consider two unsaturated (a CS and a VIS) soil layers have the same initial void ratio ($e_{initial}$), porous structure, and equal thickness. Therefore, after reaching 100% degree of saturation,

For volume-insensitive soil,

$$\text{Final water content, } w_i = \frac{e_{initial}}{G_s} \ldots\ldots\ldots\ldots\ldots\ldots\ldots\ldots\ldots\ldots\ldots(3.1)$$

For collapsible soil,

$$\text{Final water content, } w_c = \frac{e_{initial} - \Delta e}{G_s} \ldots\ldots\ldots\ldots\ldots\ldots\ldots\ldots\ldots(3.2)$$

$$\Delta w = w_i - w_c = \frac{\Delta e}{G_s} \ldots\ldots\ldots\ldots\ldots\ldots\ldots\ldots\ldots\ldots\ldots(3.3)$$

Eqn 3.1, Eqn 3.2 and Eqn 3.3 demonstrate the fact that there is a difference in the final water contents required by the two soils, depending on the change of void ratio.

'Statement 1' is again examined by comparing a collapsible soil with a relatively dense unsaturated soil. Both soils have the same initial volume ($V_{initial}$) and equal thickness. Therefore, collapsible soil has high initial void ratio than the other soil. If both soils could have the same final water content at the end of the saturation, the collapsible soil would require less water ($W_w = w * W_s$) than the other soil, by definition of water content (Eqn 3.4), this is because the non collapsible (volume insensitive to moisture

increase) soil is relatively dense, and the weight of soil solid (W_s) of non collapsible soil is greater than that of the collapsible soil.

$$w = \frac{W_w}{W_s} \dots\dots\dots\dots\dots\dots\dots\dots\dots\dots\dots\dots\dots\dots\dots\dots\dots\dots\dots\dots\dots\dots\dots(3.4)$$

The concern is if water content at the 100% saturation is same in both soils. The amount of water (W_w) in soil volume can be estimated using Eqn 3.5, which is derived using the Eqns 3.6—3.8.

$$W_w = \frac{S.e}{G_s} * W_s = \frac{S.e}{G_s} * (\gamma_{unsat} * V_{initial}) \dots\dots\dots\dots\dots\dots(3.5)$$

$$w = \frac{W_w}{W_s} = \frac{S.e}{G_s} \dots\dots\dots\dots\dots\dots\dots\dots\dots\dots\dots\dots\dots\dots\dots\dots(3.6)$$

$$S.e = w.G_s \dots\dots\dots\dots\dots\dots\dots\dots\dots\dots\dots\dots\dots\dots\dots\dots\dots\dots(3.7)$$

$$\gamma_{unsat} = \frac{W_s}{V_{initial}} \dots\dots\dots\dots\dots\dots\dots\dots\dots\dots\dots\dots\dots\dots\dots\dots\dots(3.8)$$

where, w = water content,

   W_s = weight of soil solids,

   W_w = weight of water,

   S = degree of saturation = 1 (after full saturation),

   G_s = specific gravity,

   γ_{unsat} = unsaturated unit weight, ignoring insignificant amount of water at initial
        condition, and

   $V_{initial}$ = Initial total volume.

Based on Eqn 3.5, the ratio of the weight of water in collapsible soil (W_{wc}) to that in non collapsible soil (W_{wnc}) at 100% degree of saturation is as follows:

$$\frac{W_{wc}}{W_{wnc}} = \frac{S_c.e_c.\gamma_{unsat\ (c)}}{S_{nc}.e_{nc}.\gamma_{unsat\ (nc)}} \dots\dots\dots\dots\dots\dots\dots\dots\dots\dots\dots\dots\dots\dots(3.9)$$

where, e_c = void ratio of collapsible soil, and

   e_{nc} = void ratio of non collapsible soil.

At initial unsaturated condition,

   $\gamma_{unsat(c)}$ = Initial unsaturated unit weight of collapsible soil (e.g., around 15 kN/m^3),

   $\gamma_{unsat(nc)}$ = Initial unsaturated unit weight of non collapsible soil (e.g., around 20 kN/m^3),

Therefore, $\dfrac{\gamma_{\text{unsat (c)}}}{\gamma_{\text{unsat (nc)}}} = \dfrac{15}{20} = 0.75 < 1.$

After full saturation of both soils, it is obvious that both soils have equal degree of saturation. That is, S_c (degree of saturation of collapsible soil) equals S_{nc} (degree of saturation of non collapsible soil). If both soils have the same final void ratio, (i.e., $e_c = e_{nc}$), then Eqn 3.9 reduces to Eqn 3.10.

$$\frac{W_{wc}}{W_{wnc}} = \frac{\gamma_{\text{unsat (c)}}}{\gamma_{\text{unsat (nc)}}} = K \dots\dots\dots\dots\dots\dots\dots\dots\dots\dots\dots\dots\dots\dots(3.10)$$

where, $K < 1$,

W_{wc} = the weight of water required in collapsible soil to reach 100% saturation, and

W_{wnc} = the weight of water required in non collapsible soil to reach 100% saturation. Eqn 3.10 indicates that "collapsible soil requires less amount of water than relatively dense unsaturated soil".

Eqn 3.10 is used to investigate the reason why the major collapse is sudden. However, major collapse, which is more than 85% of full collapse, is observed to occur when soil attains about 80% degree of saturation (Mahmoud, 1991). Therefore, the weight of water ($W'_{w(c)}$) required to attain major collapse is 80% of $W_{w(c)}$.

$$W'_{w(c)} \approx 0.8 * W_{w(c)} \dots\dots\dots\dots\dots\dots\dots\dots\dots\dots\dots\dots\dots(3.11)$$

Based on Eqn 3.10,

$$W'_{w(c)} = 0.8 * K . W_{w(nc)} \dots\dots\dots\dots\dots\dots\dots\dots\dots\dots\dots(3.12)$$

Therefore, if the value of K is taken 0.75, the water requirement to attain major collapse ($W'_{w(c)}$) is only 60% of the water ($W_{w(nc)}$) to reach 100% saturation by non collapsible soil. In other words, the major collapse can occur due to the increase in soil moisture equivalent to make the other non collapsible soil 60% saturated.

The following demonstrates how fast the void ratio of collapsible soil may decrease, when subjected to inundation.

Consider a collapsible soil (having collapse potential 10% or more) experiences significant collapse and can attain easily the void ratio as same as the other soil (e.g. having void ratio of 0.4).

By definition of collapse potential, C_p

$$C_p = \frac{\Delta e}{1 + e_{initial}} \dots\dots\dots\dots\dots\dots\dots\dots\dots\dots\dots\dots\dots\dots\dots\dots\dots\dots\dots\dots\dots\dots(3.13)$$

Also,

$$C_p = \frac{\Delta V}{V_{initial}} = \frac{\Delta e / e_{initial}}{(1 + e_{initial})/e_{initial}}$$

Therefore,

$$C_p = \frac{\Delta V}{V_{initial}} = \frac{\Delta e}{e_{initial}} \cdot \frac{1}{(\frac{1}{e_{initial}} + 1)}$$

$$C_p = \frac{\Delta V}{V_{initial}} = \frac{\Delta e}{e_{initial}} \cdot M \dots\dots\dots\dots\dots\dots\dots\dots\dots\dots\dots\dots\dots\dots\dots(3.14)$$

$$\frac{\Delta e}{e_{initial}} = \frac{C_p}{M} \dots\dots\dots\dots\dots\dots\dots\dots\dots\dots\dots\dots\dots\dots\dots\dots\dots\dots\dots(3.15)$$

$$M = \frac{1}{(\frac{1}{e_{initial}} + 1)} < 1$$

$$\frac{1}{e_{initial}} = 1.25 - 1.7.$$

Initial void ratio of collapsible soil usually ranges from 0.55 to 0.8, and therefore, the value of M ranges 0.37–0.44. The $\Delta e / e_{initial}$ ratio is greater than the ratio $\Delta V / V_{initial}$ (i.e. collapse potential, C_p in Eqn 3.14). From Eqn 3.15, it can be noted that the void ratio change (i.e., decrease) could be as high as 50% of the initial void ratio, though the soil can have collapse potential of 20%. The average value of M is considered 0.4. Eqn 3.14 converts to Eqn 3.16, after including the effect of inundation pressure.

$$\frac{C_p}{200} \cdot (\sigma + \gamma h) = \frac{\Delta e}{e_{initial}} \cdot M \dots\dots\dots\dots\dots\dots\dots\dots\dots\dots\dots\dots\dots\dots(3.16)$$

Where, γh = overburden stress (kPa) and

σ = Surcharge on soil surface (kPa).

By definition, collapse potential (C_p) is the percentage of volume change under the inundation pressure of 200 kPa, and it is directly proportional to the inundation pressure up to 400 kPa, as experimentally observed previously by Nouaouria (2008). The inundation pressure ($\sigma + \gamma h$) is high, when a given collapsible soil is located at a depth greater than 10 m or subjected to load from foundation (σ). Overburden stress is about

200 kPa for a collapsible bed, when the overlying non collapsible layer (unit weight, 20 kN/m^3) is 10 m deep.

3.4.1 Staged Construction to Incorporate the Effect of Inundation

The numerical model, developed to study the case of soil at constant moisture content, is extended here to study the performance of a foundation, supporting load from the structure, in collapsible soil during inundation induced collapse. During inundation, volume reduction is a characteristic problem of collapsible soil, while all types of unsaturated soils (including collapsible soil) undergo strength reduction. In order to incorporate the effect of inundation of collapsible soil, a framework of staged construction is proposed (Kakoli et al., 2009), as shown in Figure 3.14.
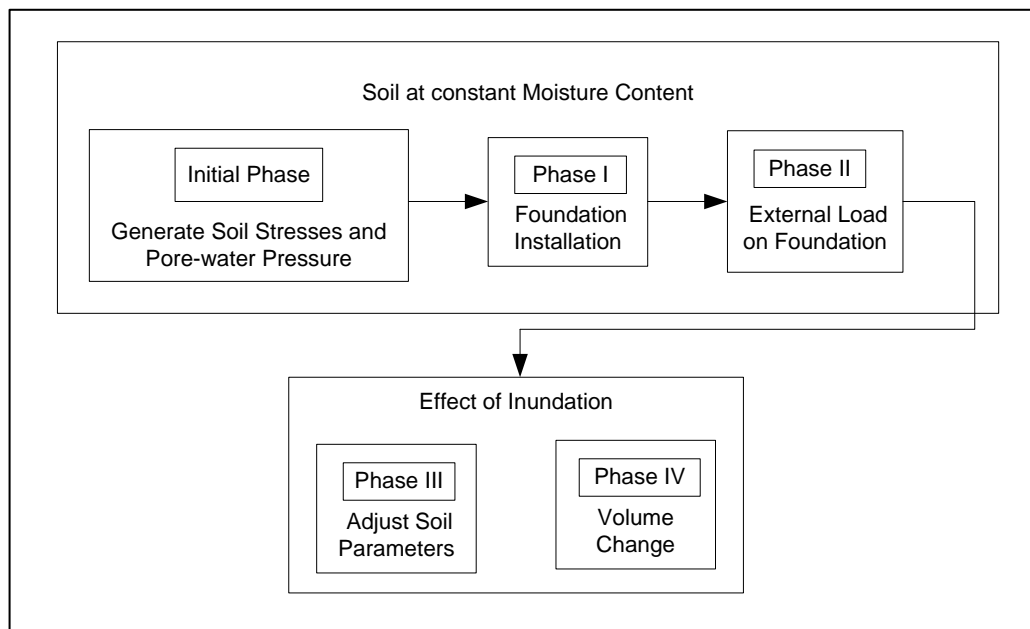
Figure 3.14: Principle/framework of the proposed staged construction

In case of collapsible soil at constant moisture content, only three calculation phases (including Initial Phase, Phase I and Phase II) have to be defined, as shown in Figure 3.15. In Phase I, foundation is installed. For example, installation of the pile
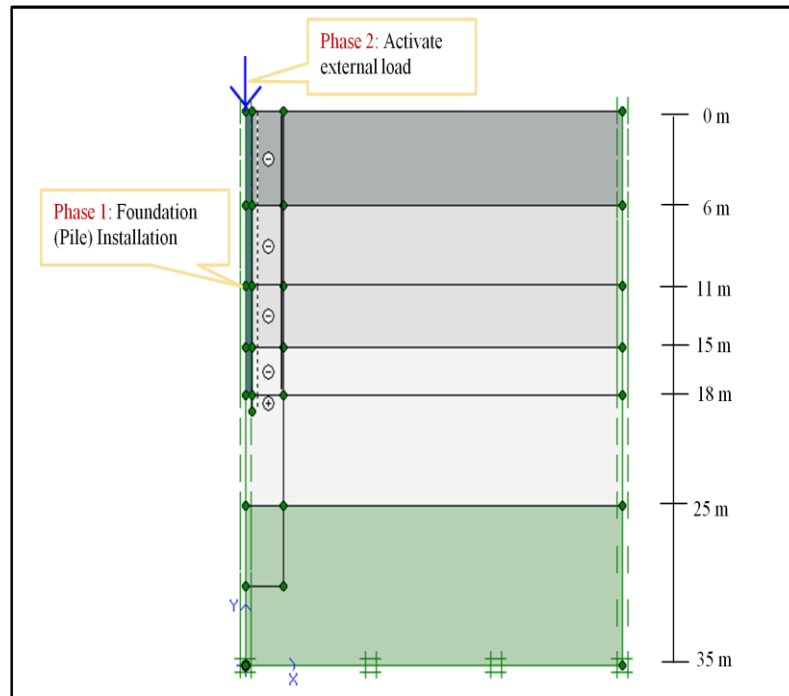
Figure 3.15: Staged Construction: Soil at Constant Moisture Content

foundation (bored) is already demonstrated in previous sections. If unsaturated clusters remain at constant moisture content, the last calculation phase is Phase II, where the external load on the foundation is applied, as demonstrated in Figure 3.15.

The proposed framework, as given in Figure 3.14, includes the effect of inundation by adding two calculation phases (Phase III and Phase IV). Figure 3.16 presents staged construction when a layer (11-15 m in this example) of collapsible soil is subjected to full saturation. These two phases are elaborated in the following sections. Phase III adjusts the properties of unsaturated soil clusters, as inundation causes changes in soil stress state (e.g. shear strength). The corresponding changes in the stress state (strength parameters) are estimated and are used to make a new data set, incorporated into the finite element calculation by reassigning the soil properties of the corresponding clusters, which was previously unsaturated but experience collapse during inundation. Phase IV applies volume change (decrease) by applying prescribed displacement/volumetric strain to the unsaturated clusters, subjected

75
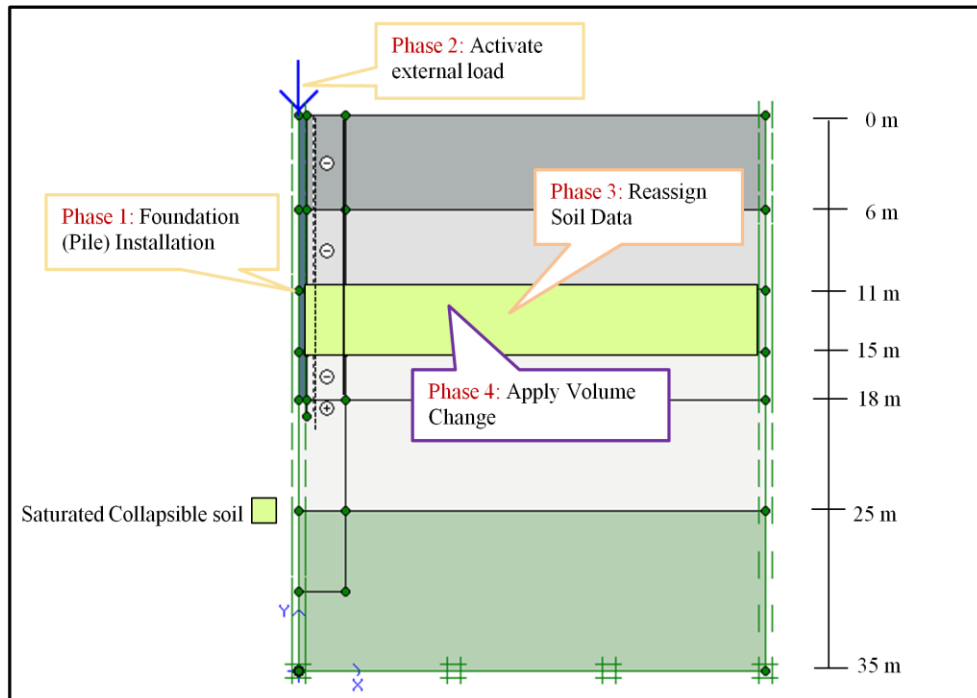
Figure 3.16: Staged construction: collapsible soil subjected to inundation

to inundation. While generating initial condition, all clusters, including the one representing foundation in the geometry model, are given soil properties, according to the soil profile. Unsaturated and saturated clusters are given the corresponding unsaturated and saturated soil properties, respectively. Initial soil stresses are generated according to K_0 procedure, and initial pore water pressure is generated according to general phreatic line. Matric suction in the unsaturated clusters, above the general phreatic line, is ignored.

The numerical model incorporating the effect of inundation of collapsible soil is applicable to any type of foundation, which is constructed on unsaturated collapsible soil and resisted loads from the structure, and after a while the collapsible soil is subjected to inundation and accordingly collapses.

3.4.1.1 Adjustment of Soil Parameters (Phase III)

The present study utilizes two independent stress state variables: namely, net normal stress ($\sigma - u_a$) and matric suction ($u_w - u_a$); for predicting the values of shear strength parameters of collapsible soil at any stage of inundation. As addressed in the literature review, soil input parameters (e.g., c and φ) can be estimated using unsaturated property

functions at any partially saturated state, as a function of matric suction. That means, at any stage of inundation, c or φ can be estimated, if matric suction (ψ) corresponding to that saturation level is known. Soil water characteristic curve (SWCC), by relating amount of water and matric suction, plays an important role in this respect.

In incorporating the effect of inundation to the numerical model, unsaturated soil clusters subjected to inundation require adjustment of soil parameters, replacing its initial data by a new soil dataset. The soil parameters (e.g., cohesion, c) at the intermediate stage (corresponding degree of saturation, S_{inter}) of inundation are used to make the 'new soil dataset', which is applied in Phase III of staged construction. S_{inter} is the average degree of saturation of the initial degree of saturation (S_b) and the final degree of saturation (S_f) reached at the end of inundation experienced by a given layer.

Eqn 3.18 is a part of the shear strength function (Eqn 3.17), given by Vanapalli et al. (1996) and Fredlund for unsaturated soil. Eqn 3.18 can estimate cohesion contribution (Δc) due to matric suction in the primary transition zone in SWCC. However, in the secondary transition zone, Eqn 3.18 either over-estimates or under-estimates the value of Δc, as compared to experimental values reported by Escario and Juca (1989).

$$\tau = \left[c' + \left(\sigma_n - u_a \right) * \tan\varphi' \right] + \Theta^{\kappa} \left(u_a - u_w \right) * \tan\varphi' \ldots\ldots\ldots\ldots(3.17)$$

Therefore, the cohesion of unsaturated soil, $c = c' + \Theta^{\kappa} \left(u_a - u_w \right) * \tan\varphi'$;
and cohesion contribution due to matric suction,

$$\Delta c = \Theta^{\kappa} \left(u_a - u_w \right) * \tan\varphi' \ldots\ldots\ldots\ldots\ldots\ldots\ldots\ldots(3.18)$$

This study introduces a correction factor (α) (in Eqn 3.19) into the shear strength function (Eqn 3.17). This factor is only required to estimate the cohesion in the secondary transition zone. Based on the experimental results of Escario and Juca (1989), a relation between the correction factor (α) and the plasticity index (I_p) is found, as shown in Figure 3.17, at the middle of secondary transition zone.

$$\tau = \left[c' + \left(\sigma_n - u_a \right) * \tan\varphi' \right] + \alpha . \Theta^{\kappa} \left(u_a - u_w \right) * \tan\varphi' \ldots\ldots\ldots(3.19)$$

Where, α_i = correction factor = $\left[\frac{\Delta c_{measured}}{\Delta c_{predicted}}\right]_{(u_a - u_w)}$

The data points, in Figure 3.17, correspond to the three soils, studied by Escario and Juca (1989). The correction factor is recommended only for the secondary transition zone, while its value is close to 1 in the primary transition zone.

The chart shows the fitted line with:
$$\alpha = 0.0318(I_p) + 0.2006$$
$$R^2 = 0.996$$

with y-axis labelled "Correction Factor, α" and x-axis labelled "Plasticity Index, I_p (%)".
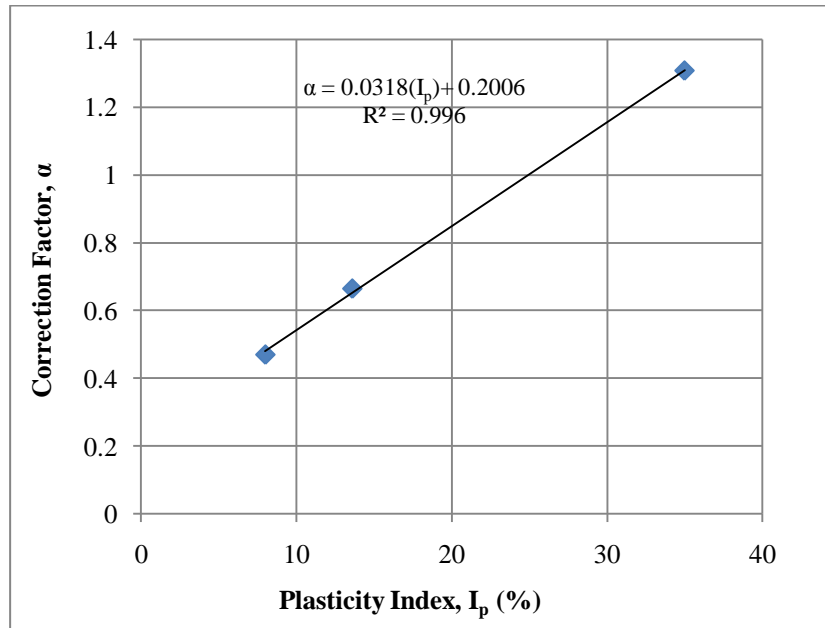
Figure 3.17: Correction factor in cohesion vs. matric suction relation

This correction factor is low, when soil has low plasticity index (I_p). Instead, matric suction of those soils (having low plasticity index, I_p) cannot be very high, as compared to those having relatively high plasticity index (I_p), at the middle of the secondary transition zone or at the residual state. As a result, the last part in Eqn 3.19 becomes very small for soils with low I_p. Therefore, reduction of cohesion due to matric suction reduction (during inundation) can reasonably be ignored for the soils having low I_p. The importance of considering cohesion reduction for only highly plastic soil (plasticity index > 8 or more) is noted in this study. It is also found that cohesion does not change significantly due to inundation, if plasticity index falls below 8. Otherwise, Δc has to be estimated using Eqn 3.19, Figure 3.17 and SWCC of the given soil to obtain the cohesion value. The sum of cohesion at saturated condition and the Δc at a specific

matric suction (or degree of saturation) is the cohesion at the corresponding partially saturated state.

By defining Phase III, the change of any soil parameters, used as soil data input, can be applied to study their effects on the foundation performance using finite element analysis.

3.4.1.2 Applying Volumetric Strain (Phase IV)

Volume change behavior of collapsible soil during inundation can be applied through volumetric strain or prescribed displacement in the program (PLAXIS). Applying volumetric strain is preferred than prescribed displacement, as volumetric strain can handle collapse of a soil cluster, existing near ground or at depth. On the other hand, prescribed displacement can only be used, while simulating collapse of a soil cluster near ground or wetting from top. To validate the simulation results obtained by applying prescribed displacement, it is difficult to get reasonable results experimentally. If water is allowed to flow from top to down, it follows the shortest route. As a result, it is difficult to predict the percentage of collapse attained. In the proposed procedure, the cluster of collapsible soil, subjected to volume change during inundation, is given input of volumetric strain (-ve), estimated according to the extent of inundation.

The magnitude of volumetric strain that should be applied in finite element program depends on the expected collapse strain due to the inundation under consideration. Volumetric strain is known from the collapse strain and a calibration factor, as given in Eqn 3.20.

$$\varepsilon_v = C * \varepsilon_c \dots\dots\dots\dots\dots\dots\dots\dots\dots\dots\dots\dots\dots\dots\dots\dots\dots..(3.20)$$

where, ε_v = Volumetric strain,

ε_c = Collapse Strain, and

C = Calibration Factor.

If degree of saturation (S_r) after partial inundation is known, then collapse strain can be estimated using Eqn 3.21 for partial inundation. There exists a linear relation between the percentage of full collapse experienced (P) and the degree of saturation (S) in the major collapse phase (Mahmoud, 1991). In case of full inundation (if final degree of saturation is about 80 % or more), the value of P in Eqn 3.21 is equals 1. It is also

practical to apply full volumetric strain in one calculation phase, as collapsible soil is subjected to a sudden volume change during inundation.

$$\varepsilon_c = P * \frac{C_p}{200} * (\sigma + \gamma h_m)\ldots\ldots\ldots\ldots\ldots\ldots\ldots\ldots\ldots\ldots\ldots\ldots(3.21)$$

where, P = percentage of collapse experienced during partial inundation,

C_p = Collapse potential,

σ = Surcharge or stress due to foundation load,

γh_m = Overburden stress at the mid height of the collapsible layer subjected to inundation, and

h_m = Depth to the mid section (point) of the collapsing layer from ground.

Performance of any foundation in collapsible soil subjected to inundation can be investigated using the proposed simulation procedure. The percentage of full collapse, depending on the extent of inundation (partial or full), can be controlled in this procedure. The procedure is applicable to highly plastic to non plastic collapsible soil.

3.5 Validation of Numerical Model for Pile in Collapsible Soil during Inundation

This section presents the calibration and the validation of the proposed numerical model. The reduced-scale model pile test results (Mashhour, 2009) are used to calibrate the numerical model. The geometry model is developed using the scale of the reduced scale model pile test setup. Full-scale pile test results (of Grigoryan, 1997) are further used to validate the calibration factor established. In numerical model validation, indirect load due to negative skin friction and positive skin frictional resistance, developed on the pile interface, are compared.

3.5.1 Modeling of Model Pile Test by Mashhour (2009)

The proposed numerical model is used to model the soil collapses, occurred in five model pile tests by Mashhour (2009), for calibration purpose. The objectives of the experimental program, conducted by Mashhour at Concordia University, were to investigate the consequences of soil collapse of different magnitudes in terms of indirect load due to NSF on pile. Three hypothetical prototype thicknesses (from 5 to 11 m) of collapsible

soil bed, overlying a deep bed of strong layer (e.g., bedrock), were considered in designing the reduced scale pile test setup. The model pile was of end bearing type. In Mashhour (2009), model pile tests were conducted to measure the indirect load (Q_n) due to negative skin friction (NSF), resulting from collapse of collapsible soil subjected to inundation from bottom. During experimental setup, the model pile was first installed in the test tank. Then, the tank was filled with collapsible soil in multiple layers and each layer was compacted well. Three different collapsible soils were used in that experimental program. Each collapsible soil was prepared as a homogeneous mix of fine sand and clay (i.e. of kaolin type) in different proportions to obtain different collapse potentials, within a range of 4 to 12.5.

Table 3.13: Scaling factors for pile-soil model (Sedran et al., 2001)

Parameter	Symbol of Scaling Factor	Particular Set of Scaling Factors
Length	λ_L	L_m/L_p
Area	λ_{area}	λ_L^2
Volume	λ_{volume}	λ_L^3
density	λ_ρ	1
Mass	λ_M	λ_L^3
Stress	λ_σ	1
Strain	λ_ε	1
Force	λ_F	λ_L^2
Modulus of Elasticity	λ_E	1

The size of the tank was determined considering a reasonable volume of soil mix required. Practically, the tank was filled with collapsible soil to conduct each test and the soil was removed from it at the end of each test. A pile with 0.0254 m diameter is selected to eliminate the edge effect for the chosen dimension of the tank, which is 0.5 m (length) x 0.5 m (width) x 0.6 m (height). The edge of the tank is at a distance of 10 times the pile diameter (D) from the pile axis, coincide the centerline of the tank. In each test, the embedded length of the model pile was 0.5 m ± 0.03 in collapsible soil. Table 3.13

presents a particular set of scaling factors applied in this study. Table 3.14 presents the scaling factors applied to obtain geometric similarity.

Table 3.14: Scaling Factors for Geometric Similarity

Hypothetical Prototype		Model	L/D	Scaling Factor λ_L (=L_m/L_p)
Length, L (m)	Diameter, D (m)	Surcharge, σ (kPa)		
5.3	0.269	40		1 : 10.6
8	0.406	60	19.7	1 : 16
10.6	0.538	80		1 : 21.2

Both the scaling factors of density and stress (or strain) were made equal 1 for the designed experimental model setup, so that scaling of material properties, including angle of internal friction (φ), cohesion (c), modulus of elasticity (E), Poisson's ratio (υ), etc., were not required. When both the model and the prototype have identical density and stresses, constitutive similarity is easily achieved without scaling of material properties (Sedran et al., 2001). The scaling factor of density (λ_ρ) was possible to keep equaled 1, as the same soil as that in the prototype (hypothetical) was used in the model test. However, reducing the grain size is not practical, as it may result in adverse changes in the material properties of the soil. Further, the influence of grain size, as concern arises for not being scaled, is considered negligible to produce any distortion in model response, according to an established rule of thumb criterion. The rule of thumb criterion is that the influence of grain-size effects on model response can be neglected when the ratio D/d_{grain} is greater than 30 (Ovesen, 1980 Franke and Muth, 1985; Tagaya et al., 1988 and Sedran et al., 2001). In this test program, the pile diameter-to-diameter of sand grain (D/d_{grain}) ratio varied from 30 to 50 for 90% sand particles, as the sand (having D_{60} = 0.5 mm) used in the mixture, i.e., poorly graded. The scaling factor of stress (λ_σ) was maintained equal 1, by applying a surcharge on the soil surface in the model test setup. The overburden stress at the mid-depth of the collapsible layer in prototype was applied as surcharge in the reduced scale model in each case. Therefore, three different surcharges were applied to have similitude of three prototype depths (i.e. 5.3 m, 8 m and 10.6 m, as in Table 3.15) of

collapsible soil. Therefore, collapsible soils in both the model and the prototype were subjected to the same stress through this special arrangement. It is important to note that the experimental study, by Mashhour (2009), investigated the effect of soil collapse under its own gravity. As the gravitational acceleration (g) is not scaled, application of surcharge allowed to attain the same inundation pressure in the model and to have the similitude of the prototype. Table 3.15 presents the scope of the experimental program by Mashhour (2009) considering soil properties, collapse potential, depth of collapsible soil (in prototype) and surcharge (in the reduced scale model).

Table 3.15: Scope of the experimental program by Mashhour (2009)

Test	Soil	Collapse Potential, Cp (%)	Prototype Soil Depth (m)	Model Surcharge (kPa)
1		12.5	5.3	40
2	CS-1	12.5	8	60
3		12.5	10.6	80
4	CS-2	9	10.6	80
5	CS-3	4.2	8	60

Collapsible soils, used in the model tests, were found strong that is a characteristic property of unsaturated collapsible soil at initial moisture condition (5% water content approximately). Before inundation, small settlements (7 mm on an average), were observed even under a surcharge (40, 60 or 80 kPa) applied on the soil surface, as given in Table 3.16. In each test, a particular surcharge was applied incrementally in several steps, while the collapsible soil remains at its initial moisture content in the tank. When the effect of surcharge on the soil volume diminished, collapsible soil was subjected to inundation from bottom. Therefore, in each test, collapsible soil experienced volumetric strains resulting from two different reasons: application of surcharge on soil surface and inundation. Volumetric strain due to surcharge on the soil surface occurred due to the adjustment/repositioning of particles. On the other hand, collapsible soil settled significantly due to inundation (as in Table 3.17), though the soil showed high resistance for further collapse just before the inundation was commenced. It should be noted here

that the soil settlement (i.e., collapse) due to inundation (as in Table 3.17) was relatively high, as compared to the soil settlement caused by surcharge.

Table 3.16: Effects of surcharge: soil settlement, volumetric strain and negative skin friction (after Mashhour, 2009)

Soil	Test	Surcharge (kPa)	Collapse Potential, C_p (%)	Due to Surcharge	
				Soil settlement (mm)	Volumetric Strain (%)
CS-1	1	40	12.5	5	0.86
	2	60	12.5	5	0.9
	3	80	12.5	8	1.33
CS-2	4	80	9	8	1.42
CS-3	5	60	4.2	7	1.22

Table 3.17: Effects of inundation: soil settlement and volumetric (collapse) strain (after Mashhour, 2009)

Soil	Test	Surcharge (kPa)	Collapse potential, C_p (%)	Soil Settlement (mm)	Collapse Strain, (%)	
					Measured	Estimated
CS-1	1	40	12.5	20	3.7	2.5
	2	60	12.5	22	4.4	3.75
	3	80	12.5	30	6	5
CS-2	4	80	9	12	2.4	3.6
CS-3	5	60	4.2	6	1.2	1.26

Volumetric strain is calculated from the measured soil settlement (due to a given action; either surcharge or inundation) divided by the original soil depth (prior to the given action commenced) in the tank. Also, collapse strain is estimated for each test case, as given in Table 3.17. The estimated collapse (volumetric) strain is based on collapse potential (collapse strain at 200 kPa inundation pressure) and the concept of direct proportional relation between the collapse strain and the inundation pressure. From Table

3.17, estimated and measured collapse strains are close for all the cases, similar to the findings of Nouaouria et al. (2008). The effect of inundation pressure on soil collapse is
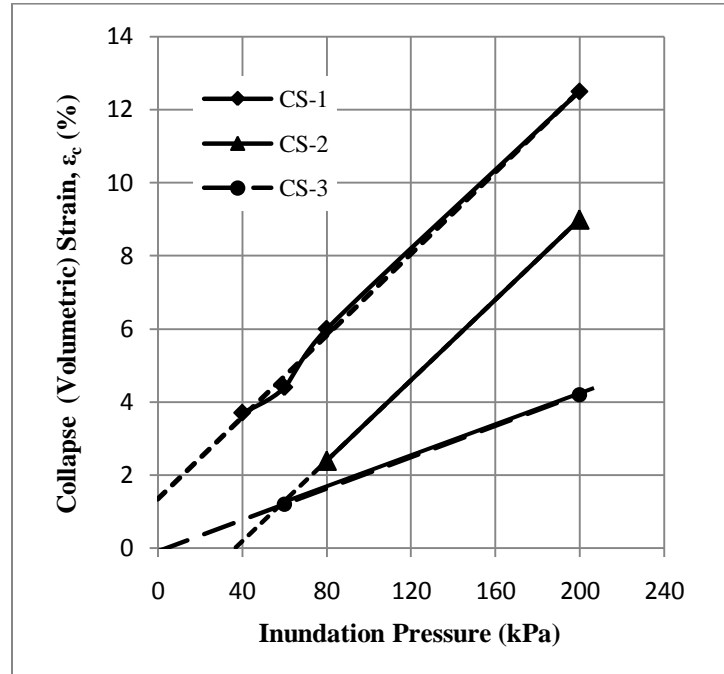
Figure 3.18: Effect of inundation pressure on collapse (volumetric) strain (after Mashhour, 2009)

studied in Figure 3.18. In this figure, the data-point, corresponding to 200 kPa inundation pressure, is the collapse potential (known from the oedometer test) of a given soil. Three collapsible soils, used in the model tests by Mashhour (2009), responded to inundation pressure in three different ways. Based on the figure, CS-1 (C_p of 12.5) showed some collapse during inundation without any pressure, while CS-3 (C_p of 4.2) experienced collapse after a critical value of inundation pressure (40 kPa).

3.5.1.1 Numerical Modeling of the Model Pile Test (by Mashhour, 2009)

The reduced scale tests (Mashhour, 2009) are numerically modeled to predict indirect load (Q_n) due to negative skin friction (NSF). No further scale effect is to consider as the same dimension of experimental model setup is used in developing its geometry model. Instead, some important issues, regarding the use of finite element program of PLAXIS (originally developed for saturated soil) are taken into considerations for modeling

collapsible soil (i.e. highly porous at unsaturated condition) during inundation. In this respect, the model of a reduced scale setup is used to calibrate the PLAXIS data input (including surcharge and volumetric strain) to make it useful for modeling the collapsible soil (initially unsaturated) subjected to inundation.

For all the collapsible soils (used by Mashhour, 2009), phase III (reassign the material dataset) in staged construction, does not have insignificant effect on the numerical results and therefore omitted, as these soils were found non-plastic or have low plasticity index (2.6). It is earlier mentioned that strength reduction during inundation, is insignificant for such soils, with low plasticity index. Three different collapsible soils, as given in Table 3.18 and Table 3.19, were used in the model test tank. By mixing different percentages of clay with sand, each collapsible soil was prepared to have different collapse potentials.

Table 3.18: Collapsible soils used in the model test (Mashhour, 2009)

Soil	Collapse Potential, C_p (%)	Clay Content (%)	Void Ratio, e	Liquid Limit, LL	Plastic Limit, PL	Plasticity Index, PI
CS-1	12.5	10	0.7	15.9	13.3	2.6
CS-2	9	8	0.69	N.A	N.A	N.A
CS-3	4.2	6	0.67	N.A	N.A	N.A

Table 3.19: Properties of collapsible soils used in model tests (Mashhour, 2009)

Soil	Cohesion, c (kPa)	Angle of internal friction, φ (°)	Modulus of elasticity, E (kPa)	Diala tanc, Ψ (°)	Coefficient of lateral earth pressure, K_0	Unsaturated unit weight γ_{un} (kN/m³)	Saturated unit weight, γ_{sat} (kN/m³)	Specific gravity, G_s
CS- 1	15.5	35	30,000	5	0.43	16.2	20	2.67
CS- 2	12.5	38.5	30,000	8.5	0.38	16.2	20	2.67
CS- 3	9	40	30,000	10	0.36	16.2	20	2.67
Dense Sand	1	40-50	45,000	10-20	0.36-0.23	18.2	21	2.67

Table 3.20: Model pile properties

Pile Geometry and Dimension		Pile Properties		
Pile Length, L_p (m)	Diameter of pile d_p (m)	Poisson Ratio υ_p	Modulus of Elasticity E_p (kN/m^2)	Unit Weight γ_c (kN/m^3)
0.5	0.025	0.33	2E+11	77

Table 3.20 presents properties of the model pile used in the experimental program. The model pile has sufficient surface roughness. Therefore, the pile interface strength is taken as 80% of the surrounding soil shear strength.

In developing the geometry model of this test setup, sufficient depth below the pile tip is provided. The clusters (i.e., representing a layer below the pile tip) are given the properties of strong soil, like dense sand, as given in Table 3.19. In the experimental test setup, the model pile was supported at the bottom of the tank, where a load cell was connected with the pile.

Collapse (volumetric) strain is an input parameter, in the finite element program, to study the effect of inundation. Therefore, volumetric strain (ε_v) is derived from the collapse (volumetric) strain attained (ε_c) in each test case. It should be mentioned here that ε_v and ε_c are not equal, rather correlated by a calibration factor as in Eqn 3.20. The collapse (volumetric) strain (ε_c) is determined from the collapse potential (C_p) after the adjustment for inundation pressure (i.e., the overburden pressure and surcharge) at the middle of each collapsing layer, as given in Eqn 3.22. The following relation, between the collapse strain and the inundation pressure, should be considered where the overburden pressure at the middle of each collapsing layer does not exceed 400 kPa, according to Nouaouria et al. (2008). Beyond this limit, collapse strain remains constant with the increase of inundation pressure.

$$\varepsilon_c = \frac{C_p}{200} * (\sigma + \gamma h_{mid}) \dots\dots\dots\dots\dots\dots\dots\dots\dots\dots\dots\dots\dots\dots\dots(3.22)$$

It is important to recognize the difference between the negative skin frictions due to the collapse of a porous soil (collapsible) and a soil with normal porosity. Pile is indirectly loaded through negative skin friction due to the collapse (volumetric) strain in the surrounding soil. The calibration factor (C) is introduced to take such effect into consideration. Negative skin friction will be obtained higher than the actual measured

one, if the calibration factor is not applied. The five model tests are used to establish the calibration factor (C). The value of C is found 0.1 consistently.

Inundation is introduced after the effect of applied surcharge on the soil volume diminished. Therefore, the effect of surcharge is included into the numerical modeling through the input value of volumetric strain, rather than applying it in defining the geometry model. Due to the application of a surcharge (40 kPa or more) on the soil surface, FE model leads to a very high settlement (about 30 mm) whereas the collapsible soil (at initial moisture condition) settled very small (5─7 mm) in the tank, as given in Table 3.16. In the finite element calculation, the effect of matric suction is ignored above the general phreatic line. Therefore, unsaturated collapsible soil, which is very strong due to high matric suction and thus preventing the soil structure to allow significant rearrangement of grains within the soil structure, cannot exhibit that strength in FE analysis. Accordingly, any surcharge (40 kPa or more), applied in PLAXIS calculation, results high settlement, which is about 6 times the experimentally measured settlement. This implies that the application of unfactored surcharge would be a source of considerable error and hence it is not included directly.

3.5.1.2 Comparison of Results between Present Study and Mashhour (2009)

Pile is numerically studied under its self weight and indirect load due to the volumetric strain (ε_v) resulting from the soil collapse. Comparison of results is carried out for indirect load (Q_n) due to inundation only. Numerically predicted Q_n due to negative skin friction (collapse) is compared with the experimental value. The experimentally measured Q_n due to inundation (collapse) is obtained from the total Q_n (due to surcharge and inundation) after subtracting Q_n due to surcharge as measured in each test. In this thesis, Q_n due NSF means the developed NSF due to inundation only

Numerical results are compared with the experimental results at two different stages of inundation when the water level raised up-to the half-depth and the three-quarter-depth from the bottom of the collapsible layer. The saturated depth of the collapsing soil (H_s) was increasing from 0 to 50 cm (average in each test) during the test period. The ratio of depth of collapsing soil (H_s)-to-pile diameter (D) was 9.8, 14.5 and 19.6 for half-depth, three-quarter-depth and full-depth saturation of collapsible soil (from bottom), respectively. Figure 3.19─Figure 3.23 compare predicted (numerically) negative

skin friction (Q_n) with experimentally measured values in five tests. In each figure, the trend-line of experimental data shows the value of negative skin friction as the level of water in the tank goes up.
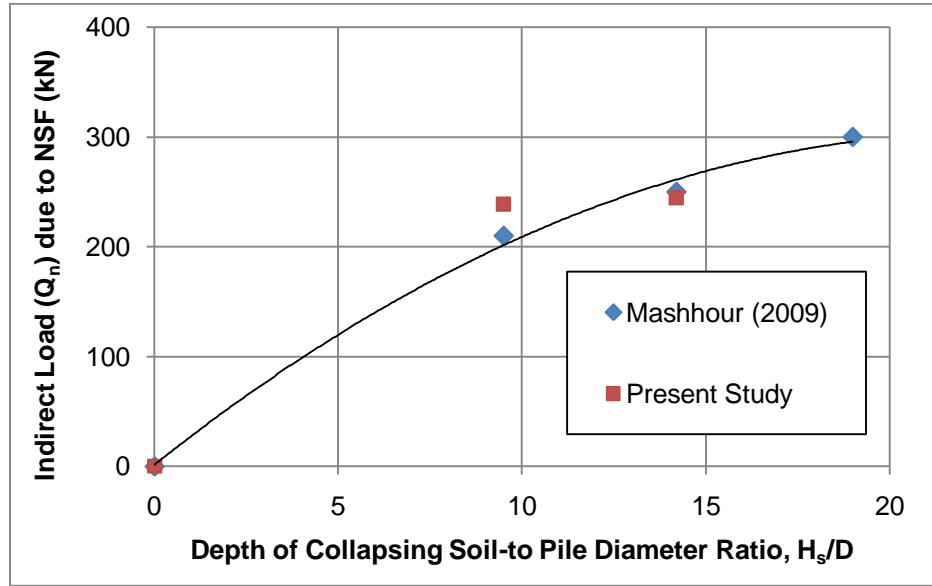
Figure 3.19: Effect of depth of collapsing soil-to-diameter (H_s/D) on indirect load (Q_n) due to NSF (Test -1 in table 3.17)
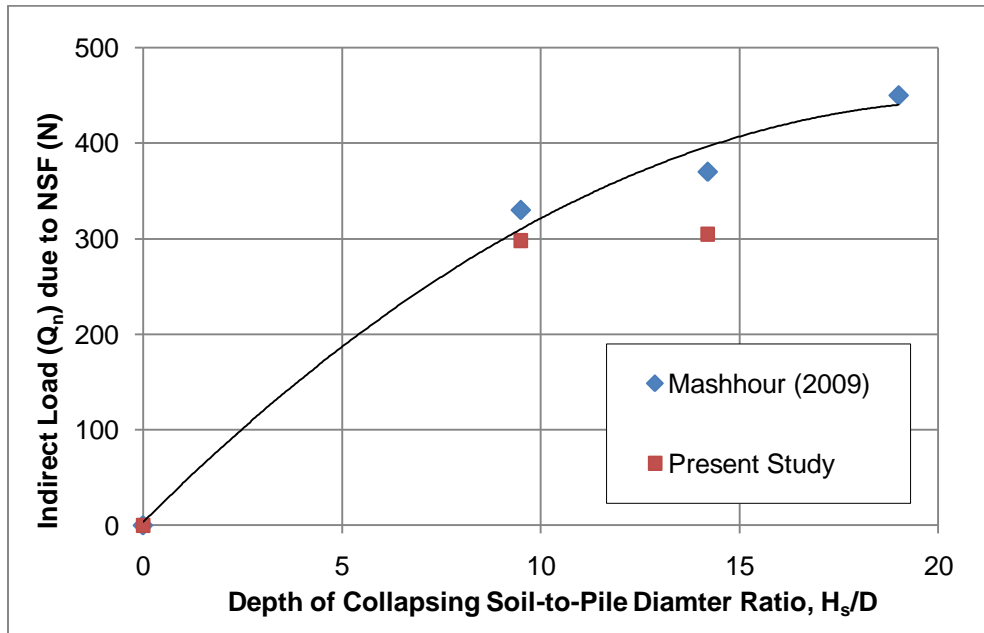
Figure 3.20: Effect of depth of collapsing soil-to-diameter ratio (H_s/D) on indirect load (Q_n) due to NSF (Test-2 in Table 3.17)
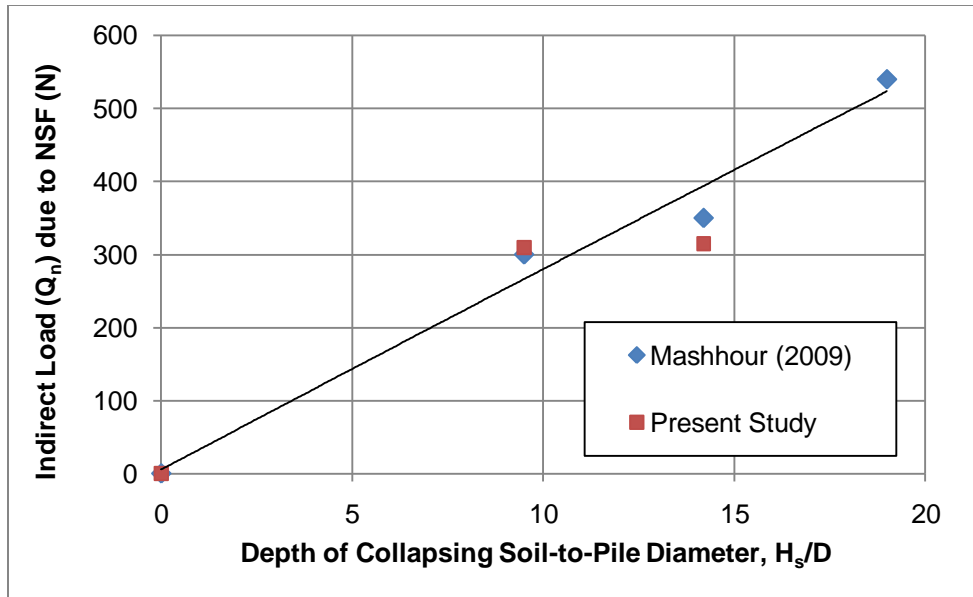
Figure 3.21: Effect of depth of collapsing soil-to-diameter ratio (H_s/D) on indirect load (Q_n) due to NSF (Test – 3 in Table 3.17)
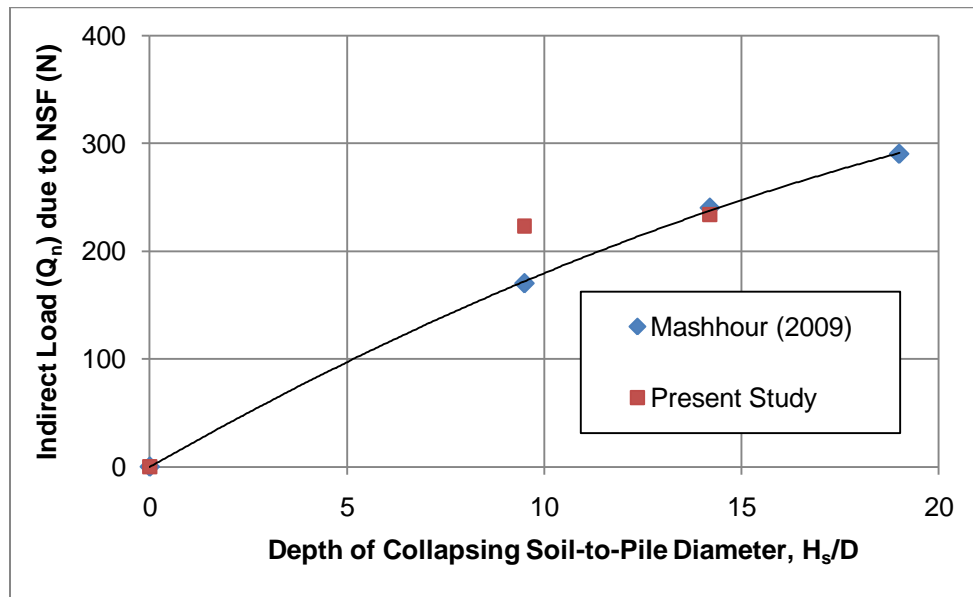
Figure 3.22: Effect of depth of collapsing soil-to-diameter ratio (H_s/D) on indirect load (Q_n) due to NSF (Test – 4 in Table 3.17)

90
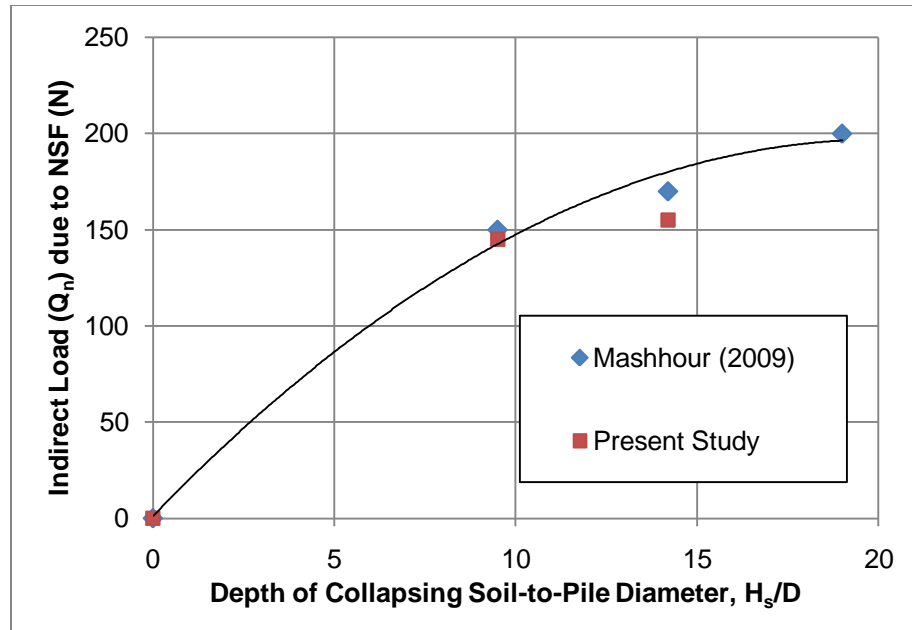
Figure 3.23: Effect of depth of collapsing soil-to-diameter ratio (H_s/D) on indirect load (Q_n) due to NSF (Test – 5 in Table 3.17)

The stage of full depth saturation of collapsible soil, when H_s/D is 19.8, is not considered in comparing numerical values with the experimental ones. Because, a deep layer of dense sand (which did not exist in the experimental setup) below the pile tip is applied while developing the numerical model. This difference in simulating the experimental model might cause considerable difference between the numerical and the experimental results, when the indirect load (Q_n) on the pile increases due to the increased depth of saturated collapsible soil (H_s). Based on the numerical results as shown in Figures 3.19–3.22, it can be stated that numerical value of Q_n will be obtained less than the experimental one at the full-depth saturation (H_s/D of 19.8). Good agreements between the numerical and the experimental results can only be expected, until additional indirect load on the pile (due to negative skin friction) exceeds the ultimate base resistance at the pile tip, or if the indirect load is not sufficient to cause any significant settlement. In the laboratory setup, the pile was of end bearing type, and therefore, even high indirect load could not cause any pile settlement. On the other hand, the pile tip in the finite element model rests on a deep layer of dense sand. In the finite element model, the pile settles into the dense sand layer, as the load (i.e., the indirect load

91

due to negative skin friction) on the pile increases with the progressive saturation of collapsible soil. As collapse commences near the bottom part of the pile, positive skin friction disappears from the entire pile surface (pile head to tip). Therefore, the limit of base resistance, due to the developed negative skin friction on the pile surface, exceeded fast due to the small tip area of the model pile. The use of dense sand properties below the pile tip could not adequately increase the base resistance, as the small size of the tip area dominated in this respect. In the finite element analysis, Q_n causes pile to settle when its magnitude exceeds a critical value (depending on the ultimate base resistance). A portion of Q_n is released due to the initiated relative movement between the pile and the collapsing soil, i.e. the pile settlement. Thus, Q_n on a pile, which is allowed to settle, is less than that on an end bearing pile (e.g. supported by rock at the pile tip).
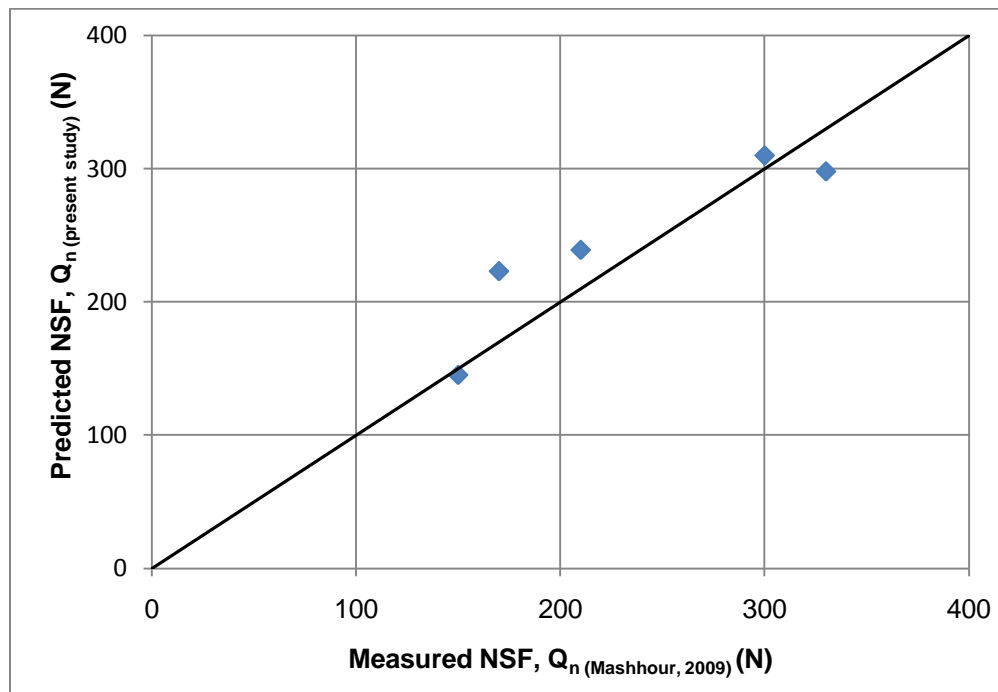
**Figure 3.24: Comparison of numerical and experimental results
(collapse of bottom half of the collapsible soil)**

For this reason, this study considers half-depth (H_s/D of 9.5) and three-quarter depth (H_s/D of 14.2) saturation stages for comparison. Approximately, Q_n due to saturation from half to three-quarter depth is found as the critical point beyond which the pile experiences considerable settlement due to the indirect load (Q_n). Figure 3.24 and

Figure 3.25 present the comparisons between the numerical and the experimental results for half depth and three-quarter depth inundation from bottom, respectively. There are good agreements between the numerical and the experimental results.
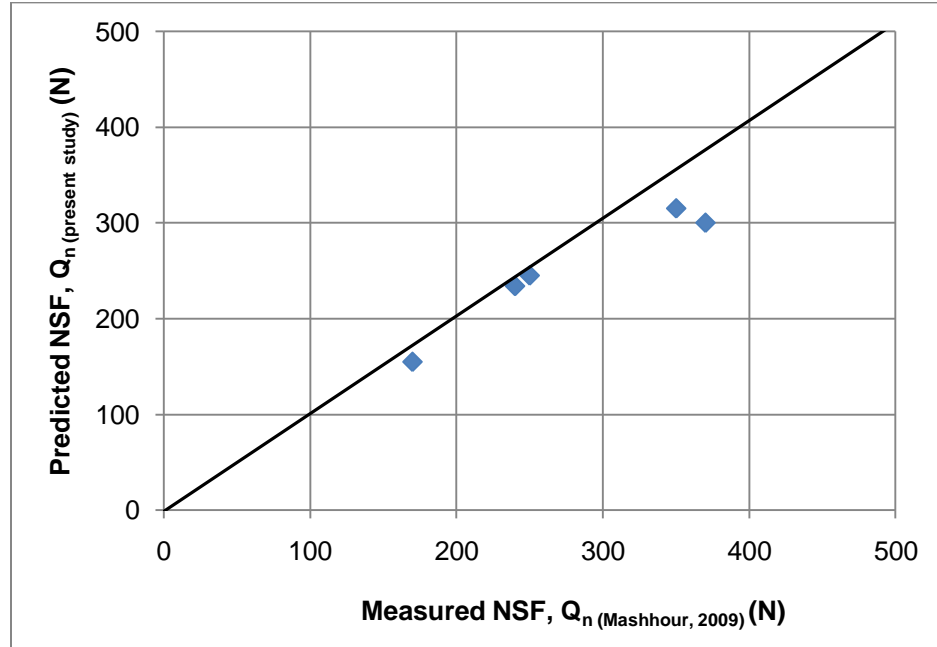
Figure 3.25: Comparison of numerical and experimental results
(collapse of three-quarter depth from bottom of the collapsible soil)

3.5.2 Modeling of Full-Scale Pile Tests (by Grigoryan, 1997)

The performance of the proposed procedure of modeling collapsible soil during inundation is tested using the full scale experimental results (Grigoryan, 1997). Two different cases, as given in Table 3.21, are addressed.

Table 3.21: Experimental investigations of full scale tests

Soil Collapse	Original Thickness of Collapsed Layer (m)	Depth of Collapsed layer from surface (m)	Collapse Potential, C_p (%)	Experimental Region	Reference
At Depth	4	11	8	Volgodon-2	Grigoryan (1997)
Near Surface	6	0	7	Nikopol	Grigoryan (1997)

In the test at Volgodon-2, a special method of local wetting the collapsible soil layer was adopted during the field test setup. A circular trench, 0.5 m wide and 1 m deep, was dug around each pile, as shown in Figure 3.26. Four equally spaced drainage holes were made from the bottom of the circular trench. Drainage holes were 0.17 m in diameter and its length was 16 m (i.e. 2 m less than the length of the test pile). Both the circular trench and the drainage holes were filled with the draining material. Throughout the test period, 500 m^3 of water was used in the circular trench and the water level was kept steady throughout the test. Local wetting around the pile was induced after the pile was installed.
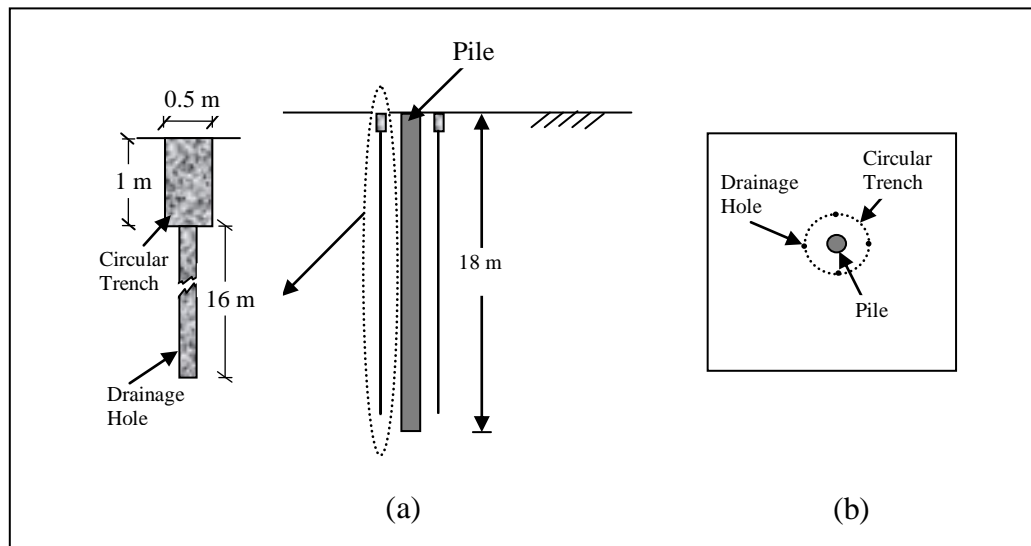
Figure 3.26: Method of local wetting of collapsible soil using circular trench and drainage holes at Volgodon-2; (a) Profile of the test setup, (b) Plan view of the test setup

In the test at Nikopol, full-scale pile test under prolonged wetting (from top) was carried out in a test pit (20 m x 20 m plan area and 1 m deep). The water level, in the test pit was maintained at a height of 0.5 m for 2.5 months. The test period covered all three collapse phases. Therefore, 6000 m^3 water was required up to the end of such a test.

In the Volgodon region, collapsible soil existed up to a depth of 15 m from the ground surface, initially unsaturated, and overlying a deep non-collapsible bed of dense loam. The test piles were 18 m long, and therefore, the last 3 m of the pile was embedded into a deep non-collapsible bed. Groundwater table was found at a depth of 25 m from the ground surface.

In the Nikopol region, collapsible soil was up to a depth of 8 m from the ground surface. Below 8 m, the soil had low collapse potential (<2%). Therefore, the last 14 m (of 22 m long pile) of the pile had contact with collapsible soil having insignificant collapse potential.

The physical and mechanical properties of the soil profile at Volgodon-2 and Nikopol regions are summarized in Table 3.12. In both regions, unsaturated collapsible soils, having plasticity index around 8, did not have very high cohesion, actually ranges between 14 and 24 kPa. The reduction of cohesion was low for such soils subjected to inundation, and accordingly the strength reduction is ignored in the numerical investigation.

The full scale test piles were of bored and cast-in-situ type. At different pile sections, measuring devices were installed to record stress or strain, i.e. a function of the axial load at that level.

The pile, tested in Volgodon, was equipped with three vibrating wire type dynamometers, at the depths of 5 m, 11 m and 15 m from the pile head. A ground dynamometer (designed by the Research Station of Gidroproekt) was set up at the base level of the pile. The steel wire (an element of a dynamometer) caused a variation in the vibration frequency due to any change in the axial load at that section. Therefore, the longitudinal force (at a pile section) and the normal stress at the pile base were interpreted from the dynamometer readings by Grigoryan (1997).

The pile, tested in Nikopol, was equipped with three strain gauge dynamometers at 9.2 m, 12.3 m and 22 m (pile tip) from the pile head. The strain gauge dynamometer was specially designed with electrical sensors, developed at the Central Scientific-Research Institute (TsNIIK in Russian). The dynamometer was installed within the pile stem, so that the full longitudinal force could pass through it. The principle component of a strain gauge dynamometer was the elastic ring, made of high strength steel. The elastic ring was placed between two steel plates of 10 mm thick. The steel plates, with the elastic ring inside, were covered by rubber casings, of 3─4 mm thick. The rubber casing was used for the protection of the steel plates and the elastic ring. Individual pile section was welded to the steel plates. Each cable (wire), attached to the elastic ring, was brought to the ground through separate pipe. Pipes were covered with bitumen to prevent cohesion

between the pipe and the concrete. In the laboratory, the gauge reading showed no effect of moisture and temperature variations, insulation condition of conductors and oxidation of contacts. Dynamometer measures deformation gave the magnitude of the axial load at the point where it was installed. This dynamometer was calibrated in the laboratory and recalibrated after the pile installed in the ground. The calibration was made up to a load of 1000 kN.

Table 3.22 presents the dimensions and properties of the piles used in the full scale experiments at Volgodon-2 and Nikopol (Grigoryan, 1997). The length-to-diameter ratio (L/D) is 18 and 44 for the piles at Volgodon and at Nikopol, respectively.

Table 3.22: Pile geometry, dimension and properties

Experimental Region	Pile Geometry and Dimensions		Pile Properties		
	Pile Length, L (m)	Diameter of pile D (m)	Poisson Ratio υ_p	Modulus of Elasticity E_p (kN/m^2)	Unit Weight γ_c (kN/m^3)
Volgodon-2	18	1	0.33	3E+07	24.5
Nikopol	22	0.5			

The full scale pile tests in collapsible soil are modeled by defining three phases; Initial Phase, Phase I (pile installation) and Phase IV (applying volumetric strain). Phase III is omitted since the unsaturated cohesion of the collapsible soil was not high and the plasticity was low.

3.5.2.1 Comparison of Results between Present Study and Grigoryan (1997)

The calculation of negative skin frictions, based on the experimental results of Grigoryan (1997), is given in Table 3.23 and Table 3.24.

Table 3.23: Estimation of negative skin friction and pile resistances from full-scale pile test results at Volgodon

External Load, P (kN)	-	0	No Load Condition
Self Weight of the Pile Section 5-15m: $W_{(5-15m)}$ (kN)	-	192	-
Axial Load at 15m: P_{15} (kN) During Inundation	-	740	-
Negative Skin Friction, Q_n (kN) due to collapse of 11-15m	Calculated from experimental data	548	$Q_n = P_{15} - W_{(5-15)}$
Negative Skin friction, Q_n (kN)	Numerical result	518	-

Table3.24: Estimation of negative skin friction and pile resistances from full-scale pile test results at Nikopol

External Load, P (kN)	-	600	-
Self Weight of the pile section 0-9m: W_9 (kN)	-	43	-
Axial Load at 9m: P_9 (kN)	P_{9b}	40	P_{9b} (before inundation)
	P_{9max}	550	P_{9max} (during inundation)
Increase in Axial Load at 9m: Due to inundation	ΔP_9	510	$\Delta P_9 = P_{9max} - P_{9b}$
Positive Skin Friction, Q_s (kN): Before Inundation	$Q_{s(0-9m)}$	603	$Q_{s(0-9m)} = P + W_9 - P_{9b}$
Negative Skin Friction, Q_n (kN) due to collapse of 0-6m	$Q_{s(0-6m)}$	301	$Q_{s(0-6m)}$
	Calculated from experimental data	209	$Q_n = \Delta P_9 - Q_{s(0-6m)}$
Negative Skin Friction, Q_n due to collapse of 0-6m	Numerical result	180	--

Table 3.25 compares finite element results, obtained in this study, with the experimental data from Grigoryan (1997). In both conditions, numerical results of Q_n are reasonably well as compared to the experimental data; using the calibration factor established from the numerical modeling of Mashhour (2009) reduced scale tests. Furthermore, the numerical and the experimental results are in good agreement for positive skin frictional and end resistances (for collapse at depth in Volgodon-2), as in Table 3.25.

Table 3.25: Comparison between the full-scale test and the finite element analysis results

Case	Resistances	Experimental (Grigoryan, 1997)	FEM (Present Study)
Collapse at Depth (Volgodon-2)	Negative Skin Friction (kN)	548	518
	Positive Skin Friction (kN)	650	606
	End Resistance (kN)	235	251
Collapse near Ground (Nikopol)	Negative Skin Friction (kN)	186	180

When the pile at Volgodon was subjected to negative skin friction, the pile was under no external load condition. On the other hand, the pile at Nikopol was under 600 kN external load, and negative skin friction caused additional indirect load on the pile.

3.6 Sensitivity of Numerical Results to Deformation Theories

Sensitivity of the numerical results is tested for small and large deformation theories used in finite element calculations. The numerical model validation and calibration is carried out in this chapter using small deformation theory, because models were of small size and the collapse was also small. Moreover, the derived calibration factor that is used to determine the input volumetric strain into the program makes the calculation preference towards small deformation theory. However, as the problem related to collapse shows apparent involvement of large deformations, updated mesh analysis (i.e., a technique in PLAXIS to accommodate large deformation problem) is explored to test sensitivity of the numerical model. Both the small deformation theory and the updated mesh analysis are carried out for some selected cases, as presented in Table 3.26. The definitions of thickness of collapsible soil (H), depth of collapsing soil (H_s), radius of wetting (h) and collapse potential (C_p) are described in Figure 4.6.

Table 3.26: Selected cases in comparing the predicted values obtained from small deformation theory and updated mesh analysis

Case #	Thickness of collapsible soil, H (m)	Depth of collapsing soil, H_s (m)	Radius of wetting h (m)	Collapse potential, C_p (%)
1	14	7	5	5
2	8	4	10	5
3	10	5	5	7
4	12	6	5	10
5	12	6	5	10
6	12	6	10	5
7	14	7	15	3
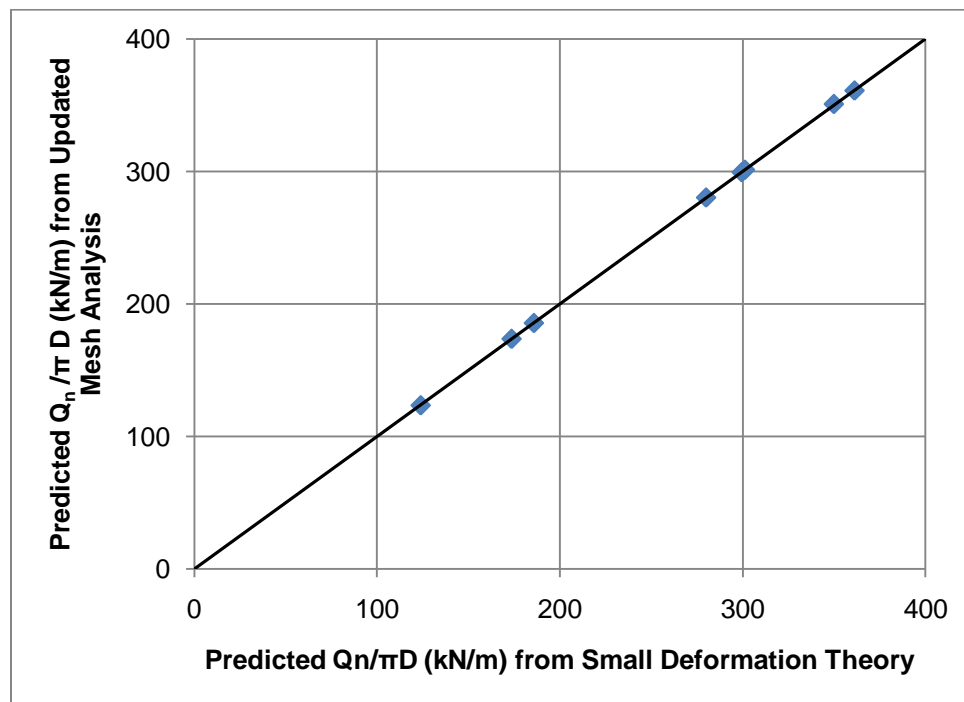
Figure 3.27: Comparison between unit negative skin friction ($Q_n/\pi D$) values predicted from small deformation theory and updated mesh analysis

The values of unit negative skin friction ($Q_n/\pi D$) from both types of finite element calculations (in Figure 3.27) are found comparable. Therefore, the numerical model can be executed using small deformation theory.

3.7 Development Numerical Model for Pile Design in Collapsible Soil subjected to Inundation

This section introduces a numerical approach to assist pile design, subjected to both the direct (external) and the indirect (due to negative skin friction) loads. The magnitude of the drag force, Q_n due to the volume decrease of a known thickness of inundating collapsible soil, is required in implementing this approach. The value of Q_n can be known from the analytical models (presented in Chapter 5). The resultant drag force and the external loads are applied at the centre of the pile cross-section at the bottom of the collapsible soil subjected to inundation, as a point load (force per radian). Further, mobilization of any skin friction in the pile interface, which is in contact with the collapsible soil showing volume decrease, is restricted by adjusting the 'Interface' material set. For the interface with the collapsing soil and also with the layers overlying collapsing one, the cohesion (c) and the angle of shearing resistance (φ) of the 'Interface' material set are set 1 kPa and zero, respectively. Otherwise, the interfaces are assumed to have reduced strength using an interface strength reduction factor to the corresponding soil layer.

Table 3.27: Frictional and base resistances under inundation

External Load on Pile Head (kN)	Inundation Condition	Skin Frictional Resistance (kN)		Base Resistance (kN)	
		Experimental (Grigoryan 1997)	FEM	Experimental (Grigoryan 1997)	FEM
0	Yes	650	598	235	248

The numerical results are compared well with the experimental data. This modeling approach benefits the Geotechnical Engineers in designing the pile foundation under a given inundation condition.

3.8 Discussion

This chapter presents detail of the numerical model developed to incorporate the effect of inundation of collapsible soil on the performance of pile. The developed model is validated using available experimental results from the literature. The numerical model is found to predict negative skin friction resulting from the inundation of the collapsible soil successfully, while it was not possible previously. According to Grigoryan (1997), each full scale pile test under such test condition, took about 2─3 months excluding the time for experimental setup. Moreover, instrumented pile is difficult to construct and install. Measuring devices are very sensitive to inundation and method of installation as well. Therefore, after installing pile and commencing wetting, it was commonly found that some of the devices were not working. Full scale pile test are time consuming, expensive and difficult to achieve sensible results. Similarly, model pile tests are also difficult to conduct, as experienced by Mashhour (2009). Furthermore, model pile test results cannot provide direct knowledge about the negative skin friction under the field condition. Moreover, the effects of length and diameter of the pile and the radius of wetting front could not be examined based on the model pile test results. In designing pile foundation in collapsible soil, several parameters are involved, as discussed in Chapter 4. In addition to that, wetting from top is difficult to achieve, while the test program of Mashhour (2009) studied the case of wetting from bottom only. When soil is subjected to inundation from top, induced wetting is usually non uniform, and it takes long time to saturate the soil as the soil cannot be flooded with the required water at the beginning. The advantage of model pile test is taken in the validation of the numerical model, while its limitations are handled with caution. First of all, the results of the model test are not extrapolated to full scale data. Rather, the numerical model is developed as same as the model test setup in the laboratory. Then, the edge effect is eliminated in both cases by taking a reasonable dimension of the tank, as compared to the pile dimensions. Also, model test results can give useful information on relative effect of parameters and help in understanding the influence of various parameters. In this study, the model test results are used to calibrate the model, relating the input volumetric strain and the expected collapse strain based on the collapse potential. The calibration factor for volumetric strain input is found as a relative adjustment factor. Most importantly, good agreements between the numerical and

the full scale pile test results are noted in predicting negative skin friction, for the same calibration factor, as established based on the model pile tests of Mashhour (2009). The developed numerical model and the calibration factor can be used to predict negative skin friction on the pile under any geo-environmental condition. It requires simply the volumetric strain attained at the moment of interest.

Also, a procedure is presented here to study the performance of pile (in terms of shaft and pile tip resistances) if collapsible soil is subjected to inundation, provided the magnitude of indirect load due to negative skin friction is known. The advantage of the later modeling procedure over the former numerical model is that pile performance can be easily examined and suitable pile geometry can be obtained without calculating the volumetric strain, strength reduction of collapsible soil, etc.

CHAPTER 4

RESULTS AND ANALYSIS

4.1 General

The factors, affecting the magnitude of indirect load (Q_n) due to negative skin friction (NSF), are not identified yet due to the limited data available in the literature. With the present knowledge, for a given case of soil and inundation conditions, only the increase of Q_n due to the increase in pile diameter (D) can be predicted. Instead, several factors such as thickness and location of collapsing soil, collapse potential, pile geometry and roughness, radius of wetting, direction of inundation, etc., may have combined effects on the performance of a pile in collapsible soil subjected to inundation. In this chapter, the proposed numerical model is used to investigate NSF developed on the pile interface due to soil collapse. Analysis of experimental results, of small scale pile load tests in collapsible soil subjected to inundation, from Mashhour (2009) provides a basis in the parameter identification. This study conducts an extensive numerical investigation to examine the effects of such parameters on the development of NSF resulting from full inundation of a given collapsible layer in a single event.

4.2 Analysis of Experimental Results of Mashhour (2009)

The experimental data from Mashhour (2009) are analyzed here to understand the relative influences of some factors, such as inundation pressure (σ), depth of collapsing soil-to-pile diameter ratio (H_s/D) and volumetric strain (ε_v) on the indirect load (Q_n) due to NSF.

Figure 4.1 presents the effect of inundation pressure on Q_n due to NSF using the results of the tests 1–3. In these tests, the same soil (CS-1) was used to fill the test tank and also the same test procedure (briefly discussed in Chapter 3) was followed. The only exception is the magnitude of surcharge (i.e., inundation pressure) applied on the soil surface in each test. The applied surcharges are 40, 60 and 80 kPa and the corresponding volumetric strains are measured 3.6, 4.4 and 6%, for Test 1, Test 2 and Test 3,
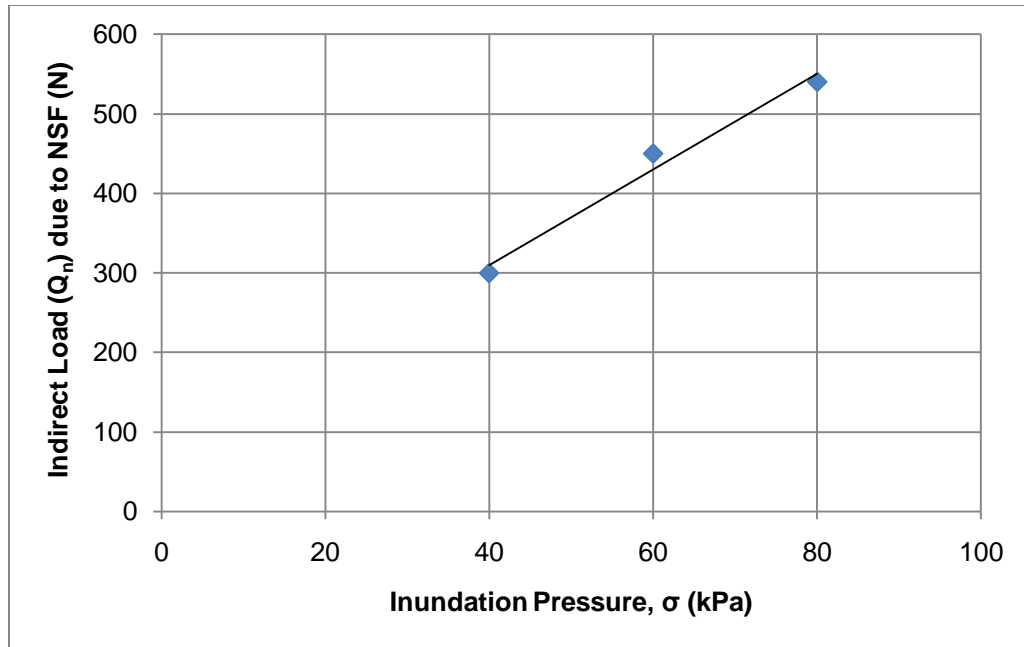
Figure 4.1: Effect of inundation pressure (σ) on indirect load (Q_n) due to negative skin friction (NSF), when $H_s/D = 19.8$

respectively. The data-points (of Figure 4.1) represent the measured values of Q_n in three tests (1–3) at the full-depth of inundation stage (i.e., attained at the end of each test). Q_n is found directly proportional to inundation pressure (σ). This implies that the thickness of the soil layer (related to inundation pressure), overlying the collapsible layer subjected to inundation, is an important factor, as its own overburden weight is an unavoidable source of inundation pressure for the underlying collapsible soil layer. It can be explained from two other points of view: thicknesses of collapsible soil (in prototype configuration) and volumetric strains. Firstly, the value of the indirect load (Q_n) due to NSF increases if the thickness of collapsible soil layer increases. Test 3, having the thickest layer (10.6 m) of collapsible soil and the largest pile diameter among three prototype configurations of tests 1–3, gives the highest value of Q_n resulting from the collapse. Secondly, the higher the volumetric strain (ε_v), the higher the Q_n is. In Test 3, collapsible soil (in the test tank) experiences the highest average volumetric strain, because of the greatest overburden pressure at the mid-depth of the collapsible layer. It is to note that these are the statements for a given soil.

104
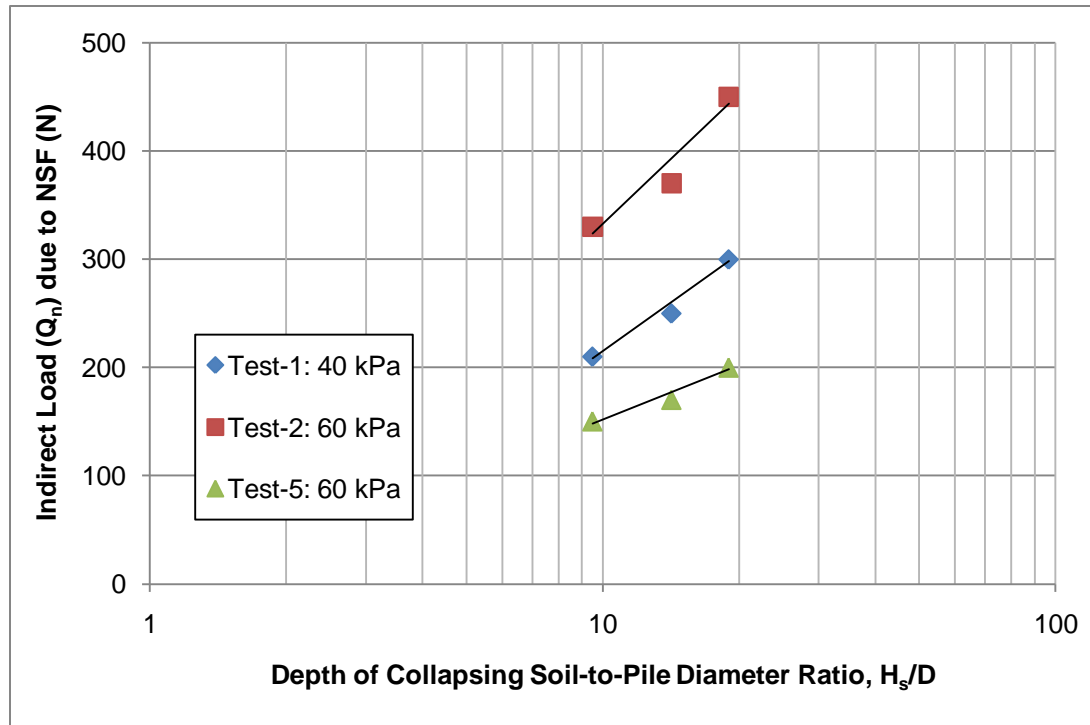
Figure 4.2: Effect of H_s/D ratio on indirect load (Q_n) due to NSF

Two statements, just made based on Figure 4.1 (i.e., the case of full inundation), are also noticed at two other stages of the progressive inundation from the bottom of the tank, as shown in Figure 4.2 and Figure 4.3. The H_s/D ratio, a non-dimensional parameter, represents the stage of progressive inundation for a given test setup. For the first statement, the results of Test 1 and Test 2 in Figure 4.2 can be compared. For the second statement, results of Test 2 and Test 5 in Figure 4.2, and Test 3 and Test 4 in Figure 4.3 can be studied. The developed NSFs are found higher in Tests 2 and 3 than those in Tests 5 and 4, respectively, though all the tests are carried out under the same inundation pressure (model test) or the test setups are of same prototype thickness of collapsible layer. Therefore, the trend of NSF can be predicted for a given thickness of collapsible soil (or inundation pressure) based on the volumetric strain. Second statement also explains the observations of Test 1 and Test 2. Test 2 gives the higher NSF than Test 1, because the soil experiences greater volumetric strain in Test 2 at a given stage of inundation, H_s/D (i.e., non dimensional). Therefore, the first statement can be eliminated and the second one can stand alone.
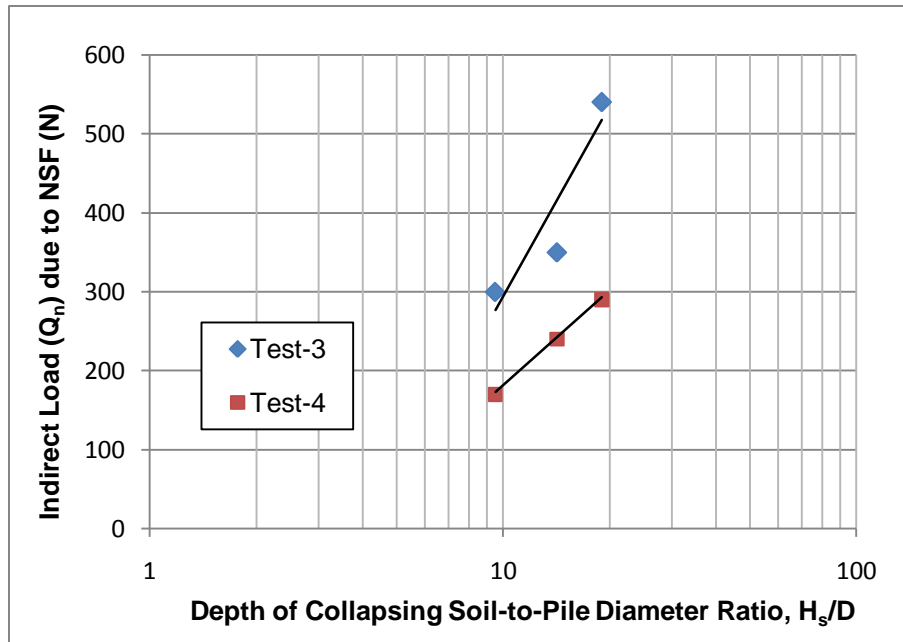
Figure 4.3: Effect of H_s/D ratio on indirect load (Q_n) due to NSF, inundation pressure (σ) = 80 kPa
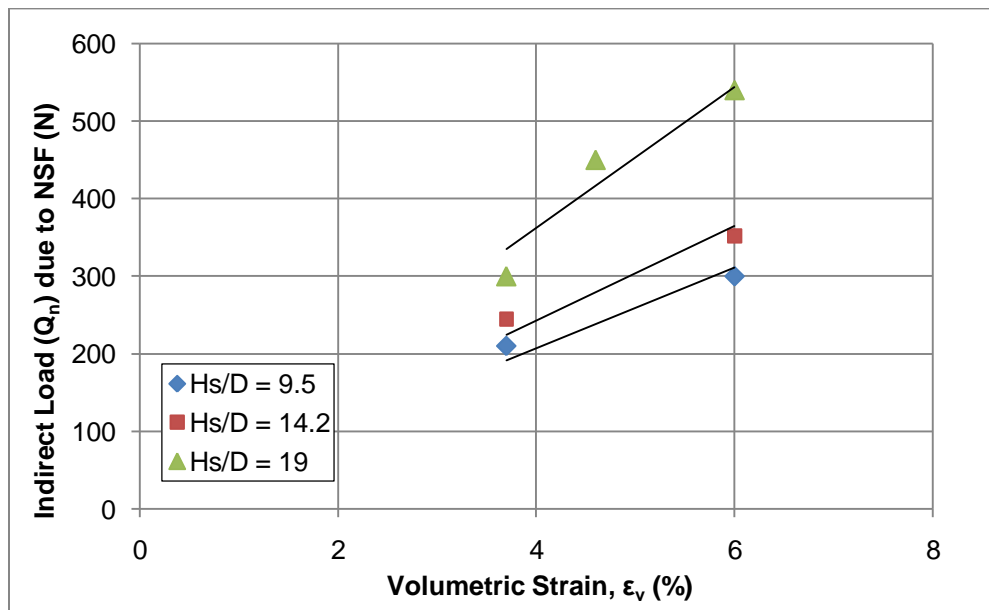

Figure 4.4: Effect of volumetric strain (ε_v) on indirect load (Q_n) due to NSF

The effect of volumetric strain on indirect load (Q_n) due to NSF is studied for a given collapsible soil and also for different collapsible soils in Figure 4.4 and Figure 4.5,

respectively. In Figure 4.4, it is found that Q_n increases with the increase of volumetric strain for a given stage of inundation and a given collapsible soil. In Figure 4.5, the same effect of volumetric strain is noted, while considering the results of five tests (using three collapsible soils) together.
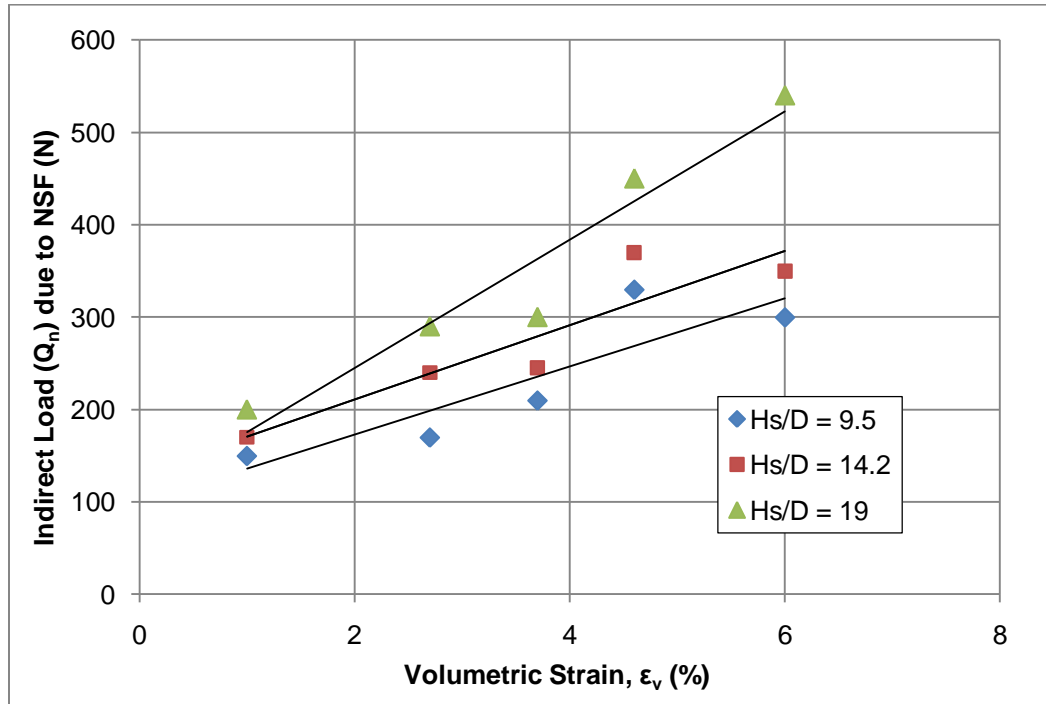
Figure 4.5: Effect of volumetric strain (ε_v) on negative skin friction

Note that the analysis of experimental results is limited to some extents, since pile diameter (D), pile length-to-diameter ratio (L/D), pile roughness, direction of wetting, radius of wetting, etc. are constants. The experimental program examines the effects of inundation pressure, depth of collapsing soil-to pile diameter ratio (H_s/D) and volumetric strain (ε_v) for the case of inundation from bottom. Direction of inundation from top and depth of embedment into the non collapsible soil (underlying the collapsible soil) cannot be studied experimentally.

4.3 Scope of the Parameter Identification

The proposed numerical model is used to identify the parameters seemed to govern both the negative skin friction and the depth of neutral axis. This chapter examines the effects

of different parameters including soil angle of internal friction (φ), collapse potential (C_p), pile length (L) and diameter (D), pile length-to-diameter ratio (L/D), depth of collapsible soil (H), depth of collapsing soil (H_s), radius of wetting front (h), embedded pile length (d_e) in non collapsible soil and interface strength reduction factor (ISRF) on the developed NSF during inundation of collapsible soil. The effect of both small and large deformation theories on the predicted results is also investigated. The term 'collapsing soil' is used for a certain part of the collapsible soil, which is subjected to inundation and experiences collapse (volumetric strain).

Table 4.1 presents the ranges of the parameters varied for both directions of inundation (from bottom and top). Figure 4.6 and Figure 4.7 show the details of the case studied schematically.

Table 4.1: List of parameter variations

Type	Parameters	Unit	Ranges
Soil Properties	Cohesion (c)	kPa	20
	Soil angle of internal friction (φ')	°	20 – 40
	Collapse Potential (C_p)	%	5 – 15
Geometrical Properties	Depth of collapsible soil (H)	m	8 – 15
	Depth of collapsing soil (H_s)	m	4 – 7.5
	$x = H_s/H$	-	0.5
	Length of pile (L)	m	12 – 30
	Diameter of pile (D)	m	0.2 - 1
	Pile length-to-diameter (L/D)	-	20 - 75
	Embedded pile length in non collapsible soil-to full pile length ratio (L_e/L)	-	0.3 – 0.75
	Radius of wetting front (h)	m	3 - 10
	Interface strength reduction factor (ISRF)	-	0.6 – 0.9
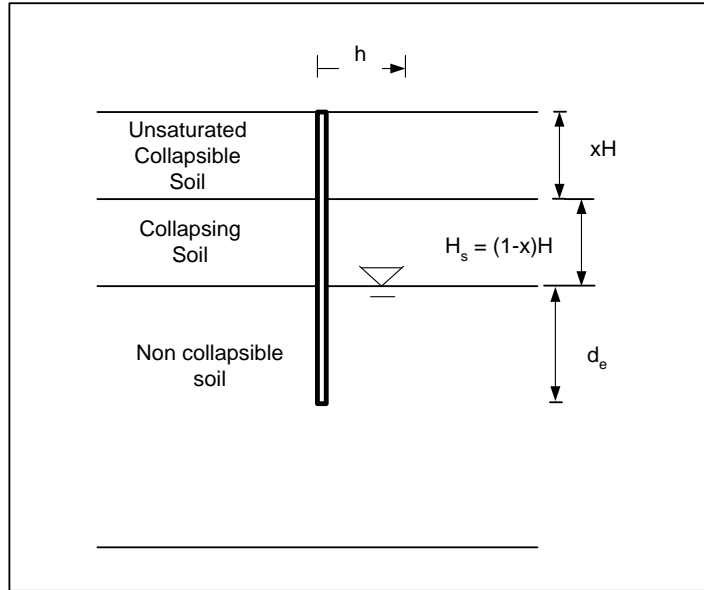
**Figure 4.6: Schematic diagram of the case studied: inundation from bottom**
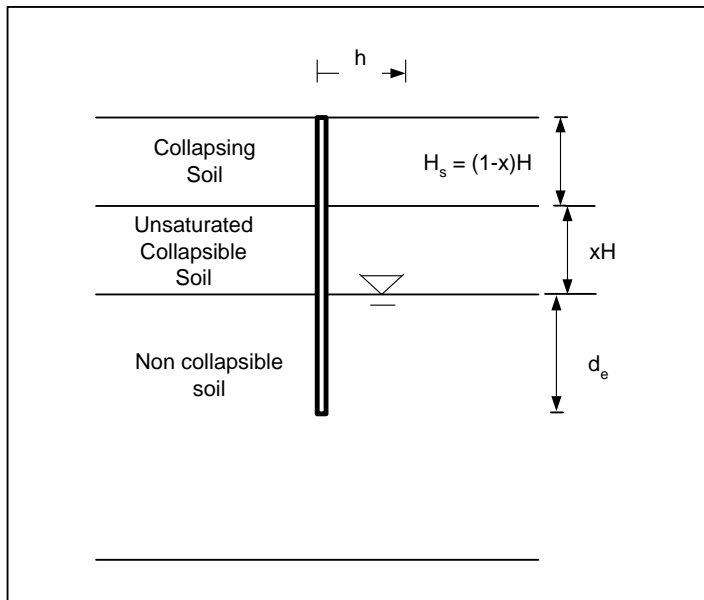
Figure 4.7: Schematic diagram of the case studied: inundation from top

This study considers non plastic collapsible soil, which usually has cohesion from 15 to 25 kPa at the unsaturated state and experience very small decrease during inundation. As already discussed in Chapter 3, for collapsible soil with low or no

plasticity, cohesion at the unsaturated state has a small contribution due to matric suction. Thus, this small matric suction contribution is ignored here, and the value of cohesion is always taken as 20 kPa. As a result, the step for adjusting soil parameters in the proposed numerical procedure is excluded from the numerical investigations conducted in this chapter. The value of angle of internal friction of collapsible soil is taken as 20˚, 30˚ and 40˚, as it usually ranges 20-40˚ in the literature. Both collapsible and non collapsible soils are given the same shear strength parameters.

The strength of pile-soil interface is based on the associated soil properties, reduced by interface strength reduction factor (ISRF). Dilatancy index (ψ) of interface element is kept zero, though the soil may have non zero values of it. The ground water table coincide the bottom line of the collapsible layer. Collapsible soil is overlying non collapsible bed, as shown in Figure 4.6. Two different directions of wetting (i.e., from bottom and from top) are considered in this investigation.

4.4 Sensitivity Analysis

Negative shear stress (i.e., NSF) develops on pile interface, if soil around the pile settles faster than the pile. During soil collapse, both the negative part (due to NSF) and the positive part (due to positive skin friction) constitute the shear stress distribution at the pile interface, as shown in Figures 4.8–4.11. Depth of neutral axis (N.A.) is the depth to the point of zero shear stress (in the shear stress distribution on the pile interface) from the ground.
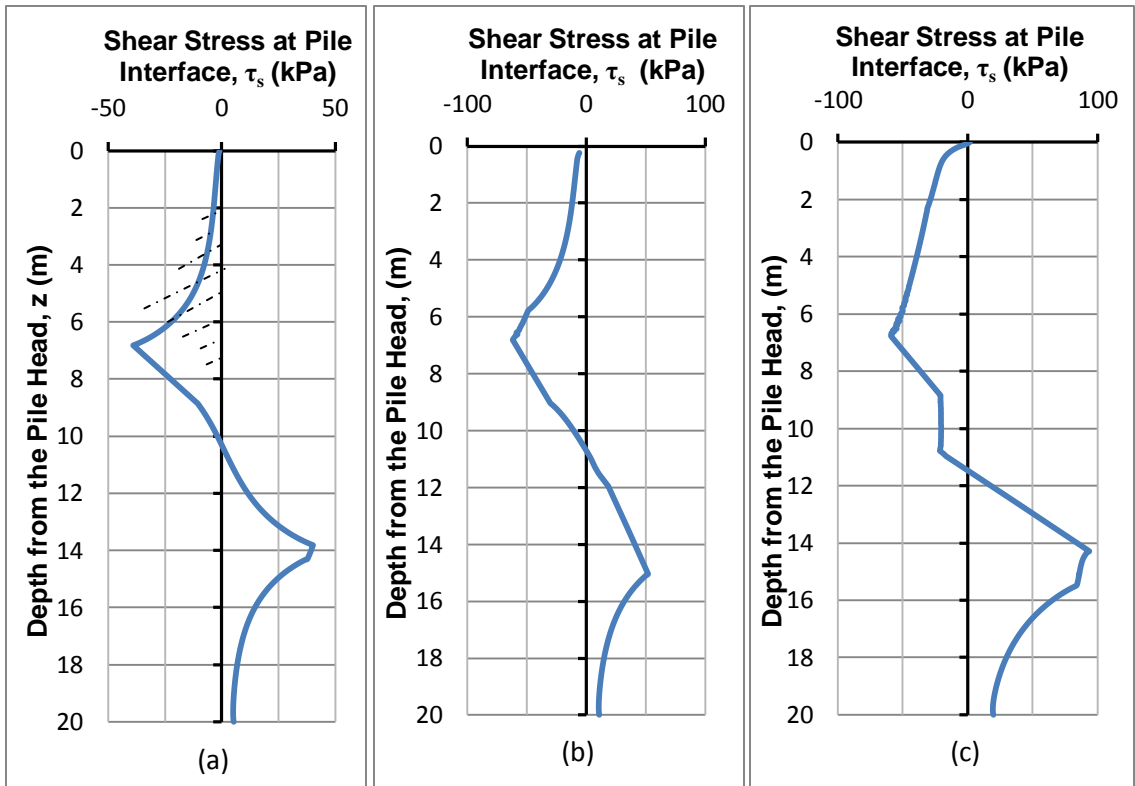
Figure 4.8: Shear stress distribution (inundation from bottom) when h = 3m;
**(a) C_p = 5%, (b) C_p = 10%, and (c) C_p = 15%**
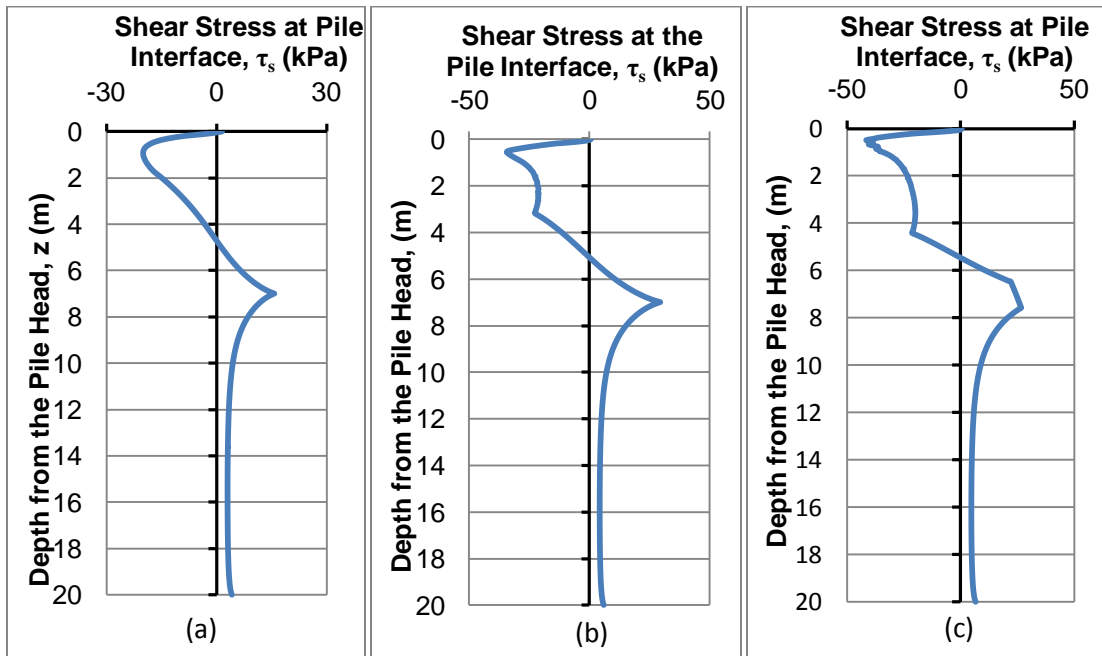
Figure 4.9: Shear stress distribution (inundation from top), when h = 3m;
**(a) C_p = 5%, (b) C_p = 10%, and (c) C_p = 15%**
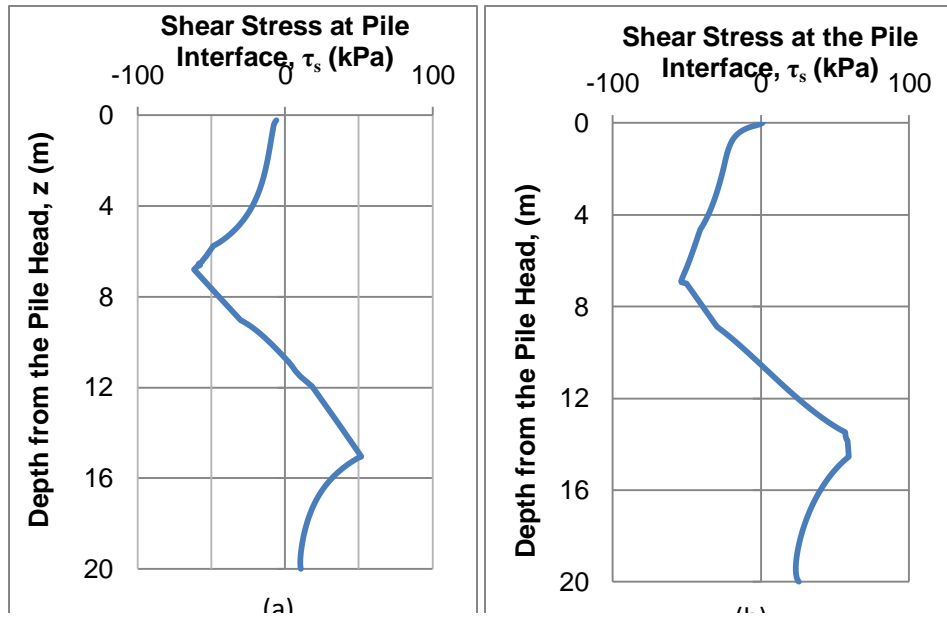
Figure 4.10: Shear stress distribution (inundation from bottom), when $C_p = 5\%$; (a) h = 3m, and (b) h = 7m
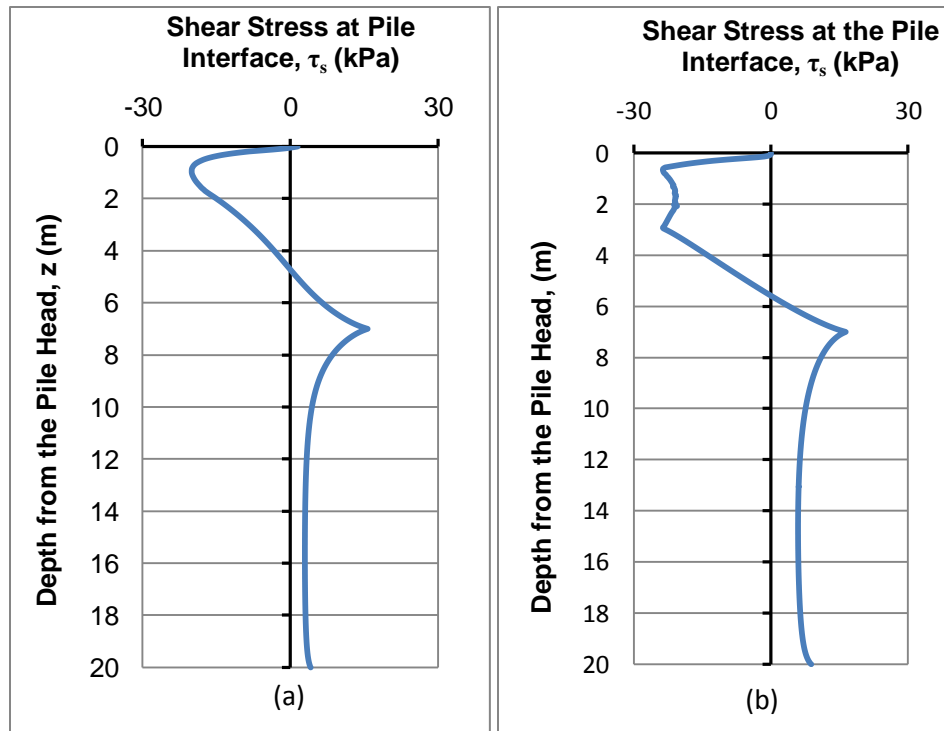

Figure 4.11: Shear stress distribution (inundation from top), when $C_p = 5\%$; (a) h = 3m, and (b) h = 7m

The indirect load (Q_n) due to NSF is the area bounded by the negative part of the shear stress distribution (i.e., the shaded area in Figure 4.8a) times the pile perimeter (πD). Therefore, the sensitivity of the pattern of shear stress distribution to different factors, such as collapse strain (i.e., volume reduction), radius of wetting front and direction of inundation, is analyzed here for a given soil and a pile. A significant influence of collapse strain (i.e., volume reduction) of a given collapsible soil layer subjected to inundation is noticed for both the directions of inundation (i.e., from the bottom and from the top), as shown in Figure 4.8 and Figure 4.9. For greater collapse strain, Q_n increases, because of the increase in the area bounded by the negative part of the shear stress distribution. The effects of the radius of wetting front (h) on the shear stress distribution are examined in Figure 4.10 and Figure 4.11 for the cases of inundation from bottom and top, respectively. The area bounded by the negative part of the shear stress distribution increases with the increase of the radius of wetting front, and the indirect load due to NSF increases, accordingly. While comparing the results of both directions of inundation, the location of neutral point is found lower in the case of inundation from the bottom than that in the case of inundation from the top, though the thickness of collapsing soil is the same in both the cases.

Figure 4.8 and Figure 4.10 can be compared with Figure 4.9 and Figure 4.11 respectively. This implies that the case of inundation from the bottom is more critical than that from the top. In case of inundation from the top, positive skin friction could develop in greater portion of the pile length. The values of Q_n are calculated for this condition only, while investigating the effects of angle of internal friction, length and diameter, and L/D ratio. In this section, the interface strength reduction factor is taken 0.9. The effect of pile roughness on the development of NSF is also addressed later.

4.4.1 Effect of the Angle of Internal Friction (φ)

The effect of the angle of internal friction (φ) on the indirect load (Q_n) due to NSF and the depth of neutral axis (N.A) is studied through 95 numerical test results on 36 cases. Figure 4.12–Figure 4.15 show that the angle of internal friction (φ) has almost no effect
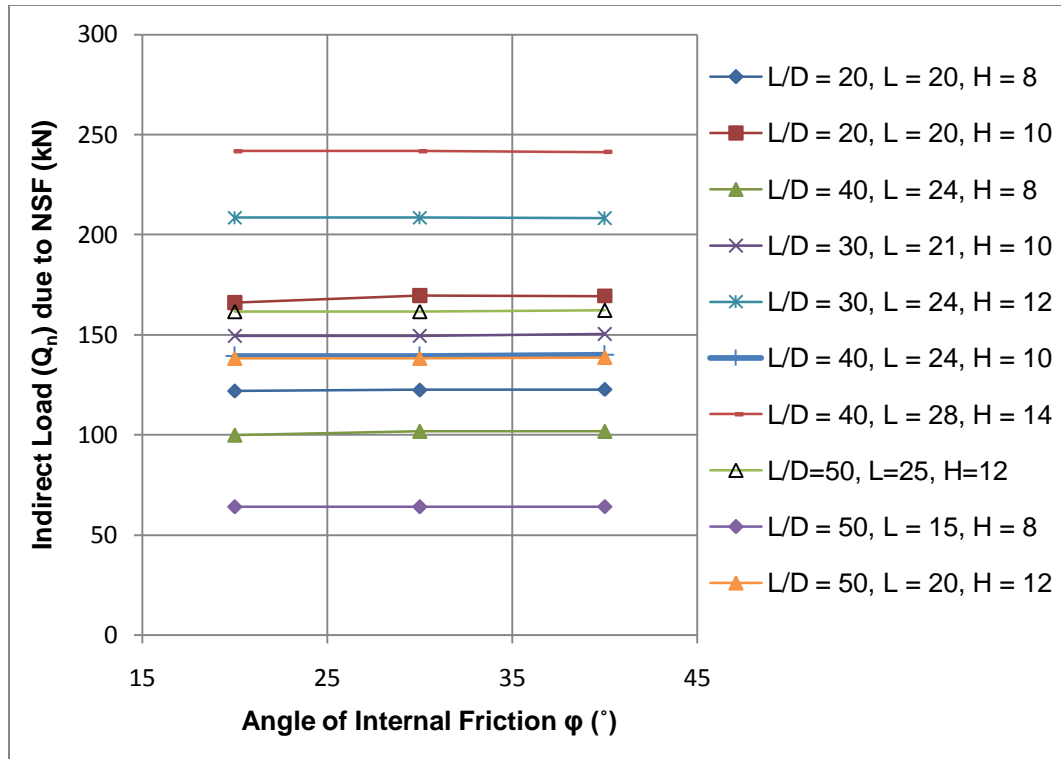
Figure 4.12: Indirect load (Q_n) due to NSF vs. angle of internal friction (φ), when h=3m, and $C_p = 5\%$

on negative skin friction. For any value of φ, the shear stress mobilized on the pile interface and the neutral depth are found identical.

Among 95 numerical tests, only 9 tests give slight variation in the calculated indirect load (Q_n) due to NSF. It is equally important to mention here that the variation is less than 5% in each case. In those few cases, the calculated value of Q_n is less, as the difference ΔQ_n is released by causing the pile to settle. It happens when the load on the pile is high due to Q_n and the ultimate pile resistances (i.e., positive skin friction and end resistances) are not adequate to support the load. Several points can be noted in this respect. Those 9 cases involve some or all of the factors: a) relatively thick bed of collapsing soil layer at greater depths, high collapse potential and wide radius of wetting front, b) large L/D ratio of long pile, and c) low angle of internal friction at the pile base. The factors, mentioned in category (a), have potential to make the situation for the development of high Q_n.
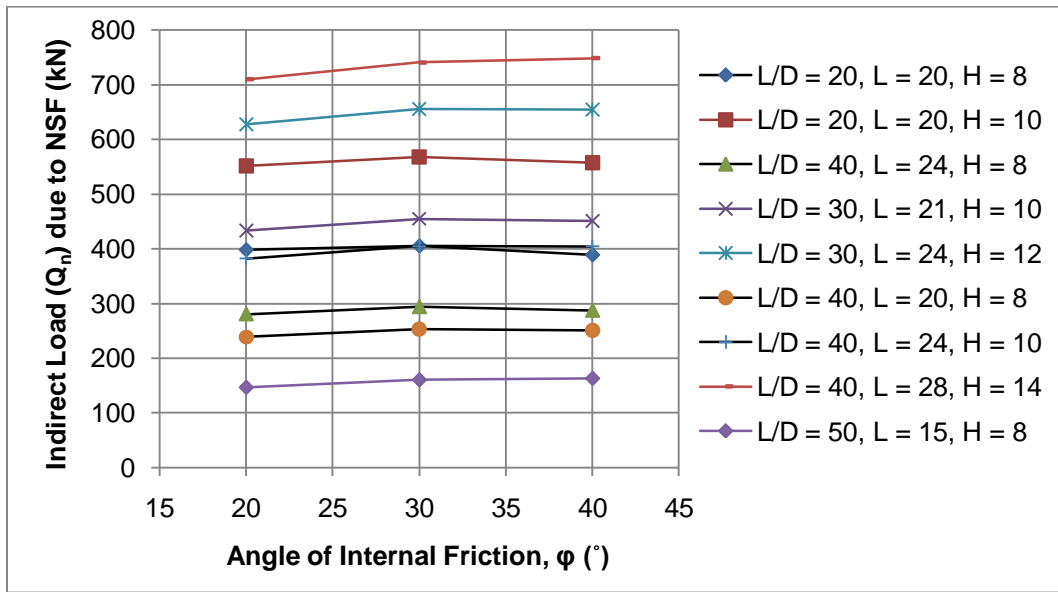
Figure 4.13: Indirect load (Q_n) due to NSF vs. angle of internal friction (φ), when h=3m, and $C_p = 15\%$
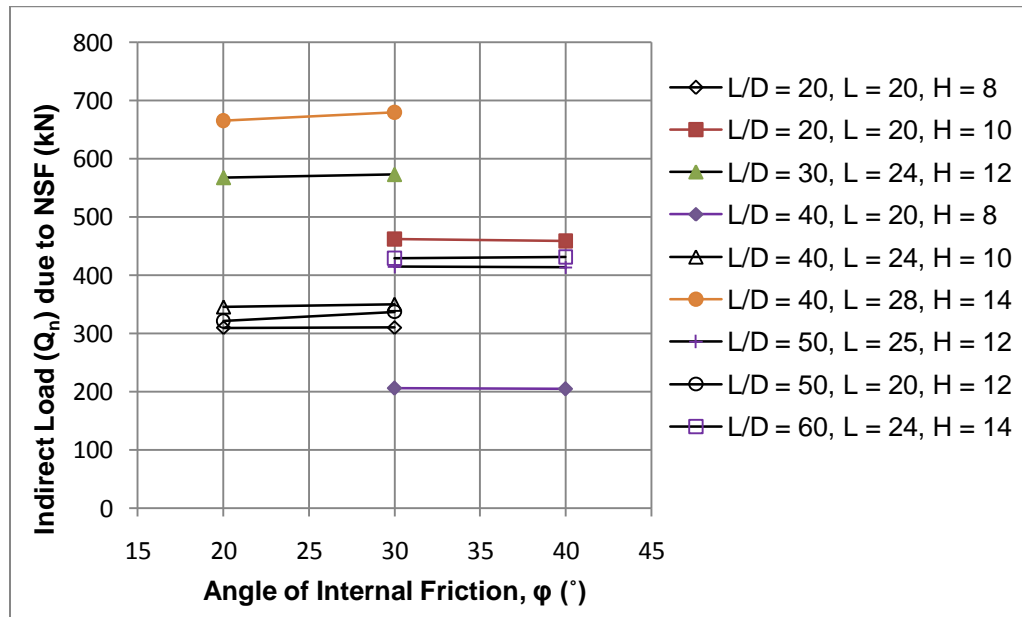
**Figure 4.14: Indirect load (Q_n) due to NSF vs. angle of internal friction (φ), when h=7m, and $C_p = 5\%$**
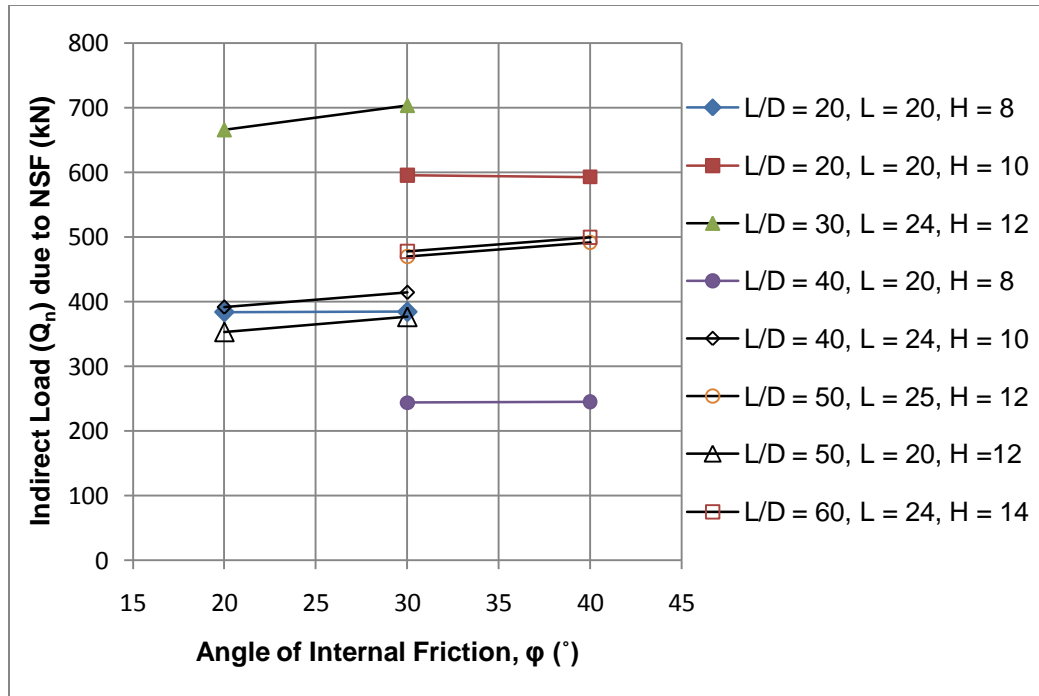
Figure 4.15: Indirect load (Q_n) due to NSF vs. angle of internal friction (φ), when h=10m, and $C_p = 5\%$

In addition to that, long pile with small diameter (i.e., large L/D) can also develop insufficient positive skin frictional resistance due to small pile diameter. During soil collapse, positive skin frictional resistance can develop on the pile surface embedded into the non collapsible soil underlying collapsible soil. Also due to shallow embedment into non-collapsible soil, positive skin frictional resistances could not develop sufficiently in the cases mentioned above, as relatively a small part of the pile length (L) was left to mobilize positive skin friction and the major part of L mobilizes NSF.

Moreover, the use of low angle of internal friction, especially when it is 20˚ at the pile base level, can develop inadequate end resistance. As mentioned earlier that both non collapsible soil and collapsible soil were given the same shear strength properties (c and φ). Therefore, the soil near the pile tip was given 20˚ as the value of φ, while investigating the effect of φ (equal 20˚) on the value of Q_n. Even for a long pile, relatively large depth of collapsing soil (e.g., 5–7 m) suffers from the release of ΔQ_n (or pile settlement) especially with small diameter (i.e., high L/D ratio).

116

It can be stated that Q_n, calculated with φ equals 20˚, is originally equal to those calculated with other φ values before the pile settles under Q_n. Therefore, the angle of internal friction (φ) is not considered a governing parameter to predict Q_n and the depth of neutral axis (N.A.) and therefore excluded from any consideration in the following parametric study.

4.4.2 Effects of Pile Length (L), Pile Diameter (D) and L/D Ratio

The effects of pile length (L), pile diameter (D) and length-to-diameter ratio (L/D) on the indirect load (Q_n) are studied for around 50 different pile geometries. This study considers piles having L/D ratio of 20, 30, 40, 50, 60 and 75. For each L/D ratio, different pile lengths, ranging 12–30 m are chosen. In addition to that, 8 m and 14 m deep beds of collapsible soils are considered. Figure 4.16–Figure 4.19 show the effect of L/D ratio on Q_n for a given set of condition, including radius of wetting front (h), depth of collapsing soil (H_s) and collapse potential (C_p). The H_s represents the depth of collapsing soil (i.e., half of the collapsible soil layer from its bottom), shown in Figure 4.6 for the results presented in this section. Each set of condition shows the same trend in influencing the Q_n. At a constant L/D ratio, Q_n increases with the decrease in pile length (L), as pile diameter (D) also decreases to maintain the constant L/D ratio. fQ_n is directly related to the pile diameter (D), as it is the product of the area of negative shear stress mobilized on the pile interface and the pile perimeter (πD). For a given L, as high L/D ratio corresponds to low pile diameter, any pile experiences decrease in Q_n if L/D ratio increases, as shown in Figure 4.16–Figure 4.19.

These figures provide additional information regarding the effect of collapse potential (C_p) on Q_n. Figure 4.16 and Figure 4.18 can be compared to Figure 4.17 and Figure 4.19 respectively, to note the considerable effect of collapse potential (C_p) on the value of Q_n. Consider an example case of 30 m long pile with L/D ratio equals 60, where the developed Q_n may be 90 kN (i.e., in Figure 4.16) and 238 kN (i.e., in Figure 4.17) for 5% and 15% of collapse potential respectively. Depending on different factors, pile can experience indirect load Q_n as high as 600 kN, as shown in Figure 4.19.
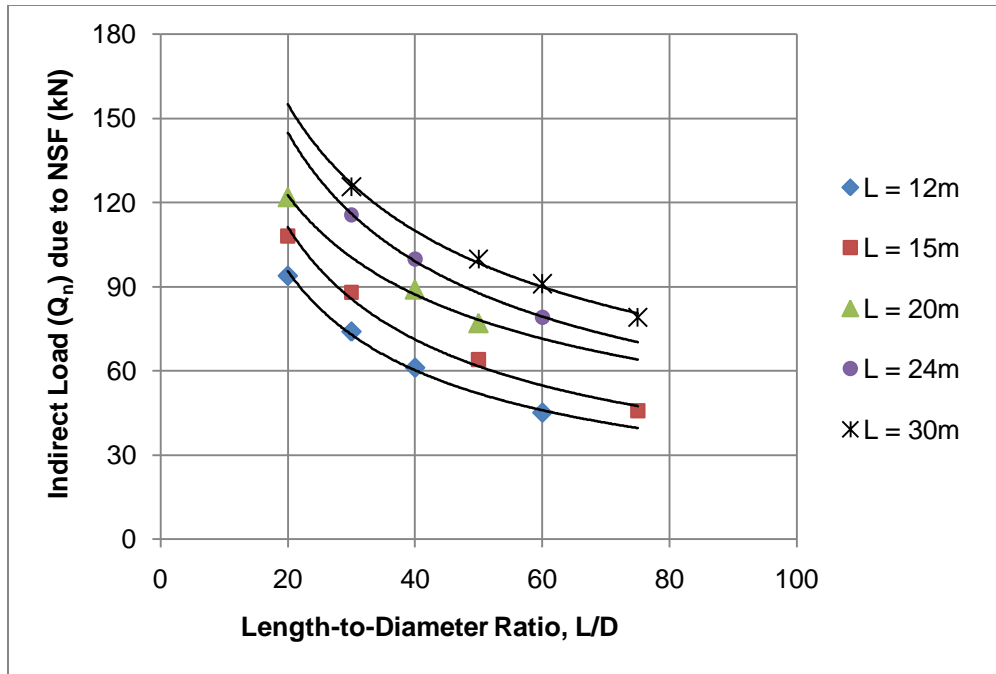
Figure 4.16: Indirect load (Q_n) due to NSF vs. length-to-diameter ratio (L/D), when h = 3 m, H_s = 4 m and C_p = 5%
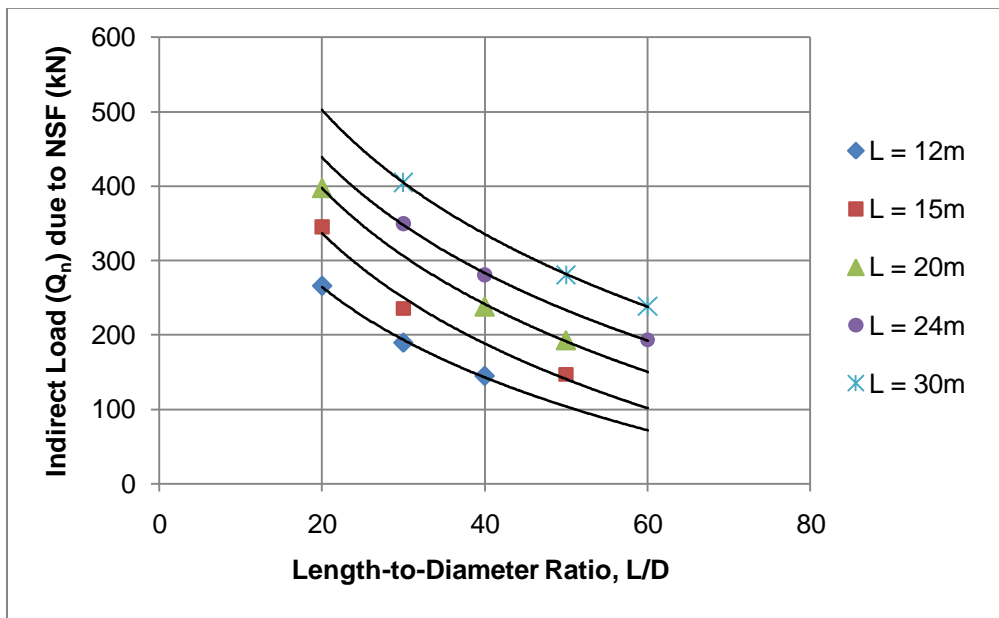
Figure 4.17: Indirect load (Q_n) due to NSF vs. length-to-diameter ratio (L/D), when h = 3 m, H_s = 4 m and C_p = 15%
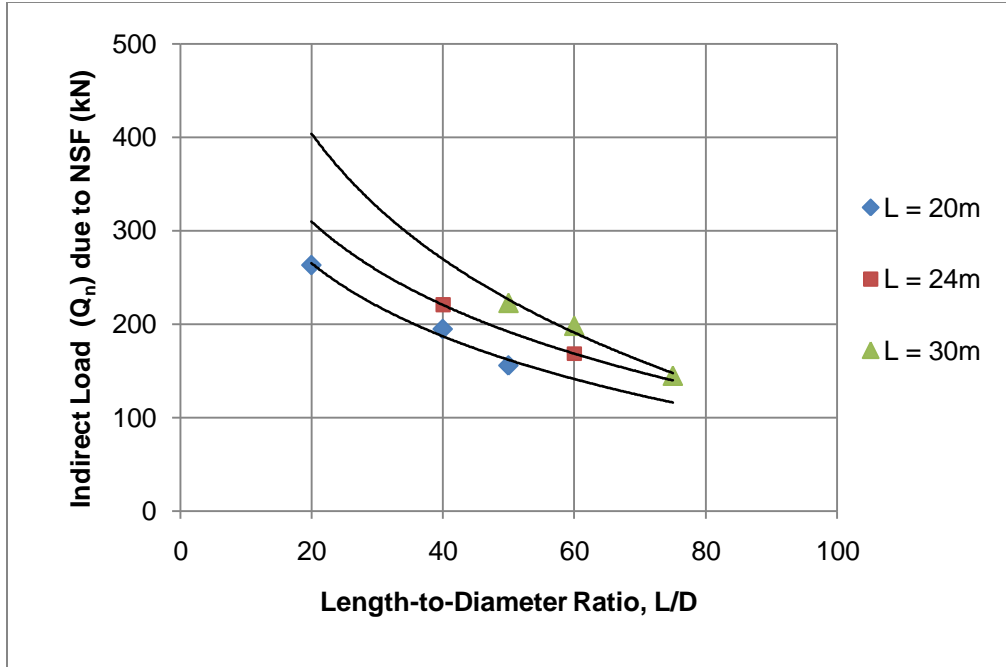
**Figure 4.18: Indirect load (Q_n) due to NSF vs. length-to-diameter ratio (L/D), when h = 3 m, H_s = 7 m and C_p = 5%**
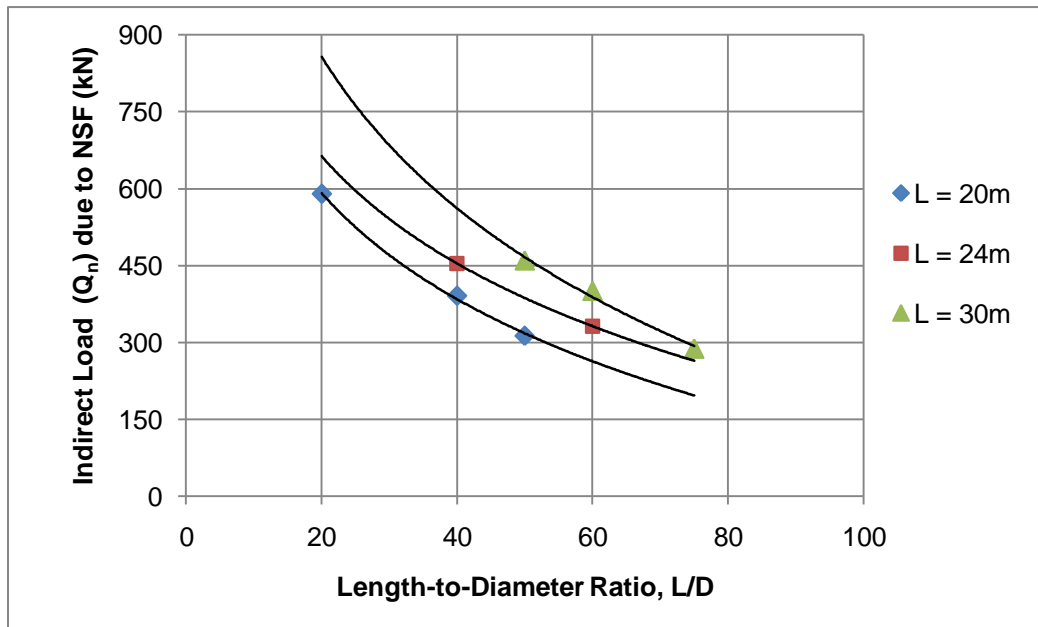

Figure 4.19: Indirect load (Q_n) due to NSF vs. length-to-diameter ratio (L/D), when h = 3 m, H_s = 7 m and C_p = 10%
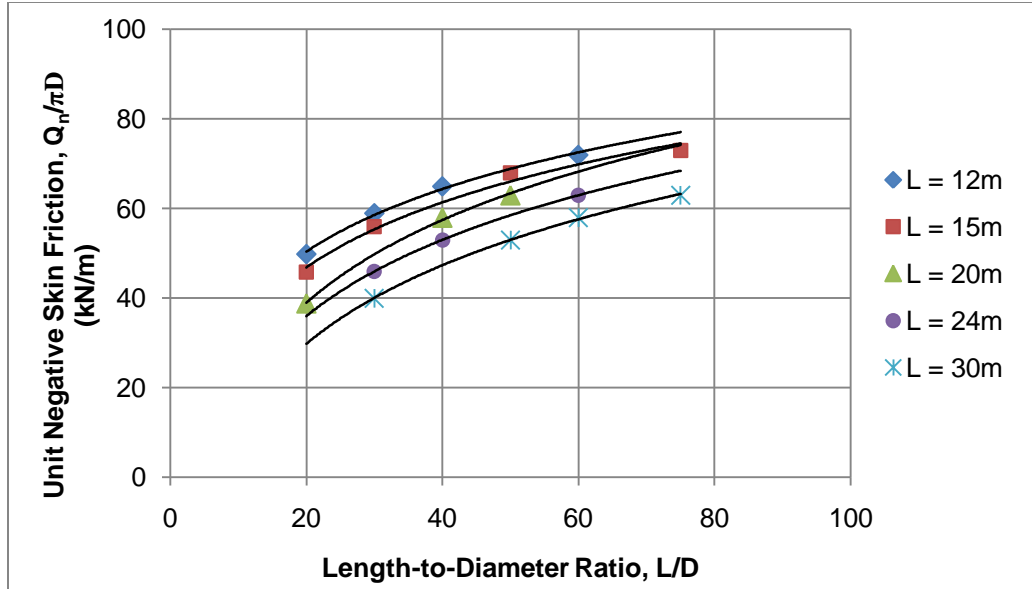
Figure 4.20: Unit negative skin friction ($Q_n/\pi D$) vs length-to-diameter ratio (L/D), when h = 3 m, H_s = 4 m and C_p = 5%

The considerable effect of the radius of wetting front (h) is also clearly noted in these figures. The effects of C_p and h are investigated later on. Figure 4.20 presents the indirect load (Q_n) due to NSF as unit negative skin friction (i.e., the Q_n per unit perimeter, $Q_n/\pi D$), or the shaded area in Figure 4.8(a) to discard the effect of pile diameter (D). Indirect load (Q_n) and unit negative skin friction ($Q_n/\pi D$) show different trends with the increase of L/D. However, the explanation for getting parallel curves is same in both cases. There exists no unique relation between unit negative skin friction and L/D.

Further, indirect load (Q_n) due to NSF is studied in terms of average negative shear stress (q_n). Average negative shear stress (q_n) is the integration of the negative shear stress mobilized along the part (N.A.) of the pile length divided by the depth of neutral axis (N.A.). In this format, the influence of pile diameter and the depth of neutral axis are eliminated. However, for the previously defined set of conditions (including h, H_s and C_p), no further conclusion can be derived regarding the effect of L/D on average negative skin friction (q_n), as shown in Figure 4.21.
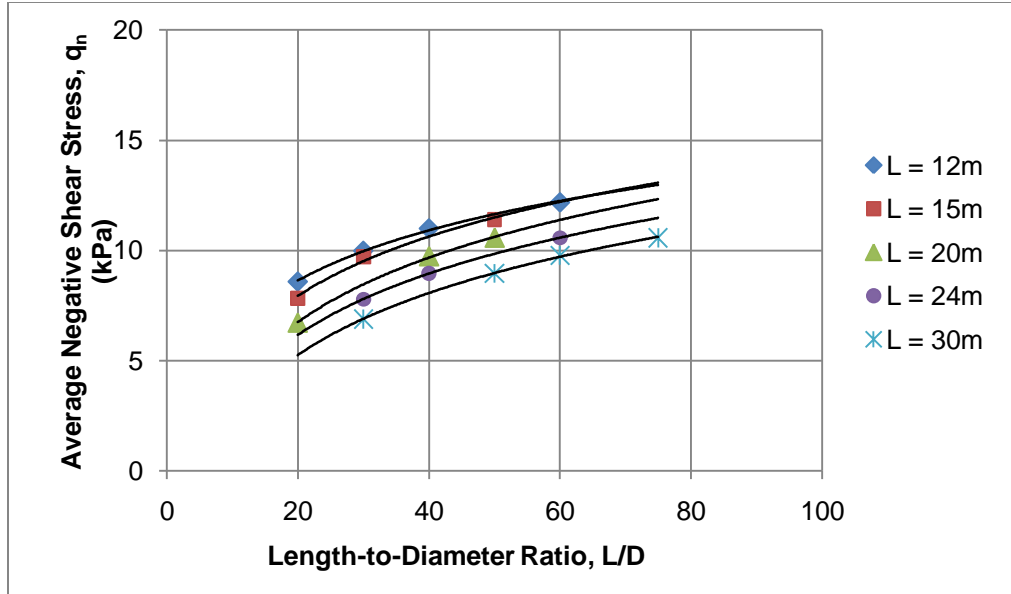
Figure 4.21: Average negative shear stress (q_n) vs. length-to-diameter ratio (L/D), when h = 3m, H_s = 4m and C_p = 5%

Therefore, a new set of conditions is defined by the radius of wetting front (h), the depth of collapsing soil-to-pile diameter ratio (H_s/D) and the collapse potential (C_p), where the effect of pile diameter (D) is further eliminated from the depth of collapsing soil (H_s). The average negative shear stresses (q_n) for different L/D is compared for the cases having the same radius of wetting front (h), collapse potential (C_p) and H_s/D. Figure 4.22–Figure 4.25 present the variation of average negative skin friction (q_n) with L/D ratio for a new set of conditions (i.e., h, H_s/D and C_p). It can be noted that the L/D ratio has no effect on average negative shear stress (q_n) if h, H_s/D and C_p remain constant.
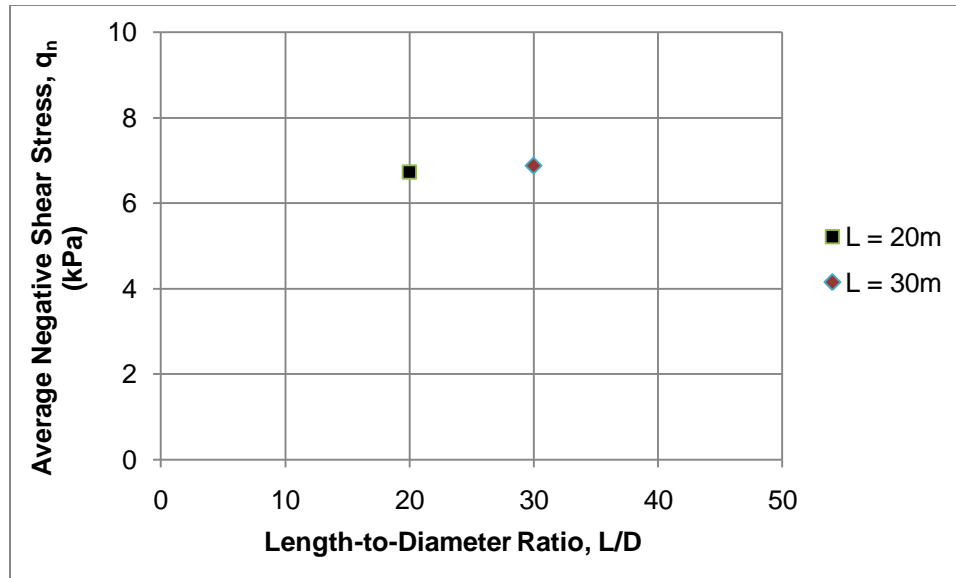
Figure 4.22: Average negative shear stress (q_n) vs length-to-diameter ratio (L/D), when h = 3 m, H_s/D = 4, and C_p = 5%
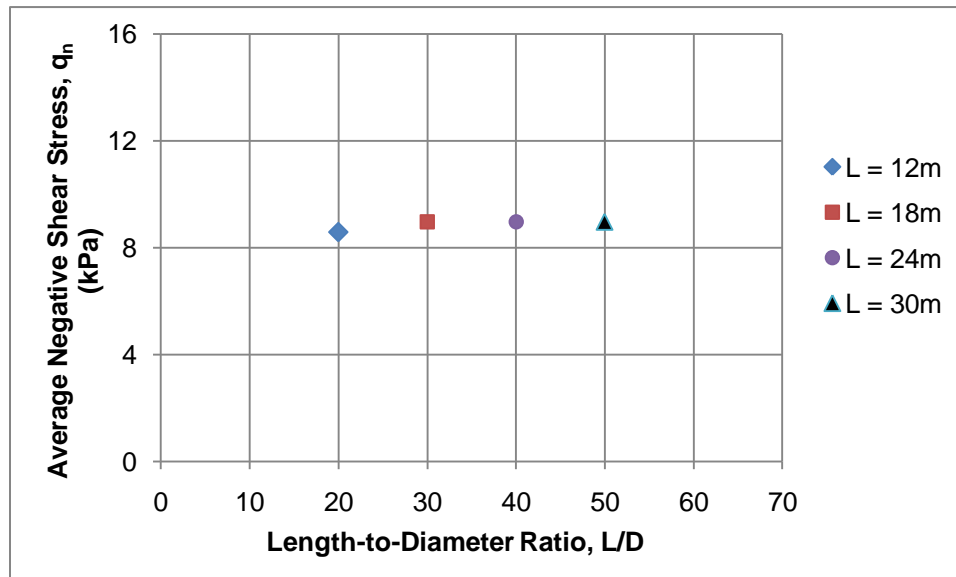
Figure 4.23: Average negative shear stress (q_n) vs length-to-diameter ratio (L/D), when h = 3 m, H_s/D = 6.6, and C_p = 5%
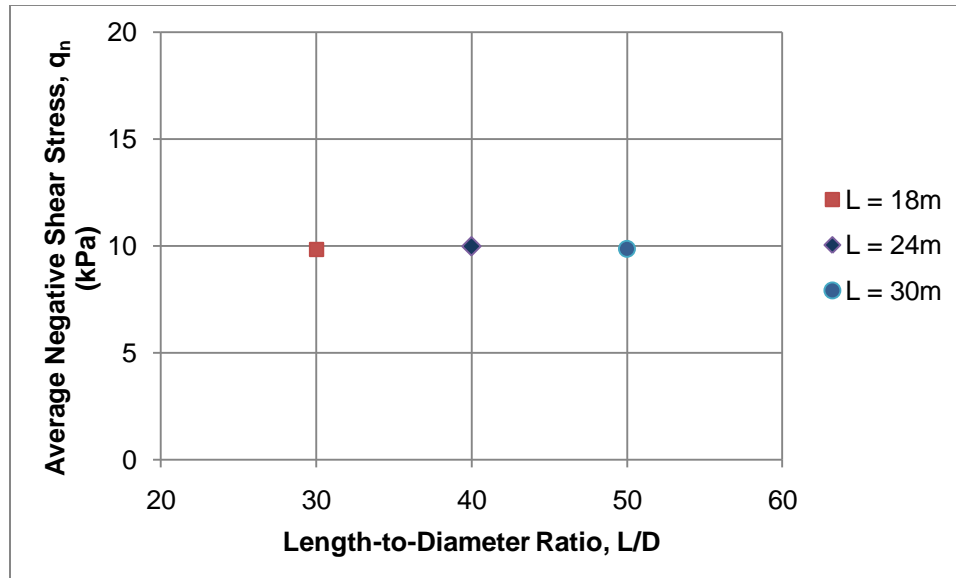
Figure 4.24: Average negative shear stress (q_n) vs length-to-diameter ratio (L/D), when h = 3 m, H_s/D = 8.33, and C_p = 5%
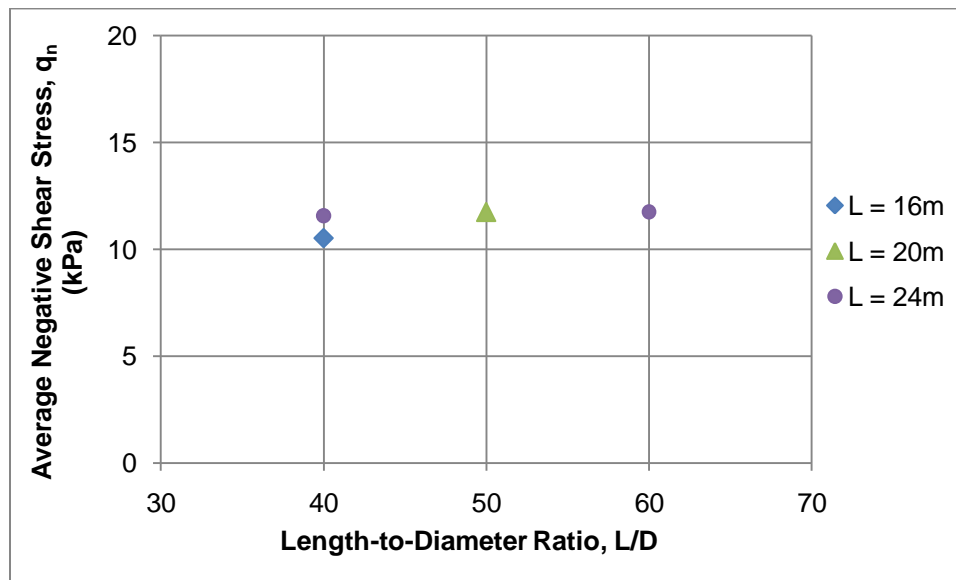
Figure 4.25: Average negative shear stress (q_n) vs length-to-diameter ratio (L/D), when h = 3 m, H_s/D = 12.5, and C_p = 5%
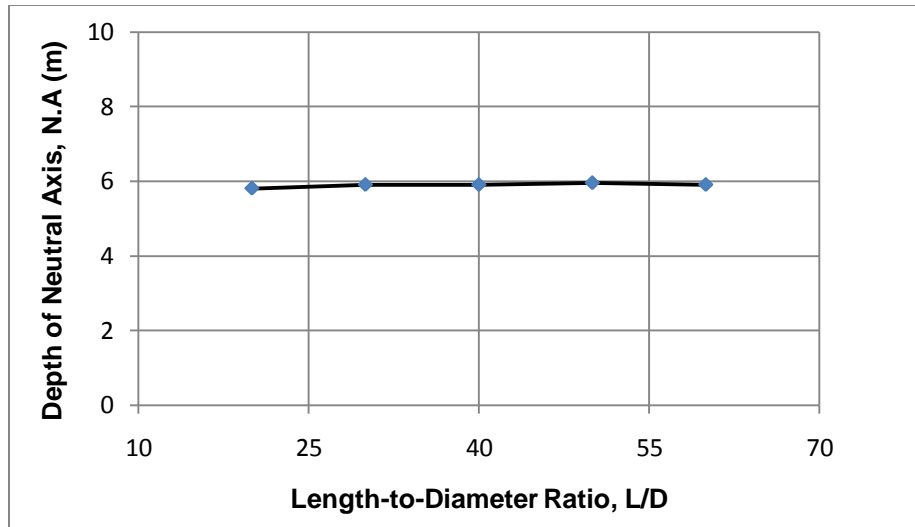
**Figure 4.26: Depth of neutral axis (N.A) vs length-to-diameter ratio (L/D),
when h = 3 m, H$_s$ = 4m and C$_p$ = 5%**
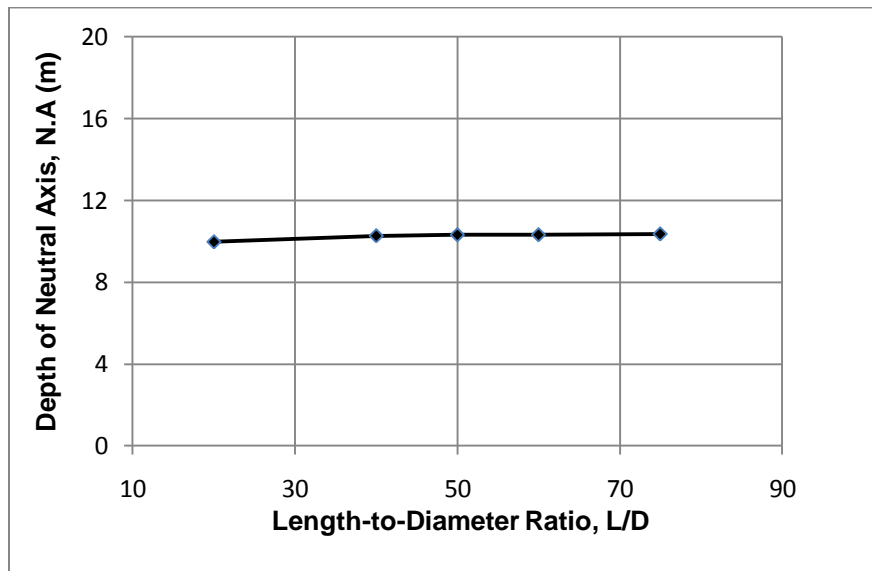
**Figure 4.27: Depth of neutral axis (N.A) vs length-to-diameter ratio (L/D),
when h = 3 m, H$_s$ = 7m and C$_p$ = 5%**

The effect of L/D ratio on the depth of neutral axis (N.A.) is studied. Figure 4.26 and Figure 4.27 demonstrate that L/D ratio has no considerable effect on the depth of

neutral axis (N.A) for a given set of h, H_s and C_p. The points on the figures are obtained for different pile lengths as well. It becomes clear that average negative shear stress (q_n) and depth of neutral axis (N.A) have no influence of L/D ratio.

4.4.3 Effect of the Embedded Length (L_e) in Non-collapsible soil

The effect of embedded length-to-full pile length ratio, (L_e/L) is studied on the average negative shear stress (q_n). Figure 4.28 and Figure 4.29 show that the ratio L_e/L has no considerable influence on the average negative shear stress (q_n), if H_s/D ratio is constant. In this study, L_e/L ratio is varied from 0.3 to 0.73.
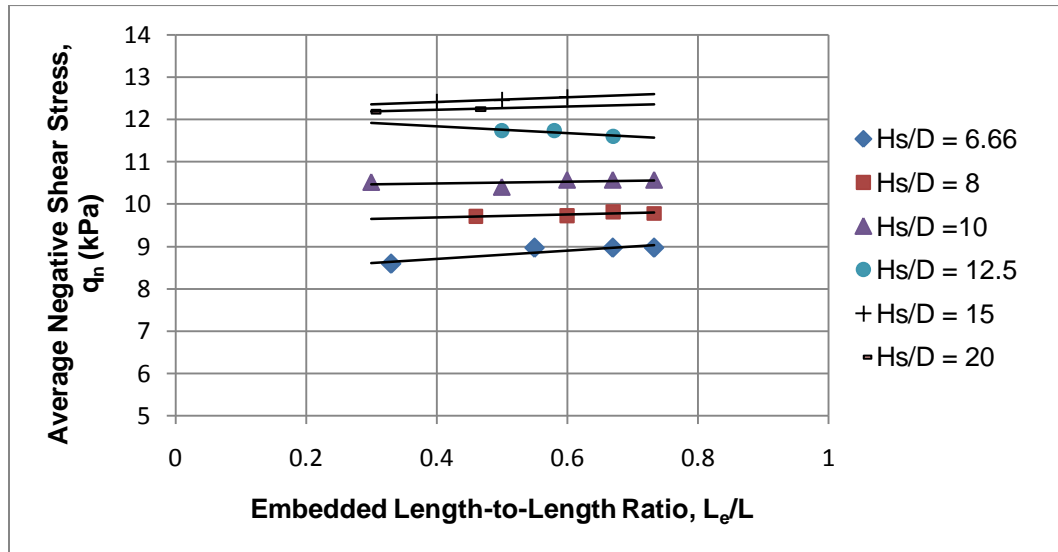
Figure 4.28: Average negative shear stress (q_n) vs (L_e/L) ratio, when h = 3 m, and C_p = 5%

125
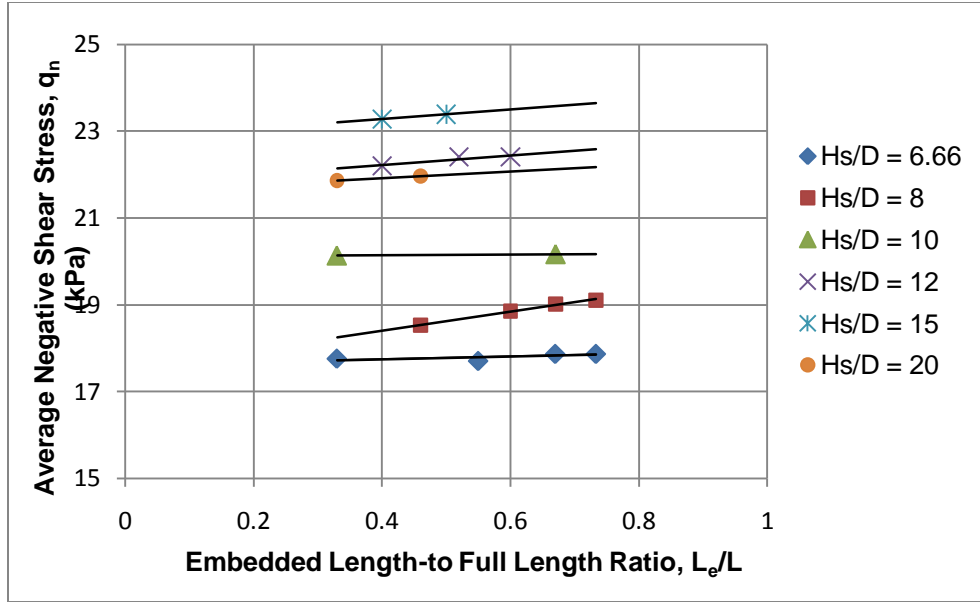
Figure 4.29: Average negative shear stress (q_n) vs (L_e/L) Ratio, when h = 3 m, and C_p = 10%

In Figure 4.29, it can be noted that the average negative shear stress (q_n) is slightly less for the cases having low L_e/L ratio. As the embedded pile length into non collapsible soil is not enough to develop positive skin frictional resistance, a portion of Q_n is reduced due to pile settlement. Before the pile experiences settlement, q_n developed on the pile having low L_e/L ratio equals that developed on the pile having high L_e/L ratio. However, the concept of building structures on pile in collapsible soil is not to experience any sudden settlement due to NSF. Therefore, the maximum value of q_n that may be caused due to the inundation of collapsible soil should be considered to avoid any pile settlement. For this reason, L_e/L ratio is not considered an influencing parameter, as it should be considered in designing the pile length when the indirect load (Q_n) due to NSF is known.

4.5 Parametric Study for the Case of Inundation from Bottom

The depth of collapsing soil-to-pile diameter ratio (H_s/D), the radius of wetting front (h) and the collapse potential (C_p) are found to influence the average negative shear stress (q_n) and the depth of neutral axis (N.A.). The effects of such parameters on q_n are examined to analyze the results in the following sections for interface strength reduction

126

factor (ISRF) equal 0.9. Pile is embedded adequately into non-collapsible soil not to experience any pile settlement to obtain maximum value of Q_n developed.

4.5.1 Effect of Depth of Collapsing soil-to-Pile Diameter Ratio (H_s/D)

The effect of the depth of collapsing soil-to-pile diameter ratio (H_s/D) on average negative shear stress (q_n) is studied in this section. The reason of considering H_s/D, instead of H_s, is already discussed in the previous section. Figure 4.30–Figure 4.35 show the variation of average negative shear stress (q_n) with H_s/D ratio for different sets of conditions (i.e., defined by h and C_p). It can be noted that average negative shear stress (q_n) has a linear relation with H_s/D ratio in a semi-logarithmic plot. Data points on the figures are the numerical results obtained for the entire range of each parameter considered in this study. For example, 17 different embedded length-to-full pile length ratios (L_e/L) are considered to obtain 65 data points (representing 65 cases) in Figure 4.30 for a given h and C_p.
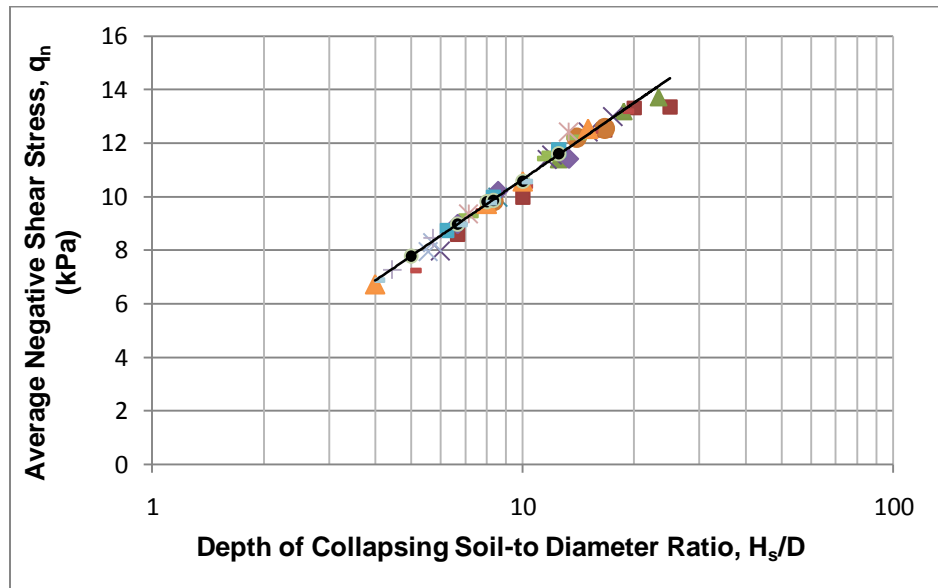
Figure 4.30: Average negative shear stress (q_n) vs. H_s/D ratio, for different Embedded Length-to-Full Length ratio (L_e/L), when h = 3 m, and C_p = 5%
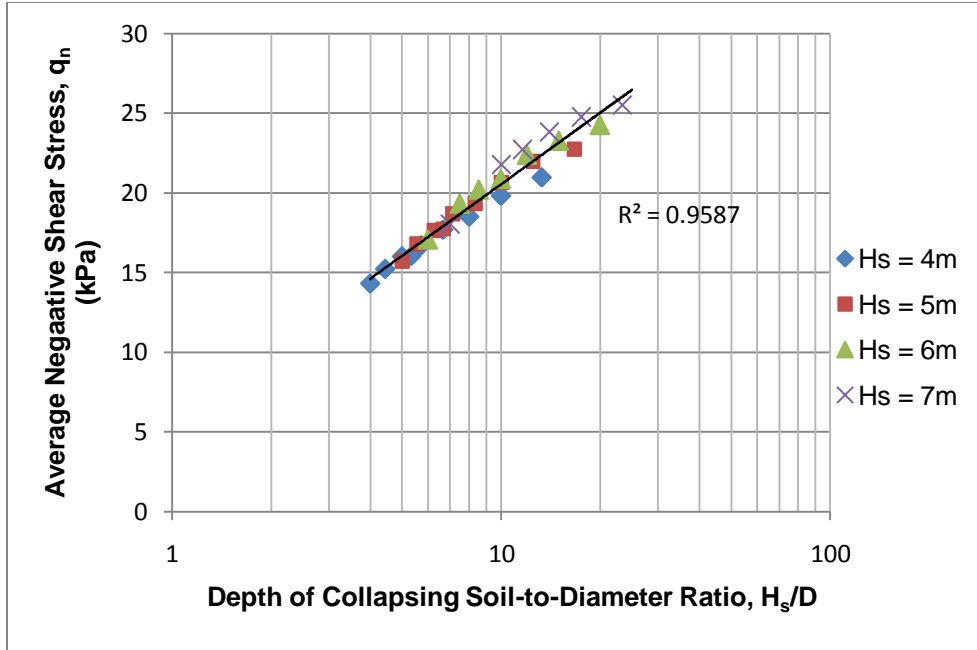
Figure 4.31: Average negative shear stress (q_n) vs. H_s/D ratio, when h = 3 m, and C_p = 10%
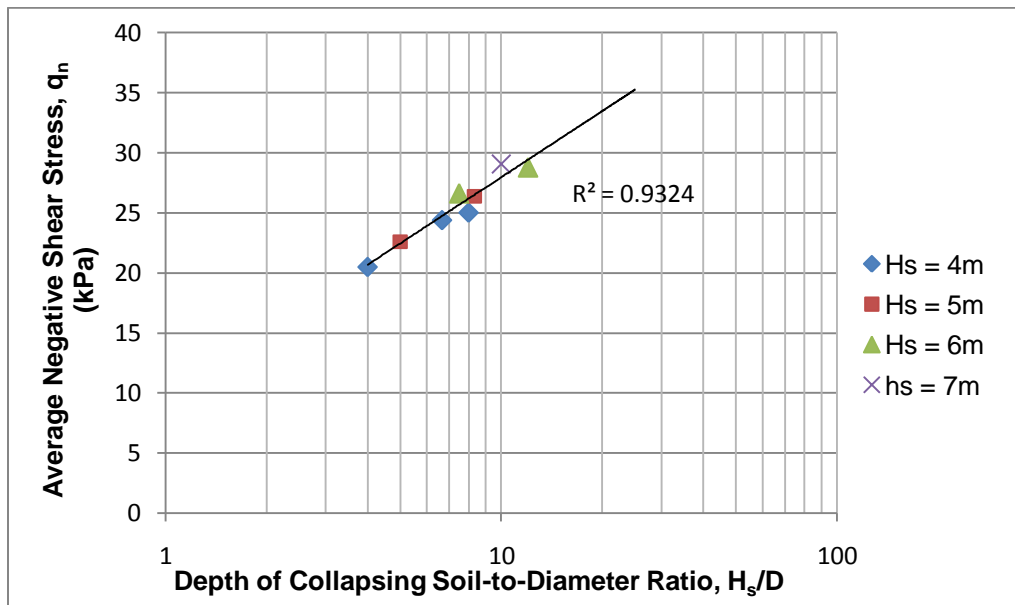

Figure 4.32: Average negative shear stress (q_n) vs. H_s/D ratio, when h = 3 m, and C_p = 15%
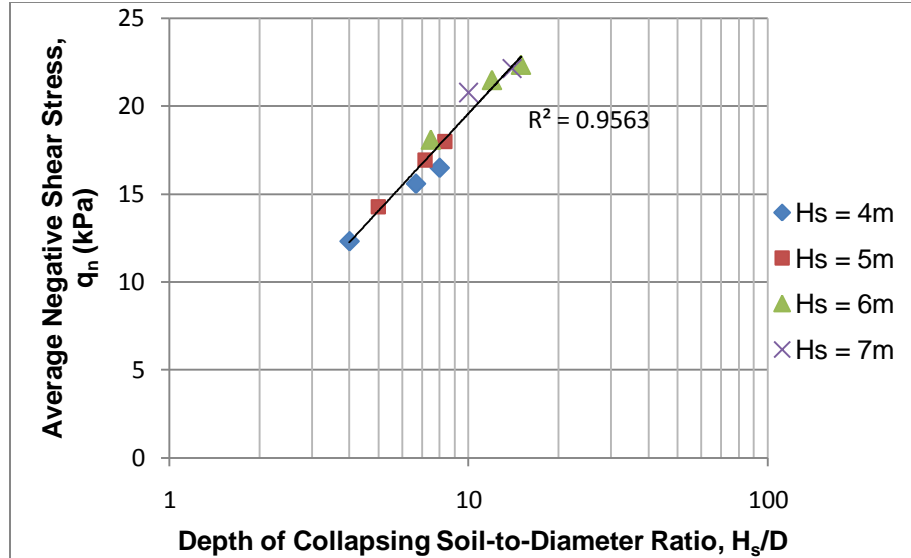
Figure 4.33: Average negative shear stress (q_n) vs. H_s/D ratio, when h = 5 m, and C_p = 5%

The linear relation between q_n and H_s/D ratio in a semi-logarithmic plot (as shown in Figure 4.31–Figure 4.35), is found unique for a given C_p and h. However, slope of q_n vs. H_s/D relation varies with the variation of C_p and h.

The value of H_s/D is considered up to 25 in this study. Therefore, the values of H_s/D ratio are 23 and 35 for pile diameter (D) of 0.3 m and 0.2 m respectively, as the maximum depths of collapsible and collapsing soils are considered 14 m and 7 m. Based on the numerical results, it should be reported that the increase of average negative shear stress (q_n) continues until the value of H_s/D is 14. Beyond this condition, q_n does not show any further increase due to any increase in H_s/D ratio. For this reason, Figure 4.30–Figure 4.35 have data points up to H_s/D ratio of 14. Average negative shear stress (q_n) is found to vary from 14 kPa to 35 kPa, depending on the H_s/D ratio, h and C_p.
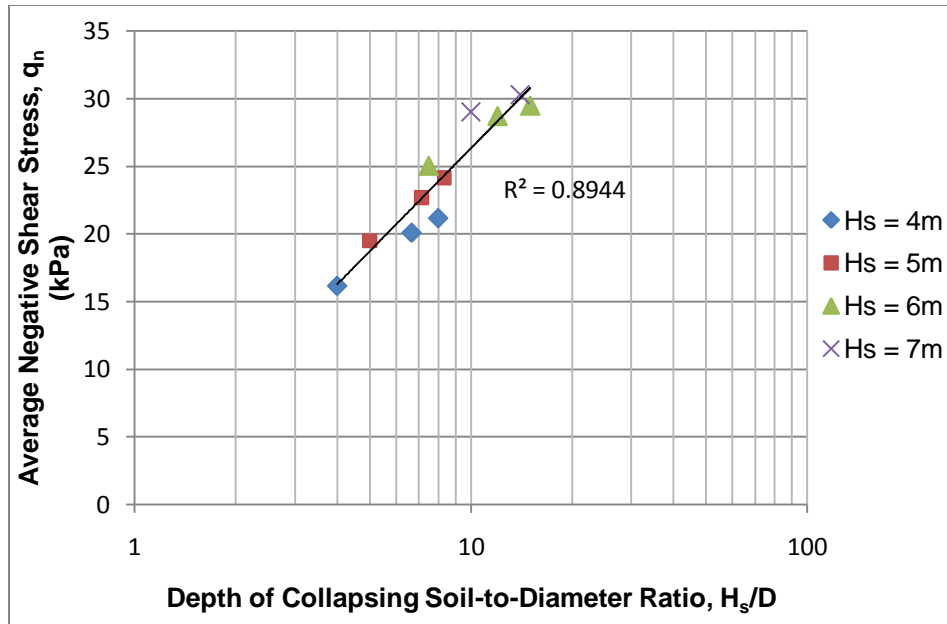
Figure 4.34: Average negative shear stress (q_n) vs. H_s/D ratio, when h = 7 m, and C_p = 5%
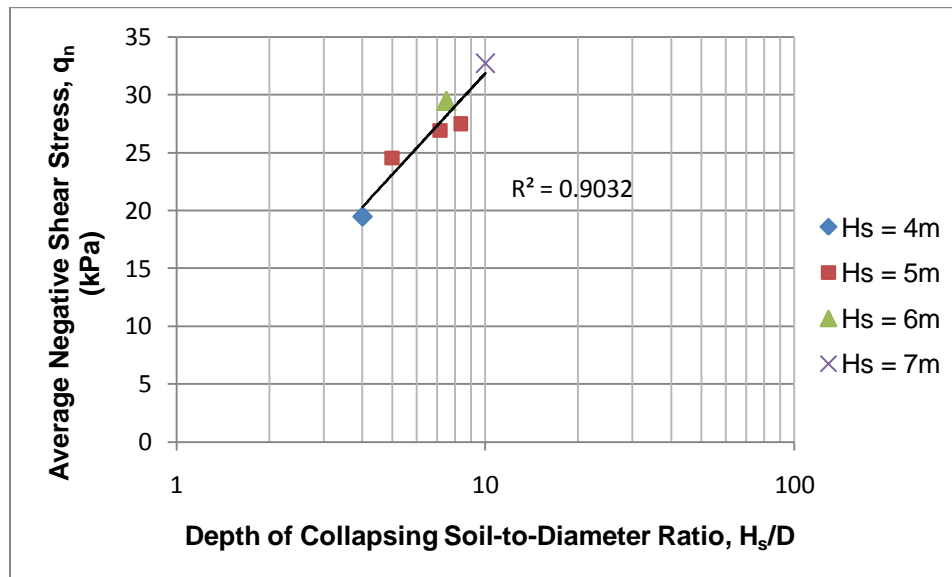
**Figure 4.35:** Average negative shear stress (q_n) vs. H_s/D ratio, when h = 10 m, and C_p = 5%
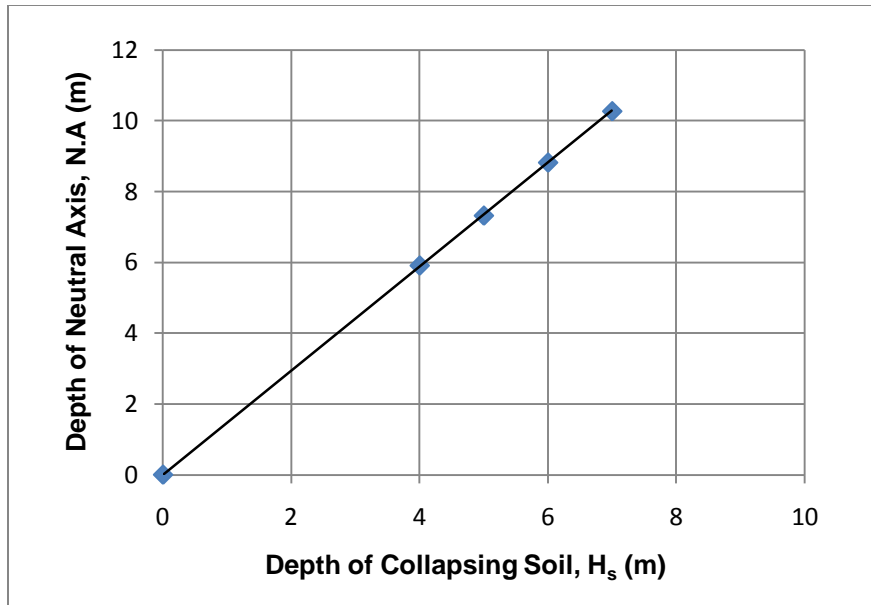
Figure 4.36: Depth of Neutral Axis (N.A) vs. H_s, when h = 3 m, and C_p = 5%
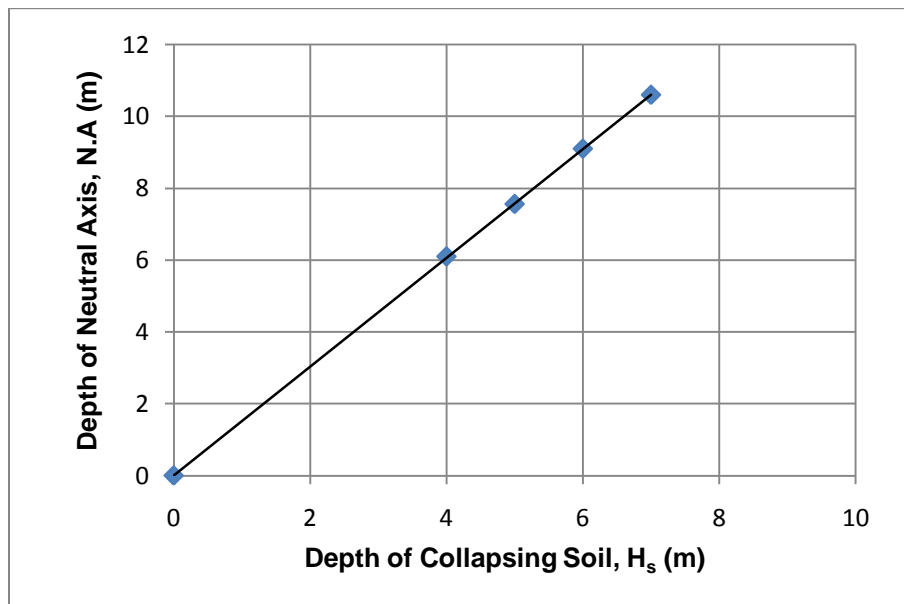
Figure 4.37: Depth of Neutral Axis (N.A) vs. H_s, when h = 3 m, and C_p = 10%
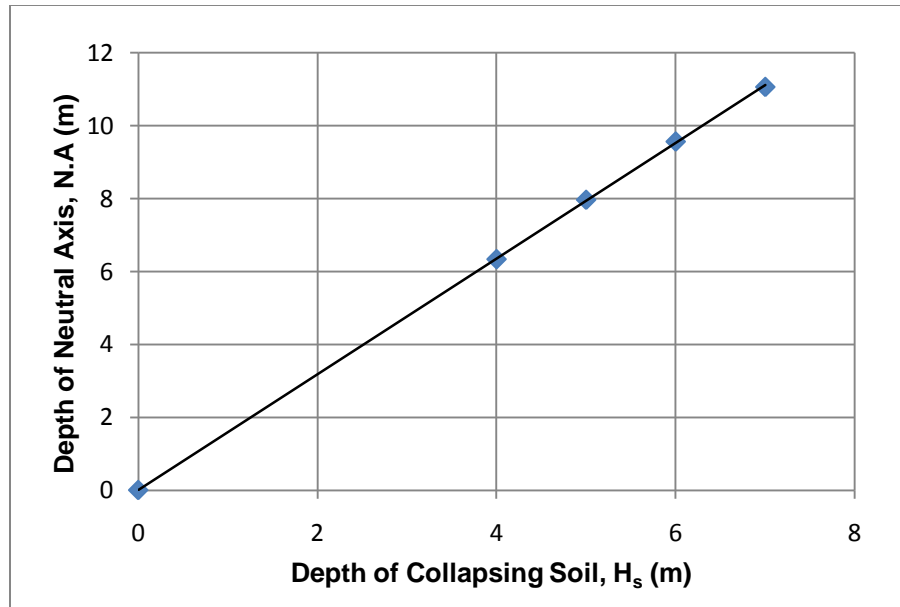
Figure 4.38: Depth of Neutral Axis (N.A) vs. H_s, when h = 3 m, and C_p = 15%

The variation of the depth of neutral axis (N.A.) with the depth of collapsing soil (H_s) is studied in Figure 4.36–Figure 4.38. It is noted that the depth of neutral axis increases linearly with the increase of the depth of collapsing soil. If the collapsing soil is located at greater depth from the ground, the depth of neutral axis (N.A.) is also very high.

4.5.2 Effect of the Radius of Wetting

The effect of the radius of wetting (h) is investigated on the average negative shear stress (q_n) in Figure 4.39, for the collapse potential (C_p) equals 5%. Average negative shear stress (q_n) increases with the increase in the radius of wetting front (h), for given values of H_s/D and C_p.

The results related to higher collapse potential and the maximum limit of C_p that can have significant effect on q_n are discussed later on. In case of wide wetting front (h), it is noted that high collapse potential (C_p) does not increase average negative shear stress (q_n).
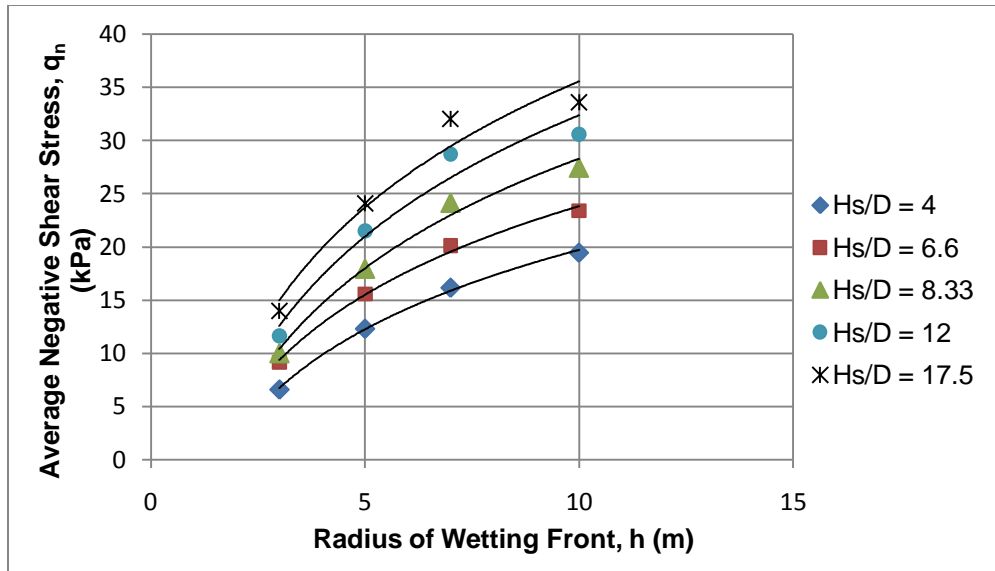
**Figure 4.39: Average negative shear stress (qn) vs. radius of wetting front (h)
when Cp = 5%**

4.5.3 Effect of Pile Interface Strength Reduction factor

Interface strength reduction factor (ISRF) is taken as 0.9 in the numerical investigations presented in the above sections. This section investigates the effect of ISRF on the q_n, as shown in Figure 4.40–Figure 4.43, for different H_s/D ratio, h and C_p.
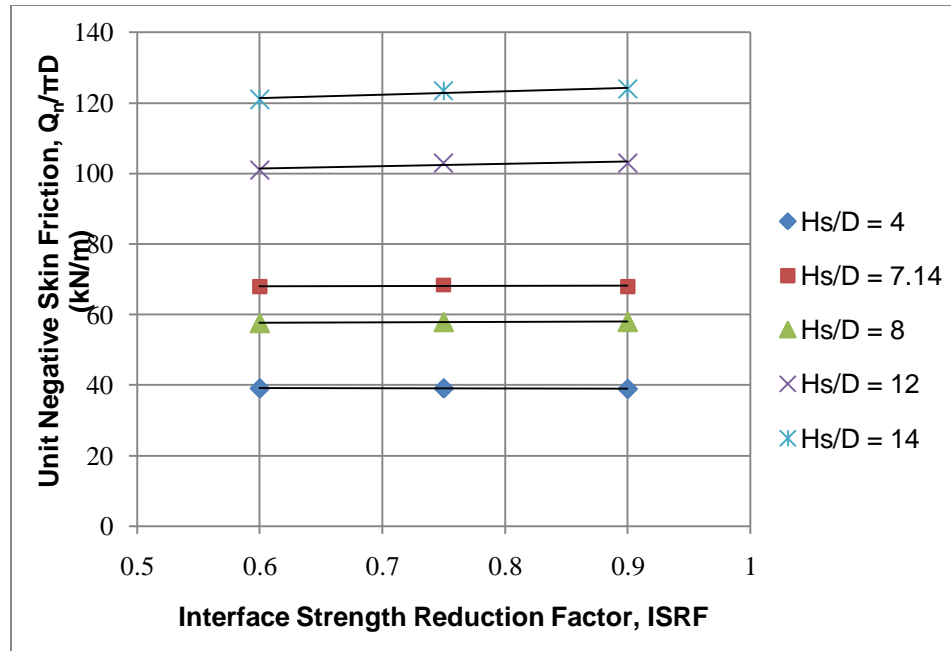
Figure 4.40: Effect of Interface Strength Reduction Factor (ISRF) on unit negative skin friction ($Q_n/\pi D$), where h = 3 m and C_p = 5%
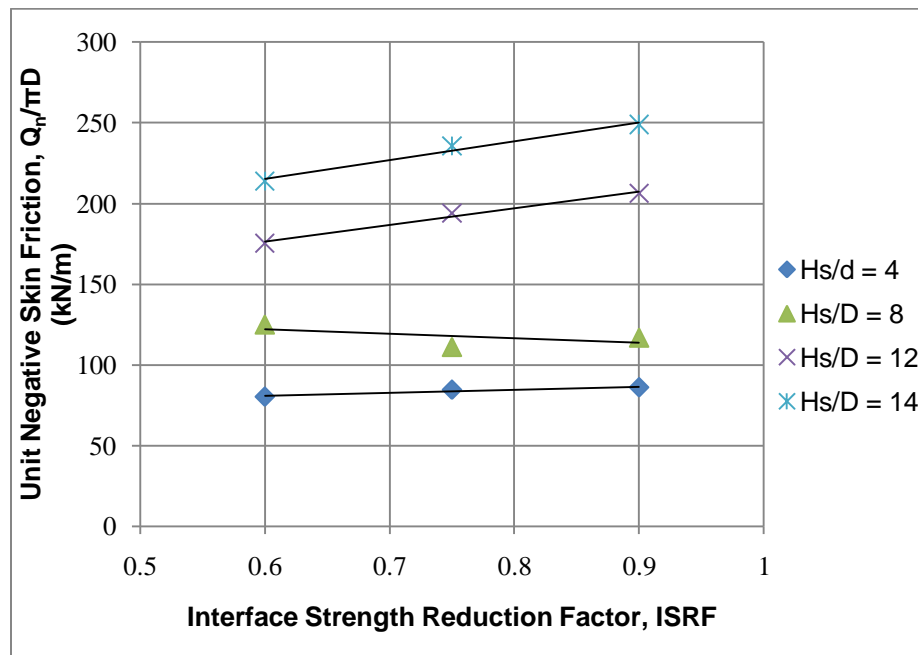
Figure 4.41: Effect of Interface Strength Reduction Factor (ISRF) on unit negative skin friction ($Q_n/\pi D$), where h = 3 m and C_p = 10%
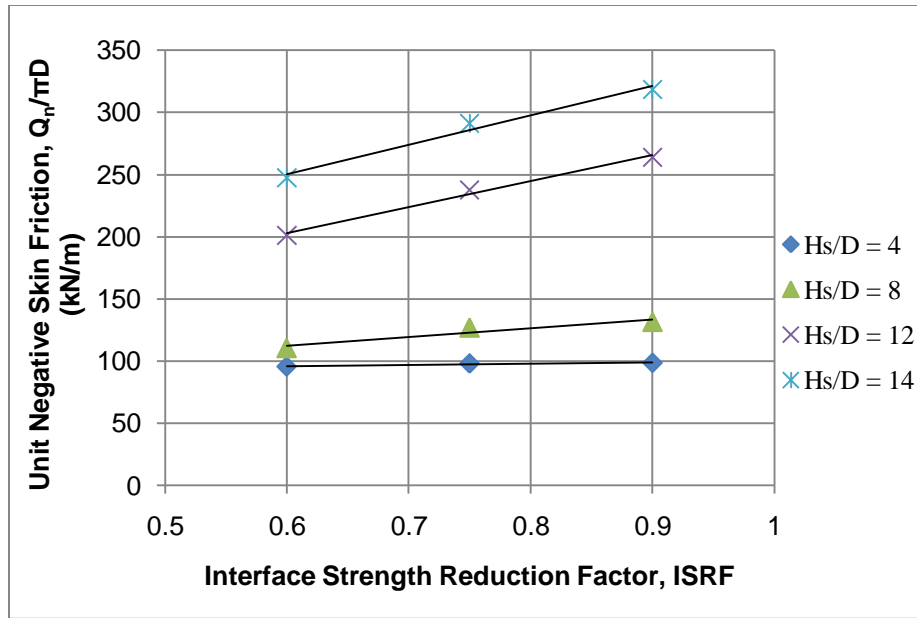
Figure 4.42: Effect of Interface Strength Reduction Factor (ISRF) on unit negative skin friction ($Q_n/\pi D$), where h = 7 m and C_p = 5%
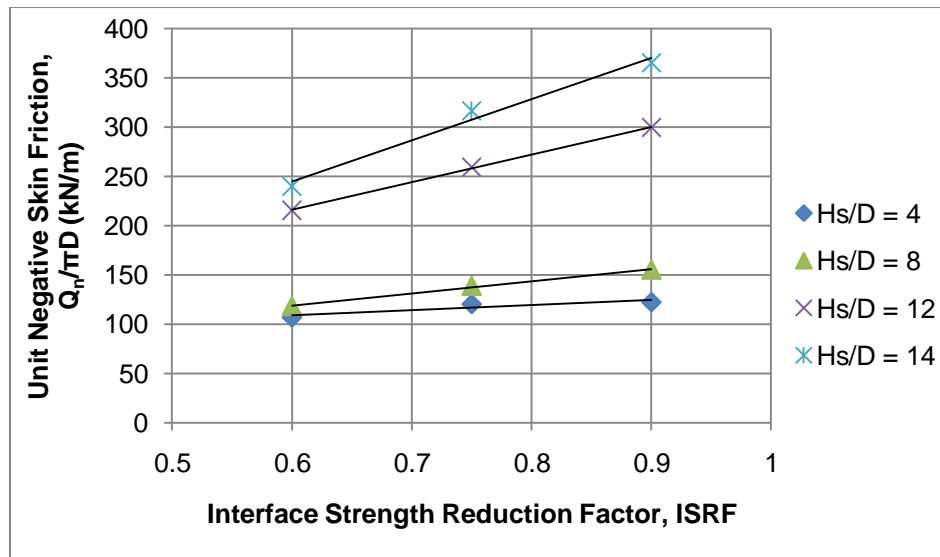
Figure 4.43: Effect of Interface Strength Reduction Factor (ISRF) on unit negative skin friction ($Q_n/\pi D$), where h = 10 m and C_p = 5%

It is to note that ISRF has insignificant influence on the unit negative skin friction $(Q_n/\pi D)$, when H_s/D, h and C_p are close to their respective lower limits, where Q_n, $Q_n/\pi D$ or q_n is naturally low. Instead, Q_n, $Q_n/\pi D$ or q_n increases if any of the sensitive parameters (i.e., H_s/D, h and C_p) increases. Whenever any of the sensitive parameters is close to its upper limit, the effect of ISRF in predicting the value of indirect load (Q_n) on pile due to NSF should be taken into considerations. Alternately, the reduced value of Q_n should be taken into consideration in pile design, if any sensitive parameter is close to its lower limit.

4.5.4 Effect of Collapse Potential

The effect of collapse potential (C_p) on average negative shear stress (q_n) is studied in this section. Figure 4.45–Figure 4.47 shows the variation of q_n with C_p for different h. It is noted that there exists a linear relation between average negative shear stress (q_n) and collapse potential (C_p) in each case. For a given radius of wetting front (h), the straight line in q_n vs C_p plot passes through origin.
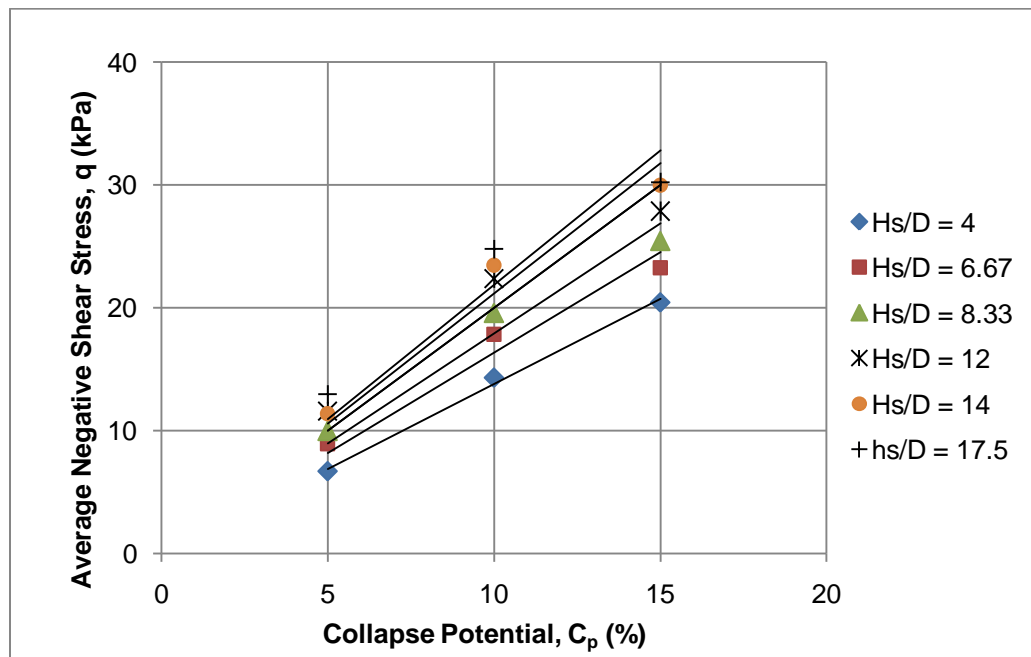
Figure 4.44: Average negative shear stress (q_n) vs. collapse potential (C_p), when h = 3 m
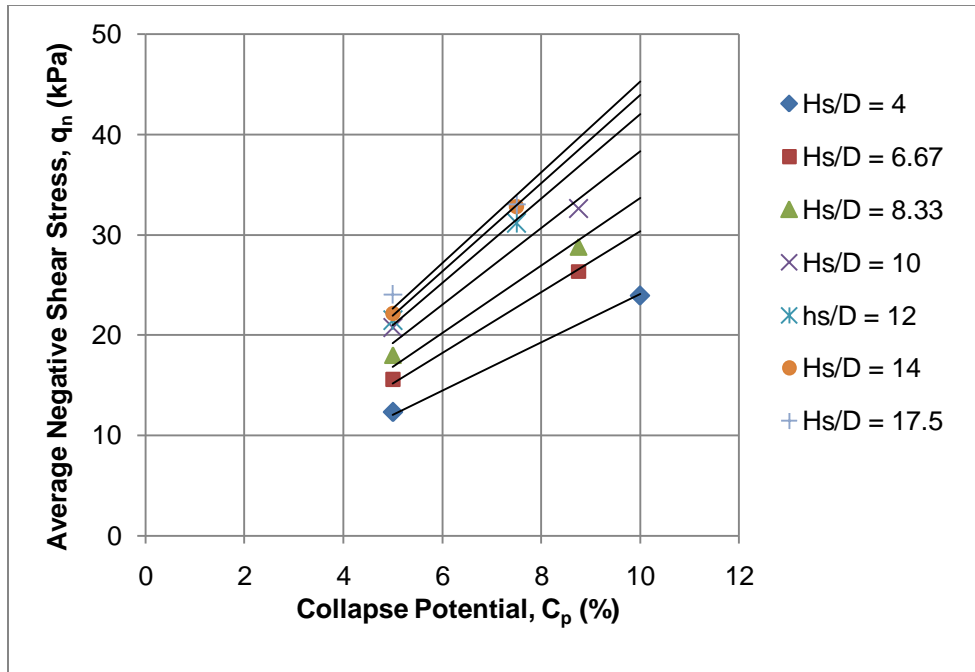
Figure 4.45: Average negative shear stress (q_n) vs. collapse potential (C_p), when h = 5 m
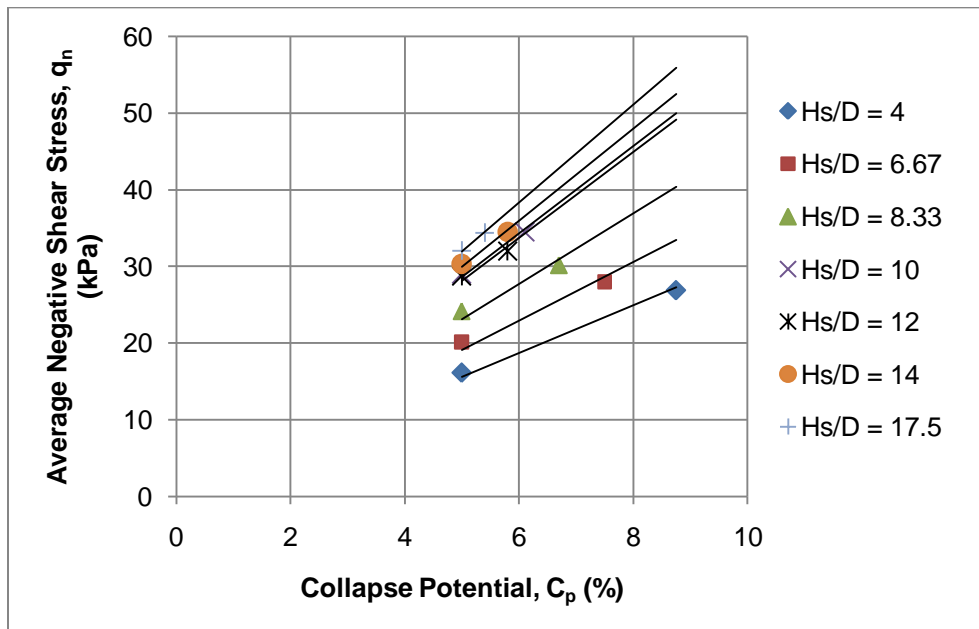
Figure 4.46: Average Negative Shear Stress (q_n) vs. Collapse Potential (C_p), when h = 7 m
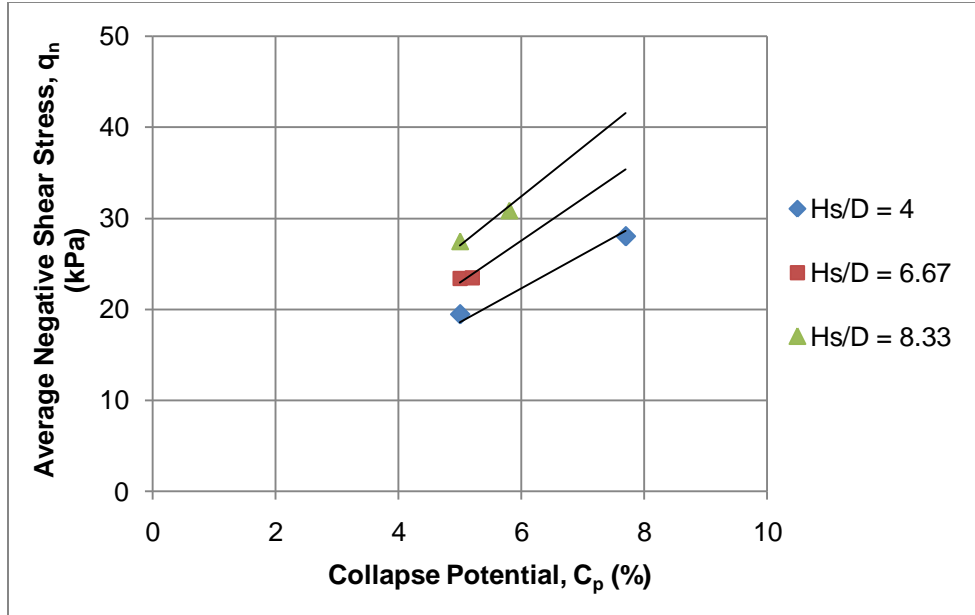
Figure 4.47: Average negative shear stress (q_n) vs. collapse potential (C_p), when h = 10 m

It can be noted that the proportional coefficient relating q_n and C_p varies with H_s/D. The value of proportional coefficient also increases if the H_s/D ratio is less than 14, for a given radius of wetting. A combined effect of C_p and h on the maximum value of NSF developed is noticed, and will be addressed further in Chapter 5.

4.6 Parametric Study for the Case of Inundation from Top

The effect of the depth of collapsing soil-to-pile diameter ratio (H_s/D), the radius of wetting front (h) and the collapse potential (C_p) are studied in case of inundation of collapsible soil from top. The indirect load due to NSF is studied in terms of unit negative skin friction ($Q_n/\pi D$). For a given thickness of collapsing soil and pile, inundation from the top causes less Q_n than inundation from the bottom. ISRF is taken 0.9 in the following cases.

4.6.1 Effect of H_s/D Ratio

Unit negative skin friction ($Q_n/\pi D$) shows linear variation with the increase of H_s/D ratio, as shown in Figure 4.48–Figure 4.50. High collapse potential of the collapsing soil and wide wetting front are found to increase the intensity of the effect of H_s/D ratio on $Q_n/\pi D$.
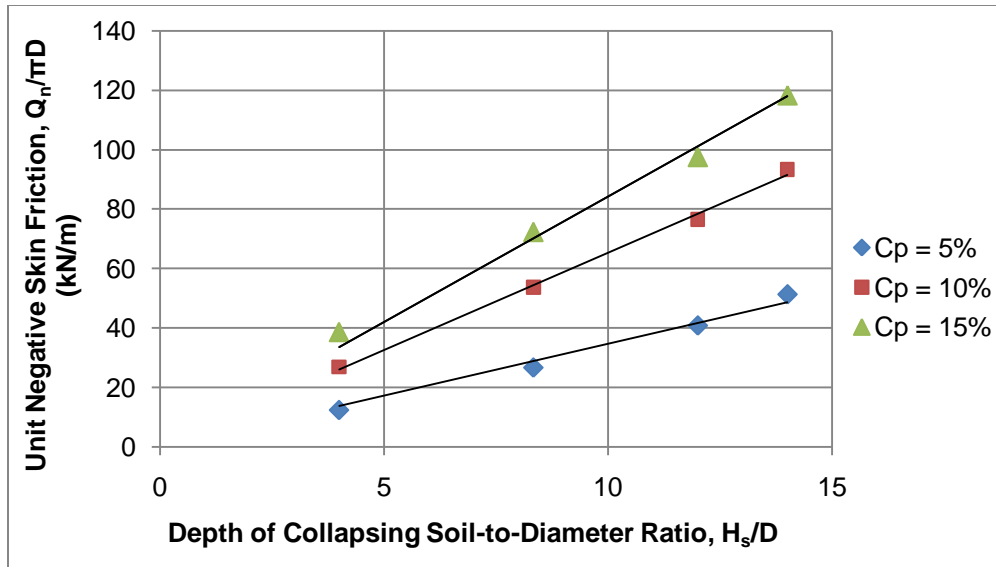
Figure 4.48: Unit negative skin friction ($Q_n/\pi D$) vs. H_s/D ratio, when h = 3 m
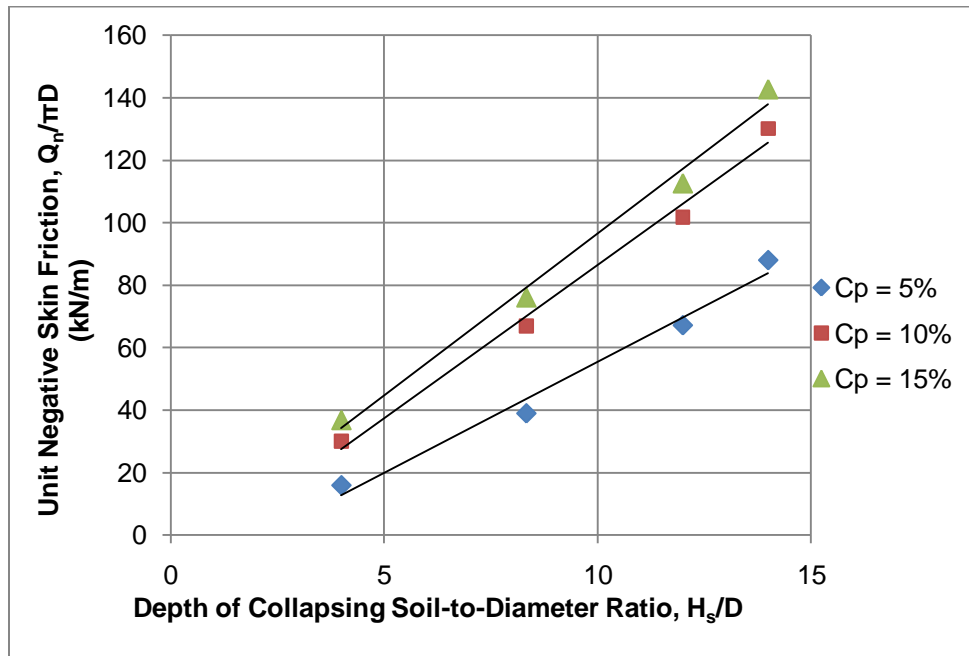
Figure 4.49: Unit negative skin friction ($Q_n/\pi D$) vs. H_s/D ratio, when h = 7 m
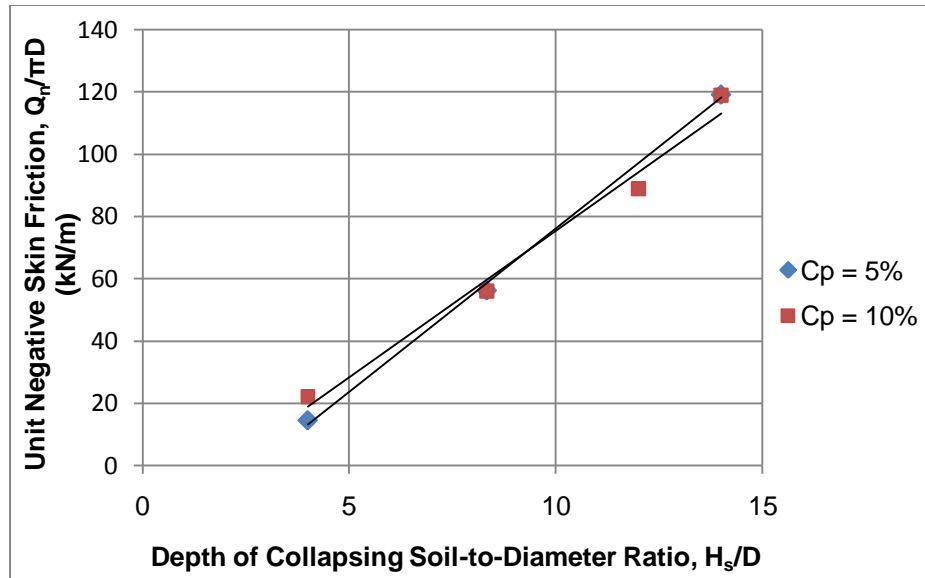
Figure 4.50: Unit negative skin friction ($Q_n/\pi D$) vs. H_s/D ratio, when h = 10 m

In case of 10 m radius of wetting front, collapse potential is not found to have significant influence on $Q_n/\pi D$, as shown in Figure 4.50. It is possible that $Q_n/\pi D$ already reaches its maximum value due to the wetting of 7 m radius front. Beyond this level, soil becomes detached from the pile. Therefore, any increase in the radius of wetting front and the collapse potential could not further increase the value of $Q_n/\pi D$.

4.6.2 Effect of Radius of Wetting

Figure 4.51–Figure 4.53 show the effect of the radius of wetting front on $Q_n/\pi D$, for different H_s/D ratio and C_p. It is found that $Q_n/\pi D$ does not increase infinitely with the increase of h. Figure 4.52 demonstrates that $Q_n/\pi D$ attains its maximum value due to wetting of 7 m of radius front.

140
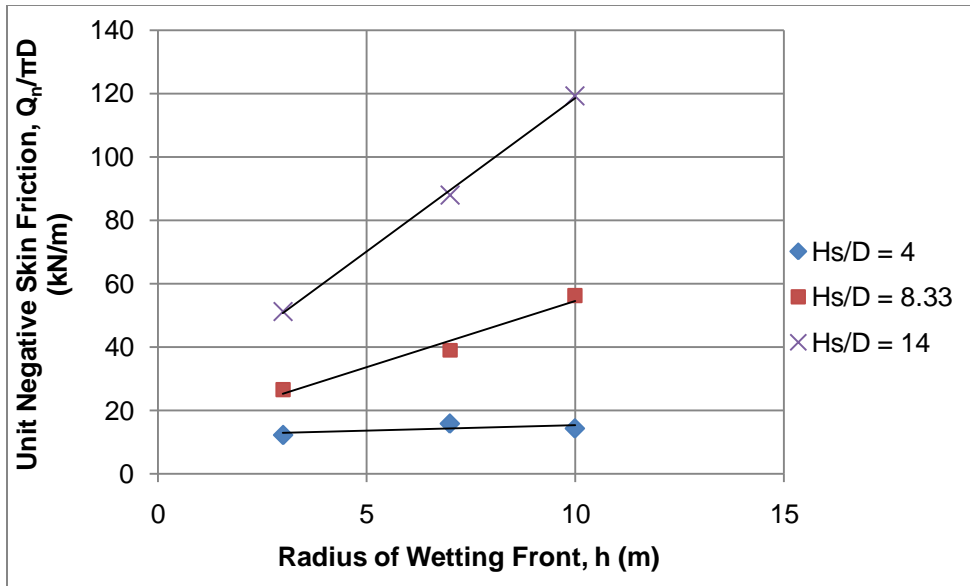
Figure 4.51: Effect of radius of wetting front (h) on unit negative skin friction $(Q_n/\pi D)$, when $C_p = 5\%$
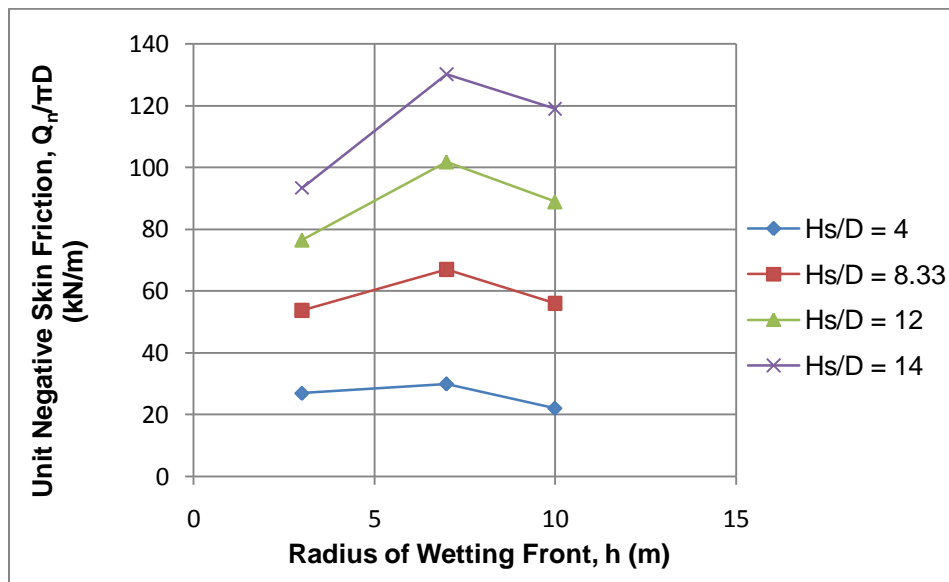
Figure 4.52: Effect of radius of wetting front (h) on Unit negative skin friction $(Q_n/\pi D)$, when $C_p = 10\%$
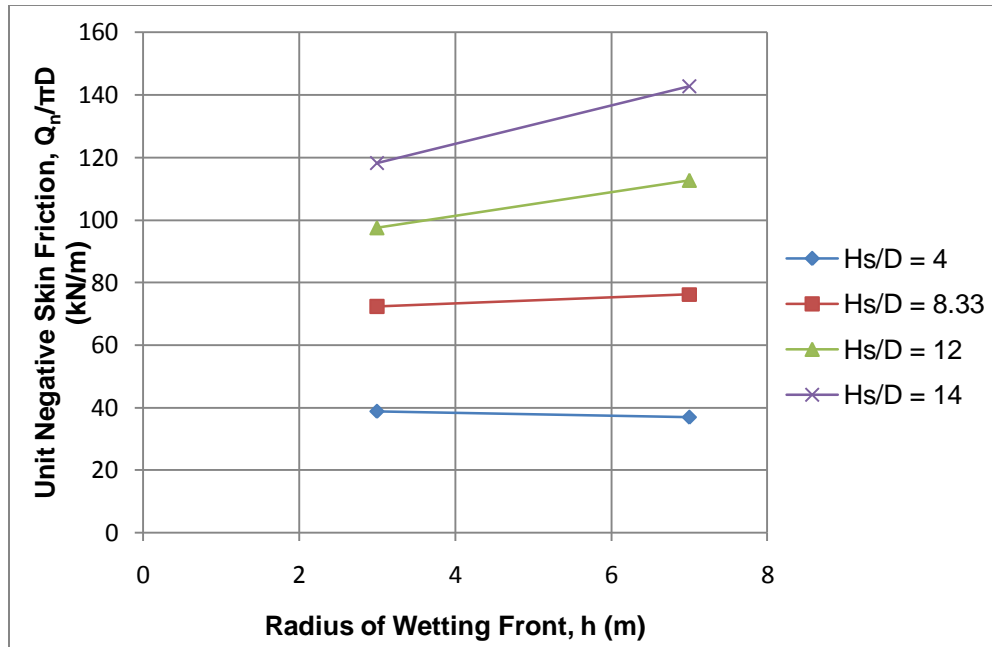
Figure 4.53: Effect of radius of wetting front (h) on unit negative skin friction $(Q_n/\pi D)$, when $C_p = 15\%$

4.6.3 Effect of Collapse Potential

Figure 4.54–Figure 4.56 show the effect of collapse potential (C_p) on $Q_n/\pi D$, for different H_s/D ratio and h. Between 5–10% of collapse potential, the effect of C_p is more pronounced than any other condition beyond this range. Moreover, h and C_p have influence on $Q_n/\pi D$ in this respect.
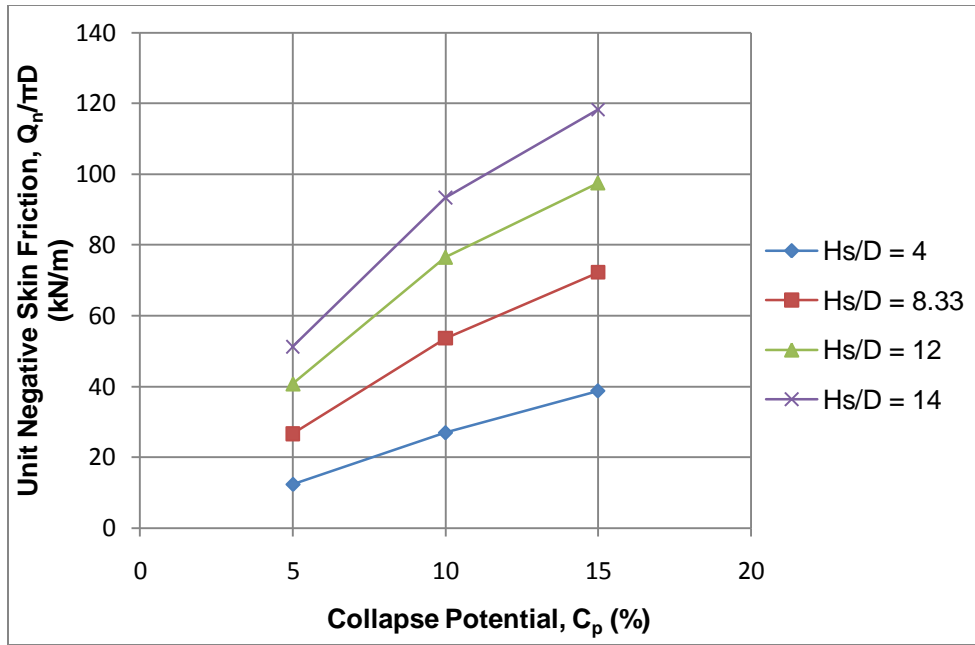
Figure 4.54: Effect of collapse potential (C_p) on unit negative skin friction ($Q_n/\pi D$), when h = 3 m
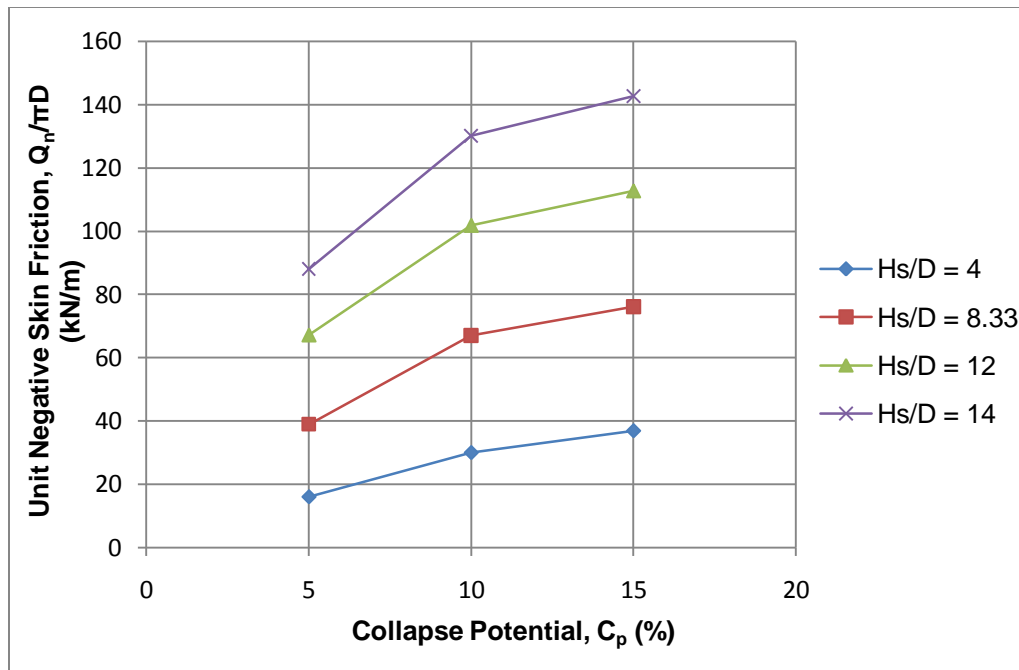
Figure 4.55: Effect of collapse potential (C_p) on unit negative skin friction ($Q_n/\pi D$), when h = 7 m
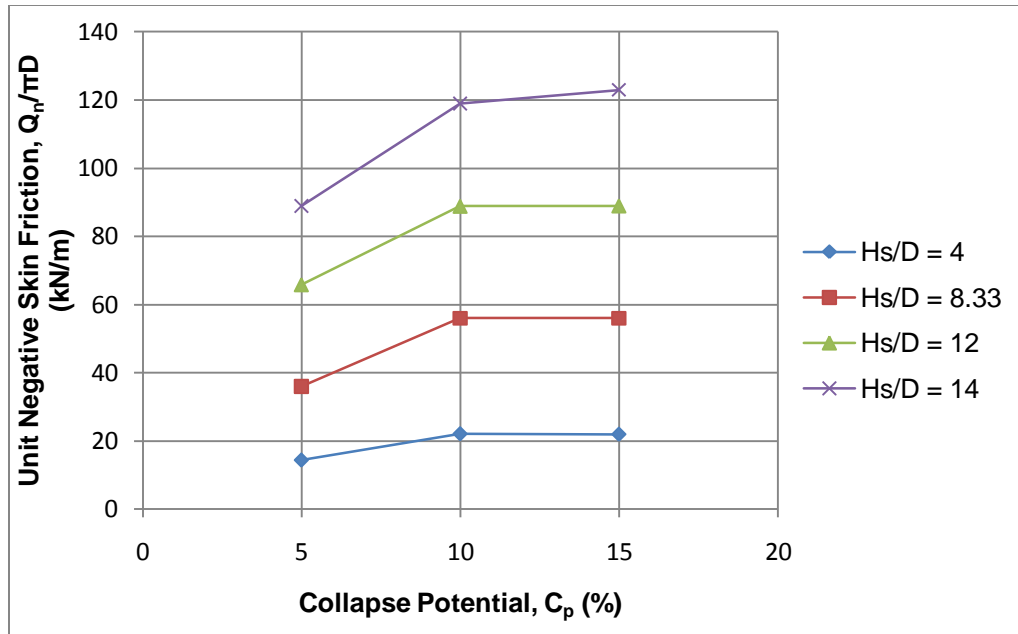
Figure 4.56: Effect of collapse potential (C_p) on unit negative skin friction ($Q_n/\pi D$), when h = 10 m

4.7 Discussion

Based on the numerical results, collapse potential, radius of wetting, direction of wetting (from bottom or top) and interface strength reduction factor are found to have significant influence on the shear stress developed on the pile interface during inundation of collapsible soil around the pile. Instead, angle of soil internal friction (φ), L_e/L and L/D ratios have no effect on average negative shear stress (q_n). Further, H_s/D ratio governs the magnitude of average negative shear stress.

In this study, it is found that the value of the average negative shear stress usually varies between 12 to 30 kPa. Note that the experimental results of Chen et al. (2008) also confirm this range.

CHAPTER 5

ANALYTICAL MODELING

5.1 General

In the literature, no analytical model is presently available to predict the indirect load on pile due to negative skin friction (NSF), caused by the inundation of collapsible soil (around the pile). Moreover, the combined effects of different factors (related to soil and inundation conditions, and pile geometry) on the development NSF were not known from previous studies. Based on the numerical results and analysis, this study presents the analytical models to determine the indirect load on the pile due to NSF for both the directions of inundation—from the bottom and the top—for any given set of conditions. To our knowledge, the first design procedure that can provide adequate positive skin friction and pile capacity in accommodating indirect load due to NSF, is given here to design a single pile foundation in collapsible soil that may experience inundation.

5.2 Development of Analytical Models for the Case of Inundation from Bottom

Analytical models are developed to determine average negative shear stress (q_n) and the depth of neutral axis (N.A.), as the product, of q_n and N.A., is the unit negative skin friction ($Q_n/\pi D$), in case of inundation of collapsible soil from bottom up to half depth of the layer. Based on the numerical investigations, q_n is found directly proportional to collapse potential (C_p). Therefore, q_n can be defined by Eqn 5.1.

$$\text{Average negative shear stress, } q_n = k*C_p \ldots\ldots\ldots\ldots\ldots\ldots..(5.1)$$

Where, k = Proportional constant = $f(H_s/D, h)$,

C_p = Collapse potential (%).
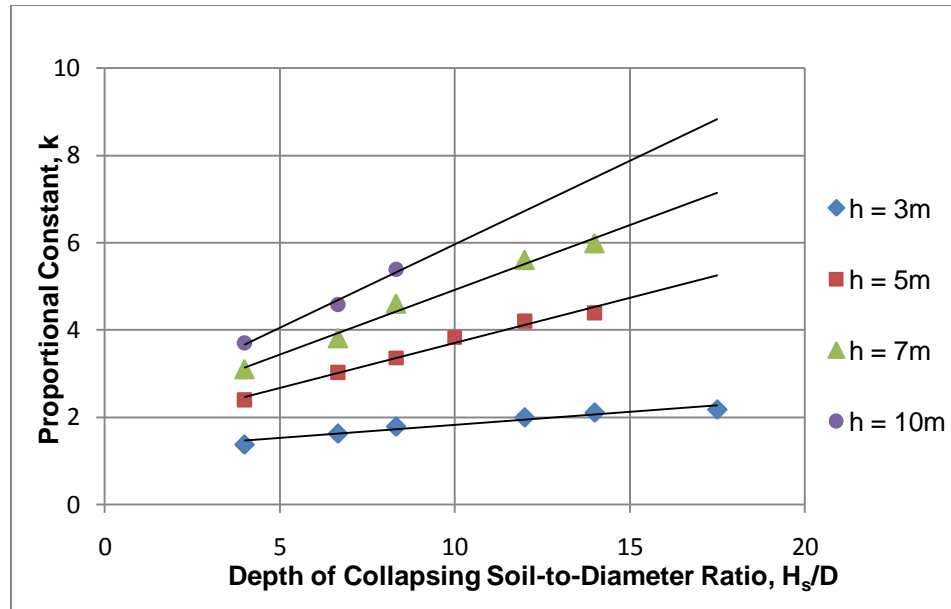
Figure 5.1: Proportional constant (k) vs. H$_s$/D ratio for different radius of wetting front (h)

The value of proportional constant (k) depends on H$_s$/D and the radius of wetting (h), as shown in Figure 5.1. It can also be determined using the relations, given in Eqns 5.2–5.5, obtained from Figure 5.1..

For h = 3m,

$$k = 0.0597 \, (H_s/D) + 1.226 \ldots\ldots\ldots\ldots\ldots\ldots\ldots\ldots\ldots\ldots\ldots\ldots\ldots (5.2)$$

For h = 5m,

$$k = 0.206 \, (H_s/D) + 1.647 \ldots\ldots\ldots\ldots\ldots\ldots\ldots\ldots\ldots\ldots\ldots\ldots (5.3)$$

For h = 7m,

$$k = 0.2966 \, (H_s/D) + 1.958 \ldots\ldots\ldots\ldots\ldots\ldots\ldots\ldots\ldots\ldots\ldots\ldots (5.4)$$

For h = 10m,

$$k = 0.3825 \, (H_s/D) + 2.140 \ldots\ldots\ldots\ldots\ldots\ldots\ldots\ldots\ldots\ldots\ldots\ldots (5.5)$$
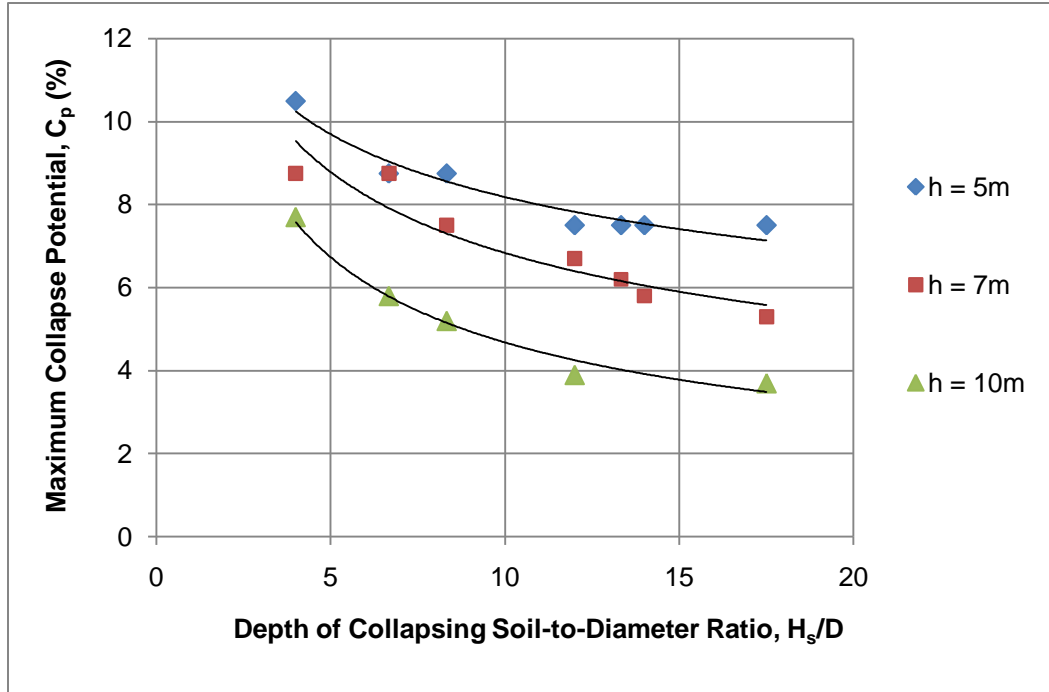
Figure 5.2: Maximum collapse potential

The combined effects of H_s/D ratio and h on the collapse potential (C_p) that can effectively contribute to the increase in q_n are established in Figure 5.2, based on the numerical results. This indicates that q_n does not increase infinitely due to the increase in any of the influencing factors such as H_s/D ratio, h or C_p, though the proportional constant (k) increases with the increase of H_s/D ratio and h. The maximum value of C_p (from Figure 5.2) can also be determined using Eqns 5.6–5.8, for a given condition (i.e., defined by H_s/D ratio and h).

For h = 5 m,

$$C_p = 14.385 * \left(\frac{H_s}{D}\right)^{-0.245} \dots\dots\dots\dots\dots\dots\dots\dots\dots\dots\dots\dots\dots\dots(5.6)$$

For h = 7 m,

$$C_p = 15.75 * \left(\frac{H_s}{D}\right)^{-0.363} \dots\dots\dots\dots\dots\dots\dots\dots\dots\dots\dots\dots\dots\dots(5.7)$$

For h = 10 m,

$$C_p = 15.698 * \left(\frac{H_s}{D}\right)^{-0.526} \dots\dots\dots\dots\dots\dots\dots\dots\dots\dots\dots\dots\dots\dots(5.8)$$

Therefore, the maximum possible value of q_n can be determined using Eqn 5.1.

The analytical model to predict the depth of neutral axis (N.A.) (i.e., required to estimate indirect load (Qn) due to NSF) is proposed. Based on the numerical results, it is found that the depth of neutral axis (N.A.) from the ground is less than the depth of the bottom of the collapsible soil (H = 2 * Hs). N.A. is the sum of the depth of unsaturated collapsible soil (H_s) and N´ (the portion of N.A. in contact with collapsing soil). Alternately, N´ is equal to the depth of neutral axis (N.A.) minus the depth of unsaturated collapsible soil (overlying the collapsing soil), as given in Eqn 5.9. N´ is defined by Eqn 5.10, since it is proportional to the depth of collapsing soil for a given radius of wetting (h) and Cp, as shown in Figure 5.3 and Figure 5.4.
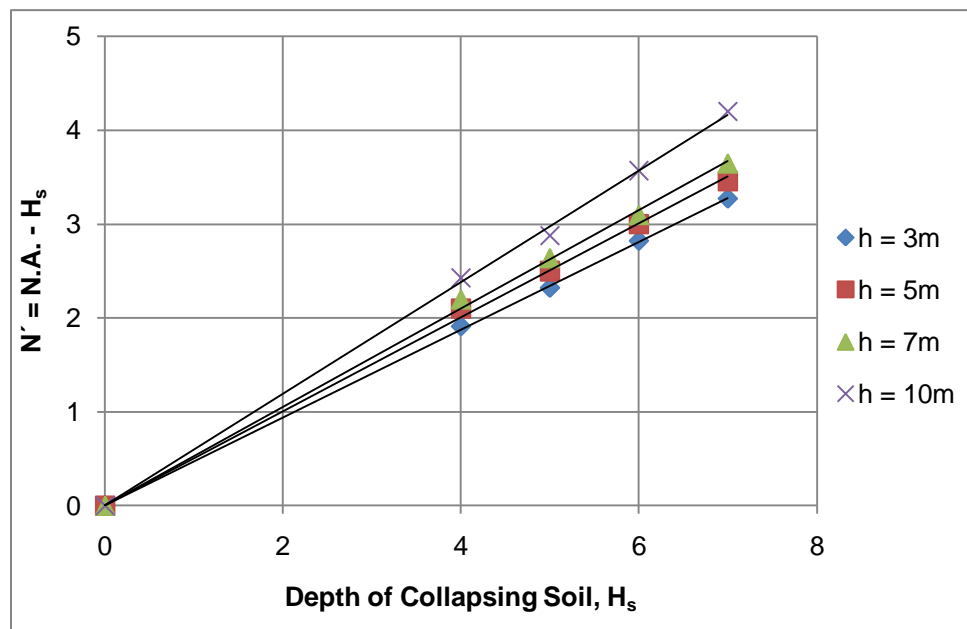
Figure 5.3: Effect of depth of collapsing soil (H_s) on N´, when Cp = 5%

Therefore,

$$N´ = N.A - H_s \dots\dots\dots\dots\dots\dots\dots\dots\dots\dots\dots\dots\dots\dots\dots\dots\dots(5.9)$$

$$N´ = m * H_s \dots\dots\dots\dots\dots\dots\dots\dots\dots\dots\dots\dots\dots\dots\dots\dots\dots\dots\dots\dots(5.10)$$

Where, m = Proportional coefficient relating to H_s and N´

= f (C_p, h).
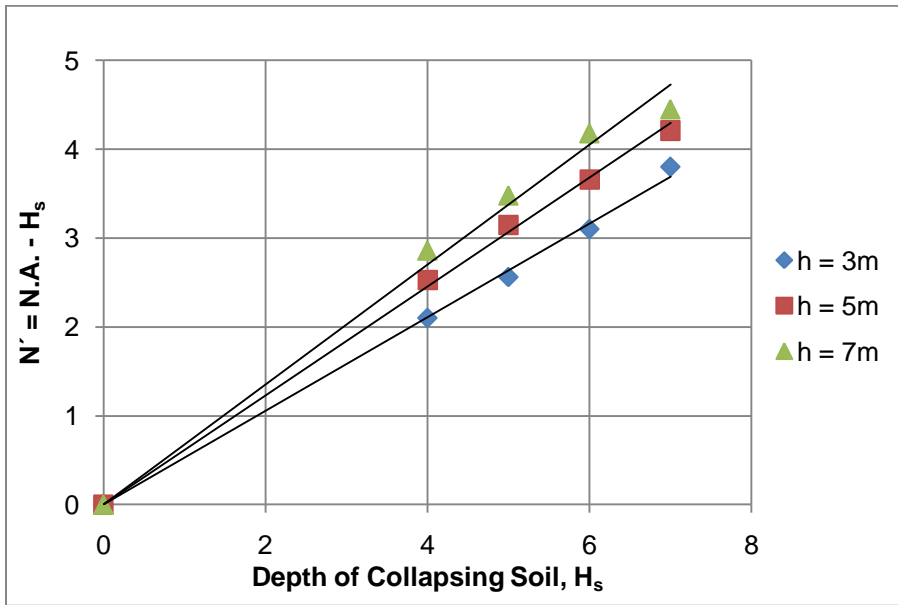
**Figure 5.4: Effect of depth of collapsing soil (H_s) on N´,
when C_p = 10%**

The value of 'm' depends on C_p linearly, as shown in Figure 5.5, for any radius of wetting (h). This relation can be defined by Eqn 5.11, for a given 'h'.

$$m = m_1 * C_p + m_2 \dots\dots\dots\dots\dots\dots\dots\dots\dots\dots\dots\dots\dots\dots(5.11)$$

Where, $m_1 = f(h)$, as shown in Figure 5.6,
and m_2 = Constant for any radius of wetting = 0.4
From Figure 5.6,

$$m_1 = 0.0045\ h - 0.0012\dots\dots\dots\dots\dots\dots\dots\dots\dots\dots\dots..(5.12)$$

Based on Eqns 5.9–5.12, Eqn 5.13 is developed and is proposed to predict the depth of neutral axis (N.A.).
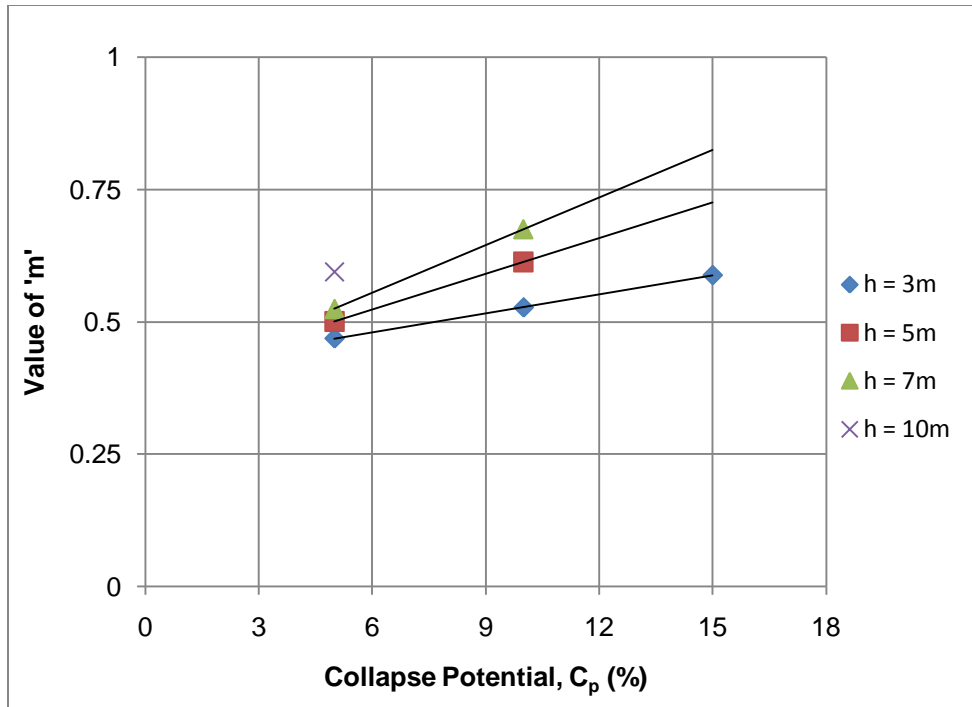
Figure 5.5: Effect of collapse potential (C_p) on the value of 'm'
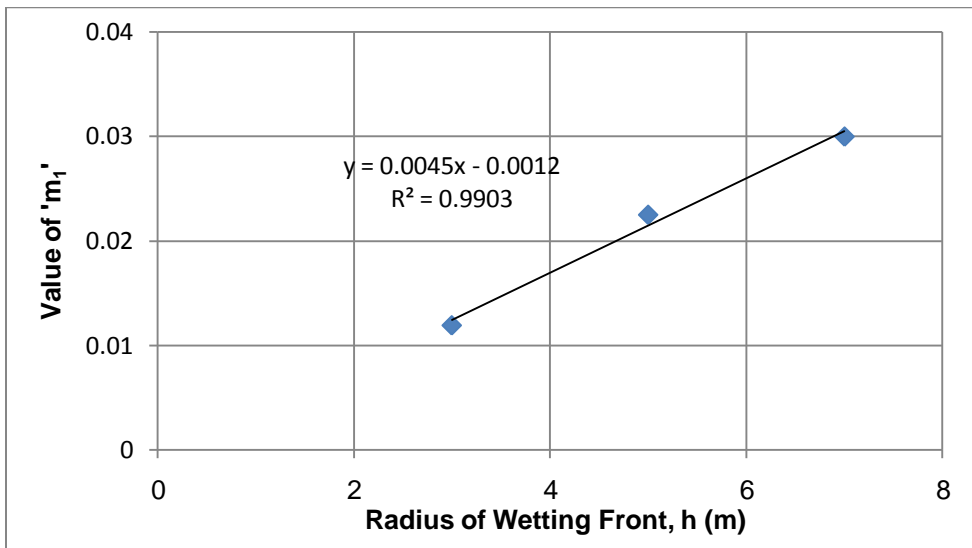
Figure 5.6: Effect of radius of wetting (h) on the value of 'm_1'

$$\text{N.A.} = m*H_s + H_s$$
$$= (m + 1) * H_s$$
$$= (m_l *C_p + b + 1) * H_s$$
$$= (m_l *C_p + 1.4) * H_s$$
$$= \{(0.0045\,h - 0.0012) * C_p + 1.4\}\, H_s \dots\dots\dots\dots\dots\dots\dots\dots\dots\dots\dots\dots(5.13)$$

Eqn 5.13 is used to determine the neutral depth for some selected cases to verify that predicted values are in good agreements with the values obtained directly from numerical investigation (as shown in Figure 5.7).
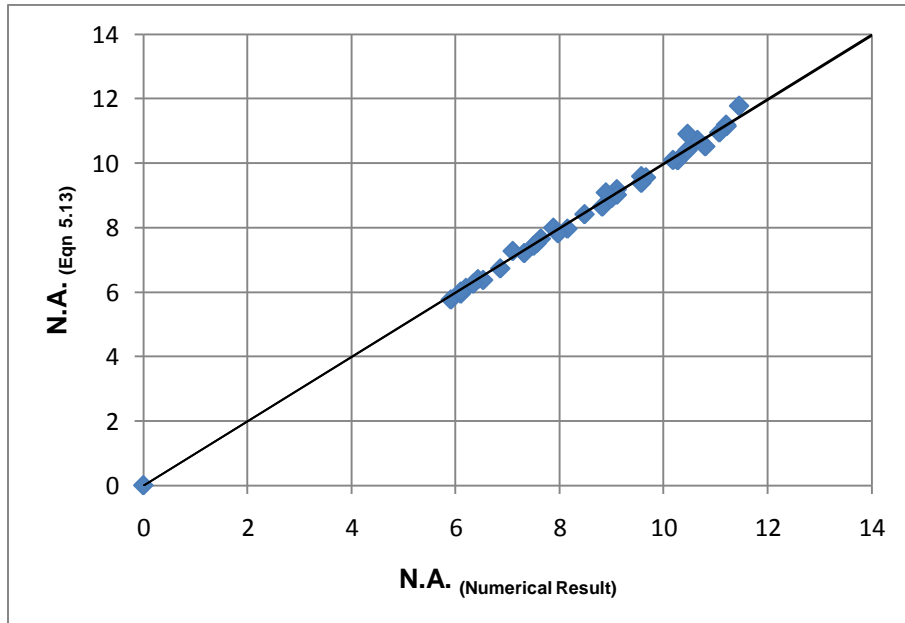
Figure 5.7: Comparison between numerical and predicted values of neutral depth

Once the values of 'k' (Eqns 5.2–5.5) and N.A. (Eqn 5.13) are known, the indirect load (Q_n) due to NSF can be predicted using Eqn 5.14.

$$Q_n = q_n * \text{N.A.} * \pi D \dots\dots\dots\dots\dots\dots\dots\dots\dots\dots\dots\dots\dots\dots(5.14)$$

Where, D = pile diameter.
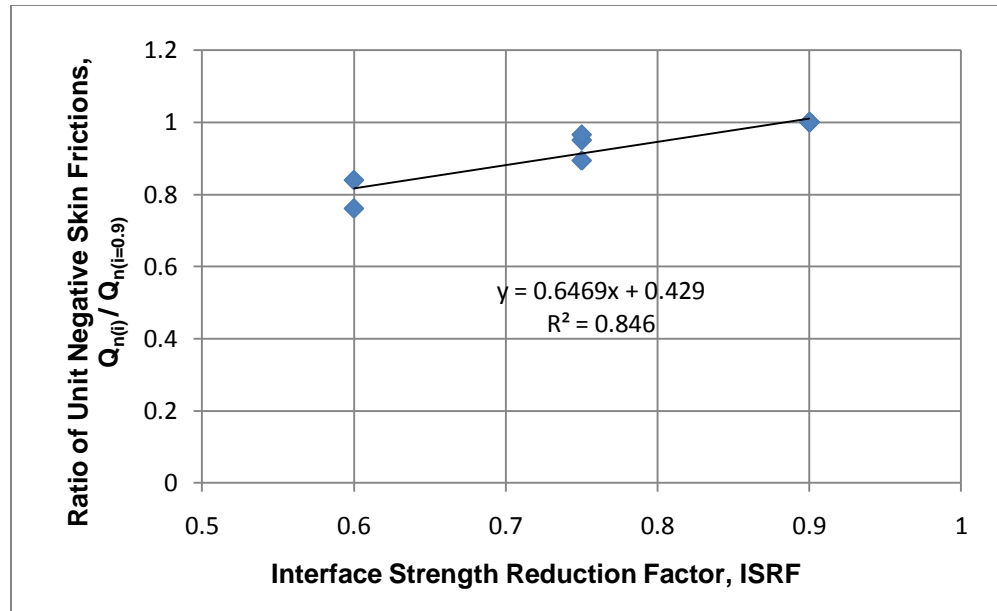
Figure 5.8: Effect of Interface Strength Reduction Factor (ISRF) on unit negative skin friction ($Q_n/\pi D$), when $H_s/D = 8$

The above equations are developed for the interface strength reduction factor (ISRF) of 0.9. A factor is recommended to apply on the indirect load (Q_n) to accommodate the effect of pile roughness. For a given H_s/D ratio, the ratio of indirect load at any ISRF to indirect load at 0.9 ISRF (Eqn 5.1, Eqn 5.13 and Eqn 5.14) has a linear relation with the ISRF, which is shown in Figure 5.8. Q_n for any pile interface roughness (applying the corresponding ISRF) can be estimated using Eqn 5.15.

$$Q_{n(i)}/ Q_{n(0.9)} = I_M * (ISRF) + I_c \ldots\ldots\ldots\ldots\ldots\ldots\ldots\ldots\ldots\ldots(5.15)$$

Note that the values of I_M and I_c are known from Figure 5.9 and Figure 5.10 respectively.
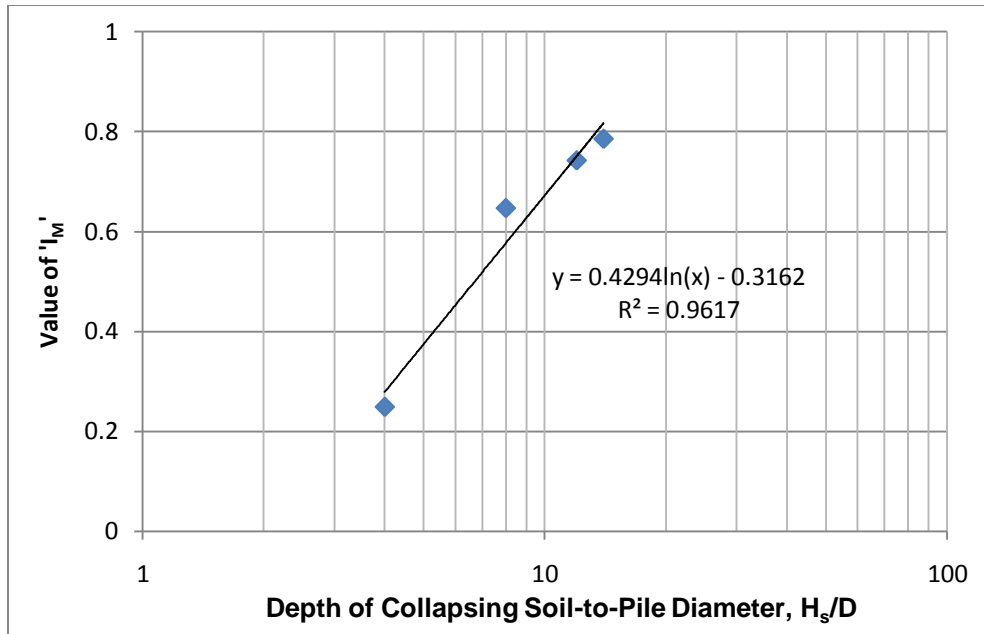
Figure 5.9: Value of I_M for different depth of collapsing soil-to-pile diameter ratio (H_s/D)
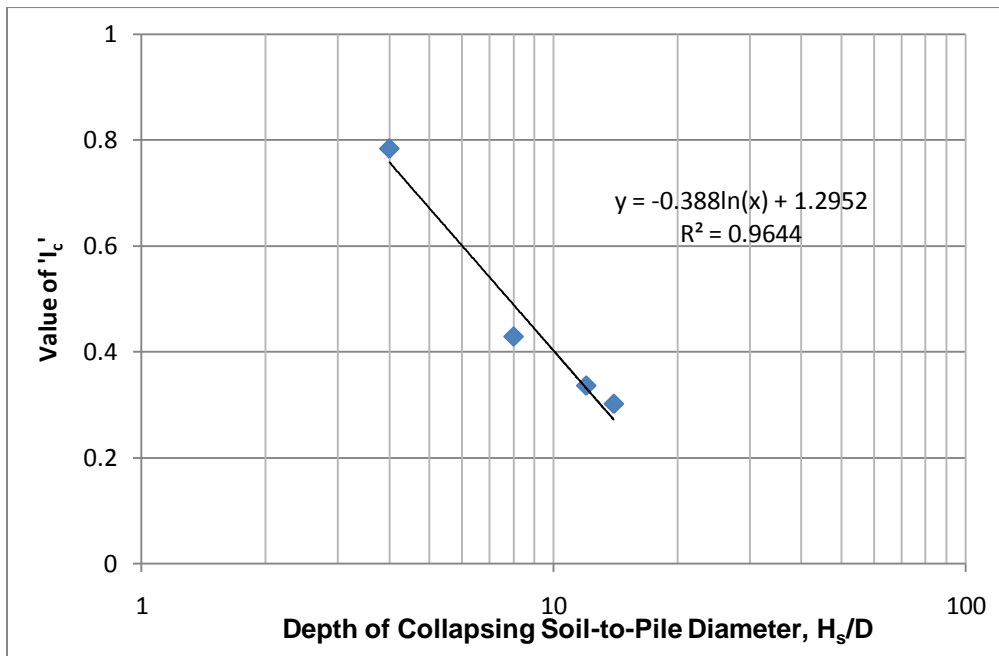
Figure 5.10: Value of I_c for different depth of collapsing soil-to-pile diameter ratio (H_s/D)

5.3 Development of Analytical Models for the Case of Inundation from Top

This section presents the analytical models to predict indirect load (Q_n) due to NSF resulting from the inundation of collapsible soil from the top. Based on the numerical results, unit negative skin friction ($Q_n/\pi D$) has a linear relation with H_s/D, as defined by Eqn 5.16.

$$Q_n/\pi D = I_a * (H_s/D) + I_b \ldots\ldots\ldots\ldots\ldots\ldots\ldots\ldots\ldots\ldots\ldots\ldots\ldots..(5.16)$$

The values of I_a and I_b depends on the collapse potential (C_p), as $Q_n/\pi D$ shows two slopes between 5–10% of collapse potential and 10–15% of collapse potential for a given H_s/D ratio. The values of I_a and I_b depends on H_s/D ratio, as shown in Figure 5.11–Figure 5.14.
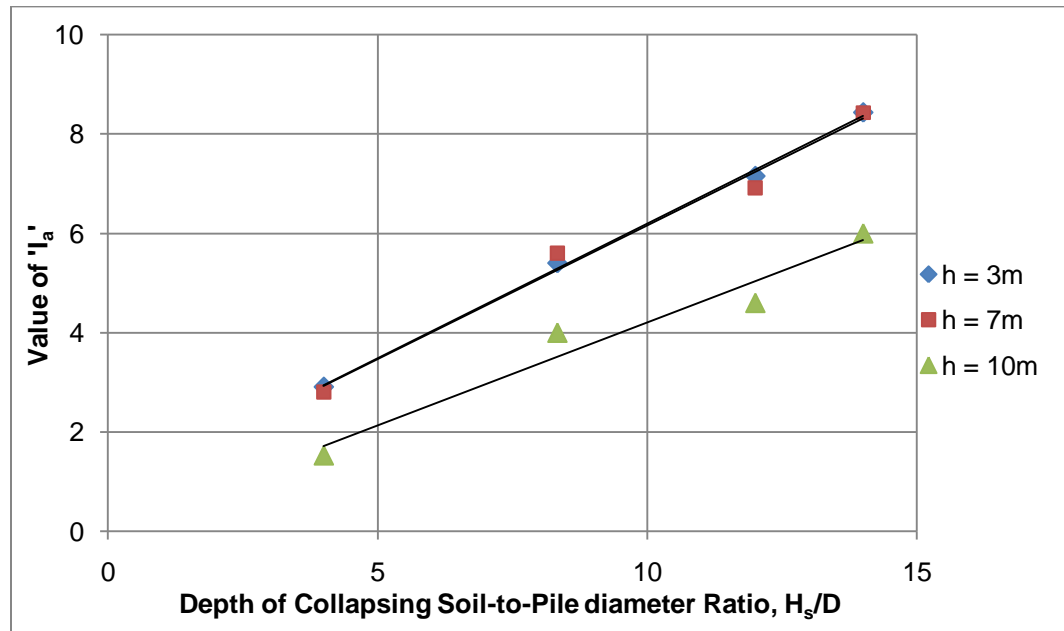
Figure 5.11: Value of I_a for different H_s/D and h, when C_p = 5–10%
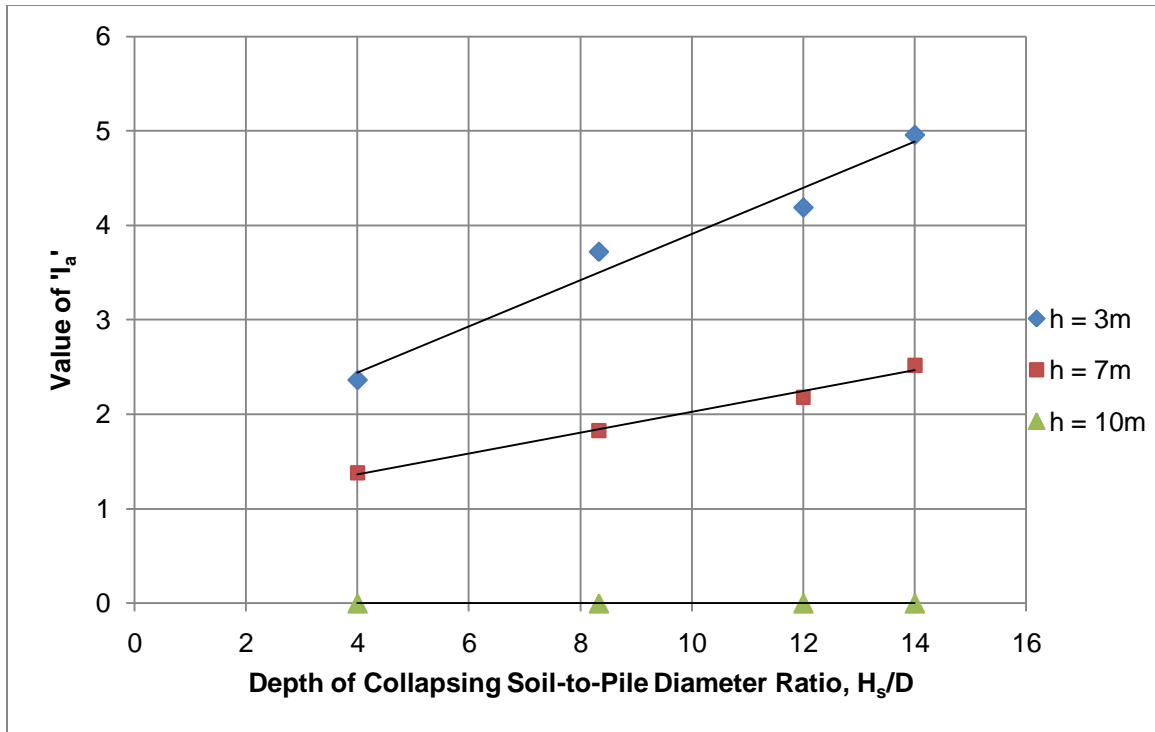
Figure 5.12: Value of I_a for different H_s/D and h, when C_p = 10–15%

The value of I_a can be found from Eqn 5.17 – Eqn5.19 and Eqn 5.20 – Eqn 5.22 for C_p between 5-10% and 10-15%, respectively.

For h = 3 m and C_p between 5-10%,
$$I_a = 0.5425 \, (H_s/D)^2 + 0.7738 \quad\text{..} \quad (5.17)$$

For h = 7 m and C_p between 5-10%,
$$I_a = 0.5392 \, (H_s/D) + 0.7705 \quad\text{..} \quad (5.18)$$

For h = 10 m and C_p between 5-10%,
$$I_a = 0.4144 \, (H_s/D) + 0.0613 \quad\text{..} \quad (5.19)$$

For h = 3 m and C_p between 10-15%,
$$I_a = 0.2445 \, (H_s/D) + 1.4641 \quad\text{..} \quad (5.20)$$

For h = 7 m and C_p between 10-15%,

$$I_a = 0.1103 \, (H_s/D) + 0.9207 \ldots\ldots\ldots\ldots\ldots\ldots\ldots\ldots\ldots\ldots\ldots\ldots\ldots\ldots \quad (5.21)$$

For h = 10 m and C_p between 10-15%,

$$I_a = 0 \ldots\ldots\ldots\ldots\ldots\ldots\ldots\ldots\ldots\ldots\ldots\ldots\ldots\ldots\ldots\ldots\ldots\ldots \quad (5.22)$$
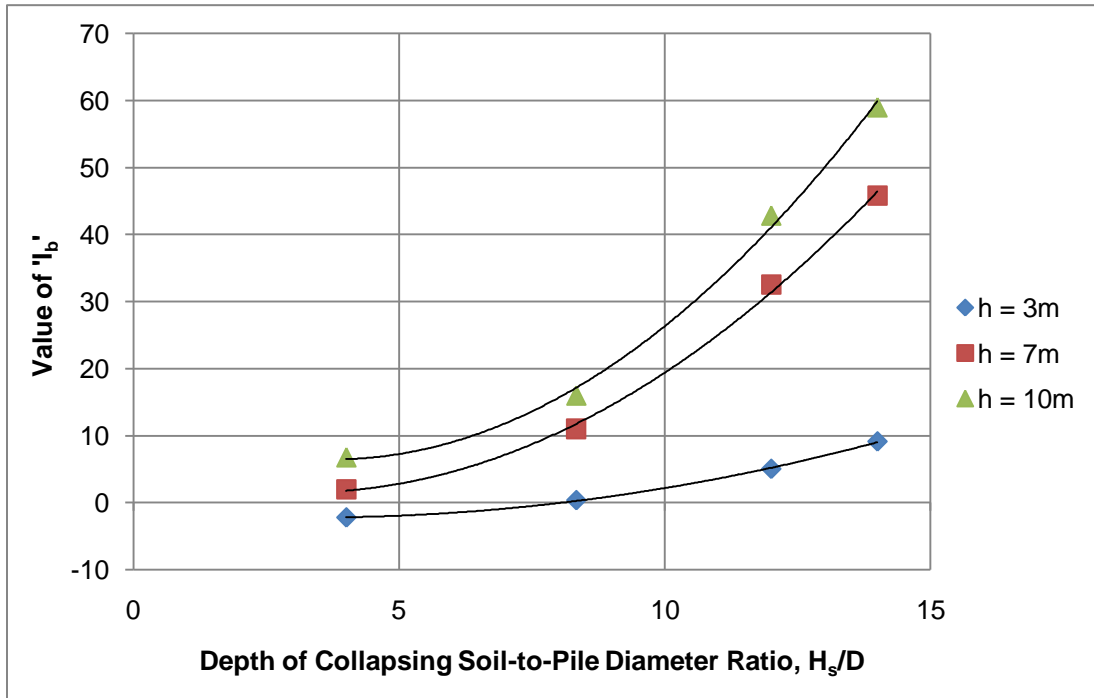
Figure 5.13: Value of I_b for different H_s/D and h, when C_p = 5–10%

The value of I_b can be found from Eqn 5.23 – Eqn5.25 and Eqn 5.26 – Eqn 5.28 for C_p between 5-10% and 10-15%, respectively.

For h = 3 m and C_p between 5-10%,

$$I_b = 0.098 \, (H_s/D)^2 - 0.6545 \, (H_s/D) - 1.13 \ldots\ldots\ldots\ldots\ldots\ldots\ldots\ldots \quad (5.23)$$

For h = 7 m and C_p between 5-10%,

$$I_b = 0.381 \, (H_s/D)^2 - 2.4 \, (H_s/D) + 5.29 \ldots\ldots\ldots\ldots\ldots\ldots\ldots\ldots\ldots \quad (5.24)$$

For h = 10 m and C_p between 5-10%,

$$I_b = 0.508 \ (H_s/D)^2 - 3.8 \ (H_s/D) + 13.56 \dots\dots\dots\dots\dots\dots\dots\dots\dots\dots \ (5.25)$$

For h = 3 m and C_p between 10-15%,

$$I_b = 4.0933 \ (H_s/D) - 14.72 \dots\dots\dots\dots\dots\dots\dots\dots\dots\dots\dots\dots\dots \ (5.26)$$

For h = 7 m and C_p between 10-15%,

$$I_b = 8.707 \ (H_s/D) - 21 \dots\dots\dots\dots\dots\dots\dots\dots\dots\dots\dots..\dots\dots\dots \ (5.27)$$

For h = 10 m and C_p between 10-15%,

$$I_b = 8.76 \ (H_s/D) - 14.5 \dots..\dots\dots\dots\dots\dots\dots\dots..\dots\dots\dots\dots\dots \ (5.28)$$
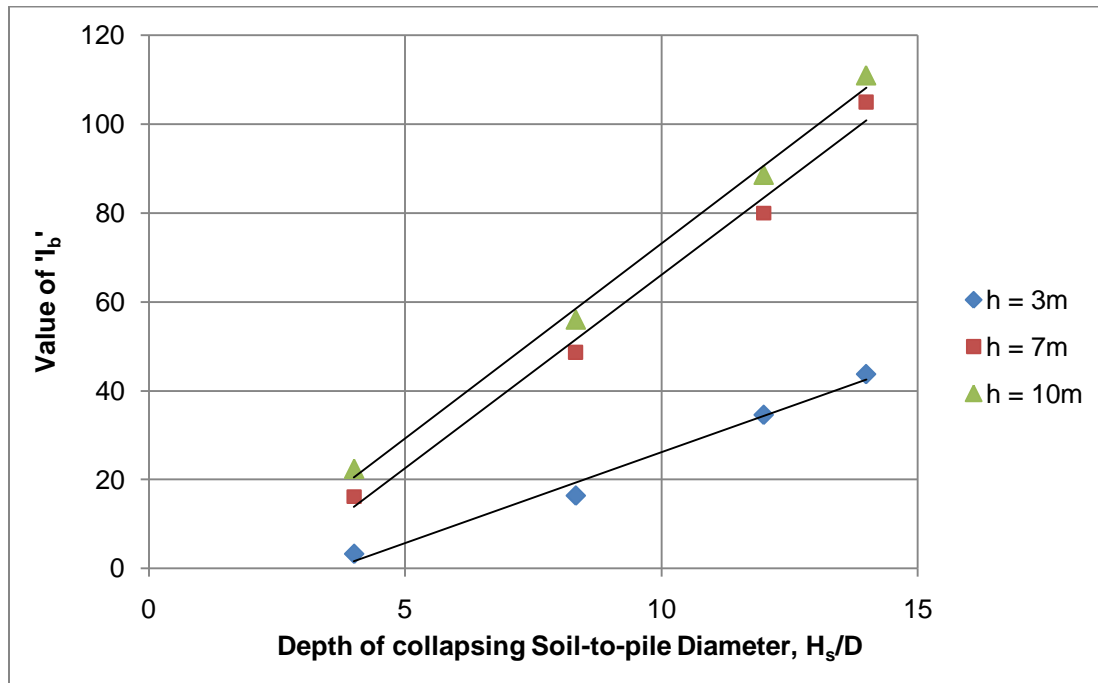
Figure 5.14: Value of I_b for different H_s/D and h, when C_p = 10–15%

Therefore, the indirect load (Q_n) due to NSF (at ISRF 0.9) can be predicted from the value of the unit negative skin friction (using Eqn 5.16) multiplied by perimeter (πD) for the case of inundation from the top.

157

5.4 Design Procedure

In order to design a single pile in collapsible soil subjected to inundation, the following procedure is proposed.

1. Predict unit negative skin friction $(Q_n/\pi D)$ on pile interface due to full saturation of a given collapsible soil layer.

   a. In case of inundation causing collapse of bottom half of the collapsible layer, estimate the value of k and the maximum possible collapse potential (C_p) causing negative skin friction using Eqns 5.2–5.5 and Figure 5.1, respectively, based on the H_s/D ratio and h. Eqn 5.1gives the value of average negative shear stress (q_n) under the condition stated. Unit negative skin friction $(Q_n/\pi D)$ is determined from the average negative shear stress (q_n) multiplied by the depth of neutral axis from the ground surface (N.A.). Eqn 5.13 gives the N.A. value based on C_p, H_s and h.

   b. In case of inundation of collapsible soil from the top, estimate the values of I_a and I_b using Figures 5.11–5.14, based on C_p and h. Eqn 5.16 gives the value of unit negative skin friction $(Q_n/\pi D)$ under the condition stated.

2. Adjust the value of unit negative skin friction $(Q_n/\pi D)$ for the interface strength reduction factor, using I_M and I_c. The values of I_M and I_c are known from Figure 5.9 and Figure 5.10 respectively. This adjustment factor is developed for the inundation of the bottom half of collapsible soil. Since the negative skin friction due to inundation from the top is significantly smaller than that due to the inundation from the bottom, this step can be omitted for the case of inundation from the top.

3. Calculate the indirect load (Q_n) due to the negative skin friction resulting from full inundation of the collapsible soil of a given thickness from the value of unit negative skin friction $(Q_n/\pi D)$ multiplied by the perimeter of the pile.

4. The sum of the predicted indirect load and the external load can be applied in the proposed numerical model to investigate the pile performance in terms of shaft and pile tip resistances. Depending on the pile tip resistance that can be achieved from the given soil condition, a suitable length of pile can be chosen to provide adequate positive skin frictional resistance during inundation.

CHAPTER 6

CONCLUSIONS

6.1 General

There is a high possibility of wetting collapsible soil (i.e., supporting the foundation) and of experiencing inundation induced collapse accordingly, during the lifetime of the structure, as inundation is likely to occur with a high degree of probability or accidentally. Corrective measures, of fixing collapse induced foundation and structural problems, are expensive, Thus, it is important to design foundation in collapsible soil considering the effect of inundation so that structures could survive during soil collapse without having any sign of distress. To date, all currently available solutions (soil treatment and shallow foundation, stone column, compaction, etc.) can support only relatively light structures in collapsible soil. While pile foundation, driven to an existing bearing stratum underlying the collapsible soil layer, is considered the only available alternative, the negative impact of collapsible soil subjected to inundation is identified on its capacity (due to the development of negative skin friction) and performance (e.g., separation of the pile from the pile cap due to reduction in pile capacity) during the lifespan of the structure. The influence of different factors (such as thickness and location of collapsing soil, collapse potential, pile geometry and roughness, radius of wetting, direction of inundation, etc.), affecting the magnitude of indirect load (Q_n) due to negative skin friction (NSF), are not identified yet due to the limited data available in the literature. Investigation of foundation in collapsible soil requires high cost and the length of time, and the difficulty associated in obtaining reasonable experimental results. Numerical models of foundations in problematic soils, such as moisture sensitive soil (including collapsible soil and expansive soil) and soil sensitive to cyclic loading (i.e., sensitive clay), have not yet been developed due to the complexities in describing the problematic behavior of such soils numerically. In the literature, there is no analytical model presently available to predict indirect load on pile due to negative skin friction (NSF), caused by inundation of collapsible soil (around the pile). Though numerical

modeling of collapsible soil, without any change of soil moisture, can be achieved easily, it is inapplicable in examining the performance of foundation in collapsible soil during inundation, however. During inundation, collapsible soil affects the performance of pile significantly due to its radical volume change behavior. Present study is the first attempt in developing numerical model to incorporate the effect of inundation of collapsible soil, in order to study the performance of an axially loaded vertical pile and to propose a pile design procedure in this respect.

This chapter summarizes the conclusions drawn from the present study. Recommendations for future research are also given.

6.2 Conclusion

The following conclusions can be drawn:

1. A numerical model capable of incorporating the effect of inundation of collapsible soil was developed to investigate foundation performance during soil collapse using finite element technique. The numerical model was used to evaluate indirect load (Q_n) due to negative skin friction on pile resulting from inundation of collapsible soil. The model was validated with experimental data available in the literature.

2. Volumetric strain resulting from full saturation can be applied in a single calculation phase. Present study explains that collapsible soil reaches 100% degree of saturation with less amount of water than other moisture insensitive unsaturated soils and its void ratio decreases relatively fast.

3. Small deformation theory and Updated mesh analysis (using PLAXIS) give comparable results.

4. The numerical model is capable to investigate the effect of inundation (on a single vertical pile performance) from the bottom of collapsible soil (e.g., due to rise in ground water table) and also from the top (due to rainfall). The results of numerical model showed that a collapsible layer existing at a depth causes more severe problems than that existing near surface for a given thickness of collapsible soil subjected to inundation.

5. The numerical model was used to identify parameters influencing the development of negative skin friction on pile. The results of the numerical model showed that

angle of soil internal friction has no effect on the developed negative skin friction (NSF) on pile.

6. The following are noted for the case of inundation from the bottom:

    a. Collapse potential (C_p) influences average negative shear stress (q_n) and has no effect on depth of neutral axis (N.A.).

    b. There is a maximum radius of wetting (h) that can influence the magnitude of negative skin friction and the maximum limit depends on other factors. The radius of wetting does not have any significant effect on depth of neutral axis (N.A.).

    c. Pile roughness (in terms of pile interface strength reduction factor) is found to have significant influence on the development of negative skin friction on pile, when any of the parameters such as the radius of wetting (h), the H_s/D ratio, and the collapse potential (C_p) is close to their respective upper limits.

    d. Pile length (L) and pile length-to-diameter ratio (L/D) has no effect on average negative shear stress (q_n), if the radius of wetting (h), the H_s/D ratio, the pile roughness and the collapse potential (C_p) remain constant.

    e. Pile embedment into non collapsible soil (underlying collapsible soil) to full length ratio (L_e/L) has no influence on average negative shear stress (q_n), when the radius of wetting (h), the H_s/D ratio, the pile roughness and the collapse potential (C_p) remain constant. For low L_e/L ratio, indirect load (Q_n) developed by negative skin friction may be low, as pile settles for not developing adequate positive skin frictional resistance.

    f. For a given soil condition (e.g., defined by C_p) and inundation condition (e.g., defined by h), average negative shear stress (q_n) depends on H_s/D ratio linearly, in a semi logarithmic plot. The slope of this relation varies with the soil and inundation conditions.

7. The following are noted for the case of inundation from the top:

    a. Unit negative skin friction ($Q_n/\pi D$) has linear relation with H_s/D ratio in a semi logarithmic plot, for given h and C_p.

    b. Unit negative skin friction ($Q_n/\pi D$) does not increase infinitely due to the increase of h.

161

    c. Collapse potential (C_p) influences unit negative skin friction ($Q_n/\pi D$) more than depth of neutral axis (N.A.).

8. Another modeling procedure is proposed to design the pile (length below the collapsible soil, diameter, etc.) when the indirect load due to NSF is known.

9. Analytical models those can be used to predict the indirect load due to negative skin friction are developed for both the cases of inundation condition (from bottom and top).

10. Application of the proposed procedure will reduce the cost of construction, litigation and remediation.

6.3 Recommendations for Future Studies

1. Study the developed negative skin friction (NSF) on a single pile at different stages of partial inundation (in terms of degree of saturation).

2. Examine sensitivity of hysteresis property of SWCC on the developed NSF developed for partial inundation.

3. Extend the current study to investigate the performance of a single pile in terms of rotation, bending moment, etc., when the pile is subjected to inclined/lateral load during inundation of collapsible soil.

4. Extend the proposed model to cover the cases of battered pile and group piles.

5. Extend the proposed procedure of modeling soil collapse to investigate the performance of shallow foundation.

6. Study the combined effect of pile installation and inundation on the neighboring pile.

BIBLIOGRAPHY

Abbeche, K., Hammoud F., and Ayadat T. 2007. Influence of relative density and clay fraction on soils collapse. Experimental Unsaturated Soil Mechanics [C], Springer Proceedings in Physics, 2007, 112, pp. 3–9.

Abdrabbo, F.M., and Abdelaziz, T.M. 2006. Study of the infiltration of water through collapsible soil. Geotechnical Special Publication. n 147, in Proceedings of the Fourth International Conference on Unsaturated Soils, pp. 1049–1060.

Arya, L.M., and Paris, J.F. 1981. A physicoempirical model to predict the soil moisture characteristic from particle-size distribution and bulk density data. Soil Science Society of America Journal, 45: 1023–1030.

ASTM D 5333-03, 1998. Standard test method for the measurement of collapse potential of soils, ASTM International, West Conshohocken, Available at, http://www.astm.org.

Ayadat, T., and Hanna, A.M. 2007. Identification of collapsible soil using the fall cone apparatus. Journal of Geotechnical Engineering, 30(4): 312–323.

Ayadat, T., and Hanna, A.M. 2005. Encapsulated stone columns as a soil improvement technique for collapsible soil. Journal of Ground Improvement, 9(4): 137–147.

Basma, A.A., and Kallas, N. 2004. Modeling soil collapse by Artificial Neural Networks. Geotechnical and Geological Engineering, 22(3): 427–438.

Booth, A.R. 1977. Collapse settlement in compacted soils. Council for Scientific and Industrial Research Report 324, National Institute for Transport and Road Research Bulletin 13, pp. 1–34.

Brandon, T.L., Duncan, J.M., and Gardner, W.S. 1990. Hydrocompression settlement of deep fills. Journal of Geotechnical Engineering, 116(10): 1536–1548.

Brooks, R.H., and Corey, A.T. 1964. Hydraulic properties of porous media. Colorado State University Hydrology, Paper No.3, Fort Collins, Colo.

Brutsaert, W. 1967. Some methods of calculating unsaturated permeability. Transactions of the ASAE, American Society of Agricultural Engineers, 10(3): 400–404.

Chen, Z.H., Huang, X.F., Qin, B., Fang, X.W., and Guo, J.F. 2008. Negative skin friction for cast-in-place piles in thick collapsible loess. Unsaturated Soils. Advances in Geo-Engineering, D.G. Toll, C.E. Augrade, D. Gallipoli, and S.J. Wheeler, Taylor and Fracis 2008, pp. 979–985.

Clemence, S.P., and Finbarr, A.O. 1981. Design considerations for collapsible soils. Journal of Geotechnical Engineering, 107(3): 305–317.

Cox, D.W.1978. Volume change of compacted clay fill. In Proceedings of the Institution of Civil Engineers Conference on Clay Fills, London, pp. 79–86.

Derbyshire, E.; Dijkstra, T.A., and Smalley, I.J. 1998. Genesis and properties of collapsible soils. Nato Asi Series, Vol. C468.

Dijkstra, J., Brorere, W., and van Tol, A.F. 2006. Numerical investigations into stress and strain development around a displacement pile in sand. In H.F. Schweiger (ed.), Numerical methods in Geotechnical Engineering, pp. 595–600.

Dudley, J.H. 1970. Review of collapsing soils. Journal of Soil Mechanics and Foundation Division, 96(3): 925–947.

El-Mossallamy, Y. 1999. Load settlement behavior of large diameter bored piles in overconsolidated clay. In G.N. Pande, S. Pietruszczak, and H.F. Schweiger (eds), Numerical Models in Gemechanics; Proceeding of the 7th international symposium, Graz, Rotterdam, Balkema, the Netherlands.

Escario, V., and Juca, J. 1989. Strength and deformation of partly saturated soils. In Proceedings of the 12th International Conference on Soil Mechanics and Foundation Engineering, Rio de Janerio, pp. 43–46.

Evans, R.D., Jefferson, I., Northmore, K.J., Synac, O., and Serridge, C.J. 2004. Geophysical investigation and in-situ treatment of collapsible soils. Geotechnical Special Publication, n 126 II, Geotechnical Engineering for Transportation Projects: Proceedings of Geo-Trans, pp. 1848–1857.

Evstatiev, D. 1995. Design and treatment as loess bases in Bulgaria. In Genesis and properties of collapsible soils. Edited by Ed. Derbyshire, T. Dijkastra, J. Smalley, NATO ASI Series C: Matematical and Physical Sciences vol. 468, Kluwer Akad. Publishers, pp. 375–382.

Fellenius, B.H. 1972. Downdrag on piles in clay due to negative skin friction. Canadian Geotechnical Journal, 9(4): 323–337.

Feng, M., and Fredlund, D.G. 1999. Hysteretic influence associated with thermal conductivity sensor measurements. In Proceedings of the 52nd Canadian Geotechnical Conference, Regina, Sask., 24-27 october, BiTec Publishers Ltd., Richmond, pp. 651–657.

Franke, E., and Muth, G. 1985. Scale effect in 1g model tests on horizontally loaded piles. In Proceedings of the 11th International Conference of Soil Mechanics and Foundation Engineering, San Francisco, Calif. Vol. 2, pp. 1011–1014.

Fredlund D.G., and Morgenstern N.R. 1977. Stress state variables for unsaturated soils. ASCE J. Geotech. Eng. Div. GT5, 103, pp. 447–466.

Fredlund D.G., Morgenstern N.R., and Widger R.A. 1978. The shear strength of unsaturated soils. Canadian Geotechnical Journal 15(3): 313–321.

Fredlund, D.G., and Rahardjo, H. 1993. Soil mechanics for unsaturated soil, John Wiley & Sons, New York.

Fredlund D.G., and Xing A. 1994. Equations for the soil-water characteristic curve. Canadian Geotechnical Journal 31(4): 521–532.

Fredlund, D. G., and Gan, J. K-M. 1995. The collapse mechanism of a soil subjected to one-dimensional loading and wetting. Genesis and Properties of Collapsible Soils, edited by E. Derbyshire, T. Dijkstra and I. J. Smalley, NATO ASI Series, Vol. 468, Kluwer Academic Publishers, pp. 173–205.

Fredlund, M.D. 1999. The role of unsaturated soil property functions in the practice of unsaturated soil mechanics. PhD dissertation, University of Saskatchewan, Saskatoon, Sask.

Fredlund, D.G. 2006. Unsaturated soil mechanics in engineering practice. Journal of Geotechnical and Geoenvironmental Engineering, 132(3): 286–321.

Fredlund, D.G., and Houstan, S.L. 2009. Protocol for the assessment of unsaturated soil properties in geotechnical engineering practice. Canadian Geotechnical Journal, 46(6): 694–707.

Futai, M.M., Almeida, M.S.S., and Lacerda, W.A. 2006. The shear strength of unsaturated tropical soils in Ouro Perto, Brazil. In Miller et al. (Eds.) Proceedings of the 4th International Conference on Unsaturated Soils. Carefree, AZ, ASCE Geotechnical Special Publication, 147: 1201–1211.

Gan, K.J., and Fredlund, D.G. 1988. Multistage direct shear testing of unsaturated soils. Geotechnical Testing Journal, 11(2): 132–138.

Gao, X.J., Wang, J.C., and Zhu, X.R., 2007. Static load test and load transfer mechanism study of squeezed branch and plate pile in collapsible loess foundation. Journal of Zhejiang University - Science A, 8(7): 1110–1117.

Gardner, W.R. 1958. Some steady state solutions of the unsaturated moisture flow equation with application to evaporation from a water table. Soil Science, 85(4): 228–232.

Grigoryan, A.A., and. Grigoryan, R.G. 1975. Experimental investigation of negative-friction forces along the lateral surface of piles as the soils experience slum-type settlement under their own weight. Osnovaniya, Fundamenty i Mekhanika Gruntov, No. 5, pp. 10–13.

Grigoryan, A.A., and Chinenkov, Yu. A. 1990. Experience gained with construction on long piles with broadened heels in soils prone to slump-type settlement. Osnovaniya, Fundamenty i Mekhanika Gruntov, No. 4, pp. 2–5.

Grigoryan, A.A. 1991. Construction on Loess Soils. Osnovaniya, Fundamenty i Mekhanika Gruntov, No. 1, pp. 24–27.

Grigoryan, A.A. 1997. Pile Foundations for buildings and structures in collapsible soil. A.A. Balkema Publishers, Brookfield, USA.

Hanna, A.M., and Sharif A. 2006. Drag force on a single pile in clay subjected to surcharge loading. International Journal of Geomechanics, 6(2): 89–96.

Hilf, J.W. 1956. An investigation of pore-water pressure in compacted cohesive soils. Tech. Memo. 654. U.S. Bureau of reclamation, Design and construction Div. Denver. CO.

Holtz, W.G. 1948. The determination of limits for the control of placement moisture in high rolled earth dams. American Society for Testing and Materials, Proceedings, 48, pp. 1240–1248.

Hormdee, D., Ochiai, H., and Yasufuku, N. 2005. Advanced direct shear testing for collapsible soils with water content and matric suction measurement. Geotechnical Special Publication, n 130–142, Geo-Frontiers, pp. 2281–2290.

Houstan, S.L., Mahmoud, H.H., and Houstan, W.N. 1995. Down-Hole collapse test system. Journal of Geotechnical Engineering, 121(4): 341–349.

Isaev, B.N., Badeev, S.Y., and Zetenskii, V.Y. 1989. Pile foundations on stabilized bases in type II collapsibility soils. Soil Mechanics and Foundation Engineering, 26(4): 149–151.

Jennings, J. E., and Knight, K. 1975. A guide to construction on or with material exhibiting additional settlement due to collapse of grain structure. In Proceedings of the 6th Regional Conf. of Africa on SMFE, pp. 99–105.

Kakoli, S.T.N., Hanna, A.M., and Ayadat, T. 2009. Simulation of collapsible soil subjected to inundation. 17th International Conference on Soil Mechanics and Geotechnical Engineering, Alexandria, Egypt.

Kalashnikova, O. P. 1976. Investigation of the behavior of piles in a collapsible soil stabilized through a leading hole. Soil Mechanics and Foundation Engineering journal, 13(1): 16–19.

Katzenbach, R., and Arslan, U. and Holzhäusher, J. 1995. Geotechnische Meßüberwachung des 300 m hohen Commerzbank-Hochhauses in Frankfurt am Main. Proceedings Pfahl Symposium '95. Mitteilungen des institutes und der Versuchsanstalt für Geotechnik der Technischen Universität Darmstadt: Heft 48: 233–244.

Kenneth, D.W., Houstan, W.N., and Houstan, S.L. 1993. Evaluation of in-place wetting using soil suction measurements. Journal of Geotechnical Engineering, 119(5): 862–873.

Khalili, N., and Khabbaz, M. H. 1998. A unique relationship for the determination of the shear strength of unsaturated soils. Geotechnique, 48(5): 1–7.

Klukanova, A., and Frankovska, J. 1995. The Slovak Carpathians loess sediments, their fabric and properties. Genesis and Properties of Collapsible Soils, Derbyshire et al. (Eds.), pp. 129–147.

Kodikara, J., Barbour, S.L., and Fredlund, D.G. 1999. Changes in clay structure and behavior due to wetting and drying. In Proceedings of the 8th Australia, Newzealand Conference on Geomechanics, Hobart, pp. 179–186.

Lawton, E. C., Fragaszy, R. J., and Hardcastle J. H. 1991. Stress ratio effects on collapse of compacted clayey sand. Journal of Geotechnical Engineering, 117(5): 714–730.

Lawton,E.C.; Fragaszy, R.J., and Hetherington, M.D. 1992. Review of wetting-induced collapse in compacted soil. Journal of Geotechnical Engineering, 118(9): 1376–1394.

Lee, C.J., Bolton, M.D., and Al-Tabaa, A. 2001. Recent findings on negative skin friction in piles and pile groups in consolidating ground. 5th International Conference on Deep Foundation Practice, Singapore, April, pp. 273–280.

Leong, E.C., and Rahardjo, H. 1997. Permeability functions for unsaturated soils. Journal of Geotechnical and Geoenvironmental Engineering. 123(12): 1118–1126.

Lim, Y.Y., and Miller, G.A. 2004. Wetting-induced compression of compacted Oklahoma soils. Journal of Geotechnical and Geoenvironmental Engineering, 130(10): 1014–1023.

Lu, N., and Likos, W.J. 2004. Unsaturated soil mechanics. Wiley Publishers.

Lutenegger, A.J., and Saber, R.T. 1988. Determination of collapse potential of soils. Geotechnical Testing Journal, 11(3): 173–178.

Mal'tsev, A.T., and Sazhin, V.S. 1980. Behavior of short piles in collapsible soils under the action of inclined forces. Soil Mechanics and Foundation Engineering, English Translation of Osnovaniya Fundamenty i Mekhani, 17(6): 235–239.

Mahmoud, H. 1991. The development of an in-situ collapse testing system for collapsible soils. Ph.D dissertation, Arizona State University, Tempe, Arizona.

Mashhour, I. 2009. Negative skin friction on single piles in collapsible soils. MA.Sc thesis, Concordia University, Montreal, Quebec.

Maswoswe, J. 1985. Stress-paths for compacted soil during collapse due to wetting. PhD dissertation, Imperial College of Sciences and Technology, England.

Mckee, C.R., and Bumb, A.C. 1984. The importance of unsaturated flow parameters in designing a monitoring system for hazardous wastes and environmental emergencies. In Proceedings of Hazardous Materials Control Research Institute National Conference, Houstan, Texas, pp. 50–58.

Mckee, C.R., and Bumb, A.C. 1987. Flow-testing coalbed methane production wells in presence of water and gas. Society of Petroleum Engineers (SPE), Richardson, Texas Formation Evaluation No. 1, pp. 599–608.

Miranda. A.N. 1988. Behavior of small earth dams during initial filling. Ph.D. dissertation, Colorado State University, Fort Collins, Colorado.

Nouaouria, M.S., Guenfoud, M., and Lafifi, B. 2008. Engineering properties of loess in Algeria. Journal of Engineering Geology, 99(1-2): 85–90.

Öberg, A.-L., and Sällfors, G. 1997. Determination of shear strength parameters of unsaturated silts and sand based on the water retention curve. Geotechnical Testing Journal, 20(1): 40–48.

Ovesen, N.K. 1980. The use of physical models in design. In Proceedings of the 7th European Conference of Soil Mechanics and Foundation Engineering, Brighton, U.K. Vol. 4, pp. 319–323.

Pereira, J.H.F. 1996. Numerical analysis of the mechanical behavior of small collapsing earth dams during first reservoir filling. PhD dissertation, University of Saskatchewan, Saskatoon, Canada.

Pereira, J.H.F., and Fredlund, D.G. 1999. Numerical Analysis of the post-filling performance of small collapsing dams. In Proceedings of the Eleventh Pan American Conf. on Soil Mechanics and Geotechnical Engineering, Iguanzu Falls, Brazil, 3, pp. 1129–1140.

Pereira, J.H.F., and Fredlund, D.G. 2000. Volume change behavior of collapsible compacted gneiss soil. Journal of Geotechnical and Geoenvironmental Engineering, 126(10): 907–916.

Pereira, J.H.F., and Fredlund, D.G., Neto, M.P.C., and Gitirana Jr., G.F.N. 2005. Hydraulic behavior of collapsible compacted gnesis soil. Journal of Geotechnical and Geoenvironmental Engineering, 131(10): 1264–1273.

Pham, H.Q. 2001. An engineering model of hysteresis for soil-water characteristic curves. M.Sc. thesis, University of Saskatchewan, Saskatoon, Saskatoon, Canada.

Pham, H.Q., and Fredlund, D.G., and Barbour, S.L. 2002. A simple soil-water hysteresis model for predicting the boundary wetting curve. In Proceeding of the 55th Canadian Geotechnical Conference, Ground and Water-Theory to Practice, Niagara Falls, Ontario, October 20-23, BiTech Publishers Ltd., Richmond, B.C., pp. 1261–1267.

Pham, H.Q., and Fredlund, D.G., and Barbour, S.L. 2003. A practical hyteresis model for the soil-water characteristic curve for soils with negligible volume change. Géotechnique, 53(2): 293–298.

PLAXIS BV, PLAXIS 2D Foundation. Available at, http://www.plaxis.nl/.

Poulos, H.G. 1997. Piles subjected to negative friction: A procedure for design. Geotechnical Engineering, Southeast Asian Geotechnical Society, 28(1): 23–44.

Rawls, W. J., and Brakensiek, D. L. 1985. Prediction of soil water properties for hydrologic modeling. In Proceedings of the American Society of Civil Engineers Watershed Management in the Eighties Symposium, ASCE, New York, pp. 293–299.

Rollins, K.M., Rollins, R.L., Smith, T.S., and Beckwith, G.H. 1994. Mitigation measures for small structures on collapsible alluvial soils. Journal of Geotechnical Engineering, 120(9): 1533–1553.

Rollins, K.M., Jorgensen, S.J., and Ross, T.E. 1998. Optimum moisture content for dynamic compaction of collapsible soils. Journal of Geotechnical and Geoenvironmental Engineering, 124(8): 699–708.

Scheinost, A.C., Sinowski, W., and Auerswald, K. 1997. Regionalization of soil-water retention curves in a highly variable landscape: I-Developing a new pedo-transfer function. Geoderma, 78(3-4): 129–143.

Sedran, G., Stolle, D.F.E., and Horvath, R.G. 2001. An investigation of scaling and dimensional analysis of axially loaded piles. Canadian Geotechnical Journal, 38(3): 530–541.

Sharma, R.S., and Singhal, S. 2006. Preliminary observation on volumetric behavior of unsaturated collapsible loess. Geotechnical Special Publication, in Proceedings of the Fourth International Conference on Unsaturated Soils, 147, pp. 1017–1024.

Sommer, H., and Hammbach, P. 1974. Groβpfahlversuche im Ton für die Gründung der Talbrücke Alzey. Der Bauingenieur, Vol 49, pp. 310–317.

SoilVision Systems, SoilVision V2.0, Available at, http://www.soilvision.com/.

Tadepalli, R., and Fredlund, D.G. 1991. The collapse behavior of a compacted soil during inundation. Canadian Geotechnical Journal, 28(4): 477–488.

Tadepalli, R., Rahardjo, H., and Fredlund, D.G. 1992. Measurements of matric suction and volume changes during inundation of collapsible soil. Geotechnical Testing Journal, 15(2): 115–122.

Tagaya, K., Scott, R.F., and Aboshi, H. 1988. Scale effects in anchor pullout test by centrifugal technique. Soils and Foundations, 28(3): 1–12.

Tani, M. 1982. The properties of a water-table rise produced by a one-dimensional, vertical, unsaturated flow. Journal of Japan Forestry Society, 64: 409–418.

Tyler, S.W., and Wheatcraft, S.W. 1989. Application of fractal mathematics to soil-water retention estimations. Soil Science Society of America Journal, 53(4): 987–996.

Udomchoke, V. 1991. Origin and engineering characteristics of the problem Soil in the Khorat Basin, Northeastern Thailand. Ph.D dissertation. Asian Institute of Technology, Bangkok, Thailand.

Vanapalli, S.K., Fredlund, D.G., Pufahl, D.E., and Clifton, A.W. 1996. Model for the prediction of shear strength with respect to soil suction. Canadian Geotechnical Journal, 33(3): 379-392.

Vanapalli, S.K., and Fredlund, D.G. 2000. Comparison of different procedures to predict unsaturated soil shear strength. Advances in Unsaturated Geotechnics (GSP 99), Proceedings, Geodenver Conference, Denver, Colo., 5-8 August, Shackelford et al. (Eds.), 195–209.

Van Genuchten, M.T. 1980. A closed form equation predicting the hydraulic conductivity of unsaturated soils. Soil Science Society of America Journal, 44: 892–898.

Vereecken, H., Maes, J., Feyen, J., and Darius, P. 1989. Estimating the soil moisture retention characteristic from texture, bulk density, and carbon content. Soil Science, 148(6): 389-403.

Wehnert, M., and Vermeer, P. 2004. Numerical analyses of load tests on bored piles. In Numerical Methods in Geomechanics. NUMOG IX, pp. 505–511.

Yasufuku, N., Ochiai, H., and Hormdee, D. 2006. An empirical relationship for predicting soil collapsibility due to soaking under compression and shear. Geotechnical Special Publication, n 147, in Proceedings of the Fourth International Conference on Unsaturated Soils, pp. 1037–1048.

Zapata, C.E., Houstan, W.N., Houstan, S., and Walsh, K.D. 2000. Soil-water characteristic curve variability. Advances in unsaturated Geotechnics (GSP 99), In Proceedings of Geodenver Conference, Denver, Colo., 5-8 August, Shackelford et al. (Eds.), pp. 84–124.